Neuronal functions of RIM3γ and RIM4γ

Dissertation

zur
Erlangung des Doktogrades (Dr. rer. nat)
der
Mathematisch-Naturwissenschaftlichen Fakultät
der
Rheinischen Friedrich-Wilhelms-Universität Bonn

vorgelegt
von

Katrin Michel
aus
Heidenheim

Bonn, März 2015

Angefertigt mit Genehmigung der Mathematisch-Naturwissenschaftlichen Fakultät der Rheinischen Friedrich-Wilhelms-Universität Bonn

1. Gutachter: Prof. Dr. Susanne Schoch

1. Gutachter: Prof. Dr. Albert Haas

Tag der Promotion: 03.07.2015

Erscheinungsjahr 2015

Contents

1 Summary

The large isoforms of the Rab3 interacting molecule (RIM) family, RIM1α/β and RIM2α/β are integral components of the cytomatrix of the presynaptic active zone. Through multiple interactions with other active zone proteins they are involved in regulating several steps of presynaptic neurotransmitter release. The RIM protein family contains two additional isoforms, RIM3γ and RIM4γ, whose functions remain to be elucidated.

In this study we could show that RIM3γ and RIM4γ are key regulators in neuronal growth involved in the establishment of axons and dendrites, formation of synapses and dendritic spines. Furthermore, the loss of RIM3γ leads to a dispersion of the Golgi apparatus whereas the loss of RIM4γ induces the condensation of the Golgi in the cell's soma. These findings provide first hints that the small γ-Rims are involved in neuronal growth by regulating processes of vesicular traffic. Live cell imaging of Rab-protein marked vesicles in RIM3γ and RIM4γ knock-down neurons revealed changes in the velocity and the path length of Rab11 and Rab8 vesicles, confirming that the loss RIM3γ and RIM4γ has an effect on intracellular transport routes.

In an affinity purification mass spectrometry based search for novel γ-RIM interaction partners we identified a large set of proteins that have been associated with neuronal growth through the remodeling of the cytoskeleton or vesicular traffic and in addition a smaller group of synaptic proteins. A comparison of the individual affinity purification mass spectrometry approaches performed in different tissue fractions revealed that a cluster of new γ-RIM interaction partners was repeatedly detected. This cluster contained proteins involved in the remodeling of the cytoskeleton, site directed transport of vesicles and proteins that belong to signaling cascades important for axonal and dendritic growth. We performed first validation experiments using *in vitro* binding assays to decipherer the direct interactions of this complex. These experiments confirmed *in vitro* an interaction between γ-RIMs and the cytoskeleton regulator IQGAP3, the adhesion molecule plakophilin4 and Syd-1 an important initiator of synapse assembly.

To get further insights in the cellular functions of RIM3γ and RIM4γ we generated constitutive knock-out mouse lines for both proteins. RIM3γ and RIM4γ knock-out mice are viable and not distinguishable from wild type litters until 20 days after birth. Around an age of three weeks RIM4γ knock-out mice develop a strong episodic motor phenotype, most prominent in the hind limbs, whereas RIM3γ knock-out mice show no obvious phenotype. Behavioral tests of motor coordination revealed that RIM4γ knock-out mice suffer also during phenotypic inconspicuous periods from milder coordinative disturbances suggesting impairments in cerebellar functions. Interestingly, after the induction of neuronal activity in an animal model of epilepsy RIM4γ transcripts were strongly upregulated in the hippocampus 12 hours after status epilepticus whereas RIM3γ transcripts were downregulated in the hippocampal subregion dentate gyrus

after 36 hours. These findings suggest that the γ-RIMs might be either involved in pathological changes occurring during epileptogenesis or in neuroprotective mechanisms in response to increased network activity.

Taken together, the results of this study provide new insights into the function of RIM3γ and RIM4γ in the development and the function of a healthy brain and form the basis for future studies on the precise understanding of the role of RIM3γ and RIM4γ during the pathogenesis of neurological disorders.

2 Introduction

Introduction

Already in 1865 the German Neuroanatomist Otto Deiters described the three structurally distinct compartments of a nerve cell: the cell body, which is continuous and has a variable number of processes that frequently branch, ultimately get thinner and disappear. Besides these numerous processes the neuron exhibits one major process which when it leaves the cell body appears as a rigid hyaline mass. Today we refer to these processes as dendrites and axon. The unique molecular composition and the morphological polarization of these structures gives a neuron the ability to receive information by its dendrites, compute it, and deliver information via its axon to other neurons or muscle cells. Since the times of Otto Deiters a lot of progress has been made in the characterization of the physiological properties of axons and dendrites as well as the general cellular mechanisms, which enable the neuron to form these highly specialized compartments. Neuronal growth involves remodeling of the cytoskeleton, as well as synthesis, transport, and integration of membrane, lipids and proteins in a highly organized manner. Every compartment has its unique composition which allows the neuron to process information in a fast and precise manner. However, as much as we understood of the great picture of these mechanisms as little we understand of the precise molecular pathways and especially how they converge together.

2.1 Neuronal growth: establishment of axons and dendrites

2.1.1 Remodeling of the cytoskeleton during neuronal growth

The cytoskeleton provides structure and stability to the cell, but it is in no way just a rigid and stable scaffold. At least in parts the cytoskeleton is constantly destroyed, renewed, or newly constructed, making it a highly dynamic structure. These dynamic properties enable the cytoskeleton to participate in and to regulate multiple cellular processes [Gardner et al., 2013, Edwards et al., 2014]. The expansion of the cytoskeleton determines the cells size and shape. Remodeling of the cytoskeleton regulates formation and structural organization of cellular organelles [de Forges et al., 2012, Pollard & Cooper, 2009]. Furthermore, the cytoskeleton serves as a scaffold along which proteins and cellular organelles are transported throughout the cell [Schliwa, 2006]. The filamentous structure of the cytoskeleton is build up by intermediate filaments, microtubules and actin filaments. Structural variability and dynamics of these filaments is provided by hundreds of accessory proteins, which converge extrinsic and intrinsic signals on the cytoskeleton and regulate assembly and location of the different filamentous components [Wickstead & Gull, 2011].

2.1.1.1 Regulation of the actin cytoskeleton during neuronal growth

Forward movement and extension of neuronal branches take place at the growing tip of a neurite the so-called growth cone. The growth cone forms a hand like structure, in which actin is localized at the outline of the finger like fine tips followed by microtubules reaching from the cells soma into the center of growth cone. Remodeling of F-actin leads to local instability of the actin network and allows microtubules and other protein to enter the growth cone, leading to an extension of the neuronal branch [Witte & Bradke, 2008].

Important regulators of the actin cytoskeleton during neuronal growth are the three members of the Rho family of small GTPases, RhoA, CDC42 and Rac1. Rac1 and CDC42 have been shown to be mainly growth promoting, whereas RhoA has rather growth inhibitory effects [Luo, 2000].

Rac1 regulates actin dynamics through two major downstream effectors, the WAVE complex and p21-activated kinase (PAK) [Miki et al., 1998, Burridge & Wennerberg, 2004]. Rac1 activation of the WAVE complex leads to actin polymerization through the Arp2/3 complex [Govek et al., 2005], whereas the activation of PAK leads to the phosphorylation of Cofillin, an actin depolymerization factor, shown to be involved in neurite formation [Arber et al., 1998, Edwards et al., 1999, Meberg & Bamburg, 2000]. This shows, that both actin polymerization and depolymerization are important for neuronal growth. The balance of actin polymerization and depolymerization allows the neuron to remodel and also elongate the cytoskeleton simultaneously in an appropriate fashion. This also explains why actin polymerization or depolymerization can on the one hand be growth promotive and on the other hand growth inhibitory.

CDC42, like Rac1, regulates actin dynamics through the Arp2/3 complex and phosphorylation of cofilin. CDC42 deficient neurons exhibit defects in axon formation and reduced neurite length [Garvalov et al., 2007, Rohatgi et al., 1999, Rohatgi et al., 2000].

RhoA is mainly suggested to be growth inhibitory but contradicting findings on RhoA's function during neuronal growth have been reported. Two major downstream effectors of RhoA involved in neuronal growth are ROCK, a member of the Rho Kinase family, and a formin related protein, mammalian diaphanous (mDia) [Leung et al., 1996, Watanabe et al., 1997, Amano et al., 1996]. ROCK regulates actin bundling and accumulation of actin filaments and has been shown to mediate RhoA signaling during dendrite retraction and the inhibition of axon initiation [Nakayama et al., 2000, Bito et al., 2000, Amano et al., 1996]. mDia was suggested to initiate actin nucleation by binding to free actin monomers [Li & Higgs, 2003, Higashida et al., 2004]. However, in contrast to ROCK mDia was suggested to promote axongenesis, which could explain how RhoA is growth inhibitory or supportive [Arakawa et al., 2003]. Taken together, tight temporal and spatial control of actin dynamics is an important mechanism for a neuron to specifically regulate the different steps of dendritic and axonal growth.

2.1.1.2 Microtubule remodeling during neuronal development

Microtubules are the second group of cytoskeletal filaments playing an important role in the regulation of neuronal growth. Microtubules grow as hollow tubes and rapidly switch from growth to shrinkage (catastrophes) and shrinkage to growth (rescue). Thus microtubules never attain a

steady state length but exist either in a growing (polymerization) phase or a shrinking phase (depolymerization) [Burbank & Mitchison, 2006]. This dynamic instability allows microtubules to rapidly reorganize and differentiate spatially and temporarily in accordance to the cells context [Kirschner & Mitchison, 1986]. Ultrastructural analysis showed that microtubules form parallel bundles in axons and dendrites, which extend during neuronal growth [Yamada et al., 1971]. Additionally, pharmacological studies revealed that microtubule depolymerizing drugs inhibit growth and lead to neurite retraction [Daniels, 1973]. However, microtubule organization differs between axons and dendrites. Axonal microtubules show a uniform orientation and are complemented by the microtubule associated protein (MAP) tau whereas dendritic microtubules show a mixed orientation and are complemented by the microtubule associated protein MAP2 [Ferreira et al., 1989]. Tau has been shown to be required for axon formation and growth [Dawson et al., 2001, DiTella et al., 1996, Takei et al., 2000]. Besides stabilizing microtubules itself, tau also protects microtubules from depolymerization and interacts with components of the actin cytoskeleton during stimulated neurite outgrowth [Yu & Rasenick, 2006, Sharma et al., 2007]. In dendrites MAP2 binds along the side of microtubules and contributes to their stabilization by crosslinking adjacent microtubules. Overexpression of MAP2 in non-neuronal cells leads to the growth of dendritic like processes, whereas depletion of MAP2 in primary neuronal cultures inhibits neurite formation [LeClerc et al., 1993, Caceres et al., 1992]. Aditionally, MAP2 was also suggested to link the rough endoplasmic reticulum to microtubules of dendrites and thereby to contribute to the differential expression of organelles in axons and dendrites [Farah et al., 2005].

One specialized class of microtubule associated proteins are the microtubule plus end tracking proteins (+TIPs). +TIPs show a high affinity to the plus end of polymerizing microtubules and are involved in the control of microtubule dynamics, growth directionality, interactions with other cytoskeletal components and correct positioning of organelles, receptors, and channels. Therefore +TIPs are important regulators of neuronal growth during development and of neuronal communication in mature neurons [Jaworski et al., 2008, Temburni et al., 2004, Williams et al., 2004, Gu et al., 2006]. The first identified microtubule plus end tracking protein is the cytoplasmic linker protein 170 (CLIP170). Interactions between CLIP170 and the IQ-motif GTPase-activating protein 1 (IQGAP1), an actin binding protein, provide a possible link between microtubules and the actin cytoskeleton [Fukata et al., 2002, Watanabe et al., 2004]. IQGAP1 interacts additionally with the microtubule plus end tracking protein CLASP2 providing a further link between microtubules and the actin cytoskeleton [Watanabe et al., 2009]. Neurons deficient for CLASP2 show impairments in axon elongation and reductions in dendritic branch length. The overexpression of CLASP2 on the other hand leads to formation of multiple axons and enhanced dendritogenesis [Beffert et al., 2012]. These findings shows that the correct interplay between microtubules and actin and the concomitant distribution of organelles and proteins are important for neuronal growth, polarization and function.

2.1.2 Membrane transport processes during neuronal growth

The elongation of axons and dendrites requires, besides structural changes associated with the cytoskeleton, the addition of an enormous amount of new plasma membrane in order to carry out the vast increase in the neuronal surface area. The plasma membrane of a mature neuron can reach a surface area of about 250,000μm^2 and is thereby the neuron's biggest organ. Its correct polarized composition of lipids and proteins is fundamental for the neuron's function of receiving and propagating electrical signals. During neuronal growth new membrane is synthesized, equipped with differential sets of proteins and lipids, transported by site specific carriers and finally targeted to the place of destination, where fusion with the plasma membrane occurs [Horton et al., 2003, Pfenninger, 2009].

2.1.2.1 Controlled transport of membrane: RAB proteins

Members of the Rab protein family of small GTPases are hypothesized to act as intracellular 'cargo address labels' of vesicular membrane transport in neuronal and non-neuronal cells. With over 60 family members in mammals, Rab proteins constitute the largest family of small GTPases [Klöpper et al., 2012, Zerial & McBride, 2001]. Rab proteins function as molecular switches, by cycling between a GTP bound active form and a GDP bound inactive form. The activity status of Rab proteins, is regulated by guanine exchange factors (GEFs) and GTPase activating proteins (GAPs). GEFs are activators of Rab proteins; by binding to the GTPase they reduce its affinity for GDP and promote the exchange from GDP to GTP. GTPase activating proteins on the other hand serve as negative regulators; they increase the intrinsic GTPase activity of the Rab protein and accelerate the conversion of the GTP bound active to the GDP bound inactive form [Barr & Lambright, 2010]. The spatial and temporal distribution of GEFs and GAPs and numerous additional Rab effector proteins including motor proteins and tethering complexes, allows Rab GTPases to govern various steps in membrane trafficking, including vesicle budding, vesicle movement, site specific vesicle docking and vesicle fusion [Jordens et al., 2005, Grosshans et al., 2006].

In neurons, proteins and lipids are synthesized by the endoplasmic reticulum and subsequently transported to the Golgi apparatus, from where they are distributed either directly to the plasma membrane or further to the different compartments of the endsosome. The endosome is composed of three different kinds of vesicular compartments, the early, the late, and the recycling endosome [Bard & Malhotra, 2006, De Matteis & Luini, 2008, Horton & Ehlers, 2003]. Vesicles endocytosed by the plasma membrane are first transported to the early endosome, from where proteins targeted to degradation move to the late endosome and further to the lysosome, whereas other proteins are transported to the recycling endosome for eventual reinsertion into the plasma membrane. Additionally, all three endosomal compartments receive vesicles from and send vesicles back to the trans-Golgi network [Maxfield & McGraw, 2004] (Fig 2.1). Several Rab proteins have been implicated in regulating the various vesicular transport routes between the different secretory compartments have been shown to be crucial for neuronal growth [Villarroel-Campos et al., 2014].

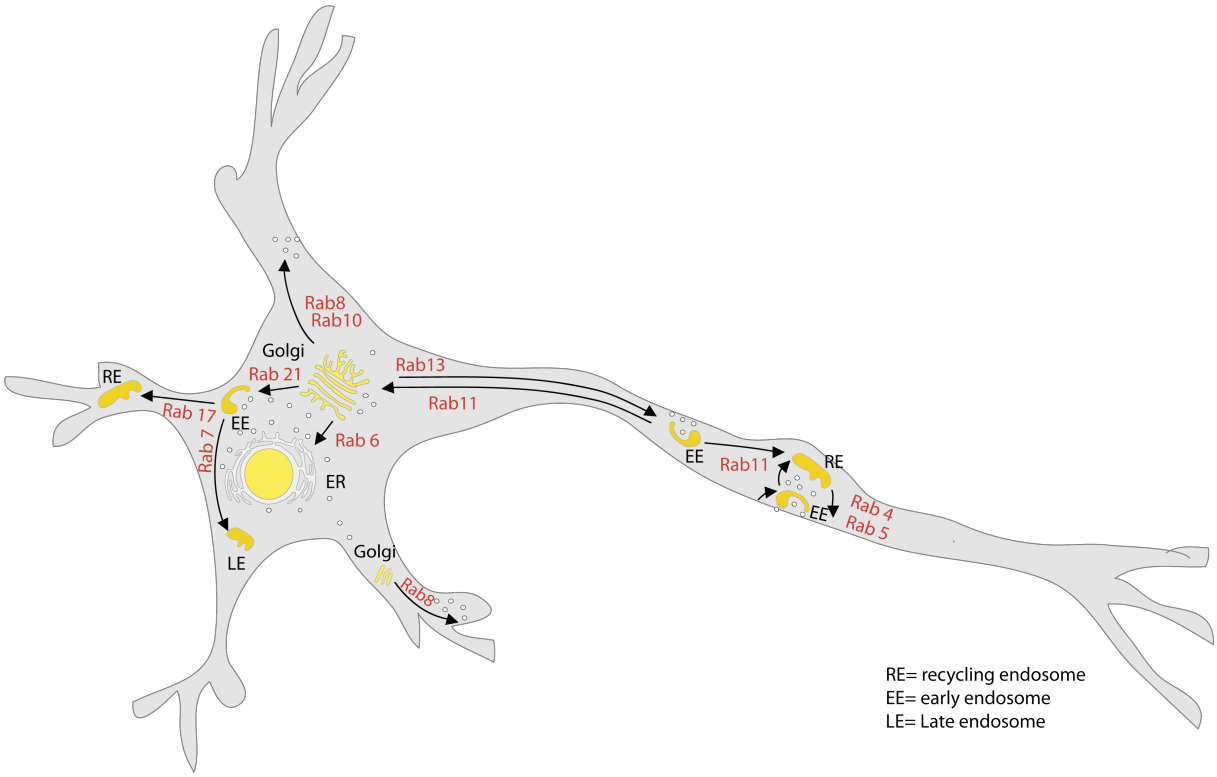

Figure 2.1: **Vesicular transport throughout the neuron is regulated by Rab proteins.** Schematic representation of the various transport routes and associated Rab proteins. In the soma of the cell the endoplasmic reticulum (ER) sends proteins to the Golgi apparatus from there cargo vesicles are distributed to the endosomal compartments the early endosome (EE), the late endosome (LE) and the recycling endosome (RE) or directly to the plasma membrane. At the plasma membrane proteins can be endocytosed and transported to the early endosome from where they are sorted either to the late endosome for degradation or to the recycling endosome for eventual reinsertion.

Among the Rab GTPases present at the trans-Golgi network, Rab6 might play a role in neurite outgrowth by regulating intra-Golgi traffic and trafficking from the Golgi to the plasma membrane [Martinez et al., 1994, Grigoriev et al., 2007]. Both, knock-down of Rab6 in hippocampal cultures and overexpression of the Rab6 negative regulator Bicaudal-D related protein 1 (BICDR-1) reduces total neurite length. BICDR-1 inhibits the trafficking of Rab6 positive vesicles to the cell periphery, supporting the idea that Rab6 mediated exocytic traffic towards the plasma membrane is involved in the membrane addition during neuronal growth [Schlager et al., 2010].

Rab8 another important regulator of the trans-Golgi network is recruited to exocytic vesicles by Rab6 [Grigoriev et al., 2011]. Additionally, Rab8 localizes to the recycling endosome, suggesting that Rab8 might be involved in several aspects of membrane trafficking important for neurite formation. Indeed, antisense suppression of Rab8 in neuronal cultures prevented initial neurite outgrowth and concentrated vesicles of the trans-Golgi-network, originally destined to the axon in the cell body. These data suggest, that Rab8 might function in neurite outgrowth by supporting exocytic traffic from the trans-Golgi network. Overexpression of Rab8 in fibroblasts, leads to the formation of neurite like protrusions and relocalization of actin filaments towards these protrusions. This effect is probably dependent on the recycling activity of Rab8 as it involves the movement of vesicular structures from the plasma membrane to the cell center and back to

the leading edge [Huber et al., 1995, Hattula et al., 2006].

Besides the Golgi apparatus, the endosome acts as an important regulatory unit of membrane traffic. In contrast to the Golgi, which sends out newly synthesized proteins to the plasma membrane, the endosome receives vesicles form the cell surface membrane and recycles them or routes them to degradation. This enables the endosome to control the density of receptors and other signaling molecules at the plasma membrane during establishment of the different functional compartments of a neuron but also in response to growth promoting signals or changes due to neuronal activity. Rab5 is a key regulator of the early endocytic pathway; it controls vesicle transport from the plasma membrane to the early endosomes as well as vesicle fusion within the early endosome [Zerial & McBride, 2001]. Studies of Rab5-GFP localization and movement in *Drosophila melanogaster* dendritic arborization (da) neurons showed, that Rab5 positive endocytic vesicles are transported out into dendrites. Further inhibition of Rab5 positive vesicle transport out into dendrites in dynein mutant Drosophila da-neurons leads to drastically reduced dendritic arbor complexity. In addition the knock-down of Rab5 simplified dendritic branching. Indicating, that Rab5 controlled endocytic traffic in dendrites might be important to induce dendritic branching [Satoh et al., 2008]. In hippocampal neurons knock-down of Rab5 or its upstream regulator Rabex-5 impairs not only dendritic but also axonal growth [Mori et al., 2013].

The recycling endosome serves as an important source of membrane during neurite extension. Additionally it regulates the availability and surface distribution of endocytosed plasma membrane receptors and thereby also the associated signaling pathways. This makes the recycling endosome to an ideal regulator of locally induced neurite branching and elongation [Platta & Stenmark, 2011, Yap & Winckler, 2012]. Rab11 is a well-known regulator of the recycling endosome, suggested to control the traffic of endocytic vesicles from the plasma membrane to the recycling endosome and from the recycling compartment back to the plasma membrane [Ullrich et al., 1996, Sönnichsen et al., 2000, Takahashi et al., 2012]. During neuronal growth Rab11 seems to be involved in axon and dendrite elongation and dendritic branching [Brown et al., 2007, Park et al., 2004, Kawauchi et al., 2010]. Overexpression of Rab11 in cortical neuronal cultures promotes axon growth and increases axon length. Consistently, knock-down of Rab11 or expression of a dominant negative version lead to the opposing effect and decrease the axonal length [Takano et al., 2012]. Further blocking the transport of Rab11 positive vesicles out into dendrites impairs dendritic elongation and branching [Takano et al., 2014a].

In summary, transport of newly synthesized membrane and its correct delivery to sites of neuronal outgrowth is primarily essential for the vast increase in neuronal surface area during neuronal growth. Control of the protein and lipid composition of the newly inserted membrane parts allows the neuron to create specialized neuronal subcompartments with divergent biochemical composition and function.

2.1.2.2 Site specific fusion: The Exocyst complex

In addition to mechanisms, which control the traffic of vesicles between the different organelles of membranous transport and the composition of cargo vesicles, it is important that the transported

vesicles are targeted to sites where new membrane and proteins are needed. The tethering of transport vesicles to their desired destination is mediated in many cases by the Exocyst complex. The Exocyst complex is an octameric protein complex of Rab effectors thought to mediate the initial interaction between transport vesicles and the acceptor membrane and therefore tether vesicles to their correct fusion sites. The Exocyst complex is highly conserved from yeast to mammals and made up of the eight tightly associated proteins Sec3, Sec5, Sec6, Sec8, Sec10, Sec15, Exo70, and Exo84 [Hsu et al., 1996, Hsu et al., 1999, TerBush et al., 1996]. In budding yeast all Exocyst components localize to the growing end of a daughter cell, but their targeting to the desired site of membrane insertion differs. Sec3 localization to the bud tip is independent from actin cables, along which vesicles are transported. Similarly Exo70 seems to only partially depend on actin cables. In contrast all other Exocyst components are associated with exocytic vesicles and their delivery to the site of membrane insertion is dependent on actin cables. This indicates, that Sec3 and Exo70 are associated with the plasma membrane and interact with the other Exocyst component on the arriving vesicles (Fig 2.2). Thus the assembly of the Exocyst complex could tether arriving transport vesicles to correct fusion sites at the plasma membrane [Boyd et al., 2004, Zhang et al., 2005].

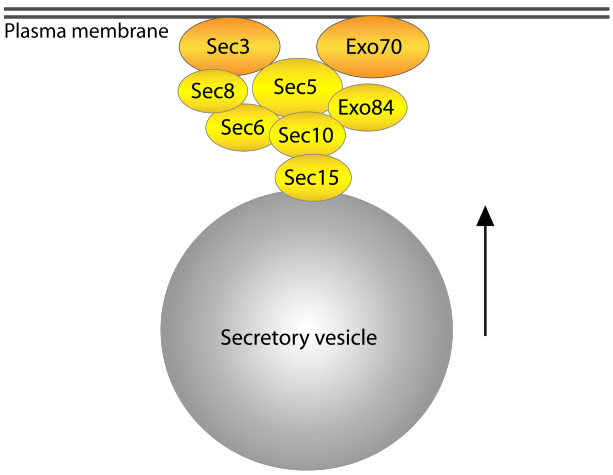

Figure 2.2: Exocyst complex assembly at the plasma membrane. Exo70 and Sec3 are directly associated with the plasma membrane whereas the other exocyst subunits are localized on arriving secretory vesicles. Exo70 and Sec3 interact with the other exocyst subunits and target thereby the secretory vesicles to the correct fusion site (modified from He et al., 2007).

Data from primary hippocampal neurons suggest, that the localization of the Exocyst complex to sites of membrane extension also holds true for neurons [Hazuka et al., 1999]. Furthermore the expression of dominant negative Sec8 or Sec10 impairs neurite outgrowth in PC12 cells and Sec5 Drosophila mutants show impairments in neurite extension [Vega & Hsu, 2001, Murthy et al., 2003]. These studies gave first evidence that Exocyst components are involved in directing membrane addition during neuronal growth. Exo70 was shown to be involved in the regulation of neuronal growth during neurite outgrowth in PC12 cells and axonal growth and polarization of hippocampal cultures in cooperation with the small GTPase TC10 [Pommereit & Wouters, 2007, Dupraz et al., 2009]. TC10 localizes to transport vesicles positive for Rab11, which plays a central role in regulating recycling pathways at the sites of neuronal growth. Therefore TC10's

interaction with Exo70 and Rab11 can connect specialized transport routes to site specific vesicle tethering. This emphasizes the importance of both protein families the Rabs as transport cargo labels to direct vesicles to correct pathways and areas where their cargo might be needed and the Exocyst family as recruiters at the sites where fusion should take place [Fujita et al., 2013].

2.1.3 Synaptic proteins in neuronal growth and development

Synapses are highly specialized subcompartments of axons and dendrites. They are intercellular junctions constituting the main site of communication between neurons and their target cells, where information is send from the presynaptic neuron to the postsynaptic cell. Synaptogenesis like neurite outgrowth relies on cytoskeletal remodeling as well as on the transport and site specific delivery of its protein and membrane complement. Cell adhesion molecules at both sites of the synapse link the two cells to each other and initiate the first contact. Later, specific pre- and postsynaptic proteins regulate the establishment of specialized protein networks at both sides of the newly forming synapse. Before a new synapse can be formed, neurons need to grow out axons and dendrites to reach their future synaptic partner cell. Interestingly, several proteins playing an important role in synapse formation have been shown to be also involved in general axonal or dendritic growth early in neuronal development.

One important presynaptic cell adhesion molecule, with a suggested dual role in dendritic development, is neurexin. Together with its postsynaptic interaction partner neuroligin, neurexin is involved in mediating the initial contact between the pre- and the postsynaptic cell and also the subsequent formation of pre- and postsynaptic compartments [Scheiffele et al., 2000, Graf et al., 2006]. In primary cultures of dissociated neurons, neurexin and neuroligin are expressed already before synapse formation, indicating that they might be involved in neuronal development. Further overexpression experiments of neuroligin in primary hippocampal neurons showed, that neuroligin can induce neurite outgrowth and elongation through its interaction with neurexin [**?**].

Another Synaptic protein with a suggested role in neuronal development is Liprin-α. Liprin-α is a key regulator in the assembly of the pre- and postsynaptic protein network. It's presynaptic function was suggested by the observation that mutants in the *C.elegans* Liprin-α homolog SYD-2 show an abnormal diffuse distribution of presynaptic markers, widening of presynaptic neurotransmitter release sites and impaired synaptic transmission [Zhen & Jin, 1999]. A function for liprin-α in dendritic growth and development was suggested by several studies. In cooperation with the leukocyte common antigen-related (LAR) family of receptor protein tyrosine phosphatases (LAR-RPTPs) Liprin-α targets the cell adhesion molecule β-catenin to dendrites promoting dendritic spine development and maintenance [Dunah et al., 2005]. Furthermore, it was shown that knock-down of LAR and disruption of the LAR-Liprin-α interaction leads to a strong simplification of the dendritic arbor in cultured hippocampal neurons [Hoogenraad et al., 2007]. The Liprin-α interaction partner GRIP1 has been proposed to regulate the targeting of newly synthesized synaptic proteins, like AMPA receptors and the EphB2 receptors from the Golgi apparatus to developing dendrites and thereby support dendritic growth. Concomitantly, knock-down of GRIP1 in hippocampal cultures leads to a reduction in the length of primary

dendrites. This indicates, that GRIP1 and Liprin-α could be involved in the regulation of dendritic growth by targeting proteins which locally induce dendrite formation and growth to the correct transport complexes [Wyszynski et al., 2002, Hoogenraad et al., 2005].

In summary synaptic proteins are not only important for synaptic signaling, but might also be involved in the regulation of neuronal growth by preassembling cargo complexes of synaptic proteins in the cell body and directing them to the correct transport routes. Additionally, synaptic proteins might be important to locally induce and promote growth and regulate thereby the fine-tuning of neuronal networks.

2.1.4 Transcriptional regulation of neuronal growth

Cellular processes like growth and development depend on the regulated expression of specific subsets of proteins, which initiate growth promoting signaling cascades and cellular processes necessary for neuronal growth. Protein expression patterns are mainly governed by the transcriptional regulation of gene expression making transcriptional programs a driving force of neuronal growth. Transcription factors can govern entire cell intrinsic developmental programs, direct distinct stages of neuronal development and alter the neurons ability to respond to extrinsic growth promoting signals. Already the expression of one set of transcription factors can determine the specific morphology and projection patterns of a single neuron [Arlotta et al., 2005, Molyneaux et al., 2007, Polleux et al., 2007]. Accordingly, the FOXO transcription factors have been discovered to regulate polarization during the early steps of neuronal development. FOXO transcription factors regulate the expression of a whole set of polarity associated genes involved in cytoskeleton remodeling and protein transport. Knock-down of FOXO by RNA interference in granule cell cultures leads to non-polarized neurons, unable to establish the morphological distinct axonal and dendritic branches [de la Torre-Ubieta et al., 2010].

Transcriptional factors regulating axonal growth of granule cell neurons are the transcription factors SnoN and Id2. Both transcription factors are targets of the CdH1-APC E3 ubiquitin ligase, which targets them to degradation and thereby restricts axonal growth [Stegmüller et al., 2006, Lasorella et al., 2006]. SnoN drives axon growth by triggering the expression of regulators of the actin cytoskeleton [Ikeuchi et al., 2009]. Id2 on the other hand is thought to promote axon growth by antagonizing the function of transcription factors, which are involved in axon repulsion [Lasorella et al., 2006].

Several transcription factors have been implicated in dendritic growth [de la Torre-Ubieta & Bonni, 2011]. For example the transcription factor NeuroD was shown to stimulate dendritic growth and arborization. Knock-down of NeuroD in granule cell cultures reduced dendritic length, but had no effect on axonal growth [Gaudilliere et al., 2004]. Furthermore, NeuroD deficient mice exhibit granule cells with shorter dendrites and impaired cerebellar and hippocampal brain development [Miyata et al., 1999]. One important feature of the transcriptional regulation of dendritic growth is its modulation by Ca^{2+}-signaling and consequently by neuronal activity. NeuroD has been shown to be phosphorylated by the activity-regulated kinase CamKII. Strikingly, phosphorylation of NeuroD triggers NeuroD dependent transcription and dendritic growth [Gaudilliere et al., 2004].

Taken together, different transcriptional programs regulate dendritic and axonal growth in their distinct developmental stages of initial branch initiation, branch elongation and pruning and pre- and postsynaptic development. Additionally, specific sets of transcriptional factors seem to be responsible for the establishment of the great variety of different neuronal populations in the brain. But to date the full set of downstream effectors, which mediate the differential growth promoting mechanisms have remained elusive.

2.2 The Synapse a highly specialized neuronal subcompartment

Neurons in the brain communicate with each other at synapses, intercellular contacts which are able to convey information with high spatial precision and speed from one cell to the other. Synapses are formed when axons reach their target cells and form stable contacts with them. The axon terminal, the so-called presynapse can send information to the opposing postsynaptic cell by releasing neurotransmitters into the synaptic cleft between both synaptic partners. The released neurotransmitter docks to receptors of the postsynapse and conveys thereby the signal send from the presynapse to the postsynapse. Fundamental for a functional synapse is therefore the close apposition of highly specialized plasma membrane regions of the two participating cells.

In the presynaptic terminal the release of neurotransmitters takes place at a highly specialized section of the of the plasma membrane the so called active zone. The active zone lies at the at the presynaptic plasma membrane facing the synaptic cleft and is composed of an electron dense protein network of scaffolding proteins, fusion proteins, ion channels, and cell adhesion molecules (Fig 2.3).

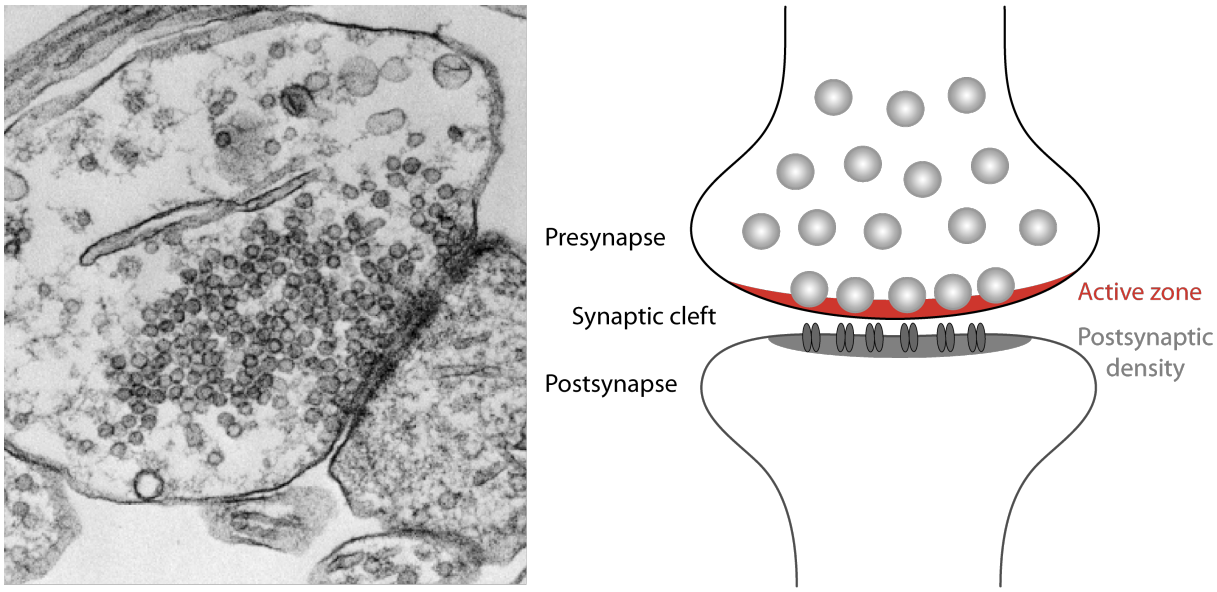

Figure 2.3: **Electron micrograph and schematic representation of the synapse.** The electron micrograph shows a hippocampal synapse. In the presynaptic terminal synaptic vesicles cluster at the active zone opposed to the postsynaptic density of the postsynaptic partner neuron. The postsynaptic density is characterized by the concentration of darker appearing electron dense material. In between the two synaptic partners cells lies the synaptic cleft.

This orchestra of proteins mediates the release of synaptic vesicles and their concomitant recycling in the molecular defined steps of the synaptic vesicle cycle. First synaptic vesicles are filled up with neurotransmitters in the center of the presynaptic terminal. From there they are transported to the active zone, the neurotransmitter release site at the presynaptic plasma membrane. After docking to the active zone synaptic vesicles are prepared for synaptic vesicle release in a multi-step maturation process called priming. When an action potential arrives at the presynaptic terminal calcium enters the presynapse through voltage gated Ca^{2+}-channels and induces the exocytosis of primed synaptic vesicles. After fusion with the plasma membrane

synaptic vesicles are rapidly reuptaken and recycled. The reuptaken empty vesicles are either immediately refilled to directly reinitiate the synaptic vesicle cycle or transported to the endosomal compartment for further sorting before they reenter the synaptic vesicle cycle [Sudhof, 2004] (Fig 2.4). A synaptic vesicle needs approximately only 60 seconds to go through the whole synaptic vesicle cycle. Fusion of the synaptic vesicle and the presynaptic plasma membrane takes even less than one millisecond, making the release of neurotransmitter to one of the fastest and spatially and temporarily, best controlled processes of membrane fusion [Betz & Bewick, 1992, Sabatini & Regehr, 1999].

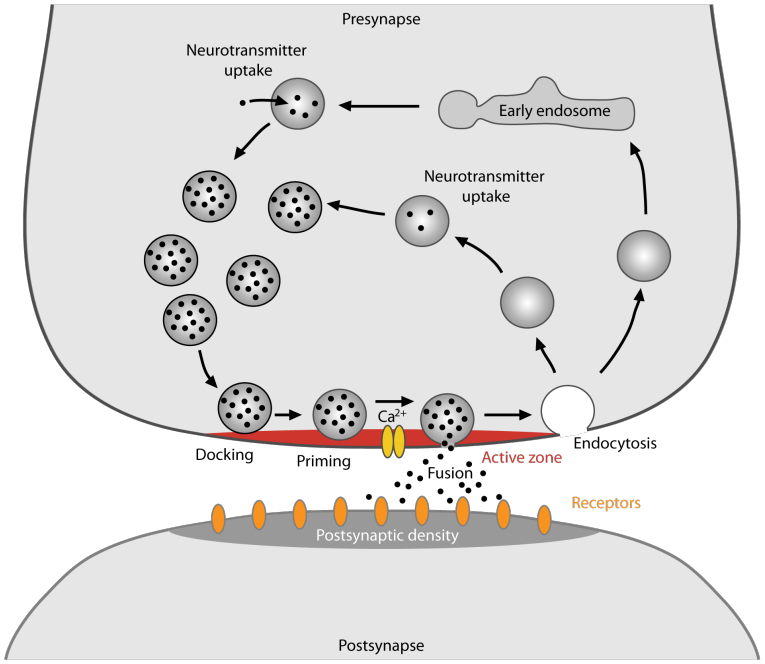

Figure 2.4: **The synaptic vesicle cycle.** Synaptic vesicles are filled with neurotransmitter, targeted to the active zone (Docking) where they are brought in a fusion competent state (Priming). Upon arrival of an action potential Ca^{2+} enters the cell through voltage gated Ca^{2+}-channels triggering the fusion of readily releasable vesicles with the presynaptic plasma membrane. The released neurotransmitters diffuses through the synaptic cleft and binds to receptors of the postsynaptic density. After fusion synaptic vesicles are either directly refilled or recycled via the early endosome.

2.3 RIM protein family

Rab3-interacting molecules (RIM proteins) are core members of the active zone protein network. RIM1α the first discovered member of the RIM protein family was identified as a putative effector of the synaptic vesicle protein Rab3 [Wang et al., 1997]. Later genetic analyses revealed that the RIM protein family consists of seven members (RIM1α, 1β, 2α, 2β, 2γ, 3γ, 4γ), which are encoded by the four different genes, RIM1-4 [Wang et al., 2000, Wang & Südhof, 2003, Kaeser et al., 2008]. The RIM1 gene encompasses two internal promoters, which lead to the expression of the two RIM1 isoforms RIM1α and RIM1β. Similarly, in the RIM2 gene three internal promoters are regulating the expression of RIM2α, RIM2β and RIM2γ. Both RIM1 and RIM2 genes are extensively alternatively spliced resulting in over 200 different variants. In strong contrast the RIM3 and RIM4 genes are not spliced and encode for only one single RIM isoform,

namely RIM3γ or RIM4γ [Wang & Südhof, 2003]. The different RIM isoforms differ in size and composition of protein domains. α-RIMs, the largest RIM isoform, are composed of the full set of RIM domains, an N-terminal zinc-finger domain, a central PDZ domain, and tow C-terminal C_2-domains (C_2A and C_2B), which are separated by an SH_3-domain binding motif. β-RIMs are identical to α-RIMs except for their N-terminal sequence, in which RIM1β lacks the Rab3-binding sequence and RIM2β lacks both the Rab-3 and the Munc-13-binding sequence. γ-RIMs are much smaller and consist of only the C-terminal C_2B domain and an isoform specific N-terminal sequence (Fig 2.5).

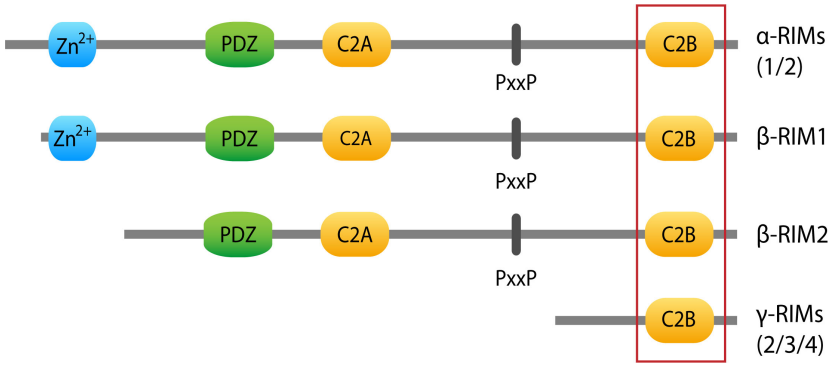

Figure 2.5: **Protein domain composition of the RIM family.** RIM1α and RIM2α compromise the full set of RIM protein domains: An N-terminal Zn^{2+}-finger domain a PDZ domain, the C_2A-domain a proline rich sequence and the C_2B domain. RIM1β lacks only all small N-terminal part whereas in RIM2β also the Zn^{2+}-finger domain is absent. In strong contrast to theses large RIM proteins the γ-RIMs are composed of only the C_2B domain and a isoform N-terminal sequence.

2.3.1 Synaptic functions of RIM1 and RIM2

The large members of the RIM protein family (Rim1α, 1β, 2α, 2β) are central organizers of the protein network at the active zone, the presynaptic neurotransmitter release site. At the active zone the large RIM proteins form a scaffold by interacting directly or indirectly with all other known active zone proteins. These multiple interactions enable RIM proteins to participate in several aspects of the presynaptic neurotransmitter release [Mittelstaedt et al., 2010]. Briefly, RIM proteins have been suggested to play a role in docking and priming of synaptic vesicles and in the recruitment of Ca^{2+}-channels to the active zone [Schoch et al., 2002, Deng et al., 2011, Han et al., 2011, Kaeser, 2011] (Fig 2.6).

A function in the docking of synaptic vesicles was suggested by the finding that synapses of RIM1/2 double knock-out mice display a reduction in the fraction of docked vesicles. Docked vesicles are synaptic vesicle that are attached to the active zone and thereby brought in close proximity to voltage-gated Ca^{2+}-channels and the presynaptic release machinery. In electron micrographs of synaptic contacts docked vesicles can be visualized as fraction of vesicles, which are attached to the electron dense meshwork of the active zone but not yet fused with the presynaptic plasma membrane. Further it was shown that RIMs interact with both Rab3, a protein present on synaptic vesicles and Ca^{2+}-channels of the active zone. This suggests, that the tripartite interaction between RIM proteins, Rab3 and Ca^{2+}-channels might bring synaptic vesicles in close proximity of voltage-gated Ca^{2+}-channels and thereby dock synaptic vesicles

to the active zone [Gracheva et al., 2008, Han et al., 2011]. After docking to the plasma membrane synaptic vesicles are brought into a fusion competent state by assembling the vesicle fusion machinery and its regulatory proteins to them. Primed synaptic vesicles compromise the readily releasable pool and determine therefore the release probability of a synapse. Cultured neurons of RIM1/2 double knock-out mice show a reduction in the synaptic release probability suggesting, that RIM proteins also function in priming of synaptic vesicles. It was proposed that this function is mediated by interaction of RIM proteins with the active zone protein Munc13. Munc13 itself brings synaptic vesicles in a fusion competent state by changing the conformation of syntaxin, a member of the vesicle fusion machinery, to allow for the assembly of the fusion machinery. Munc 13's function is inhibited, when unbound Munc13 self assembles to Munc13 homodimers. Binding of RIM1 to Munc13 disrupts these homodimers, leading to the activation of Munc13 [Richmond et al., 2001, Gerber et al., 2008, Ma et al., 2011, Deng et al., 2011].

A further important mechanism in the regulation of fast synchronous neurotransmitters release is the recruitment of voltage-gated Ca^{2+}-channels to the active zone and the alignment of Ca^{2+}-channels with the synaptic vesicle release machinery [Llinás et al., 1992, Meinrenken et al., 2002]. Presynaptic release relies predominately on N- and P/Q-type Ca^{2+}-channels, which are enriched at the active zone [Takahashi & Momiyama, 1993, Regehr & Mintz, 1994, Castillo et al., 1994, Qian & Noebels, 2001]. RIM proteins bind via their PDZ domain directly to N- and P/Q-type Ca^{2+}-channels and with their proline rich sequence between the two C_2 domains to RIM-binding proteins. They in turn bind to L-, N- and P/Q-type Ca^{2+}-channels. Synapses of RIM1/2 double knock-out mice show reduced levels of P/Q-type Ca^{2+}-channels and a desynchronization of neurotransmitter release in addition to the reduction in release probability described above. Both, the reduction in Ca^{2+}-channel levels and the desynchronization of neurotransmitter release at RIM1/2 deficient synapses can be restored by expressing only the two RIM domains that are responsible for the direct and indirect interaction between RIM proteins and Ca^{2+}-channels [Kaeser et al., 2011]. Thus, RIM proteins might tether Ca^{2+}-channels to the active zone through two parallel mechanisms: a direct interaction with N- and P/Q-type Ca^{2+}-channels and an indirect interaction with L-, N- and P/Q-type Ca^{2+}-channels via RIM-binding proteins and thereby modulate efficiency speed and synchrony of neurotransmitter release.

RIM proteins were also shown to modulate Ca^{2+}-channel openings times *in vitro.* However, if this mechanism plays a role in their function during neurotransmitter release is still a matter of debate. Several lines of evidence show that RIM proteins bind via their C_2B domain, which is shared among all RIM isforms to the β4-subunit of voltage-gated Ca^{2+}-channels and are able to shift their inactivation curve to higher voltages [Uriu et al., 2010, Kaeser et al., 2012]. But it could not be shown that the loss of this activity contributes to the impairment in Ca^{2+}influx and neurotransmitter release caused by the double knock-out of RIM1 and RIM2 *in vivo* [Uriu et al., 2010, Kiyonaka et al., 2007, Kaeser et al., 2012].

Accordingly to this multiple functions in the regulation of neurotransmitter release, RIM1α was shown to be a key player of presynaptic short- and longterm plasticity [Südhof, 2012]. Analysis of RIM1a knock-out mice revealed an impairment in presynaptic short term plasticity at excitatory Schaffer collateral synapses in the hippocampus and at cortico-LA (lateral nucleus of the

amygdala) synapses in the amygdala [Schoch et al., 2002, Fourcaudot & Gambino, 2008]. Furthermore RIM proteins have been shown to be involved in PKA dependent long-term presynaptic plasticity in the hippocampus at mossy fibers and Schaffer collateral synapses, in the cerebellum at parallel fibers to Purkinje cell synapses and in the amygdala at cortico-LA synapses [Castillo et al., 2002, Huang & Zakharenko, 2005, Lonart et al., 2003, Fourcaudot & Gambino, 2008]. However the detailed molecular mechanism how RIM proteins are involved in the different forms of presynaptic short- and long-term plasticity have remained elusive so far.

In summary, the multiple interactions of the large RIM proteins within the active zone protein network make them to powerful regulators of presynaptic neurotransmitter release. RIM proteins regulate the number of attached vesicles to the active zone and also in their ability to fuse with the presynaptic plasma membrane through different mechanisms. However, which molecular mechanism are rate limiting and how these molecular processes influence each other remains to be resolved.

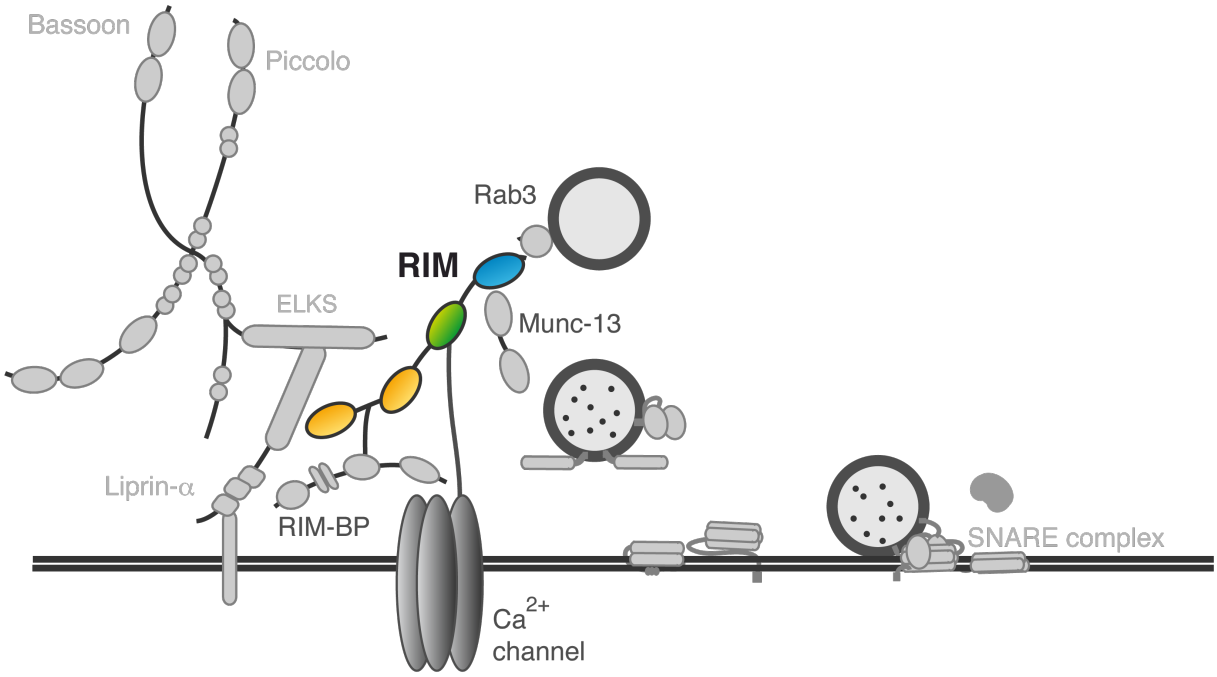

Figure 2.6: **RIM1 at the presynaptic active zone.** RIM1 is a central component of the protein network at the active zone involved in multiple steps of neurotransmitter release. Via its interaction with Rab3, RIM1 brings synaptic vesicles in close proximity of voltage-gated Ca^{2+}-channels. Through its interaction with Munc13 RIM1 participates in the priming of synaptic vesicles. The direct interaction with voltage-gated Ca^{2+}-channels and via the interaction with RIM-binding proteins (RIM-BP), allows RIM1 to tether Ca^{2+}-channel to the active zone and to regulate thereby the efficiency speed and synchrony of neurotransmitter release.

2.3.2 Function of the small RIM proteins: RIM3γ and RIM4γ

In contrast to the large members of the RIM protein family much less is known about the functional role of RIM3γ and RIM4γ. γ-RIMs are much smaller than the large α- and β-RIM proteins, as they miss most of the protein interaction domains present in the large RIM proteins and consist of only the RIM specific C_2B domain and an isoform specific N-terminal sequence. First experiments on the expression pattern of RIM3γ and RIM4γ revealed, that they are brain

specific proteins, expressed with overlapping patterns throughout the rodent brain. From birth on the expression levels of RIM3γ and RIM4γ increase during development and reach a plateau around postnatal day 20, similar to the large RIM proteins [Kaeser et al., 2008]. In Contrast to the specific synaptic localization of α- and β-RIMs, RIM3γ and RIM4γ show a broader subcellular localization. RIM3γ seems to be expressed in dendrites and axons, where it colocalizes with pre- and postsynaptic markers. In the neuronal cell body RIM3γ shows a strong enrichment to the nucleus. RIM4γ is absent from the nucleus and shows a diffuse distribution along axons and dendrites.

In search of a potential presynaptic function RIM3γ and RIM4γ were suggested to modulate presynaptic Ca^{2+} influx through direct binding to voltage-gated Ca^{2+}-channel and either modulating Ca^{2+}-channel opening times or recruit Ca^{2+}-channels to the active zone or to interfere with the anchoring of synaptic vesicles to voltage gated Ca^{2+}-channels mediated by α-RIMs. However γ-RIMs seem to be much less effective in binding to voltage-gated Ca^{2+}-channels and also in modulating neurotransmitter release than the large RIM proteins [Uriu et al., 2010, Kaeser et al., 2012]. Surprisingly shRNA mediated knock-down of RIM3γ and RIM4γ *in vitro* and *in vivo* resulted in neuronal growth defects and lead to a drastically simplified dendritic tree [Alvaréz-Baron, 2010]. This suggests that apart from a possible synaptic role RIM3γ and RIM4γ might mediate important functions during neuronal growth and development.

2.3.3 RIMs in neuronal pathologies

Neuronal networks in the brain are cascades of synaptic connections which process sensory inputs and transform them into appropriate motor outputs. This makes synapses to fundamental regulators of correct brain function. The dysregulation of neuronal networks due to inappropriate changes in synaptic function might therefore play an important role in the pathogenesis of neurological disorders like schizophrenia, autism spectrum disorders, Parkinson's disease, and epilepsy [Stephan et al., 2009, Pardo & Eberhart, 2007, Scharfman, 2008, Chandrasekaran & Bonchev, 2013]. RIM proteins and their regulatory effect on synaptic neurotransmitter release have been associated with several neurological disorders.

The changes of synaptic function in RIM1 knock-out mice lead to strong impairments in learning and memory and additionally to behaviors, which have been linked to schizophrenia [Powell et al., 2004, Lipska & Weinberger, 2000, Blundell et al., 2010b]. Two other members of the RIM family, RIM2, and RIM3γ were found to be upregulated in the amygdala of schizophrenia patients. The amygdala is a subcortical region that shows structural changes and reduced emotion evoked responses during schizophrenia and is therefore suggested to take part in the dysfunction of emotional processing in schizophrenia [Weidenhofer et al., 2006, Weidenhofer et al., 2009, Aleman & Kahn, 2005]. Further genomic expression profiles revealed, that the RIM3γ gene expression was additionally upregulated in other brain regions like the entorhinal cortex and the prefrontal cortex of schizophrenic patients [Hemby et al., 2002, Hakak et al., 2001]. Thus several members of the RIM family might be involved in the pathological changes occurring during schizophrenia.

A point mutation in the RIM1 gene has been identified in patients of autosomal dominant

cone rod dystrophy. The patients first experience reduced color vision and visual acuity, later patients have problems in seeing bright light. Interestingly, affected individuals show an increase in cognitive abilities [Michaelides et al., 2005, Sisodiya et al., 2007]. This increase in cognitive abilities is associated with a enhanced synaptic function mediated by the mutated version of RIM1. Thus the change in synaptic function might have differential effects depending on which neuronal network is affected [Miki et al., 2007].

Physiological processes like learning and memory, but also pathophysiological processes like epiletopgenesis are accompanied by an increased network activity. In response to an increase in network activity neurons can change their molecular composition and structure in order to adjust their synaptic strength [Milner et al., 1998, Scharfman, 2008]. This synaptic adaptation has been shown to be dependent on changes in gene expression, leading to the synthesis of proteins, which can modulate the composition and function of the synaptic protein network [Goelet et al., 1986, Flavell & Greenberg, 2008]. Recently, the gene expression of RIM4γ has been shown to be upregulated in the hippocampus of mice after the induction of epileptic seizures, which goes along with strong synchronous neuronal activity [Hermey et al., 2013]. Additionally, RIM1 knock-out mice have been shown to be more sensitive to strong synchronous neuronal activity, as they show an increase in spontaneous seizures after induced epileptogenesis [Pitsch et al., 2012].

Taken together all members of the RIM family could be associated to physiological and pathological changes in brain function but seem to contribute to different symptoms. Their divergent contributions could be explained on the one hand by varying expression patterns in the different brain region or in the different subcellular compartments of neurons on the other hand also by isoform specific functions.

3 Aims of the study

The RIM protein family compromises large multidomain proteins (RIM1α/β, RIM2 α/β) besides three small γ-RIMs (RIM2γ, RIM3γ, RIM4γ) that are composed of only one single RIM specific domain and a short isoform specific N-terminus. In the recent years, RIM1 and RIM2 have emerged as important regulators of synaptic transmission and plasticity. At the presynaptic active zone the large RIM proteins are integrated in a network of protein interactions allowing them to participate in the docking and priming of synaptic vesicles and the recruitment of Ca^{2+} channels. The small members of the RIM protein family, RIM3γ and RIM4γ have been suggested as important regulators of neuronal outgrowth in first shRNA mediated knock-down experiments. However, the precise function of RIM3γ and RIM4γ is still not defined, therefore we set out to address the following goals in this study.

The first aim is to characterize the full consequences of the loss of RIM3γ and RIM4γ on the development of axons and dendrites and the formation of their synaptic specializations. This will also involve analysis of vesicular transport in RIM3γ and RIM4γ knock-down neurons, to unravel if γ–RIMs promote neuronal growth trough an involvement in vesicular trafficking routes.

Secondly, we want to identify novel γ–RIM interaction partners, especially interactions that are involved in their growth promoting function, in order to elucidate the molecular mechanism underlying the role of RIM3γ and RIM4γ in the elongation of axons and dendrites. In addition to growth promoting proteins we aim to find potential synaptic γ-RIM interaction partners to gain insight into a potential synaptic function of RIM3γ and RIM4γ in accordance to the role of RIM1 and RIM2 in presynaptic vesicle exocytosis.

The third goal is to analyze which functional domains of γ-RIMs are involved in their subcellular localization. Strikingly RIM3γ shows a strong nuclear enrichment in addition to its pre- and postsynaptic localization, suggesting a function of RIM3γ in synapse to nucleus signaling.

The fourth goal is to generate constitutive RIM3γ and RIM4γ knock-out mice allowing to analyze the consequence of the ablation of the both proteins from development on and perform a first characterization of the resulting phenotypes.

Taken together this study will provide novel insights into the functional role of RIM3γ and RIM4γ in the development and function of neuronal structures in the brain.

4 Material & Methods

4.1 Material

4.1.1 Equipment

Equipment	Model	Company
Acrylamid electrophoresis system	Mini-PROTEAN 3 Electrophoresis System	BioRad
Agarose electrophoresis system	SUB-CELL GT	BioRad
Analytical balance	BP210S	Sartorius
Autoclave	HSP Laboklav	Steril Technik AG
Balance	SBC53	SCALTEC
Cat walk	Cat walk XT system	Noldus
Capillary Sequencer	3130/xl/ Genetic Analyzer	Applied Biosystems
Cell culture hood	MSC-Advantage	Thermo Scientific
Centrifuge	Function line	Heraeus
Centrifuge	5415C	Eppendorf
Centrifuge	Mikro 22R	Hettich
Centrifuge	Mikro 200R	Hettich
Centrifuge	Rotina 220R	Hettich
Cryostat	HM 560	MICROM
Confocal laser scanning microscope	Eclipse Ti	Nikon
Controller	Micro4 Controller, 4-Channel	World Precision Instruments
CO_2-controller (life cell imaging)	CO_2-controller	Pecon
Cryostat	HM 560	MICROM
Gel documentation system	AlphaImager	Alpha Innotech
Incubator (cells/cell culture)	HERAcell 150 / 150i	Thermo Scientific
Incubator (media/cell culture)	Modell 100	Memmert
Incubator small	Inkubator 1000, Unimay 1010	Heidolph
Incubator small Incubating	Mini shaker	VWR
Infrared imaging system	Odyssey	Li-cor
Inverse microscope	Axio Observer 1A	Zeiss
Inverse microscope	Axiovert 40 CF	Zeiss
Microtome	Microm HM 335 E	Microm
PCR-Cycler	UNOII	Biometra

PCR-Cycler	T3	Biometra
PCR-Cycler	T3000	Biometra
pH-meter	pHMeter 766	Calimatic Knick
Photometer	BIO	eppendorf
Power Supplies Agarose	PHERO-stab.500	BIOTEC-FISCHER
Power Supplies Agarose	Power Pack 25	Biometra
Precision Syringe	Nanofil Hamilton 10µl	World Precision Instruments
Real time PCR (Taqman)	9700HT	ABI Prism
Rotating rod	Rota-Rod ENV-575MA	Med Associates Inc.
Rotor	Type 70 Ti	Beckman Coulter
Shaker plate	Polymax 1040	Heidolph
Spectrophotometer	ND-1000	NanoDrop
Temperature controller (life cell imaging)	Tempcontrol 37-2	Pecon
Thermo shaker	MKR13	HLC
Thermo shaker	Thermomixer compact	Eppendorf
Ultrasonicator	Processor UP50H	Hielscher
Ultrasonicator	Labosonic 2000	B.Braun
Ultracentrifuge	Optima L-70K	Beckman Coulter
Vibratome Microm	HM 650V	Thermo Scientific
Vortex	Vortex-Genie 2	Scientific Industries
Vortex	Reax control	Heidolph

Table 4.1: Equipment used for this study

4.1.2 Chemicals

Chemical	**Company**
4',6-diamidino-2-phenylindolindole, dihydrocholoride (DAPI)	Life technologies
1,4-Dithiothreitol	Roche
6 x loading buffer	Fermentas
Acetic acid	Roth
Acrylamide	Roth
Agarose	peqLab
Ammoniumpersulfate (APS)	Roth
Ampicillin	Roth
Aqua ad injectabilia	Delta Select
Bovine serum albumin (BSA)	Sigma-Aldrich
Bromphenolblue	Roth

Calcium chloride	Sigma-Aldrich
Chloroform	Roth
Complete Mini Protease Inhibitor	Roche
Cryo-preserving medium (Tissue-Tek)	Dako
Dimethylsulfoxide (DMSO)	Roth
Ethylenediaminetetraacetic acid (EDTA)	Calbiochem
Ethanol	Fluka
Ethidiumbromide	Merck
Fetal calf serum (FCS)	Life technologies
Gelatin from cold water fish skin	Sigma-Aldrich
Formamide	Roth
Glucose solution 5 %	Fresenius
Glycerol	Sigma-Aldrich
HEPES	Sigma-Aldrich
HCl 2N	Merck
Iodoacetamide	Sigma-Aldrich
Isofluorane	Sigma-Aldrich
Isopropanol	Fluka
Isopropyl β-D-1-thiogalactopyranoside (IPTG)	Roth
Kanamycin	Sigma-Aldrich
Luria Broth-Agar	LabM/idg
Luria Broth-Medium	LabM/idg
Lipofectamine 2000	Invitrogen
Leptomycin B	Sigma-Aldrich
Magnesium chloride	Merck
Methanol	Merck
Milk powder	Roth
Mowiol 4-88	Roth
Paraformaldehyd	Roth
PBS	Biochrom AG
Penicilin	Sigma-Aldrich
Polyethylenimine	Polyscience
RNAse away	Molecular BioProducts
Saccharose	Sigma
Sodium acetic	Merck
Sodiumchloride	Roth
Sodiumdodecylsulfate (SDS)	Roth
Sodiumhydrogenphosphate	Merck
ß-Marcaptoethanol	Roth
TEMED	Roth

Tris-Base	Sigma
Tris-HCl	Roth
Triton-X-100	Roche
Trypan-Blue	Invitrogen
Xylol	Merck

Table 4.2: Chemicals used for this study

4.1.3 Cell culture media and reagents

Cell culture medium	**Company**
B27	Gibco
Basal Medium Eagle (BME)	Life technologies
Dulbecco's Modified Eagle's Medium (DMEM)	Gibco
Fetal calf serum (FCS)	Life technologies
Glucose	Sigma-Aldrich
Hank's Buffered Salt Solution (HBSS)	Gibco
Iscove's Modified Dulbecco's Medium (IMDM)	Gibco
L-Glutamine	Gibco
Minimum essential medium (MEM)	Sigma-Aldrich
Opti-MEM	Gibco
Papain	Sigma-Aldrich
Penicillin-Streptomycin	Gibco
Phospate saline buffer (PBS)	Gibco
Poly-D-Lysin	Sigma-Aldrich
Sodium bicarbonate	Life technologies
Sodium hypoxanthine, aminopterin, thymidine (HAT)	Life technologies
Trypsin-EDTA	Gibco

Table 4.3: Culture media used for this study

4.1.4 Antibodies

4.1.4.1 Primary Antibodies

Antibody	**Dilutions**	**Company**
β-actin mouse monoclonal (ab6276)	1:500	Abcam
β-Tubulin mouse	1:10000	BD Pharminogen
FLAG M2 mouse monoclonal	1:1000-1:5000	Sigma-Aldrich
GFP rabbit polyclonal (ab290)	1:1000	Abcam

GFP mouse monoclonal	1:1000	Santa Cruz Biotechnology
GM130 mouse	1:500	BD Transduction Laboratories
HA mouse monoclonal	1:1000	Convance
RIM3γ polyclonal	1:100	Pineda AK Service
RIM4γ polyclonal	1:100	Pineda AK Service
Synapsin 1.2 guinea pig polyclonal	1:500	Synaptic Systems
PSD-95 MAGUK scaffold protein mouse monoclonal	1:100	Neuromab

Table 4.4: List of primary antibodies

4.1.4.2 Secondary Antibodies

Antibody	**Dilutions**	**Company**
Cy3-anti mouse IgG	1:200	Jackson immuno reseearch
Cy3-anti rabbit IgG	1:200	Jackson immuno reseearch
Cy5-anti mouse IgG	1:200	Jackson immuno reseearch
Cy5-anti rabbit IgG	1:200	Jackson immuno reseearch
Cy5-guinea pig rabbit IgG	1:200	Jackson immuno reseearch
Fitc-anti mouse IgG	1:200	Jackson immuno reseearch
Fitc-anti rabbit IgG	1:200	Jackson immuno reseearch
IRDye 680-anti mouse IgG	1:20000	LI-COR Odyssey
IRDye 680-anti rabbit IgG	1:20000	LI-COR Odyssey
IRDye 800-anti mouse IgG	1:20000	LI-COR Odyssey
IRDye 800-anti rabbit IgG	1:20000	LI-COR Odyssey

Table 4.5: List of secondary antibodies

4.1.5 Kits

Kit	**Company**
BigDye® Terminator v3.1 Cycle Sequencing Kit	Applied Biosystems
Cell viability imaging kit	Roche
DNA Clean and Concentration kit	Zymo Research
DyeEx 2.0 (Purification of Sequencing)	Qiagen
Dynabeads® mRNA DIRECT™ Micro Kit	Life technologies
EndoFree Plasmid Maxi Kit	Quiagen
GeneJET™ Plasmid Miniprep Kit	Thermo Scientific
High Capacity cDNA Reverse Transcription Kit	Applied Biosystems
PureLink™ HiPure Plasmid Filter Maxiprep Kit	Life technologies

PureLink™ HiPure Plasmid Filter Midiprep Kit	Life technologies
RevertAid First Strand cDNA Synthesis Kit	Thermo Scientific
Trypsin profile IGD Kit	Sigma-Aldrich
Zymoclean DNA Clean&Concentrator kit	Zymo Research
Zymoclean Gel DNA recovery kit	Zymo Research

Table 4.6: Kits used in this study

4.1.6 Other material

Product	**Company**
Nitrocellulose membrane (Protran® 0,45 µm pore size)	Watman, GE Healthcare
Tissue tek	Sakura Finetek
Anti-FLAG M2 Magnetic Beads	Sigma-Aldrich
Glutathione−Agarose	Sigma-Aldrich

Table 4.7: List of diverse material

4.1.7 Oligo nucleotides

4.1.7.1 Cloning Primers

Template	**Direction**	**Primer 5'-sequence-3'**	**Enzyme**	**Vector**
SF-TAP	fw	GCGGAATTCACCATGGATTATAA AGATGATGATGA	EcoRI	pAAV-CMV
SF-TAP	rev	GCGTCTAGATGGTCCTGGTTTCT CGAACTGCGGGTG	XbaI	pAAV-CMV
RIM3γ	fw	GCGTCTAGAATGTTTAACGGGG AGCCTG	XbaI	pAAV-CMV
RIM4γ	rev	GCGGTCGACTTAGGAGCACGAG GGGCT	SaII	pAAV-CMV
RIM4γ	fw	GCGTCTAGAATGGAGCGCTCGC AGAG	XbaI	pAAV-CMV
RIM4γ	rev	GCGGTCGACTTAAGATCGCTCG CCACA	SaII	pAAV-CMV
RIM4γ	fw	GAATTCACCTAATGGAGCGCTC GCAGAG	EcoRI	pgex
RIM4γ	rev	GTCCGACTTAAGATCGCTCGCC ACAG	SaII	pgex

Table 4.8: Primers used for cloning.(fw: forward; rev:reverse)

4.1.7.2 Primers for site directed mutagenesis

Template	Mutation	Direction	Primer 5'-sequence-3'
pAAV-CMV-GFP-RIM3γ	NLS (42KKRR -> AAAA)	fwd	GCGACAGCCGCGGCAGCGGCG
pAAV-CMV-GFP-RIM3γ	NLS (42KK-RR -> AAAA)	rev	GCGCGCCGCTGCCGCGGCTGT
pAAV-CMV-GFP-RIM3γ	NES (64L-L -> A-A)	fwd	GGACGAGGCGGACGCGAGTGC TGTGGTCACTGGC
pAAV-CMV-GFP-RIM3γ	NES (64L-L -> A-A)	rev	GCCAGTGACCACAGCACTCGC GTCCGCCTCGTCC

Table 4.9: Sequencing primers.(fw: forward; rev:reverse)

4.1.7.3 Sequencing Primers

Template	Direction	Primer 5'-sequence-3'
pCMV β-Globin Intron	fw	GAGTCCAAGCTAGGCCCTTT
pAAV-CMV	rev	TTAGGACAAGGCTGGTGGG
pgex	fw	GGGCTGGCAAGCCACGTTTGGTG
pgex	rev	CCGGGAGCTGCATGTGTCAGAGG

Table 4.10: Sequencing primers.(fw: forward; rev:reverse)

4.1.7.4 Genotyping primers

Genotype	Primer 5'-sequence-3'	Product size
RIM3γ wild type	GGACCACACTGCAATGCTAA	324bp
	ACCAGACTCCAAAGCCCTC	
RIM3γ constKO	GGACCACACTGCAATGCTAA	618bp
	CCCTTCAGTCTTCCTGTCCA	
RIM4γ wild type	GCATGATGGGAAGGAATGCCAAGC	324bp
	GTTCAGG-CCAGGGCTTCTCCATGC	
RIM4γ constKO	GCATGATGGGAAGGAATGCCAAGC	632bp
	CCCTTCAGTCTTCCTGTCCA	

Table 4.11: Primers used for genotyping of RIM3 and RIM4 knock-out mice.(fw: forward; rev:reverse; bp: base pairs)

4.1.7.5 Primers for quantitative real time RT-PCR

Gene	Primers	Company
RIM3γ	Gene expression assay: Mm00805396_m1	Life Technologies

RIM4γ	Gene expression assay:Mm00813040_m1	Life Technologies
β-actin	Gene expression assay: Mm00607939_s1	Life Technologies
Synatophysin	Gene expression assay: Mm01289818_g1	Life Technologies

Table 4.12: Primers used for quantitative real time RT-PCR

4.1.8 Enzymes

Enzyme	**Company**
GoTaq® Flexi DNA Polymerase	Promega
DNase I	Roche
Pfu DNA Polymerase	Life technologies
Taq DNA Polymerase	Life technologies
T4 Ligase	Thermo Scientific
Restriction Enzymes	**Company**
EcoRI, SaII, XbaI, MfeI, HindIII, DpnI	Thermo Scientific

Table 4.13: List of Ezymes used in this study

4.1.9 Plasmids

Generated plasmids

Name	**Insert**	**Vector**	**Enzyme**
pAAV-SF-TAP	SF-TAP	pAAV-CMV	EcoRI, XbaI
pAAV-TAP-RIM3γ	RIM3γ	pAAV-SF-TAP	XbaI, SaII
pAAV-TAP-RIM4γ	RIM4γ	pAAV-SF-TAP	XbaI, SaII
pgex-RIM4γ	RIM4γ	pgex	EcoRI, SaII
Constructs modified by site directed mutagenesis			
pAAV-RIM3γ-mutNLS	-	pAAV-RIM3γ-GFP	-
pAAV-RIM3γ-mutNES	-	pAAV-RIM3γ-GFP	-

Table 4.14: Constructs generated during this study

Plasmids generated prior this study

pLVTHM-GFP, pLVTHM-RFP, pLVTHM-GFP-shRIM3γ, pLVTHM-GFP-shRIM4γ, pLVTHM-RFP-shRIM3γ, pLVTHM-RFP-shRIM4γ, pLenti-EGFP-RIM3γ and pLenti-EGFP-RIM4γ. These plasmids are publishes by Alvarez-Baron et al.[Alvarez-Baron et al., 2013].

Plasmids kindly provided by other labs

pEGFP-IQGAP3 Prof. Kozo Kaibuchi (Department of Cell Pharmacology, Nagoya University, Nagoya, Japan).

pEGFP-C2-IQGAP1 Dr. Dominique Brandt (Pharmakologisches Institut, Universität Marburg,

Germany).

Rab8-GFP (pEGFP-CMV), Rab6-GFP (GW), Rab11-GFP (GW) Prof. Casper C. Hoogenraad (Cell Biology, Faculty of Science, Utrecht University, Utrecht, The Netherlands).

pEGFP-N1-plakophilin4 Prof. Ilse Hofmann (Zentrum für Biomedizin und Medizintechnik, Universität Mannheim, Germany).

pCAG-Syd-1-HA Prof. Peter Scheifele (Biozentrum, University Basel, Switzerland).

4.2 Methods

4.2.1 Molecular biological methods

4.2.1.1 Polymerase chain reaction

DNA fragments were amplified by polymerase chain reaction (PCR). The PCR reaction mix contained double stranded DNA of the sequence of interest, single stranded Primers, desoxyribonucleotides (dNTPs) and the required amount of buffers and salt. The reaction was either preformed with Platinum Taq-polymerase or Pfu-polymerase in order to guarantee proof reading. Exact compositions of PCR reactions are listed below:

PCR reaction mix	Volume
10x Polymerase buffer	2µl
Magnesium chloride 25mM	1,2µl
5' primer (10pmol/µl)	0,5µl
3' primer (10pmol/µl)	0,5µl
dNTP-Mix (25mM)	0,5µl
DNA Template	2µl (50ng)
Polymerase	0,3µl
Water ad iniectabilia	ad 20µl

The reaction was performed in a thermocyler. In the initial step double stranded DNA was denaturated for 5 minutes at 95°C. Afterwards 30-35 cycles of a denaturation step for 30 seconds at 95°C, an annealing step for 40 seconds at 50-60°C and an extension step at 68/72°C for 1 minute per kilobase pair was performed. The reaction was completed by a final extension step at 68/72°C for 10 minutes.

4.2.1.2 Vector generation

For cloning DNA fragments were amplified from plasmid DNA via PCR. PCR reactions were separated on an agarose gel and the band of interest was cut out and purified (Zymoclean Gel DNA recovery kit, Zymoresearch). PCR fragments of the correct size were cut with the respective restriction enzymes for 2 hours at 37°C. In the meantime the vector of interest was cut with the corresponding restriction enzyme 1 hour at 37°C, and subsequently dephosphorylated with shrimp alkaline phosphates for 1 hour at 37°C. Following restriction, vector and PCR fragments were purified (DNA Clean and Concentration kit). Vector and PCR fragments were ligated in a molar ratio of 1:3 by T4 DNA ligase at room temperature overnight.

4.2.1.3 DNA precipitation

The volume of DNA was adjusted to 500µl and precipitated for at least 15 minutes at –80°C in the presence of sodium acetate (3,5M, 35µl) and ethanol (100%, 1ml). DNA precipitates were collected by 30 minutes centrifugation. After centrifugation the supernatant solution was

removed and the precipitated DNA pellet was washed with 70% ethanol. The solution of 70% ethanol was centrifuged again to pellet the DNA and the supernatant was removed. The washed DNA pellet was resuspended in 20µl distilled water for further use.

4.2.1.4 Chemical transformation of bacteria with plasmid DNA

50µl of chemically competent 5-alpha *e. coli* were incubated with 20µl of the ligation reaction or 1µl of plasmid DNA for 20 minutes on ice. The transformation reaction was heat shocked for 2 minutes at 42°C and shortly chilled on ice. Afterwards 200µl of LB-media were added to the reaction mix and incubated for one hour at 37°C on a thermo shaker. Subsequently, 5-alpha *e. coli* were plated on agar plates containing 100µg/ml ampicillin for selection of transformated bacteria.

4.2.1.5 Sequencing

Sequencing PCR reactions were performed with the BigDye Terminator v3.1 cycle sequencing kit and template specific primers. Reactions were purified (DNA Clean and Concentrator Kit) and sequencing was carried out using a capillary sequencer. Analysis of sequencing results was accomplished with the use of SeqMan software.

4.2.1.6 Side directed mutagenesis

Primers (Table 4.9) were designed following the instructions of the QuickChange Primer Design Program (https://www.genomics.agilent.com/). Mutations were introduce during amplification of the plasmid carrying the gene with the mutation target site by polymerase chain with the respective primers containing the desired mutation. To find the optimal conditions nine PCR reactions with 50ng,100ng, and 200ng of the plasmid carrying the gene with the mutation target site and varying $MgSO_4$ concentrations were performed with Pfu-polymerase. An initial denaturation step at 95°C was followed by 15 cycles of denaturation, annealing at 55°C for 1 minute and elongation for 2 minutes/kb of the vector at 72°C. The reaction was completed by a final extension step at 68/72°C for 10 minutes. Non mutated methylated parental DNA templates were digested by adding 1µl of the restriction enzyme DpnI to each PCR reaction over night and again 1µl DpnI the next morning for 2 hours at 37°C. After digestion all PCR reaction were pooled and the DNA concentrated by ethanol precipitation. The concentrated DNA was transformed into chemically competent 5-alpha *e. coli*. Bacteria were plated on agar plates containing 100µg/ml ampicillin for selection of transformed bacteria.

4.2.1.7 mRNA isolation and cDNA sythesis

Total mRNA was obtained from microdissected mouse brain tissue using Dynabeads mRNA DIRECT Micro Kit according to the manufacturer's (Life Technologies) instructions. CDNA was synthesized from purified mRNA by reverse transcription using the RevertAidH Minus First

Strand cDNA Synthesis Kit and compromised oligo dT primers according to the manufactures manual. CDNA samples were stored at -20°C.

4.2.1.8 Real time PCR

For quantitative real time PCR the Maxima Probe/Rox qPCR Master Mix (Thermo Fischer) together with Taqmam gene expression assays (Applied Biosystem) was used according to the following protocol.

Realtime PCR mix

Reaction component	Volume
Master mix	3,0µl
cDNA	1,25µl
Taqman gene expression assay	0,3µl
DEPC- water	1,7µl
$\sum$	6,25µl

Realtime PCR thermal profile

Step	Temperature	Time	Cycle
1	95°C	10min	
2	95°C	15sec	
3	59°C	60sec	
4	72°C	40sec	40 cycles step 2-4

Experiments were performed in triplicates on an ABI Prism 9700HT system (PE Applied Biosystems, Foster City, CA, USA). Gene expression was analyzed as relative gene expression in comparison to the internal reference gene synaptophysin. Therefore gene expression was calculated as $2^{-\Delta ct}$(Δ cycle threshold value (ct) = ct of the analyzed gene - ct synaptophysin).

4.2.2 Bioinformatic analysis

Nuclear localization signals in the sequence of RIM3γ were detected with the Nucpred bioinformatical tool (http://www.sbc.su.se/~maccallr/nucpred/cgi-bin/single.cgi). Nuclear export sequences within the protein sequences of RIM3γ and RIM4γ were identified via the bioinformatical tool NetNES1.1 server (http://www.cbs.dtu.dk/services/NetNES/). Phosphorylation sites in the sequences of RIM3γ and RIM4γ were predicted with the programs GPS_3.0_macos_201412 14.dmg for mac (http://gps.biocuckoo.org/ download.php) and http://scansite.mit.edu/.

4.2.3 Lentivirus production and *in vivo* injection

4.2.3.1 Lentiviral vectors

Lentiviral particles were generated by cotransfection of plasmids coding for the virion packaging plasmids Gag and Pol, a transfer vector carrying the gene of interest and an envelop plasmid expressing the heterologous surface glycoprotein of VSV-G (vesicular stomatitis virus) in a producer cell line HEK293FT. For the transfer of RIM3γ-GFP and RIM4γ-GFP the third generation vector plentiN-EGFP and for the transfer of shRIM3-GFP, shRIM4-GFP, shRIM3-RFP and shRIM4-RFP the second generation transfer vector PLVHTM was used. All lentiviral particles were produced with the second generation packing plasmid psPAX2 and the envelop plasmid pMD2.G. The biosafety of human immunodeficiency virus type 1 (HIV-1) based expression systems is improved by deletion of all viral accessory genes except of Tat and Rev in the second generation of lentiviral plasmids.

4.2.3.2 Transfection of HEK293T cells

HEK293FT cells growing on 15cm culture dishes with a confluence of 50-60% were transfected with one of the transfer vectors, psPAX2 and pMD2.G using polyethylenimine (PEI). The transfection mix contained 18,75µg psPAX2, 6,25µg pMD2.G, 25µg transfer vector, 100µg PEI and 500mM NaCl and was directly added to the culture medium. One day after transfection the culture medium was replaced by fresh DMEM containing 1% penicillin-streptomycin and 10% fetal calf serum. Viruses were harvested 2 and 3 days after transfection.

4.2.3.3 Viral particle production

The successful transfection of all three viral plasmids leads to the production of lentiviral particles, that are released by HEK293FT cells and accumulate in the culture media. Two days after transfection the culture media was collect and cleared from cell debris by filtering through a 0,45µm syringe membrane filter. Lentiviral particles were concentrated by ultracentrifugation (Beckman coulter counter, Ti 80) with 34400rpm at 4°C for 2 hours. The obtained viral pellet was resuspended in 10µl HBSS and stored at -80°C.

4.2.3.4 *In vivo* Injection of Lentiviral particles

Neonatal lentivirus injections

New born wistar rats were immobilized on ice for 3-5 minutes. 1µl of lentiviral particles were injected by a microinjection pump with the flow rate of 200nl per second through a hamilton syringe in the cortex and hippocampus. After the virus injection the syringe was immediately removed and pups were tattooed for later identification, warmed on a heating pad and returned to the mother. At postnatal day 21 rats were deeply anesthetized with isoflurane and perfused transcardially with PBS for 5 minutes, followed by 20 minutes of perfusion with 4% paraformaldehyde in PBS, pH 7.4. After removal, the brain was postfixed in the same fixative

for 24 h at 4°C. The cerebellum was discarded and the forebrain was cut in 100µm horizontal sections on a vibratome (Vibratome 1000; Leica Microsystems). Transduced cells were imaged with a Nikon A1/Ti-E Confocal, using a CFI Plan Apo Lambda 20x 0.75NA objective.

Postnatal day 21 lentivirus injections

21 day old wistar rats were anesthetized with 3 mg/kg xylazine (Rompun, Bayer) plus 100 mg/kg ketamine (Ketavet, Pfizer), intramuscular. When animals were deeply asleep, the heads of the rats were stabilized in a stereotactic frame and the scalp was opened in the midline for 5 mm. To prevent bleeding the periosteal connective tissue was gently removed with the blunt edge of a scalpel handle. At the coordinates 2,9mm posterior, 3,7mm lateral relative to bregma a whole was drilled with a small dental drill in the parietal skull plate at both hemispheres. A preloaded Hamilton syringe attached to a microinjection pump was slowly inserted into the brain through the opened skull. 0,5µl viral particles were inject with a flow rate of 500nl/second. The needle was kept place for two minutes moved slowly 1mm higher and again 0,5µl viral particles were injected with a flow rate of 500nl/second. After two minutes the needle was slowly removed out of the brain and the skin incision was closed by silk suture. Three weeks after the surgery rats were were deeply anesthetized with isoflurane and perfused transcardially with PBS for 5 minutes, followed by 20 minutes of perfusion with 4% paraformaldehyde in PBS, pH 7.4. After removal, the brain was postfixed in the same fixative for 24 hours at 4°C. The cerebellum was discarded and the forebrain was cut in 100µm horizontal sections on a vibratome (Vibratome 1000; Leica Microsystems). Transduced cells were imaged with a Nikon A1/Ti-E Confocal, using a CFI Plan Apo Lambda 20x 0.75NA objective.

4.2.4 Cell culture

4.2.4.1 Human embryonic kidney cells

Human embryonic kidney cells (HEK293T and HEK293FT) were grown in Dulbecco's modified Eagles medium (DMEM) containing sodium pyruvate supplemented with 10% fetal calf serum (FCS, Hyclone) and 1% penicillin/streptavidin (100 units/ml penicillin and 100 mg/ml streptavidin). Cells were passaged every 2-3 days at a confluency of 60-80% days and plated in a dilution of 1:10. Cells were maintained in humidified incubators supplied with 5% $C0_2$ at 37°C.

4.2.4.2 Transfection of HEK 293T cells

Calcium phosphate transfection

For colocalization studies of RIM proteins and fluorescence labeled Syd-1 and plakophilin4, HEK293T cells plated on poly-L-Lysin (0.1 mg/ml in borate buffer) coated coverslip in 24 well dishes were transfected. For pulldown assays and co-immunoprecipitations RIM proteins and potential interaction partners HEK293T cells in a 10cm dish were transfected. HEK293T cells were plated one day before transfection to reach a confluency of 60% on the day of transfection. 2 hours before transfection the culture medium was changed to Iscove's Modified Dulbecco's

Medium (IMDM) supplemented with 5% FCS. DNA and $CaCl_2$ were mixed and 2xHEBES was added dropwise while shaking, to allow the formation of a fine $CaPO_4$ precipitate containing the DNA. The precipitate was immediately added to the cell medium and cells were placed back into the incubator (37°C, 5% $C0_2$). The next day culture medium was changed back to DMEM. Transfected HEK293T cells for colocalization studies were fixed in 4% PFA 48 hours after transfection and further analyzed by microscopy. HEKs cells in 10cm were harvested 48 hours after transfection.

2x HEBES Buffer
50mM HEPES
280mM NaCl
1,5mM Na_2PO_4
ph7,1

Transfection mix: 2 x 24-wells	
DNA	1µg
250mM $CaCl_2$	50µl
2x HEBES Buffer	50µl

Transfection mix: 1 x 10cm dish	
DNA	10µg
250mM $CaCl_2$	600µl
2x HEBES Buffer	600µl

Polyethylenimine transfection

For pulldown assays, co-immunoprecipitations and proteomics affinity-purification mass spectrometry approaches RIM proteins and potential interaction partners HEK293T cells in a 10cm dish were transfected. HEK293T cells were plated one day before transfection to reach a confluency of 60% on the day of transfection. Culture medium was replaced by fresh DMEM (1% penicillin/streptavidin, 10% FCS) immediately before transfection. DNA was added to 250µl 250mM NaCl and 20µl Polyethylenimine (1µg/µl) were added to a second volume of 250µl 250mM NaCl. Both the DNA and the Polyethylenimine containing solutions were combined and mixed thoroughly. The transfection mix was incubated 20 minutes at room temperature and carefully added to the cells. After overnight incubation at 37°C and 5% $C0_2$ the culture medium was replaced by fresh DMEM. Cells were harvested 48 hours after transfection.

Transfection mix: 1 x 10cm dish	
DNA	10µg
150mM NaCl	500µl
Polyethylenimine	20µg

4.2.4.3 Nuclear translocation assay: Leptomycin treatment

HEK293T cells were plated in 24-well culture dishes and transfected one day later with GFP-RIM3γ by the $CaPO_4$method. Two days after transfection cells were incubated for 1 hour with 5nM Leptomycin diluted in ethanol or the same amount of ethanol as control. After the leptomycin incubation the cells were fixed with 4% paraformaldehyde and analyzed by microscopy (Zeiss Axio Observer.A1, A-Plan 10X 0.25NA objective).

4.2.4.4 NG108-15 neuroblastoma-glioma cells

NG108-15 cells were grown in Dulbecco's modified Eagles medium (DMEM) without sodium pyruvate supplemented with 10% fetal calf serum (FCS, Hyclone) and 1% penicillin/streptavidin (100 units/ml penicillin and 100 mg/ml streptavidin), 10% HAT (sodium hypoxanthine, aminopterin, and thymidine; Life technologies). Cells were passaged every 2-3 days at a confluence of 60-80% days and plated in a dilution of 1:3,5. Cells were maintained in humidified incubators supplied with 5% $C0_2$ at 37°C.

4.2.4.5 Transfection of NG108-15 cells

NG108-15 cells plated on poly-L-Lysin (0.1 mg/ml in borate buffer) coated coverslip in 24 well dishes were transfected with lipofectamine 2000 (Life technologies) with RIM proteins and GFP tagged IQGAP3 for colocalization studies. NG108-15 cells were plated one day before transfection to reach a confluency of 70% on the day of transfection. Immediately before transfection culture medium was replaced by reduced serum medium OPTI-MEM (Life technologies). DNA was added to 50µl OPTI-MEM and 1µl lipofectamine 2000 was added to a second volume of 50µl OPTI-MEM. After 5 minutes incubation at room temperature both the DNA and the lipofectamine containing solutions were combined, mixed gently and incubated for 20 minutes at room temperature. 50µl of the transfection mix were added to the culture medium of one 24-well. After 3-4 hours the medium was replaced by fresh DMEM. 48 hours after transfection NG108-15 cells were fixed with 4% PFA and further analyzed by microscopy.

Transfection mix: 1 x 24-well	
DNA	0,5µg
OPTI-MEM	50µl
lipofectamine 2000	0,5µl

4.2.4.6 Primary neuronal cell culture

A pretreatment of coverslips or wells of cell culture dishes is crucial for the optimal adhesion of neuronal cultures. Coverslips were heated up to 200°C for approximately 12 hours. Baked coverslips were placed in wells of 24 well cell culture dishes and coated with poly-D-lysine (Sigma, 0.1 mg/ml in borate buffer) overnight at 37 °C. The next day wells were washed 3 times with sterile water.

Primary neurons were prepared from E16– E19 wistar rat brains. Embryo heads were dissected and placed in a petri dish with ice-cold calcium and sodium free Hank's Buffered Salt Solution (HBSS, Invitrogen). Adhering blood vessels and membranes were removed from the brains and the cortex and hippocampus of every pup were isolated. Hippocampi and cortices were separately collected in 15 ml tubes, cut into thin slices and washed 3 times with 5 ml ice-cold HBSS. After washing HBSS was removed until a volume of 1,8ml in the case of hippocampal tissue and to 4,5ml for cortical tissue. The thin tissue slices were digested by adding trypsin,

200µl to hippocampal or 500µl to cortical tissue suspensions for 10 min at 37°C. Subsequently, the enzyme solution was removed, the preparations were washed three times with HBSS and 200µl DNAse (1mg/ml) together with pre-warmed 0.8ml Eagle's Basal Medium (BME, Invitrogen). The cells were mechanically dissociated by gentle trituration using 1 ml pipette tips. 5ml BME was added to the dissociated cells and neurons were counted in a Neubauer counting chamber. According to the cell number BME was added and 50 000 - 70 000 cells were plated in each 24 well. One day after plating the medium was replaced by fresh BME. Neurons were maintained in humidified incubators supplied with 5% $C0_2$ at 37°C. During the whole procedure BME was supplemented with 2% B27 (Invitrogen), 1% fetal bovine serum (FBS), 0.45% glucose, and 0.2mM L-glutamine.

4.2.4.7 Transfection of primary cultured neurons

Primary cortical and hippocampal neurons were transfected according to the protocol for transfection of hippocampal neurons based on DNA/Ca^{2+}-phosphate coprecipitation descibed by Köhrmann et al. [Köhrmann et al., 1999]. Neurons were transiently transfected at DIV1-5. Before transfection the original culture medium was exchanged to Minimum Essential Medium Eagle (MEM, Invitrogen), during the transfection procedure the original medium was kept in an incubator with 5% CO_2 at 37°C. Per each 24 well 1.5 µg endotoxin free DNA was used. The DNA needed for the transfection of two 24 wells was added to 60µl 250mM $CaCl_2$ and 60µl BES buffer was added dropwise while the transfection mix was vortexed for 20 seconds. The transfection mix was carefully added to the culture medium and the neurons were incubated at 2.5% CO_2 for 20 - 40 minutes. Formation of a thin Ca^{2+}-phosphate precipitate was monitored. When a precipitate was visible neurons were washed twice with HBS and 3 times with BME. In the end the original medium was added back to the cells.

4.2.4.8 Silencing of primary cultured neurons

Hippocampal neurons were transfected with a plasmid expressing GFP to visualize axons and dendrites. At DIV 2, 1 day after transfection, 2,3-dioxo-6-nitro-1,2,3,4-tetrahydrobenzo-[f]-quinoxalin-7- sulfonamide (NBQX) was added to the culture media in a final concentration of 10 or 200nM for 13 days. Control neurons were incubated in unsupplemented media. At DIV 14 neurons were fixed and analyzed using the the Sholl Analysis plug-in for ImageJ software.

4.2.4.9 Cell viability assay

Primary neurons were transfected on DIV5 with plasmids expressing GFP or GFP and the shRNA against RIM3γ or RIM4γ. Cells were fixed and analyzed on DIV 14. To identify nonviable cells propidium iodide (PI) was added to the cell culture medium 30 minutes prior to fixation. For quantification the total number of transfected neurons and PI-positive neurons were counted per micrograph image (Zeiss Axio Observer.A1, A-Plan 10X 0.25NA objective).

4.2.5 Microscopy and imaging analysis

4.2.5.1 Microscopy

Transfected primary neurons, HEK293T cells and NG108-15 cells were imaged with a light microscope (Zeiss Axiovert Observer 1A). For high magnification of cells in culture and in immunolabeled brain sections, imaging was performed with a confocal microscope (Leica TCS, Zeiss LSM710 and Nikon Eclipse Ti).

4.2.5.2 Quantification of synapse density

Cultures were transfected at DIV 3 with a plasmid expressing GFP alone (control) or together with shRNAs against RIM3γ (shRIM3) and RIM4γ (shRIM4) and immunostained at DIV 14 with anti-synapsin 1 and anti-PSD-95 antibodies. Cultured neurons were imaged with a Nikon A1/Ti-E confocal microscope using a Lambda-S CF1Apo 40X WI 1.25 NA objective. Masks representing synapsin1/PSD-95 colocalization were created with ImageJ before counting spots of overlapping synapsin/PSD-95 staining on or adjacent to the transfected neuron.

4.2.5.3 Quantification of Golgi morphology

Hippocampal neurons were transfected at DIV 3 with either shRNAs against RIM3γ (shRIM3) or RIM4γ (shRIM4), or mutated variants of both shRNAs (mutated shRIM3, mutated shRIM4), or GFP alone (control). At DIV 14 cultures were fixed and the Golgi apparatus was visualized by staining with anti-GM130 antibody. Micrograph images (Zeiss Axio Observer.A1, Plan-NEO FLUAR 40X 0.25 NA objective) of Golgi apparatus were analyzed using ImageJ. To quantify Golgi dispersion the ratio of the convex area of the Golgi outline and of the Golgi fragments was measured, and to quantify Golgi condensation the proportion of the neuron covered by the Golgi apparatus was calculated.

4.2.5.4 Axon quantification

Hippocampal neurons were transfected with either shRNAs against RIM3γ (shRIM3) or RIM4γ (shRIM4), or mutated variants of both shRNAs (mutated shRIM3, mutated shRIM4), or GFP alone (control) at DIV 1. Axonal length was measured on DIV5 using the ImageJ plug-in NeuronJ. Growth velocity was analyzed by life imaging of hippocampal cultures, transfected on DIV 7, between DIV 8 and DIV 11 and tracking axonal growth cones 24–48 hours after transfection.

4.2.5.5 Life cell imaging of Rab vesicle traffic

Live cell imaging

Cortical neurons were grown on chambered coverglas (8-well chambered borosilicate coverglas dish, LabTek). At DIV 1 neurons were cotransfected with either Rab6-GFP or Rab8-RFP or Rab11-RFP together with shRNAs against RIM3γ (shRIM3) or RIM4γ (shRIM4) or RFP alone.

4 days after transfection Rab marked vesicular traffic was imaged in living neurons. The chambered coverglas dish was placed in the a heating element with 37°C, attached to a CO_2 controller providing 5% CO_2. Fluorescent vesicles were imaged over 10 minutes with a frame rate of 6 images per minute with a Nikon A1/Ti-E confocal microscope using a Lambda-S CF1Apo 20X 1.25 NA objective.

Vesicle tracking and quantification

Vesicles were tracked manually by using the ImageJ Plugin MTrackJ (http://www.imagescience.org/meijering/software/mtrackj/). Vesicle path length and velocity were quantified with the MTrackJ plugin. Fractions of mobile and immobile vesicles were quantified with the help of ImageJ. The obtained image sequences of 10 minutes were first converted in a z-projection to create an image that contained the total vesicle amount. After subtraction of the background mobile and immobile vesicles were quantified by counting all particles on 100µm long area of the axon. An image containing only vesicles that were stable throughout the 10 minutes imaging time (immobile vesicle fraction) was created by converting the 10 minutes into a summed image and subtracting the same background as for the quantification of the total vesicle amount. Mobile vesicles were quantified in the same area as the total vesicle amount. Immobile vesicles are the difference between total vesicle amount and mobile vesicles.

4.2.6 Immunochemical methods

4.2.6.1 Immunocytochemistry

Primary neurons, HEK293T cells and NG108-15 cells were washed once with PBS and fixed with 4% paraformaldehyde in PBS for 10–15 minutes at room temperature. After washing 3 times with PBS, cells were permeabilized in 0.3% Triton X-100 in PBS for 10 minutes. Directly after permeabilization a blocking step was performed by incubating the cells in blocking buffer (10% goat serum, 1% BSA, 0.1% Triton X-100 in PBS) for at least 30 minutes, after which a primary antibody containing solution was applied and incubated overnight at 4°C. After three washes with PBS, fluorochrome-labeled secondary antibodies were applied, and incubated for 45 minutes at room temperature. Finally, cells were washed with PBS and coverslips were mounted in Moviol and left to dry overnight at room temperature.

4.2.6.2 Immunohistochemistry

Freshly dissected rat or mouse brains were incubated overnight in 4% paraformaldehyde in PBS at 4°C. After overnight fixation 100µm sagital brain slices were cut on a vibratome Microm HM650V (Waltham, USA). Brain slices were collected in 12 well culture dishes with 4% paraformaldehyde in PBS. Freefloating stainings were performed in the 12 well culture dish wells. Slices were washed once with PBS, blocked 1 hour at room temperature in PBS 10% goat serum, 0.3% Triton X-100 and labeled with first antibodies in PBS containing 5% goat serum over night at 4°C. The next morning slices were washed 3 times with PBS and incubated with

fluorochrome-labeled secondary antibodies in PBS containing 5% goat serum 2 hours at room temperature. After washing off excess antibody with PBS, slices covered using Moviol mounting medium.

4.2.7 Biochemical methods

4.2.7.1 RIM3γ and RIM4γ specific antibody production

Specific antibodies against rat RIM3γ and RIM4γ were raised against the N-terminal aminoacid sequence NH2-FNGEPGPASAGASRNC-CONH2 (RIM3γ) and NH2-CFDDEDAADSRRLKGAI QR-CO NH2 (RIM4γ) after an epitope analysis (Janin, 1979) by Pineda antibody service (http:// www.pineda-abservice.de). Antibodies were purified from rabbit immunosera by affinity chromatography on a column to which the synthetic peptide was linked covalently. The specificity of the antibodies was controlled by antigen blocking. For antigen blocking the purified RIM3γ and RIM4γ antibodies were diluted 1:100 and 1:100 in PBS containing 10% goat serum, 1%bovine serum albumin (BSA), and 0.1% Triton X-100 equally divided into two tubes. The first tube (antigen block) contained glutathione-Sepharose 4B beads bound to glutathione S-transferase (GST)-RIM3γ and GST-RIM4γ fusion protein. In the second tube (control), the glutathione-Sepharose 4B beads were bound to GST alone. Both tubes were incubated at 4°C overnight, spun at 2000 rpm for 2 minutes and supernatants were used for immunoblot analysis. Incubation with control antibody solution lead to the expected staining in immunoblot analysis, whereas incubation with preblocked antibody solutions abolished the RIM3γ and RIM4γ specific signal (appendix Fig 8.1). RIM3γ and RIM4γ antibodies were applied in Western blotting, immunocytochemistry, and immunohistochemistry at a concentration of 1:100 and 1:100, respectively.

4.2.7.2 Western blotting

Cell lysates from brain tissue were prepared from whole mouse brain or microdissected brain areas. Directly after preparation tissue samples were frozen on liquid nitrogen and either stored in -80°C or used directly. The frozen tissue samples were homogenized in 2ml/mg tissue phosphate buffered saline pH7,4 containing protease inhibitor cocktail (cOmplete, Roche) with the help of a tissue grinder. Cells in the homogenized tissue samples were lysed by adding 6xLaemlibuffer (TRIS-hydrochlorid 378mM, 30% glycerol, 12% SDS and 0,06% Bromphenolblue, 10% β-mercaptoethanol) to the samples and a 1-5 minutes incubation. Proteins were denaturated at 95°C for 5 minutes.

HEK 293T cells were lysed in phosphate buffered saline pH7,4 containing protease inhibitor cocktail and 1% triton X-100. The lysis reaction was incubated 1 hour at 4°C under rotation. After the lysis protein lysates were separated from cell debris by centrifugation at 15000rpm, 5 minutes at 4°C. 6x Laemlibuffer was added to the samples and proteins were denatured at 5 minutes at 95°C.

Proteins of the cell lysates were separated by SDS polyacryalmide gel electrophoresis (SDS PAGE) and blotted to nitrocellulose membrane over night. Membranes were incubated 1,5

hours in blocking solution of either 5% fish gelatin in PBS or 5% milk powder in TBST to avoid unspecific binding of antibodies. Proteins of interest were stained with primary antibodies against the respective proteins. Antibody staining was visualized by incubation with IRDye anti mouse 800nm or IRDye anti rabbit 680nm IgG (LI-COR) in a diluation of 1:20000 and a infrared scanning system (Odyssey, Licor). Quantification of western blots was carried using the analyze gels plugin of the FIJI software.

4.2.7.3 Protein purification from bacteria

GST(glutathione-S-transferase)-fusion proteins were expressed in *e.coli* BL21 (DE3). Bacteria expressing the GST-fusion proteins were inoculated in a 5ml liquid LB-culture medium over night at 37°C. The next morning overnight cultures were added to 500ml fresh LB-medium and grown until an optical density (OD600) of 0,5 at 600nm was reached. At this OD600 protein production was induced with 0,1mM IPTG (Isopropyl β-D-1-thiogalactopyranoside) and the cultures were incubated at 37°C for 3 hours. The bacteria were harvested by centrifugation at 4°C and lysed for 20 minutes at 4°C under rotation in PBS containing Complete Protease Inhibitor cocktail and 1% Triton X-100. Glutathione-agarose was added to the protein lysates and incubated 1 hour at 4°C in order to allow coupling of GST fusion proteins to the glutathione agarose beads. GST fusion proteins were purified in 3 washing steps. The successful protein production and the amount of coupled proteins were analyzed by SDS-PAGE and Coomassie staining.

4.2.7.4 GST Pulldown assay

GST-RIM3γ, GST-RIM4γ, GST-RIM1C2B and GST alone were in expressed in *e.coli* BL21 (DE3) and bound to glutathione-agarose beads. IQGAP3-GFP, IQGAP1-GFP, and Syd-1-HA were overepressed in HEK293T cells. 48 hours after transfection HEK 293T cells were washed once with PBS and lysed in PBS containing Complete Protease Inhibitor cocktail and 1% Triton X-100 for 1 hour at 4°C. Cell lysates were centrifuged for 2 minutes at 4°C to separate cell debris from solubilized proteins. To test binding of GST-RIM proteins to potential interaction partners, agarose coupled GST-RIMs were added to the HEK cell lysates and incubated for 2 hours at 4°C. After the binding reaction protein complexes were washed 3-5 times with PBS containing 1% Triton X-100 and analyzed by western blotting. GFP bound proteins were detected with GFP antibodies (anti-GFP mouse monoclonal Santa Cruz, 1:1000) and HA tagged proteins with antibodies against HA (anti-HA mouse Convance, 1:1000).

4.2.7.5 Co-immunoprecipitation

HEK293T cells were transfected with pairs of proteins, of which interaction should be tested, with polyethylenimine. 48 hours after transfection HEK293T cells were washed once with PBS and lysed in PBS containing Complete Protease Inhibitor cocktail and 1% Triton X-100 for 1 hour at 4°C. Cell lysates were centrifuged for 2 minutes at 15000 rpm at 4°C to separate cell debris from solubilized proteins. Protein complexes of the potential interaction partners were

purified by coupling to magnetic beads bound to antibodies against the flag sequence of the affinity tag of RIM3γ-TAP, RIMγ4-TAP and RIM1-C2A-C2B-TAP. The precipitated protein complexes were washed 5 times with PBS containing 1% Triton X-100 and analyzed by western blotting. TAP tagged proteins were detected with antibodies against flag (anti-flag, mouse, Sigma, 1:5000) GFP bound proteins with GFP antibodies (anti-GFP mouse monoclonal Santa Cruz, 1:1000), HIS tagged proteins with antibodies against HIS (anti-HIS, mouse Neuromab 1:200) and HA tagged proteins with antibodies against HA (anti-HA mouse Convance, 1:1000).

4.2.8 Mass spectrometry proteomics approach

4.2.8.1 Protein purification and preparation of tissue fractions

Protein purification from HEK cells

HEK293T cells were transfected with TAP(tandem (streptavidin-flag) affinity purification) affinity tag-tagged RIM3γ and RIM4γ and the TAP tag alone as control with polyethyleneimine. 48 hours after transfection cells were washed once with ice cold PBS and lysed in Lysisbuffer (50mM Tris HCL (pH7,5), 150mM NaCl, 2%Triton X-100 and Complete proteinase inhibitor cocktail) for 1 hour at 4°C. Cell lysates were centrifuged at 15000rpm for 2 minutes at 4°C to separate cell debris from solubilized proteins. The obtained supernatants were incubated 1 hour with prewashed magnetic beads coupled to flag-antibodies. Bound TAP tagged proteins were purified by washing the magnetic beads 2 times with a low salt buffer (50mM Tris HCL (pH7,5), 100mM NaCl, 2%Triton X-100), 2 times with high salt buffer (50mM Tris HCL (pH7,5), 500mM NaCl, 2%Triton X-100) and once with PBS.

Preparation of whole brain lysates

Brains of C57 BL/6 wild type mice were prepared freshly and the cerebellum and white matter were removed. Brains were homogenized in 2mM HEPES buffer (pH7,4) containing 0,32M sucrose, 50mM EDTA (3ml per animal) in a teflon glass potter with 7 strokes of 900rpm. Homogenates were solubilized with 20µl Triton X-100/ml for 2 hours at 4°C. The solution was clarified by centrifugation and the supernatant used for the binding reaction.

Preparation of crude synaptosomes

Brains of C57BL/6J wild type mice were prepared freshly and the cerebellum and white matter were removed. Brains were homogenized in 2mM HEPES buffer (pH7,4) containing 0,32M sucrose, 50mM EDTA (3ml per animal) in a teflon glass potter with 7 strokes of 900rpm. Homogenates were centrifuged with 3000g at 4°C for 15 minutes. The resulting supernatant was transferred to a new tube and centrifuged at with 15000 rpm at 4°C for 25 minutes. After the second centrifugation the supernatant was discarded and the obtained synaptosomal pellet was resuspended in CL144 or lysisbuffer containing 2% Triton X-100 (50mM Tris HCL, 150mM NaCl, pH 7,5, complete proteinase inhibitor) and incubated for 1 hour at 4°C. The solution was clarified by centrifugation and the supernatant used for the binding reaction.

4.2.8.2 Binding assay

Purified TAP-tagged RIM3γ and RIM4γ and the TAP tag alone coupled to magnetic beads were incubated with either crude synaptosomal fractions or whole brain lysates for four 4 hours at 4°C. Subsequent to incubation magnetic beads and coupled proteins were washed twice with low salt buffer, twice with high salt buffer and once with PBS and denaturated at 95°C in 1x loading buffer (Life technologies). Samples were separated by electrophoresis in a 12% pre-cast NuPAGE Bis-Tris gel and subsequently visualized by Coomassie Colloidal Blue over night, to control for the successful binding reaction.

4.2.8.3 In Gel tryptic digestion

Bands of the binding reactions and control reactions on the NuPAGE Bis-Tris gel were cut into equal small gel pieces and transferred to endotoxin free 1,5ml tubes. 200µl of destaining solution (Trypsin Profile IGD Kit, Sigma Aldrich) were added to each gel piece and incubated at 37°C. 30 minutes later the solution was removed and discarded and the destaining step was repeated. The destaining steps were followed by reduction and alkylation of cysteines to irreversibly break up disulfide bonds. Destained gel pieces were first dried in a centrifugal evaporator for 15-30 minutes. To reduce disulfide bonds to thiol groups, the dried gel pieces were incubated in 100µl of 20mM Dithiothreitol (DTT) in 100mM ammonium carbonate at 55°C for 30 minutes. The remaining solution was removed and 100µl of iodoacetamide was added to irreversible alkylate SH groups. After 30 minutes in the dark the remaining solution was removed and the gel pieces were incubated in 200µl of 100mM ammonium carbonate containing for 3 minutes. The supernatant was removed and the gel pieces were first incubated 5 minutes in 50% acetonitrile and subsequently 5 minutes in 100% acetonitrile. Before trypsin digestion the gel pieces were dried in a centrifugal evaporator. Each dried gel pieces was incubated with 0,4µg Trypsin in Trypsin reaction buffer (Trypsin Profile IGD Kit, Sigma Aldrich) over night at 37°C. The remaining supernatant containing the extracted tryptic peptides was transferred to a new tube and dried in a centrifugal evaporator. Dried samples were subjected to LC-MS/MS analysis.

4.2.9 Knock-out mouse generation and behavioral experiments

All procedures were performed in accordance with the guidelines of the Bonn University Medical School Care Committee. Mice were kept in an animal facility, with a maximum of 5 animals per cage with water and food provided ad libitum, and under the control of an alternating 12-hour light or dark cycle.

4.2.9.1 Generation of RIM3γ and RIM4γ knock-out mice

Null mice for either RIM3γ or RIM4γ activity were generated utilizing ES cells produced by the international Knock-out Mouse Project (KOMP) consortium. The KOMP knock-out construct is designed to create three different mouse lines (Fig. 5.19): The line obtained after germ

line transmission constitutes a "knock-out first" allele, in which insertion of a splice acceptor-lacZ gene trap cassette disrupts the endogenous RIM3γ and RIM4γ transcripts resulting in a constitutive knock-out (RIM3γconstKO and RIM4γconstKO). After FLP-mediated excision of the gene trap cassette a conditional KO is obtained (RIM3γflox and RIM4γflox); and (3) Cre-mediated recombination results in a null allele (RIM3γKO and RIM4γKO). RIM3γ knock-out mice were generated from the JM8A3.N1 ES cells carrying the RIM3γ targeting vector (IKMC Project: 34392; http://www.mousephenotype. org/martsearch_ikmc_project/ mart-search /ikmc _project/34392). RIM4γ knockout mice were generated from the JM8A3.N1 ES cells carrying the RIM4γ targeting vector (IKMC Project: 37192; http:// www.mousephenotype. org/martsearch_ ikmc_project/ martsearch/ikmc_project/37192). Es cells were injected into Balb/c mice. The resulting chimeric mice were monitored by coat color and genotyped by PCR. The following primers were used for the RIM3γ constKO line: const KO RIM3γ 5'-GGACCACACTGCAATG-CTAA-3' and 5'-CCCTTCAGTC TTCCTGTCCA-3' product size 618 base pairs; wild type RIM3γ 5'-GGACCACACTG CAATGCTAA-3' and 5'-ACCAGACTCC AAAGCCCTC-3' product size 324 base pairs. The RIM4γ constKO line was genotyped with the primers: const KO RIM4γ 5'-GCATGATGGGAAGGAATGCCAAGC-3' and 5'-CCCTTCAGT CTTCCTGTCCA-3' product size 632 base pairs; wild type 5'-GCATGATGGGAAGGAATGCC AAGC-3' and 5'-GTTCAGGCCAGGGCTTCTCCATGC-3' product size 324 base pairs. All analysis were carried out with littermates of heterozygous matings.

4.2.9.2 Gait analysis

Gait analysis of RIM4γ knock-out mice was performed with the CatWalk XT system (Noldus Information Technology). A cage with used bedding was placed at the end of the walkway to motivate the mice to cross the walkway without hesitation. While crossing the glass walkway footprints of mice were recorded with a high speed camera. To obtain comparable data mice had to cross the walkway within 10 seconds without turning or stopping in between. Mice were tested 3 times with one week recovery time in between testing days. Only data of mice that performed 3 consecutive runs meeting the criteria above were included in the quantification of the gait performance. During episodes of hind limb impairments RIM4γ knock-out mice were not able to cross the walkway within 10 seconds. Footprints of theses runs were excluded from the quantification and only used to represent the severity of the phenotype. Quantification of footprints was performed with the Catwalk XT 9.0 software (Noldus Information Technology).

4.2.9.3 Motor performance on Rotarod

Motorcoordination of mice was tested on a rotating beam (Rota-Rod ENV-575MA Five Station USB, Med Associates Inc.). Mice were tested at an age of 14-16 weeks once a week for 3 consecutive weeks. Velocity of the rotating rod was accelerated from 4 rounds per minute (rpm) to 40 rpm within 5 minutes during each testing round and the time until mice fall off the rod was monitored with a cut off at 5 minutes. Mice were first habituated on the rod for 5 minutes. After a recovery phase of 15 minutes mice had to perform 3 test rounds with again 15 minutes

recovery phases in between. The results are the means of 9 tests on 3 days.

5 Results

Results

RIM3γ and RIM4γ belong to the protein family of Rab3-interacting-molecules (RIM). The large members of the RIM protein family (RIM1α, RIM1β, RIM2α, RIM2β) are multidomain proteins enriched at the presynaptic active zone. At the active zone they form a scaffold with numerous interaction partners and govern thereby several steps of presynaptic neurotransmitter release. RIM3γ and RIM4γ are much smaller and share only the C_2B domain with the large RIMs. Also their subcellular localization differs from the large RIM proteins. RIM3γ is strongly expressed in the nucleus and shows a punctate synaptic expression pattern along axons and dendrites. RIM4γ is absent from the nucleus and shows a diffuse distribution along axons and dendrites. This already suggests that the function of the small members of the RIM protein family might differ from the synaptic function of the large RIM proteins, which show a specific presynaptic localization. First knock-down experiments in primary neuronal cultures revealed that the loss of RIM3γ and RIM4γ leads to an impairments in neuronal growth [Alvaréz-Baron, 2010]. But the full impact on neuronal morphology and the molecular mechanisms underlying the function of γ-RIMs during neuronal growth have not been analyzed yet.

5.1 RIM3γ and RIM4γ's specific subcellular localizations are governed by their N-terminal sequence

Studies on the subcellular localization of a protein can reveal its enrichment to cellular organelles or specialized compartments of a neuron and might thereby give first hints about the molecular function of a protein. The localization of a protein is on the one hand controlled by intracellular transport systems and its interaction partners, which target the protein to the desired destination. On the other hand localization signals within the amino acid sequence of a protein can determine the subcellular localization of a protein, by for example allowing the integration of the protein into the plasma membrane or into membranes of cellular organelles. The nucleus of a cell is the place of gene transcription, this process is controlled by a great variety of proteins, allowing the cell to adapt its gene expression patterns to exterior conditions. This adaptation involves the frequent import and export of proteins in and out of the nucleus. The nuclear transport of proteins is tightly regulated by proteins of the nuclear pore complex. One part of this nuclear pore complex are importin receptors, which are able to recognize nuclear localization signals within the amino acid sequence of potential cargo proteins and induce their translocation into the nucleus.

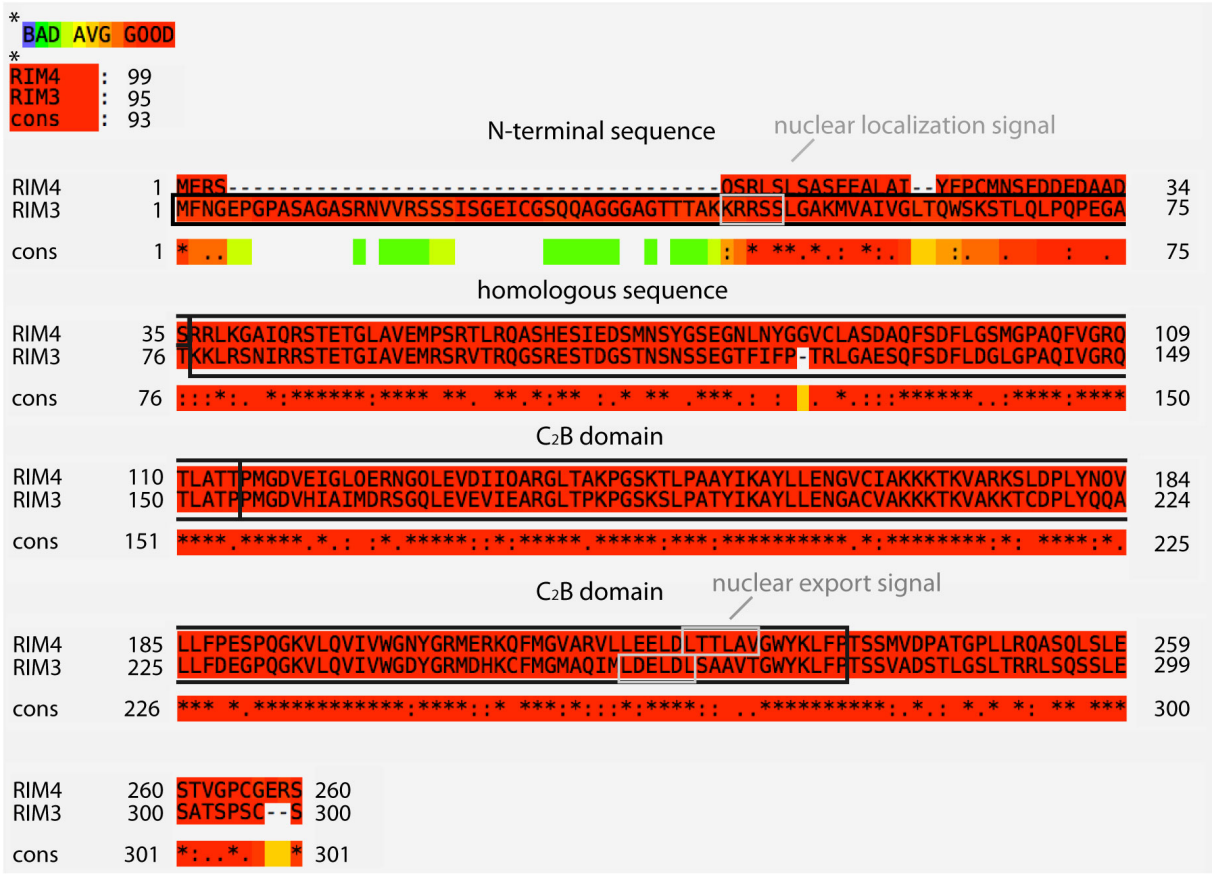

Figure 5.1: **Alignment of the RIM3γ and RIM4γ amino acid sequence reveals a high dregree of homology between both proteins.** Bioinformatical analysis identified a nuclear localization signal in the N-terminus of RIM3γ and a nuclear export signal in the C_2B domain of both γ-RIMs. Multiple sequence alignment was performed with the bioinformatical program Tcoffe (http://www.ebi.ac.uk/Tools/msa/tcoffee/).

The export of proteins out of the nucleus is regulated in a similar fashion. Exportins in the nucleus recognize nuclear export signals of export cargos and initiate their transport out of the nucleus.

Dispite their differing subcellular localization RIM3γ and RIM4γ show a high degree of sequence homology (Fig. 5.1). A bioinformatic search for nuclear import and export signals within the sequence of RIM3γ and RIM4γ revealed a nuclear localization signal in the N-terminus of RIM3γ and a nuclear export signal in the C_2B domain of both proteins. To verify the functionality of the nuclear localization signal identified in the sequence of RIM3γ, expression plasmids for truncated variants of RIM3γ comprising either the N-terminal sequence or the C_2B domain of RIM3γ were generated. Additionally, the nuclear localization signal of RIM3γ was mutated in a full-length expression plasmid of RIM3γ by exchanging the nucleotides coding for the nuclear localization signal. After transfection into NG108 neuroblastoma cells the N-terminal construct was predominantly located in the nucleus whereas the C_2B domain and the mutated version missing the nuclear localization signal were not able to translocate to the nucleus (Fig. 5.2A). This proves that the predicted nuclear localization signal in the protein sequence of RIM3γ is functional and can mediate the nuclear enrichment of RIM3γ.

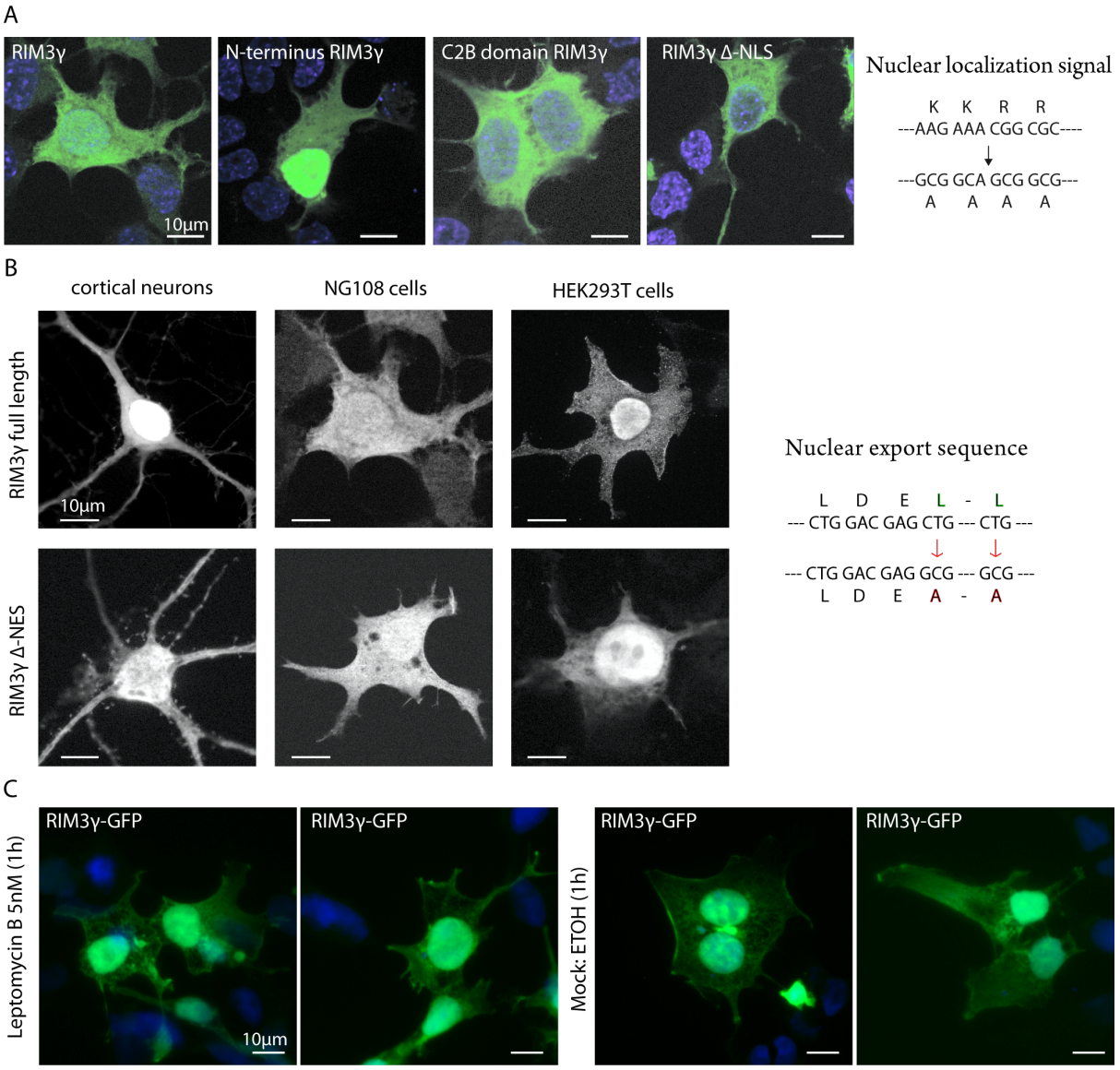

Figure 5.2: **RIM3γ's nuclear localization is governed by a nuclear localization signal in its N-terminus. A,** HEK293T cells were transfected with a vector expressing different variants of RIM3γ fused to GFP. The full-length construct and the N-terminal fragment show a strong nuclear expression whereas the C_2B domain and the construct with a mutated nuclear localization signal are absent from the nucleus. **B,** Mutations of the last two amino acids in the nuclear export signal do not change the localization of RIM3γ. Vectors expressing either RIM3γ or a mutated protein (RIM3 γ-ΔNES) fused to GFP were transfected into primary cortical neurons, NG108 neuroblastoma cells and HEK29T cells. Both RIM3γ and the its mutated variant, show similar cytosolic expression levels. **C,** Incubation of HEK293T expressing RIM3γ-GFP with 5nM Leptomycin, does not lead to the restriction of RIM3γ to the nucleus.

The nuclear export signal of RIM3γ lies in its C_2B domain and is compromised of five amino acids. Mutations of the nucleotides coding for the two last amino acids of the nuclear export sequence did not block the export of RIM3γ from the nucleus after overexpression in HEK293T cells, NG108 cells or primary cortical neurons (Fig. 5.2B). This does not exclude the functionality of the nuclear export signal, as the first three amino acids could be sufficient to maintain its function. Additionally, overexpression could mask a decreased nuclear export of RIM3γ as the protein levels after overexpression exceed by far the endogenous protein levels.

CRM1 (chromosome region maintenance 1; also referred to as exportin1) is an important nuclear export receptor, mediating the nuclear export of many proteins. This process can be blocked by the application of Leptomycin B [Fornerod et al., 1997]. To investigate if the nuclear export of RIM3γ is actively regulated by CRM1 we incubated HEK 293T cells overexpressing RIM3γ for 1 hour with 5nM Leptomycin B and subsequently fixed the cells to analyze the distribution of RIM3γ. The block of CRM1 mediated nuclear export did not restrict RIM3γ to the nucleus, as the cytosolic expression levels appeared to be unchanged after incubation with Leptomycin B and only ethanol as control (Fig. 5.2C). This again suggests, that the nuclear export sequence in the C_2B domain of RIM3 γ is not functional. However to definitively exclude active nuclear export of RIM3γ in neurons this export needs to be analyzed in a more physiological and quantitative way.

In summary, RIM3γ and RIM4γ show a more diverse subcellular distribution than the large RIM protein family members. Whereby the strong nuclear expression of RIM3γ is mediated by a nuclear localization signal in the N-terminus of RIM3γ. The amino acid sequence of RIM4γ does not exhibit a nuclear localization signal consistent with its absence from the nucleus. A nuclear export signal in the C_2B domain is conserved between both proteins. Although the functionality of this sequence could not be proven it suggests that shared functions of RIM3γ and RIM4γ are mediated by the highly homologous C_2B domain whereas isoform specific functions and also their subcellular localization might be mediated by the differing N-terminal domains.

5.2 Characterization of knock-down effects in neurons

ShRNA mediated knock-down of RIM3γ and RIM4γ leads to drastic growth impairments in cultured primary neurons [Alvaréz-Baron, 2010]. Neurons transfected with shRNAs against RIM3γ and RIM4γ on DIV3 exhibit only very few short dendrites when analyzed at DIV14. At this time point control cells transfected only with GFP have already established a complex dendritic tree. Interestingly, the phenotype could be cross-rescued, as the overexpression of RIM3γ could restore the growth deficits in RIM4γ-knockdown neurons and vice versa. Already the overexpression of the C_2B domain of RIM3γ or RIM4γ was sufficient to partially restore the growth deficits. These findings suggest, that the role of RIM3γ and RIM4γ during neuronal growth is a shared function of both proteins mediated by their C_2B domain. However, the knock-down experiments were performed early during neuronal development, leaving an possible impact on later developmental stages unresolved. Furthermore, it remained unclear so far if RIM3γ and RIM4γ's function is restricted to dendrites or affects also axonal growth.

5.2.1 RIM3γ and RIM4γ are involved in general growth promoting mechanisms

Drastic morphological changes in primary neuronal cultures after genetic manipulations like shRNA mediated protein knock-down could be a side effect of increased cell death. To rule this out in the case of RIM3γ and RIM4γ knock-down we labeled control neurons and knock-down neurons 11 days after transfection with propidium iodide. Propidium iodide is a red fluorescent DNA-intercalating dye, that is not permeant to living cells and can therefore be used to mark dead or dying cells. Primary cultured cortical neurons were transfected with either shRNAs against RIM3γ and RIM4γ together with GFP or GFP alone as control on day in vitro (DIV) 3 and fixed and stained 11 days later. The percentage of viable cells was quantified by counting the number of neurons, which expressed GFP but were not propidium iodide positive and the total number of GFP positive cells. The percentage of dead cells did not differ between control and knock-down neurons (Fig. 5.3D). These results confirm, that the reduced dendritic arborization observed after the knock-down of RIM3γ and RIM4γ is not an result of increased cell death in response to the knock-down.

Dendrites and axons share common growth regulatory mechanism but also employ signaling pathways, which specifically influence dendritic or axonal growth. This allows a neuron to built up the morphological and molecular distinct compartments of axons and dendrites. In order to investigate if RIM3γ and RIM4γ's growth promoting effects are restricted to dendritic growth or play a role in general growth promoting mechanisms we analyzed the impact of the loss of the two proteins on axonal growth. Directly after platting cultured primary neurons appear as round asymmetrical spheres. During the next 24 hours several short processes, the so-called minor neurites, are formed. About one day after plating neuronal symmetry brakes when one of the minor processes starts to grow rapidly to become the axon. The other neurites stay short until day *in vitro* 4-5 when they start to develop into dendrites. Axonal growth defects can be therefore easily visualized in primary neuronal cultures at DIV5 when neurons exhibit only one single long axonal branch and several very short dendritic protrusions.

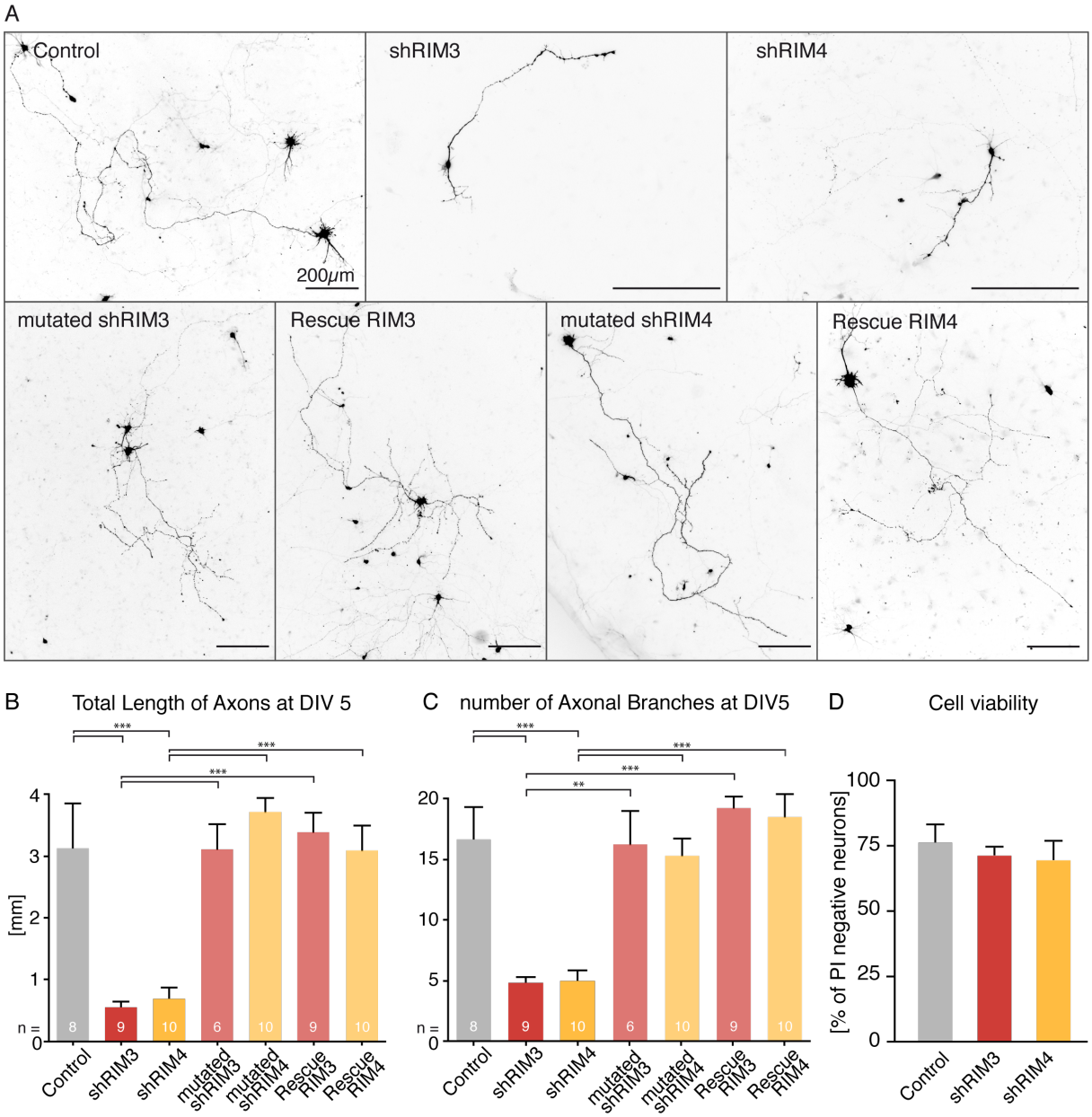

Figure 5.3: **RIM3γ and RIM4γ knock-down affects early axonal outgrowth. A,** Hippocampal neurons transfected DIV1 expressing GFP (control), shRNAs against RIM3 γ (shRIM3) and RIM4 γ (shRIM4), shRNAs with few nucleotide exchanges (mutated shRIM3 and mutated shRIM4) and coexpressing the shRNAs with the respective resistant cDNAs (rescue RIM3 γ and rescue RIM4 γ) were fixed and analyzed by confocal microscopy at DIV5. **B, C,** Quantitative analysis of total axonal length (B) and the number of axonal branches (C) showed, that axonal outgrowth and branching are strongly reduced after knock-down of RIM3γ (shRIM3) and RIM4γ (shRIM4) as compared to controls. Both parameters are unaffected after cotransfection of either shRIM3 or shRIM4 and a resistant version of the respective RIM variant (rescue RIM3γ and RIM4γ) or the transfection of mutated shRNAs against RIM3γ (mutated shRIM3) and RIM4γ (mutated shRIM4) (1-way ANOVA with Bonferoni post Test, *** $p<0.001$, ** $p<0.01$) **D,** Primary neuronal cultures were transfected on DIV5 with plasmids expressing GFP (control) or GFP and the shRNA against RIM3 γ or RIM4 γ. Cells were fixed and analyzed on DIV14. Non-viable cells were identified using Propidium Iodide (PI) staining. Neurons transfected with shRNAs showed no significant difference in viability compared to GFP transfected control cells (n=8 coverslips, 1-way ANOVA $p=0.69$).

The impact of RIM3γ and RIM4γ on axonal growth was investigated by the transfection of primary cortical neurons on DIV 1 with vectors expressing GFP alone as control or GFP together

with the respective shRNAs (shRIM3, shRIM4). Analysis of fluorescent micrographs revealed, that the knock-down of RIM3γ and RIM4γ decreased the total axonal length and the number of axonal branches (Fig. 5.3A,B,C). These effects were not observed if neurons were transfected with either a mutated non-functional shRNA or if shRNA-resistant RIM3γ and RIM4γ cDNAs were coexpressed (constructs were described in [Alvaréz-Baron, 2010] , Fig 5A,B,C). Thus, RIM3γ and RIM4γ seem to be involved in a general growth regulatory mechanism affecting the development of dendrites and axons.

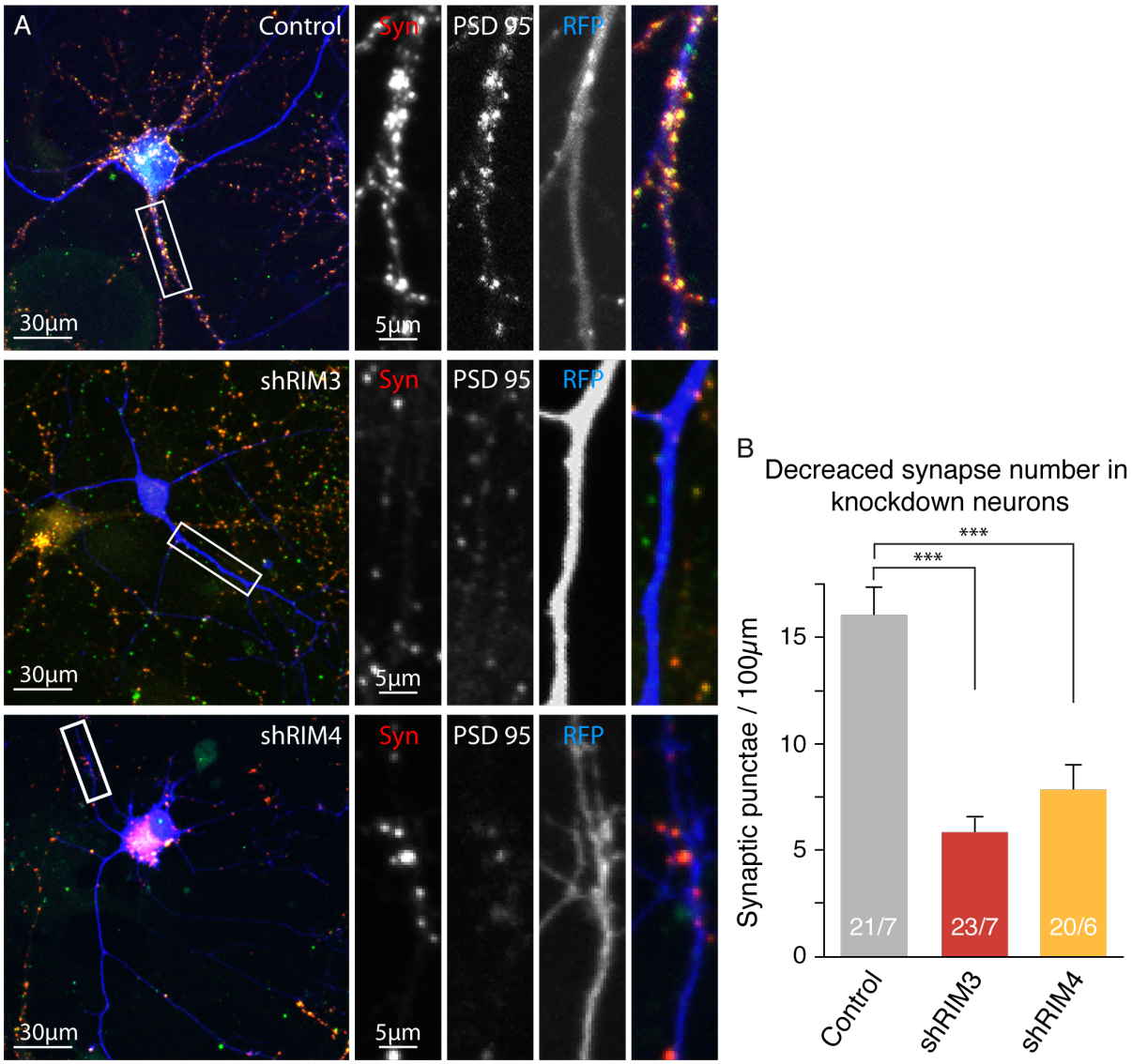

Figure 5.4: **Absence of dendritic spines and reduction in synapse density in RIM3γ and RIM4γ knock-down neurons. A,** Hippocampal neurons transfected at DIV3 with either a vector expressing GFP (control) or GFP and the shRNA against RIM3γ (shRIM3) or RIM4γ (shRIM4). All neurons were immunostained using anti-Synapsin (SYN) and anti-PSD95 (PSD95) antibodies and analyzed at DIV14 by confocal microscopy. Scale bar = 30µm, *= 5µm. **B,** Quantification of PSD95/Synapsin co-labeled synaptic punctae on RIM3γ and RIM4γ knock-down dendrites. RIM3γ-shRNA (shRIM3) and RIM4γ-shRNA (shRIM4) neurons exhibit a decreased synapse density compared to control. Quantification of Synapsin punctae density was performed using ImageJ software (n: # branches / # cells, one-way ANOVA *** $p<0.001$).

Axonal and dendritic development is not only the simple increase of a cellular or membranous protrusion it also includes the development of specific axonal and dendritic structures like the synapse with specialized presynaptic compartments in axons and postsynaptic densities in dendritic spines. The impairment in dendritic as well as in axonal growth after the loss of RIM3γ and RIM4γ suggests, that the small γ-RIMs are involved in general neuronal growth processes. This raises the question if the loss of RIM3γ and RIM4γ affects also the development of synaptic structures. To answer this question, primary neuronal cultures were transfected with shRNAs against RIM3γ and RIM4γ or a control vector at DIV3 and stained 10 days later with antibodies against the presynaptic protein synapsin and the postsynaptic protein PSD95 (Fig. 5.4A). The quantification of synapsin and PSD 95 positive synapses revealed a strong reduction in synapse density in RIM3γ and RIM4γ knock-down neurons (Fig. 5.4B).

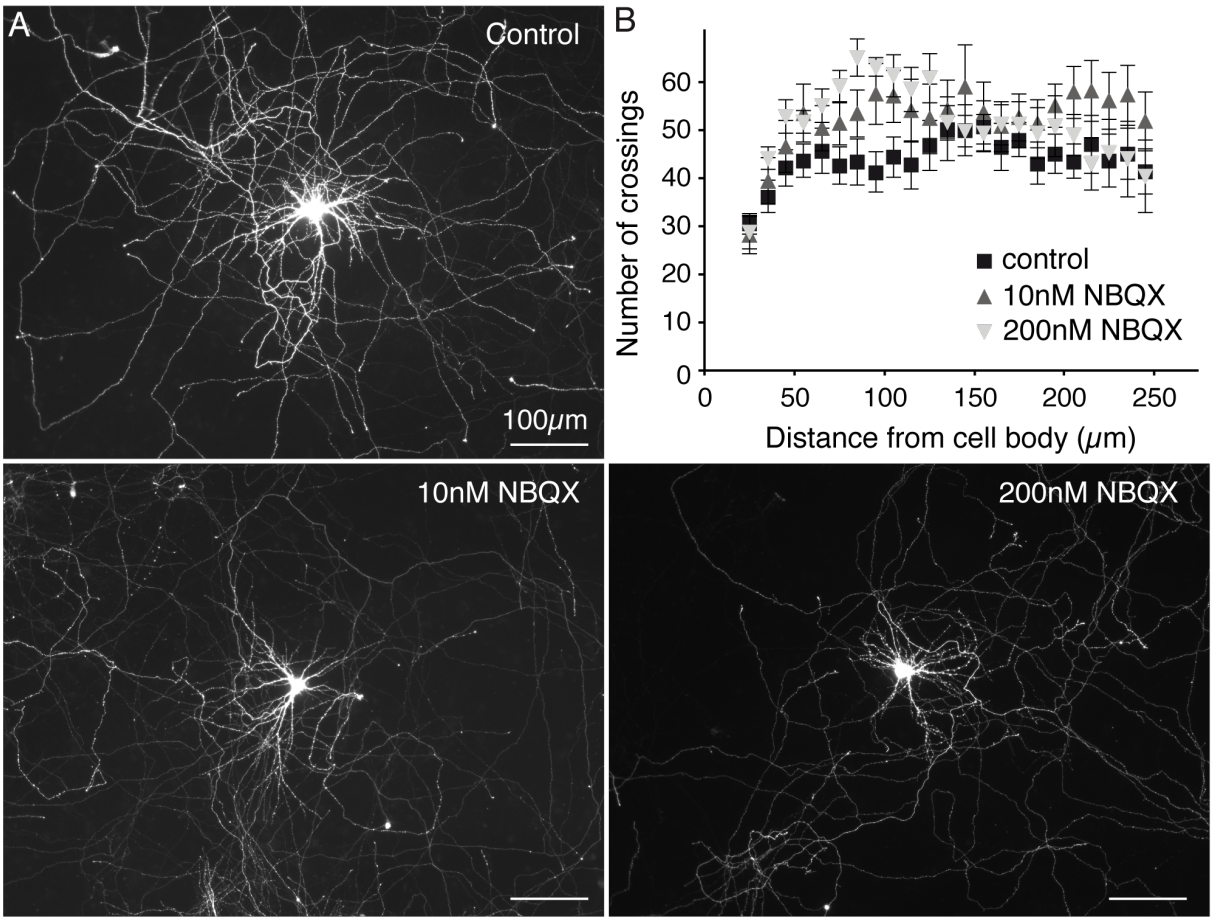

Figure 5.5: **Synaptic silencing has no effect on neuronal morphology. A,** Hippocampal neurons were transfected with a plasmid expressing GFP at DIV1 to visualize dendrites and axons. From DIV2 to DIV14 the cells were exposed to 10 nM or 200 nM 2,3- Dioxo-6-nitro-1,2,3,4-tetrahydrobenzo-[f]-quinoxalin-7-sulfonamide (NBQX). Control cells were incubated in normal media. All neurons were analyzed at DIV14. Scale bar = 100μm. **B,** Sholl analysis indicated no difference in neurite branching after synaptic silencing. In order to detect even small changes in distal dendrites Sholl analysis was performed up to 250μm from the center of the neuron.

The large members of the RIM protein family are important regulators of presynaptic neurotransmitter release but to date it is unclear if the small γ-RIMs share this function. Thus a reduction in neuronal activity due to an unknown function of RIM3γ and RIM4γ in synaptic transmission could be one reason for the growth deficits in RIM3γ and RIM4γ knock-down

neurons. Excitatory synaptic transmission is mainly mediated by AMPA (α-amino-3-hydroxy-5-methyl-4-isoxazolepropionic acid) receptors. To test if a reduction in neuronal activity could lead to the same effects as we observed in neurons deficient for RIM3γ and RIM4γ we silenced neuronal cultures with different concentrations of the AMPA receptor blocker 6-nitro-7-sulfamoylbenzo(f)quinoxaline-2, 3-dione (NBQX). One day after transfection of hippocampal cultures with GFP to visualize the cells AMPA receptor mediated synaptic transmission was partially blocked by the application of 10nM NBQX and fully by the application of 200nM NBQX until the cells were analyzed on DIV 14 [Maclean & Bowie, 2011]. Analysis of cell morphology on DIV14 revealed, that both the partial and the full block of excitatory synaptic transmission did not lead to a growth defect in primary neuronal cultures (Fig. 5.5). Therefore, a possible role of RIM3γ and RIM4γ in synaptic transmission seems not to contribute to their function during neuronal growth.

5.2.2 RIM3γ and RIM4γ *in-vivo* knock-down is growth inhibitory

Cultured primary neurons do not form the complex neuronal network present in an intact brain, where neurons establish complex and interconnected neuronal circuits and specialized substructures. In order to investigate if the knock-down of RIM3γ and RIM4γ has the same effect on the growth of a neuron, when a functional neuronal network surrounds it, we sparsely injected lentiviral particles expressing GFP only as control or the respective shRNAs (shRIM3 or shRIM4) into the ventricle of rats directly after birth (P0). The infected brains were collected and analyzed 21 days later. Cortical neurons transduced with the shRNA against RIM3γ and RIM4γ revealed drastic changes in their morphology when compared to control cells expressing only GFP. Knock-down neurons had only very few short neuronal processes whereas the control cells had developed a complex dendritic arbor (Fig. 5.6A,B). In accordance with the observed reduction in synapse density *in vitro* we detected a reduced numbers of dendritic spines in the hippocampus and cortex of 21 day old rats, which had been injected with lentiviruses particles expressing RFP together with a shRNA against RIM3γ directly after birth (Fig. 5.7A,B). To exclude possible off-target effects leading to the impaired neuronal growth after the knock-down of RIM3γ or RIM4γ *in vivo* we performed rescue experiments with a shRNA resistant RIM3γ. Newly born rats were injected with lentiviral particles expressing RFP alone or RFP together with the shRNA against RIM3γ or a combination of lentiviral particles expressing either RFP together with shRNA or GFP together with a resistant version of RIM3γ. As in our previous experiments we could observe a strong reduction in neuronal growth after knockdown of RIM3γ when compared to control neurons expressing only RFP. Whereas cells that expressed both the shRNA and a resistant RIM3γ exhibit a comparable neuronal morphology as control cells (Fig. 5.7C). These results demonstrate that decreasing the levels of RIM3γ and RIM4γ in the first 3 weeks after birth result in a dramatic alteration of neuronal morphology despite their contact with intact neighboring cells and a normal microenvironment.

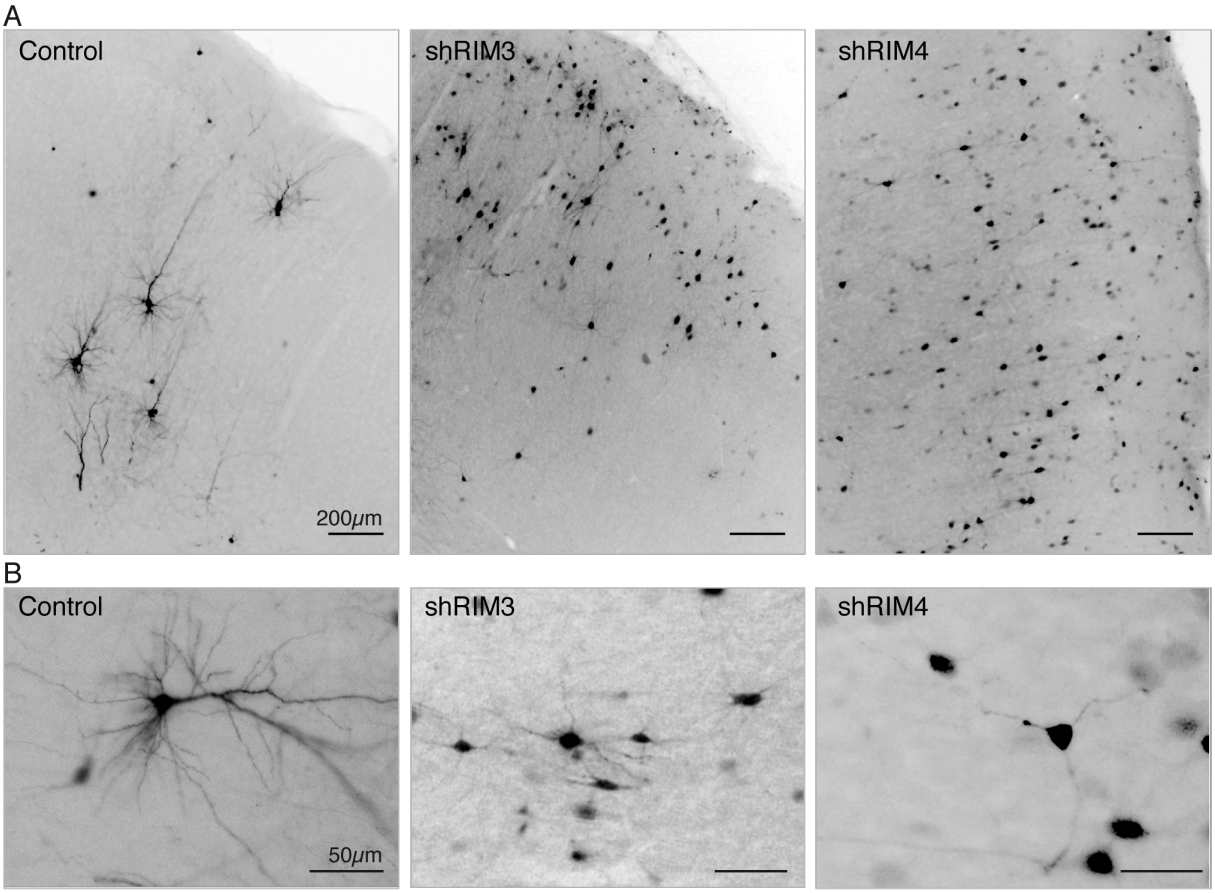

Figure 5.6: **In vivo knock-down of RIM3γ and RIM4γ leads to a drastic reduction in dendritic complexity. A,** Lentiviral particles expressing GFP alone (control) or together with shRNAs against RIM3γ or RIM4γ were injected into the ventricle of P0 rat brains. Brains were analyzed at P21 by immunohistochemistry with an antibody against GFP. Cortical control neurons displayed a normal morphology, showing regular dendritic growth. In contrast, neurons transduced with the shRNAs, exhibited a strong deficit in the number of neurites, indicating a greatly compromised neuronal branching. **B,** Higher magnification images of control and knock-down cortical neurons revealed a striking loss in the dendritic arbor of neurons with decreased levels of RIM3γ and RIM4γ as compared to control.

The reduced length of neuronal processes after the knock-down of RIM3γ and RIM4γ could be on the one hand caused by defects in neuronal branch development and maturation but on the other hand by an increase in the retraction of already formed neuronal branches. A contribution of RIM3γ and RIM4γ in the retraction of dendrites was examined by the injection of lentiviral particles expressing either RFP alone as control or together with shRNAs against RIM3γ and RIM4γ in the hippocampus of 21 days old rats. Microscopic analysis 14 days later at postnatal day 35 revealed no drastic decrease in the dendritic complexity in hippocampal RIM3γ and RIM4γ knock-down neurons in comparison to control neurons (Fig. 5.7D) pointing to a role for RIM3γ and RIM4γ during development the of neuronal branches.

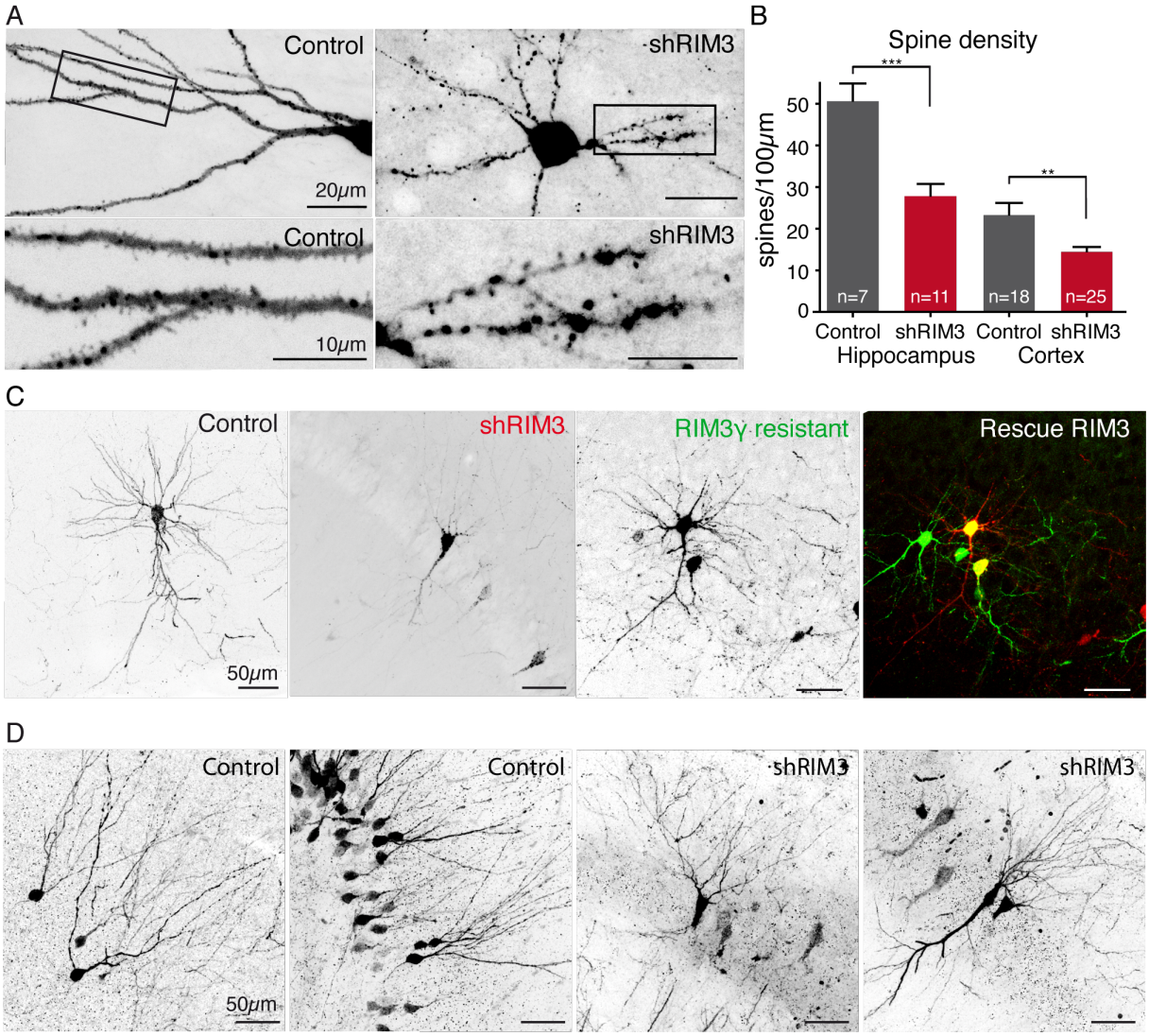

Figure 5.7: **In vivo knock-down of RIM3γ reduces spine and synapse number, has no drastic effects in the adult brain and can be rescued by coexpression of a resistant RIM3γ variant. A,** Hippocampal neurons of P21 rats show that neurons expressing the shRNA against RIM3γ exhibit a reduced number of dendritic spines in comparison to control cells expressing only RFP. **B,** Quantification of the loss in spine density in hippocampal and cortical RIM3γ knock-down neurons (T-test, Hippocampus *** p = 0.0003, cortex ** p = 0.0042). **C,** Lentiviral particles expressing RFP (control), the shRNA against RIM3γ (shRIM3) alone or together with a green fluorescent resistant variant of RIM3 (RIM3γ resitant) were injected into P0 rat brains. At P21, RIM3γ knock-down cortical neurons exhibited the expected loss in arborization, while neurons expressing both shRNA and the resistant RIM3γ were undistinguishable from control neurons expressing RFP. **D,** Hippocampal neurons of P35 rats infected with lentiviral particels expressing a shRNA agianst RIM3γ together with RFP at P21 show no obvious reduction in their dendritic complexity when compared to control neurons expressing only RFP.

5.2.3 Effects of RIM3γ and RIM4γ knock-down on intracellular vesicle trafficking

Neuronal growth is strongly dependent on continuous and highly spatially and temporally regulated transport of membrane particles, cellular organelles and proteins. This enormous logistic effort is mainly provided by vesicular transport throughout the cell. Several cellular organelles are involved in the organization of the different steps of this vesicular transport. One important regulator is the Golgi apparatus, it receives newly synthesized proteins from the endoplasmic

reticulum, sorts them and sends them either directly to the plasma membrane or to the endosomal compartment, a further vesicular sorting system. Unsurprisingly, disruption of Golgi morphology has been shown to lead to growth impairments in neurons [Beffert et al., 2012, Berto et al., 2014]. To gain first insights into the question if RIM3γ and RIM4γ are involved in Golgi apparatus controlled vesicular transport, we analyzed Golgi morphology after the loss of RIM3γ and RIM4γ in primary neuronal cultures.

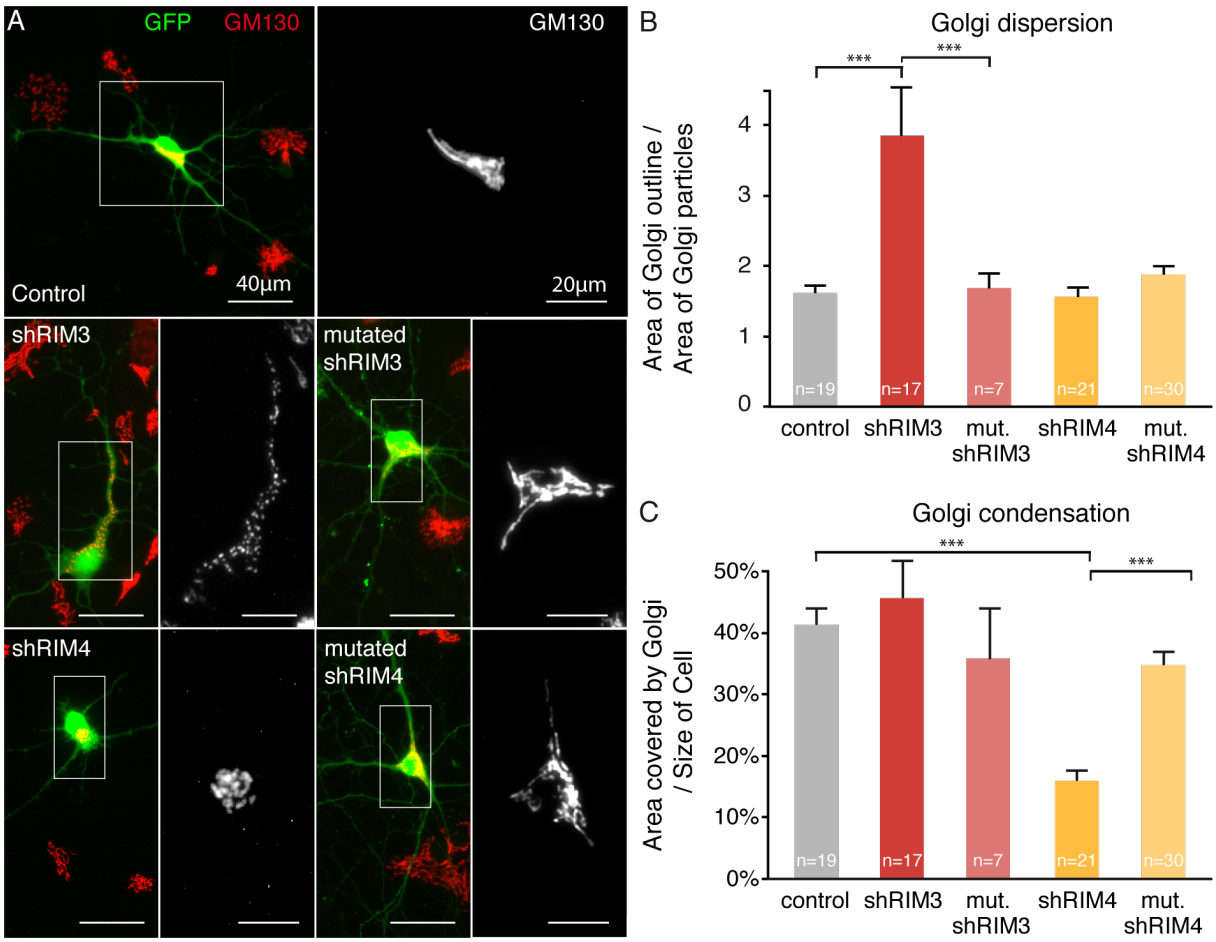

Figure 5.8: **Structural alteration of the Golgi apparatus in neurons lacking RIM3γ/4γ. A,** Confocal images of GM130 labeled cultured hippocampal neurons, transfected at DIV3 with either shRNAs against RIM3γ (shRIM3) or RIM4γ (shRIM4), or mutated variants of the both shRNAs (mut. shRIM3, mut. shRIM4), or GFP alone (control). Cells were fixed at DIV14 and stained against the Golgi marker GM130 (red). **B,** Quantification of Golgi dispersion. While Golgi dispersion in RIM4γ knock-down cells is indistinguishable from controls, RIM3γ knock-down leads to increased fragmentation and dispersion. **C,** Quantification of Golgi size shows that knock-down of RIM4γ leads to a smaller, more condensed Golgi apparatus as compared to controls. **B, C,** These structural alterations were abolished using the mutated shRNAs against RIM3γ or RIM4γ. Significance: one-way ANOVA followed by Tukey's Multiple Comparison Test, *** $p<0.0001$.

The structure of the Golgi apparatus of neurons transfected on DIV3 with either a control vector or shRNAs against RIM3γ and RIM4γ was visualized by staining with antibodies against the Golgi protein GM130. Whereas in control neurons GM130 staining revealed the typical ribbon-like structure of the Golgi apparatus, it appeared fragmented into punctate structures and dispersed throughout the cytoplasm after knock-down of RIM3γ and strongly condensed in RIM4γ knock-down neurons. Neither Golgi dispersion nor condensation was observed if non-

functional shRNAs against RIM3γ and RIM4γ with point mutations in the target sequence against the respective protein (mutated shRIM3 and mutated shRIM4) were transfected (Fig. 5.8A,B,C).

The observed changes in Golgi morphology suggest, that RIM3γ and RIM4γ play a role in neuronal growth by regulating vesicular traffic. Vesicular traffic between different sorting centers and also the plasma membrane is governed by small GTPases of the Rab protein family. Rab proteins act as 'cellular cargo address labels' marking vesicles for the specific transport routes between the different sorting centers. This makes Rab proteins ideal markers to study the vesicular transport routes in living cells. Several Rab proteins and their associated transport routes have been shown to be crucial for neuronal growth [Villarroel-Campos et al., 2014]. Three important regulators of vesicular transport during the development of neuronal arbors are Rab8, Rab11 and Rab6. Rab6 might play a role in neurite outgrowth by regulating intra-Golgi traffic and traffic from the Golgi to the plasma membrane [Schlager et al., 2010]. Rab8 is also found on vesicles of the trans-Golgi network and in addition on vesicles of the recycling endosome. Knock-down expreriments in primary neuronal cultures suggest that Rab8 is crucial for neurite outgrowth and branching [Huber et al., 1995]. Rab11 is like Rab8 found on vesicles of the recycling endosome but not present at the trans-Golgi network [Ullrich et al., 1996]. Traffic of Rab11 positive vesicles has been shown to be important for axonal and dendritic growth. In dendrites Rab11 was suggested to be involved in the cell surface expression of growth promoting receptors and thereby to locally regulate branch arborization and elongation [Lazo et al., 2013]. Because of their well established role in neuronal growth we examined if trafficking of Rab11, Rab8 and Rab6 marked vesicles is affected by the absence of RIM3γ or RIM4γ. Therefore we transfected primary neuronal cultures with shRNAs against RIM3γ and RIM4γ in combination with a plasmid expressing either Rab11, Rab8 or Rab6 fused to GFP at DIV3. On DIV7 axonal traffic of vesicles carrying Rab11, Rab8 and Rab6 vesicles was analyzed by time lapse imaging for 10 minutes with a frame rate of 10 seconds (Fig. 5.9A). For quantification the vesicles were tracked manually through the obtained videos of 10 minutes and analyzed in regard to their velocity, path length and fraction of moving and non-moving vesicles. The quantification revealed that the knock-down of RIM3γ and RIM4γ impairs transport routes of Rab8 and Rab11 positive vesicles whereas Rab6 vesicle traffic was not significantly changed. The knock-down of RIM3γ affected Rab8 and Rab11 transport routes with a decrease in the path length of both vesicle fractions (Fig. 5.9B). The knock-down of RIM4γ had a broader effect as it reduced the path length and velocity of Rab11 vesicles and changed the number of moving vesicles of Rab8 and Rab11 vesicular transport routes with an increase in Rab11 moving vesicles and a decrease in Rab8 moving vesicles (Fig. 5.9B,C,D). The number of immobile vesicles was unchanged in all conditions (Fig. 5.9E).

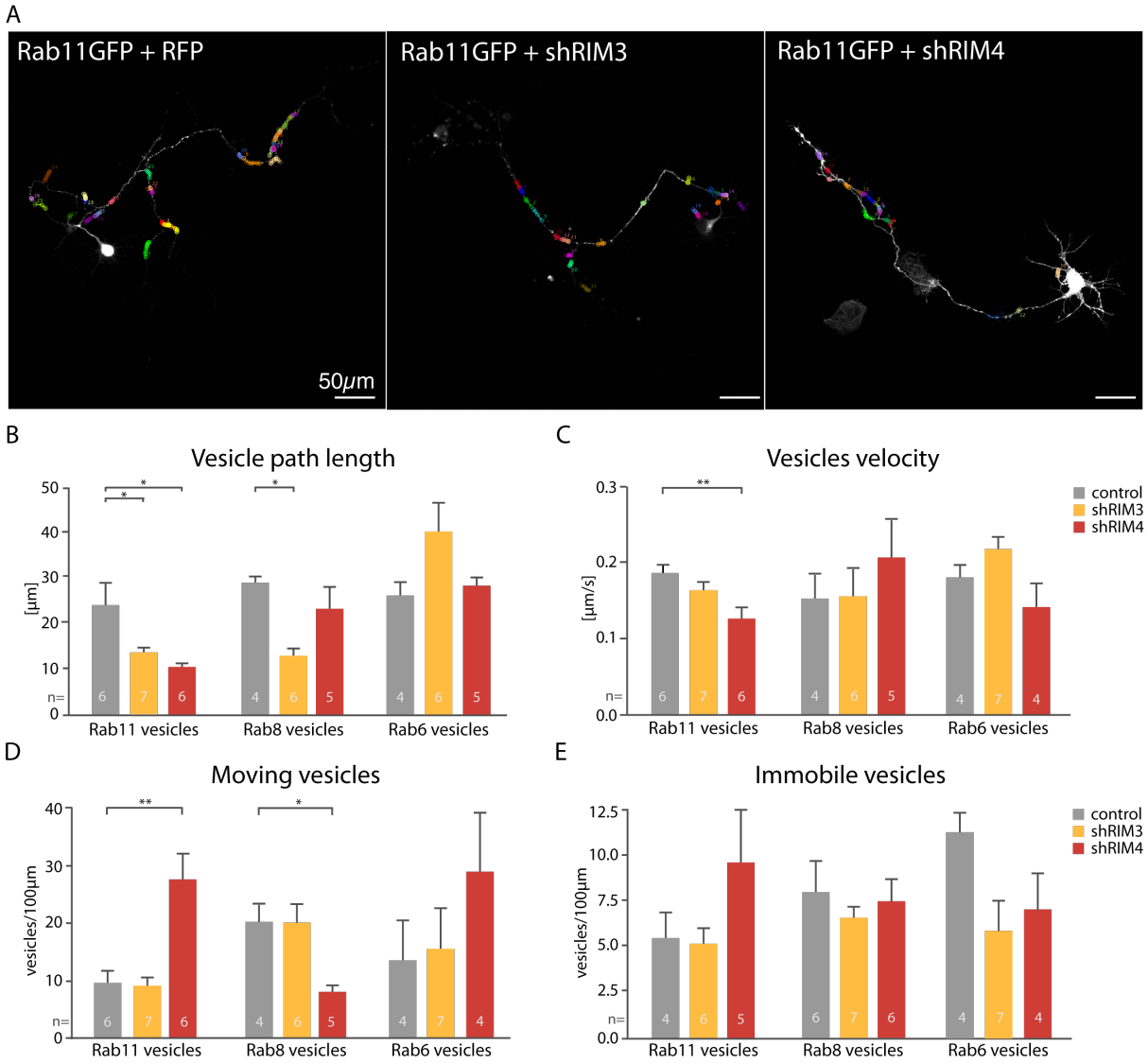

Figure 5.9: **Changed Rab11 and Rab8 vesicle dynamics after the knock-down of RIM3γ and RIM4γ.** GFP tagged Rab11, Rab8 and Rab6 constructs were coexpressed in rat primary cortical neurons together with shRNAs against RIM3/4γ and RFP or RFP alone as control. After live cell imaging at DIV7 path length, velocity and fractions of moving and non-moving of Rab6, Rab8 and Rab11 vesicles were analyzed. **A,** Exemplar stacks of confocal images (imaged every 10 sec over 10 minutes) of cortical neurons transfected with Rab11 GFP together with RFP or the respective shRNA (shRIM3, shRIM4) and RFP overlaid with manual tracks of vesicles over a time periode of 10 minutes with a frame rate of 10 seconds. **B,** Quantification of vesicle path length. **C,** Quantification of vesicle velocity. **D,** Quantification of the fraction of moving vesicles per 100µm during a 10 minutes interval. **E,** Quantification of vesicles that remained a the same position (non-moving vesicles) during 10 minutes imaging per 100µm. Significance: one-way ANOVA followed by Bonferoni post test * p> 0,05 ** p<0.001; n=number of cells.

Taken together, the knock-down of both γ-RIMs drastically decreases neuronal growth in early developmental stages, affecting dendritic and axonal growth and synapse development. Additionally, the loss of RIM3γ and RIM4γ impairs Golgi morphology and also vesicular transport of Rab11 and Rab8 vesicles. This suggest that the small γ-RIMs have a general growth promoting function during the establishment of neuronal arbors, possibly by regulating vesicular transport routes. The isofrom specific changes in Golgi morphology and Rab11 and Rab8 vesicle transport imply, that RIM3γ and RIM4γ are either involved in intracellular traffic at different steps or

have additional isoform specific functions.

5.3 Identification of novel γ-RIM binding partners

Protein interactions are the fundament of signal transduction in cells. Signaling cascades of protein interactions govern all cellular processes form DNA transcription and protein translation to cellular growth and movement as well as cell specific functions like propagation of vesicle fusion and regulated secretion of signaling molecules, hormones and neurotransmitters. In order to elucidate the function of a protein it is important to know its interaction partners and the signaling pathways in which the protein participates. To date very little is known about molecular interaction partners of RIM3γ and RIM4γ. The high sequence homology between the C_2B domain of RIM3γ and RIM4γ and all other RIM proteins suggests that the small γ-RIMs might have common interaction partners with RIM1/2. Consistently it was shown, that RIM3γ and RIM4γ like the large RIM proteins bind to Liprins and the β-subunit of voltage-gated Ca^{2+}channels [Wang & Südhof, 2003, Uriu et al., 2010]. However, these suggested interaction rather indicate a synaptic function than explaining the role of RIM3γ and RIM4γ in neuronal arborization.

5.3.1 Proteomics: affinity purification - mass spectrometry screen for novel interaction partners

The identification of new γ-RIM specific interaction partners might help to understand their role in neuronal arborization and to elucidate further γ-RIM functions in the cell. Analysis of purified protein complexes by mass spectrometry is a well established approach to identify new interaction partners of a protein. The stability of protein interactions can differ depending on the presence of cofactors, post translational protein modifications and secondary interactions with other proteins. Therefore the results of a mass spectrometry proteomic approach can show a high variation depending on the exact experimental conditions. Taking this into account we performed multiple independent mass spectrometry experiments with differing experimental conditions to identify robust but also transient protein interaction partners of RIM3γ and RIM4γ.

5.3.1.1 Affinity purification - mass spectrometry of whole brain fractions and crude synaptosomal fractions

The brain is composed of multiple different cell types like neurons, astrocytes, oligodendrocytes, microglia and endothelial cells. Each cell type expresses a specific set of proteins which defines their cellular identity. Homogenates of whole brain fractions contain this large variety of proteins found in the brain and thus also all RIM3γ and RIM4γ interaction partners. However, the great variety of proteins makes it difficult to detect interaction partners that are present in the brain at only very low amounts. Therefore, we performed a mass spectrometry approach of the whole brain fraction to identify interaction partners of all cellular compartments of a neuron and of the crude synaptosomal fraction to identify interactions with less abundant synaptic proteins. In a first approach expression plasmids of RIM3γ and RIM4γ fused to a GFP-biotin affinity tag were generated and overexpressed in HEK293T cells. The overexpressed bait proteins were purified via their biotin tag and incubated with whole mouse brain homogenates solubilized with Triton X-100, allowing the formation of RIM3γ and RIM4γ protein complexes. After the

incubation step RIM3γ and RIM4γ and their bound interaction partners were again purified via the biotin tag. The bound proteins were separated according to their molecular weight by gel electrophoresis and subsequently digested with trypsin into short peptides, which were analyzed by mass spectrometry. To control for unspecific binding to the GFP-biotin affinity tag we performed the same experiment with only GFP-biotin. As an additional control the C_2A-C_2B domain of RIM1 was included in the experiment to reduce the background of proteins showing a general affinity to C_2 domains and detect γ-RIM specific interactions (Fig. 5.10A). In our second screen for RIM3γ and RIM4γ interaction partners we tried to increase the amount of neuron specific proteins, especially synaptic proteins, by using purified synaptosomal fractions solubilized with CL114. Cl114 is a detergent of unknown composition, which is able to solubilize the Triton-X 100 resistant cytomatrix of the active zone. To reduce unspecific bindings to the bait proteins streptavidin-flag affinity tag (TAP) overexpression plasmids were used instead of the larger GFP-biotion tag of the first experiment (Fig 5.10B).

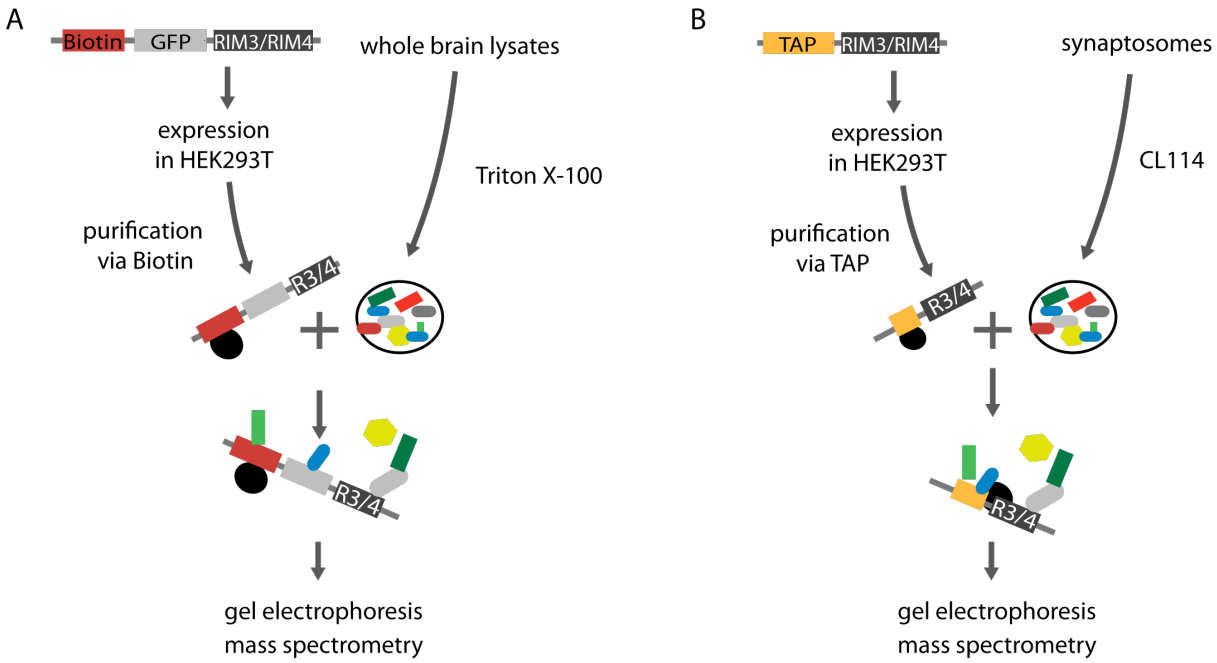

Figure 5.10: **Affinity purification - mass spectrometry experimental flow. A,** Screen for RIM3γ and RIM4γ interaction partners in whole mouse brain fractions: GFP-biotin labeled RIM3γ, RIM4γ, RIM1 C2A-C2B-domains or only GFP-biotin were overexpressed in HEK293T cells, purified via the biotin tag and incubated with Triton X-100 solubilized whole mouse brain homogenates. Bait proteins and bound interaction partners were purified again via the biotin tag. The purified protein complexes were separated by gel electrophoresis and analyzed by mass spectrometry. **B,** Screen for RIM3γ and RIM4γ in crude synaptosomal fractions: streptavidin-flag (TAP) tagged RIM3γ, RIM4γ, RIM1 C2A-C2B-domains or only streptavidin-flag were overexpressed in HEK293T cells, purified via the flag sequence and incubated with CL114 solubilized crude synaptosomal fractions. Bait proteins and bound interaction partners were purified again via the Flag tag. The purified protein complexes were separated by gel electrophoresis and analyzed by mass spectrometry.

The mass spectrometer is able to resolve the amino acid sequences of the digested peptides. These peptide sequences are compared with protein databases to identify the composition of the analyzed protein complex. The obtained results can be displayed in different values characterizing the probability of the identified protein to be present in the sample. The peptide number corresponds to the numbers of identified peptides from one protein and determines the sequence

coverage of the protein. Peptide spectrum matches (PSM) are the number of mass spectrometer spectra, which can be related to one protein. The protein score is composed of the number and probability of peptide identifications corresponding to one single protein. To eliminate proteins bound to the beads or the affinity tag of bait proteins we subtracted proteins that were as well found in mass spectrometry data of the control reactions (GFP-biotin, steptavidin-flag). Proteins which were detected in control and γ-RIM binding reactions but had more than a twofold higher protein score in the datasets of RIM3γ or RIM4γ were still taken into account. Furthermore, we excluded proteins from our analysis that were also present in the mass spectrometry data of RIM1 C_2A-C_2B-domains binding reactions. This approach lead to the identification of 50 potential novel RIM3γ interaction partners and 44 novel RIM4γ interaction partners in whole brain fractions, whereby 38 of these proteins were found in the data sets of both proteins (see appendix table 8.1). The great overlap of both data sets suggests that the γ-RIMs have shared functions, this is consistent with the observed growth deficit after the knockdown of RIM3γ as well as RIM4γ. The novel binding partners were grouped into functional categories by literature research. The largest groups of identified proteins from whole brain homogenate could be associated to signaling cascades related to growth and neuronal development (22-20%), adhesion molecules (21-18%), proteins involved in intracellular traffic (16-21%) and cytoskeletal proteins (16-17%) (Fig 5.11A). These functional categories were represented in RIM3γ and RIM4γ data sets to similar amounts whereby cytoskeletal proteins were more abundant in the data of RIM4γ. The novel RIM3γ and RIM4γ interaction partners overlapped mostly in the groups of intracellular vesicle and protein traffic with 100% overlap. In lower amounts we found synaptic proteins and two channel proteins. As specific interaction partners of RIM3γ we could identify nuclear proteins like importins and the two calcium binding proteins reticulocalbin1 and 2 in whole brain fractions (Fig 5.11A, appendix 8.1). Importins are nuclear import receptors; they recognize nuclear localization signals of target proteins and initiate their transport into the nucleus. The sequence of RIM3γ compromises such a nuclear localization signal and is actively transported into the nucleus (chapter 5.1). Thus the identified importins might mediate the nuclear translocation of RIM3γ. The relatively low amount of synaptic proteins with only 10-6,5% could be on the one hand due to a low level of synaptic proteins in the used whole brain fractions. On the other hand the whole brain fractions were solubilized with the detergent Triton X-100, a detergent that is not able to break up the tight cytomatrix of the presynaptic active zone leading again to lower levels of active zone specific protein in the whole brain fraction.

Proteins identified from the synaptosomal homogenate were analyzed in the same manner as described above. Percentages of identified protein categories reveal that the use of crude synaptosomal fractions drastically increased the amount of synaptic interaction partners. Additionally the second experimental strategy strongly reduced the amount of proteins identified as shared interaction partners of RIM3γ and RIM4γ and revealed a larger fraction of RIM3γ or RIM4γ specific binding proteins. In this second screen we identified 74 novel RIM3γ interaction partners and 34 novel RIM4γ interaction partners, of theses 98 proteins only 9 were found in the data sets of RIM3γ and RIM4γ (see appendix table 8.2). Grouping of the novel interaction partners into functional categories upon literature research revealed as largest group synaptic proteins

(18-26,4%) followed by cytoskeletal proteins (12-23,5%) and proteins involved in intracellular traffic (31-22%). In lower amounts we found adhesion molecules (5,5- 14,7%), channel proteins (18-6%) and nuclear proteins (13-6%) (Fig 5.11B).

Figure 5.11: **Functional categories of novel interaction partners suggest a role in vesicular traffic and remodeling of the cytoskeleton. A,B,** First 3 columns show categories and percentages of proteins identified as novel interaction partners of RIM3γ (yellow), of RIM4γ (orange) and shared γ-RIM binding partners (grey). The last column represents all detected proteins: grey represents the proteins found in the data sets of RIM3γ and RIM4γ, yellow RIM3γ specific proteins and red RIM4γ specific proteins. **A,** Proteins detected in whole brain homogenates solubilized with Triton X-100. **B,** Proteins identified in crude synaptosomal fractions solubilized with Cl114.

As RIM3γ specific interaction partners we could again identify one member of the importin family and the calcium binding protein reticulocalbin 2. The composition of the identified func-

tional categories supports that the small γ-RIMs might have a functional role at the synapse and an additional role in the promotion of neuronal growth by regulating intracellular traffic and the remodeling of the cytoskeleton. According to literature research we selected a subset of proteins from the whole set of novel RIM3γ and RIM4γ interaction partners that had a high protein score and additionally seemed to be promising candidates to be involved the molecular mechanism underlying the function of RIM3γ and RIM4γ in neuronal growth. These most promising candidates are listed in the table below (table 5.1). Variations in the calibration of the mass spectrometer can cause high variations in the protein scores of identified proteins explaining the much lower values in the second experiment. In whole mouse brain homogenates we found the adhesion molecules δ-catenin, plakophilin2 and plakophilin4 with relatively high protein scores. These proteins belong to a subfamily of armadillo repeat proteins that has been associated with the regulation of dendritic growth possibly by an involvement in the remodeling of the cytoskeleton [Elia et al., 2006, Keil & Hatzfeld, 2013]. In the synaptosomal fraction we only detected the more distantly related armadillo repeat protein 3. In both tissue fractions a large group of proteins involved in intracellular protein and vesicle transport was identified. Interesting candidates that might explain the function of RIM3γ and RIM4γ in neuronal growth and also the changes in Golgi morphology in RIM3γ and RIM4γ knock-down neurons are members of the Exocyst complex. The Exocyst complex is involved in the site directed fusion of several vesicular transport routes ensuring the correct delivery of vesicular cargos to the correct fusion site. In whole brain homogenates we identified Exocyst complex component 1 (sec3) and Exocyst complex component 4 (sec8) as novel binding partners of both γ-RIMs and in crude synaptosomes Exocyst complex component 3 (sec6) as RIM3γ interacting protein. Further important regulators of intracellular vesicular traffic are Rab proteins. In accordance to the observed changes in intracellular traffic of Rab marked vesicles after the knock-down of RIM3γ and RIM4γ we found various Rab proteins in the synaptosomal fractions. The correct remodeling of the cytoskeleton is a crucial mechanism during neuronal growth. From synaptosomes and the whole brain fraction we could identify two members of the IQGAP family. IQGAPs are involved in the crosstalk between actin and microtubules and have been shown to play an important role in the development of axons and dendrites. As further cytoskeleton regulating proteins we identified the CDC42 effector protein 1 in whole brain fractions as interaction partner of RIM4γ and the CDC42 effector protein 5 as interaction partner of RIM3γ. Synaptic proteins were mainly detected in the synaptosomal fractions. One interesting candidate detected in whole brain fractions is the synapse defective protein Syd-1. Syd-1 is involved in the early stage of synapse assembly and contributes to the recruitment of the RIM binding partner Liprin-α to the active zone [Owald et al., 2012]. Syd-1 was not found in synaptosomal fractions however several other members of the active zone like RIM1, the large scaffolding proteins Bassoon and piccolo and proteins of the SNARE complex for instance SNAP25. Importins were identified in both screens as specific interaction partners of RIM3γ. Protein interactions resolved in a proteomics approach might not always be primary interactions but can also be secondary and tertiary interactions, this depends strongly on the sensitivity of the protein interaction to the experimental conditions like protein abundance in the used tissue fraction, composition of the used buffers and sensitivity to trypsin digestion. Therefore the overlapping patterns of protein

categories can already give an idea in which cellular functions RIM3γ and RIM4γ might be involved. Further it has to be taken into account that peptides of trypsin-digested proteins show different protein specificity, depending on the sequence homology of for example different members of the same protein family. Thus a peptide with a relatively low specificity could be correlated with several protein family members. Taken together the large fraction of proteins directly involved in neuronal growth or in cellular processes underlying neuronal growth support a functional role of RIM3γ and RIM4γ in neuronal development, whereby the composition of the functional categories of the identified binding partners differed among both γ-RIMs. This suggests that RIM3γ and RIM4γ have isoform specific function and might contribute differentially to growth regulating processes. The identified synaptic proteins propose an additional synaptic function in accordance to the presynaptic role of the large RIM proteins.

gene ID	identified protein	protein score RIM3γ		protein score RIM4γ	
		whole brain	synaptosomes	whole brain	synaptosomes
Adhesion molecules					
70882	Armadillo repeat-containing protein 3				34
1500	Catenin (cadherin-associated protein), delta 1	502		285	
5318	Plakophilin2			769	
8502	Plakophilin4	129		442	
Intracellular protein and vesicle traffic					
55763	Exocyst complex component 1 (Sec3)	491		164	
211446	Exocyst complex component 3 (Sec 6)		35		
60412	Exocyst complex component 4 (Sec8)	404		291	
104886	Ras-related protein Rab-15		31		
19338	Ras-related protein Rab-33B		57		
270160	Ras-related protein Rab-39A		19		19
67295	Ras-related protein Rab-3C		57		
19341	Ras-related protein Rab-4A		57		

19346	Ras-related protein Rab-6A		57		
cytoskeletal and cytoskeleton regulating proteins					
11135	CDC42 effector protein (RhO GTPase binding) 1			484	
58804	Cdc42 effector protein 5		30		
10788	Ras GTPase-activating-like protein IQGAP2				32
128239	IQ motif containing GTPase activating protein 3 (IQGAP3)	158		603	
synaptic proteins					
12217	Bassoon		35		37
26875	Piccolo		30		
116837	Regulating synaptic membrane exocytosis protein 1		68		121
85360	Synapse defective 1, Rho GTPase, homolog 1 (syd-1)	246			
20614	Synaptosomal-associated protein 25		51		
nuclear proteins					
79711	Importin 4	150			
3843	Importin 5	188			
10526	Importin 8	119			
76582	Importin-11		33		
Calcium binding proteins					
5954	Reticulocalbin 1, EF-hand calcium binding domain	658			
26611	Reticulocalbin-2	396	88		

Table 5.1: Novel RIM3 and RIM4 interaction partners repeatedly identified in whole brain and synaptsomal fractions.(Protein score= the number and probability of peptide identifications corresponding to one single protein)

5.3.1.2 Comparative mass spectrometry analysis of RIM3γ and RIM4γ binding partners in whole brain and crude synaptosomal fractions

The experimental conditions of the two above described proteomic approaches, did not only differ in the used tissue fractions, detergents and purification tags of bait proteins but also in the used mass spectrometers. To obtain more comparable results, which only differ in the cellular fraction and in the used detergents we repeated the experiment in a combined approach. In this experimental strategy we combined a search for novel interaction partners in whole brain fraction solubilized with Triton X-100, crude synaptosomes solubilized with Triton X-100 and crude synaptosomes lysed with the detergent CL114. All tissue samples were obtained from one brain preparation to exclude variations within the tissue fractions. Bait proteins (streptavindin-flag tagged RIM3γ and RIM4γ) used for the binding reactions with the three protein homogenates were purified from one batch of HEK cells to ensure the same amount of bait protein in all experiments. After incubation of the flag purified bait proteins with the different tissue homogenates protein complexes were purified via the flag tag and separated by gel electrophoresis on the same gel. Also the trypsin digestion of all samples was carried out in one experimental procedure before peptides were analyzed by LC-MS/MS (Liquid chromatography–mass spectrometry-mass spectrometry) (Fig 5.12A). After analysis of the mass spectrometry data by literature research and subtraction of unspecific binding partners as described above (5.3.3.1) we grouped identified proteins of each binding reaction in the functional categories cytoskeleton regulating proteins, kinase and phosphatases, transcriptional proteins and nuclear proteins, proteasomal proteins, synaptic proteins, channel proteins, Ca^{2+}-sensors and adhesion molecules.

The percental distribution in functional categories revealed similar results for the whole brain fraction and synaptosomes lysed with Cl114 regarding cytoskeletal proteins and proteins involved in intracellular traffic. Synaptosomes lysed with Triton X-100 however revealed only a small percentage of cytoskletal proteins and proteins involved in intracellular traffic. Overall we found only a small fraction of synaptic proteins in synaptosomes and whole brain homogenates, whereby the use of the detergent Cl114 slightly increased the amount of this group in the crude synaptosomal fractions (Fig 5.12A-C, appendix table 8.3). In this combinatory screen for novel γ-RIM interaction partners we could not exactly reproduce the results of he first two experiments, however a comparison of the identified proteins in all experiments reveals several protein complexes or protein families that were found in multiple experiments. We could repeatedly identify cyclin dependent kinases, calcium/calmodulin dependent kinases, IQGAP proteins, CDC42 effector proteins, Fascins, microtubule associated proteins, kinesins, members of the Exocyst complex, GIT1, rab proteins, Ephrin receptors, synaptosomal associated proteins, synaptogyrins, synaptotagmin, synapsin, voltage dependent anion channels, importins and reticulocalbins (see appendix table 8.4 for details). The repeated identification of these protein families proposes strongly that they might indeed interact with RIM3γ and RIM4γ *in vivo*. Furthermore, the proteins detected in several experiments were associated with the functional categories adhesion molecules, intracellular traffic, cytoskeleton, synaptic proteins and nuclear proteins.

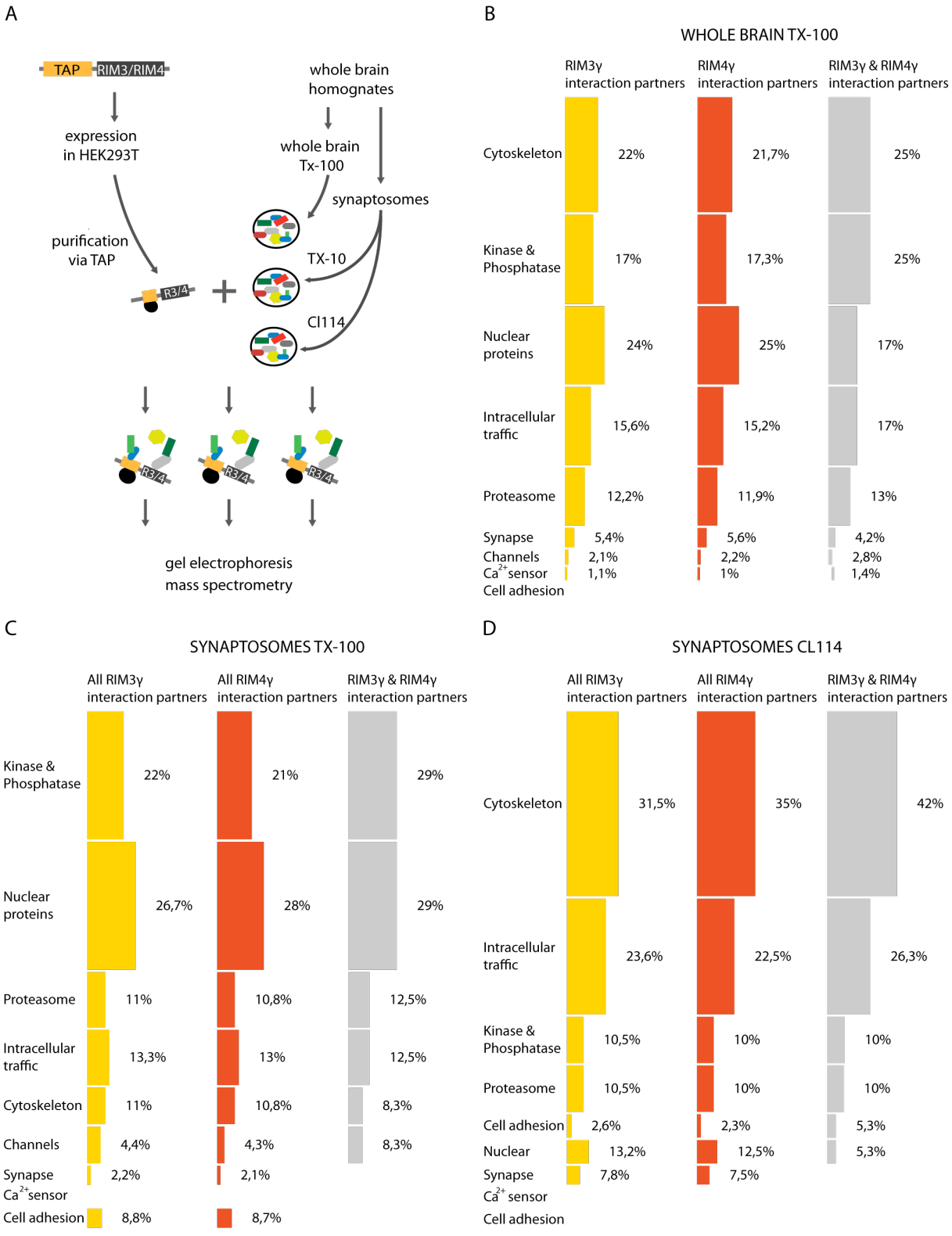

Figure 5.12: **Results of combinatory mass spectrometry approach. A,** Experimental strategy: RIM3γ and RIM4γ fused to a streptavidin-flag tag (TAP) were overexpressed in HEK 293T cells and incubated with whole brain homogenates solubilized with Triton X-100, synaptosomal fractions solubilized with Triton X-100, synaptosomal fractions solubilized with CL114. All cell lysates were obtained from one tissue preparation. After the incubation step the formed protein complexes were purified via the flag tag of the bait proteins and further analyzed by gel electrophoresis and mass spectrometry. **B,** Functional categories and percentages of potential RIM3γ and RIM4γ interaction partners detected in lysates of whole brain homogenates, **C,** proteins identified in synapsomal fractions lysed with Triton X-100, **D,** proteins identified in synaptosomal fractions lysed with CL114.

These categories were most prominent in all screens for novel γ-RIM interaction partners, suggesting that these novel interactions might have functional relevance in the molecular mechanism underlying the growth promoting effect of RIM3γ and RIM4γ. In the last combinatory affinity purification mass spectrometry experiment we identified a large number of kinases. To get first insight in the question if a phosphorylation by these kinases might have a physiological relevance we performed a bioinformatic search for phosphorylation sites in the amino acid sequences of RIM3γ and RIM4γ. This analysis revealed a phosphorylation sites in the sequence of both γ-RIMs by the repeatedly identified kinases Cyclin dependent kinase 5 (CDK5) and Calcium calmodulin dependent kinase 2 (CAMKII) (table 5.2).

RIM3γ		
Kinase	**Site**	**Sequence**
CAMKII	S104	SRVTRQGSRESTDGS
CAMKII	L298	RRLSQSSLESATSPS
CDK5	T181	VIEARGLTPKPGSKS
RIM4γ		
Kinase	**Site**	**Sequence**
CAMKII	S63	SRTLRQASHESIEDS
CAMKII	S254	GPLLRQASQLSLEST
CDK5	S190	QVLLFPESPQGKVLQ

Table 5.2: In affinity-purification mass spectrometry screen for novel -RIM interaction partners identified kinases and predicted binding sites (http://scansite.mit.edu/).

Taken together, besides a general variation in the results of individual experiments we were able to reproduce the results regarding functional categories and even to identify a cluster of proteins that are promising candidates to understand the cellular function of RIM3γ and RIM4γ repeatedly in multiple experiments. In addition by changing the tissue fraction and detergent properties we were able to increase the amount of potential synaptic interaction partners.

5.3.2 Analysis of potential novel γ-RIM binding proteins

5.3.2.1 The adhesion molecule plakophilin4

Plakophilin4 was identified as potential interaction partner of RIM3γ and RIM4γ in the first proteomic approach performed with Triton X-100 solubilized whole mouse brain homogenates. Plakophilin4 also known as P0071 belongs to a subfamily of armadillo repeat proteins composed of p120catenin, δ-catenin/NPRAP, ARVCF and the more distantly related plakophilins1-3. Armadillo repeat proteins, are characterized by a central domain of a series of approximately 40 - 45 amino acid long repeated sequence motifs, called arm-repeats. This sequence repeats built the scaffold for various protein interactions, which allow armadillo repeat proteins the involvement in several cellular processes like intracellular signaling, cell adhesion and cytoskeletal remodeling [Peifer & McCrea, 1992]. Plakophilin4 and related proteins were first identified as components of

adherens junctions, where they cluster and stabilize cadherins and control thereby intercellular adhesions. In addition to this local function at the plasma membrane plakophilins have been shown to be present in the cytosol, where they are involved in the regulation of RhO GTPases during several cellular processes like cell motility, cell division and neurite outgrowth [Elia et al., 2006, Kim et al., 2007, Martinez et al., 2003].

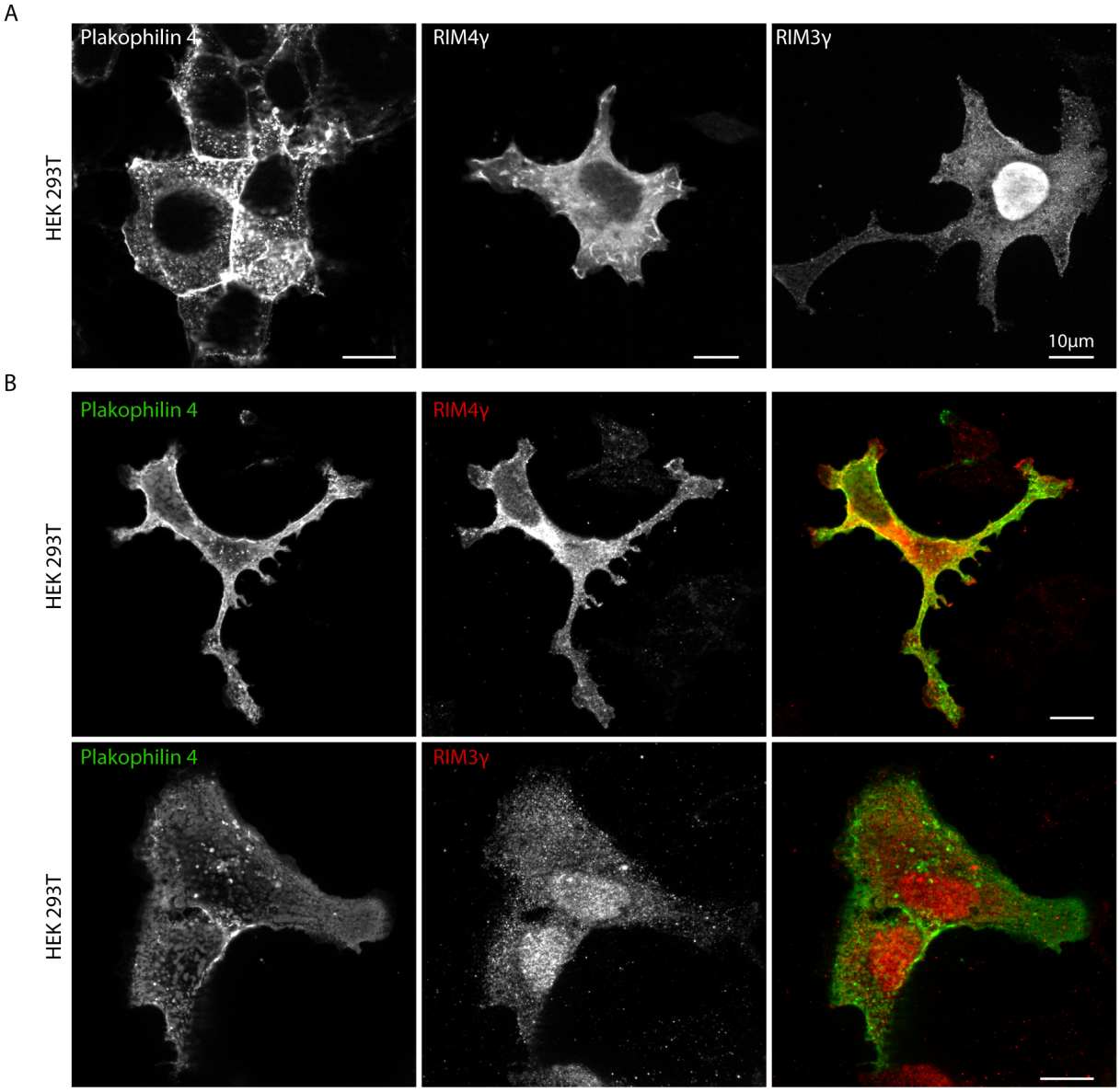

Figure 5.13: **Plakophilin4 is present in the same cellular compartments as RIM3γ and RIM4γ in HEK293T cells. A,** overexpression of plakophilin4, RIM3γ and RIM4γ fused to GFP in HEK293T cells show the specific expression patterns of the three proteins. All proteins show a diffuse cytosolic expression. Aditionally plakophilin4 is enriched at the plasma membrane, RIM3γ is in the nucleus and RIM4γ to lamelipodia of the cell. **B,** HEK293T cells were transfected with plakophilin4 fused to GFP together with either RIM3γ and RIM4γ. Antibody stainings against RIM3γ and RIM4γ two days after transfection reveal that all three proteins reside in the cytoplasm and do not alter the localization of each other.

Plakophilin4 is most closely related to δ-catenin and shows like δ-catenin a high expression level in neuronal tissue. δ -catenin is involved in the regulation of dendritic morphology and dendritic spine number by is interaction with RhoGTPases [Kim et al., 2007, Martinez et al., 2003]. A

specific function of plakophilin4 in neuronal growth was not shown yet however a screen for interaction partners of plakophilin4 revealed a high number of cytoskeletal proteins and also a large fraction of proteins involved in vesicular and intercellular traffic [Keil & Hatzfeld, 2013, Keil et al., 2013]. The identified interaction partners suggest that plakophilin4 like δ -catenin plays an important role in neuronal outgrowth and makes it to an interesting potential γ-RIM interaction partner, which might help to elucidate the specific function of RIM3γ and RIM4γ in neuronal growth. As a first step to examine if RIM3γ and RIM4γ interact in vivo we tested in human embryonic kidney cells (HEK293T) if their subcellular localization is altered by the coexpression of plakopilin4 in the same cell and if they are present in the same subcellular compartments. The overexpression of only plakophilin4-GFP revealed an enrichment of plakophilin4 at the plasma membrane and a diffuse cytsosolic distribution. γ-RIMs fused to GFP exhibit diffuse expression in the cytoplasm of HEK 293T cells. RIM3γ is additionally enriched in the nucleus whereas RIM4γ localizes to lamelipodia (Fig 5.13 A). After overexpression of plakophilin4-GFP together with either RIM3γ or RIM4γ and antibody stainings against RIM3γ and RIM4γ a colocalization was mainly observed in the cytosol (Fig 5.13 B). The potential interaction between plakophilin4 with RIM3γ or RIM4γ was further characterized *in vitro* by co-immunoprecipitation. RIM3γ and RIM4γ fused to a flag-streptavidin affinity purification tag (TAP) were coexpressed in HEK293T cells together with plakophilin4 fused to GFP. After 48 hours the cells were lysed and RIM3γ-TAP and RIM4γ-TAP together with bound partners were purified via their flag tag. The purified protein complexes were seperated by gel electrophoresis and analyzed by western blotting (Fig 5.14A).

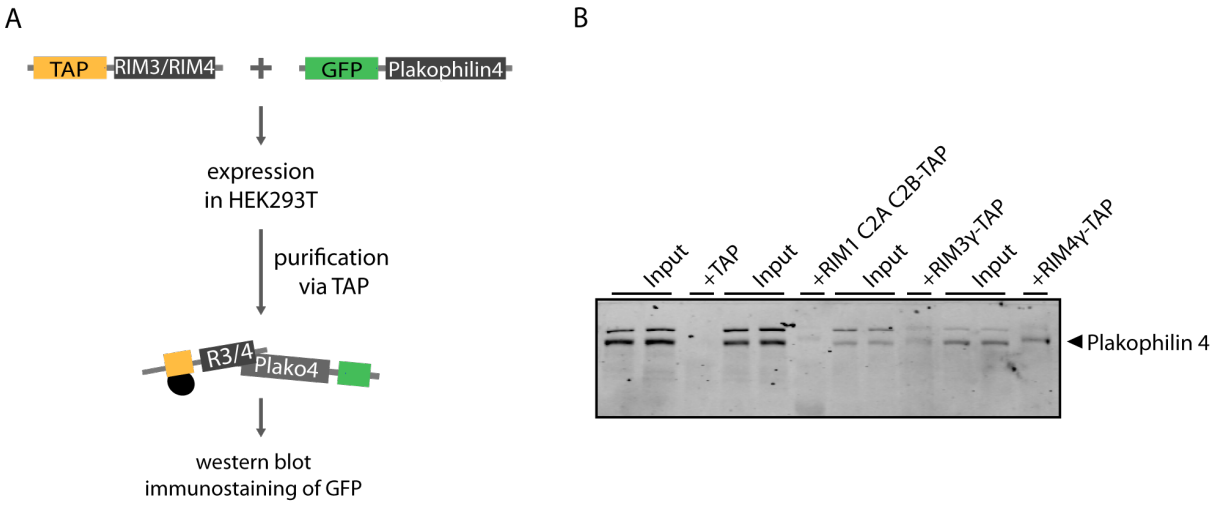

Figure 5.14: ***In vitro* binding of plakophilin4 to RIM3γ and RIM4γ. A,** Co-immunoprecipitation (Co-IP) experimental procedure: RIM3γ and RIM4γ fused to a streptavidin-flag affinity tag (TAP) were coexpressed with plakophilin4–GFP in HEK293Tcells. After cell lysis the formed protein complexes were purified via the flag tag of RIM3γ and RIM4γ and separated by gel electrophoresis. A positive binding was detected on the western blot by immunostaining against GFP. **B,** Immunoblotting of Co-IP reveals an *in vitro* binding of plakophilin4 to RIM3γ and RIM4γ and no binding to both controls (TAP and RIM1 C2A-C2B-domain-TAP). Number of individual experiments n=2.

Plakophillin4-GFP was detected on the western blot by antibody staining against the GFP tag. To control for unspecific binding the experiment was performed with only the TAP tag alone

and to control for a general binding affinity of plakophilin4 for C_2 domains with the RIM1-C_2A-C_2B-domains fused to TAP. Both control reactions were negative, whereas binding reactions of plakophilin4 and RIM3γ and RIM4γ revealed a plakophilin4 specific band on the western blot (Fig 5.14B). Therefore, the results of the co-immunoprecipitation support the identification of plakophilin4 as novel γRIM binding partner.

5.3.2.2 The cytoskeleton regulator IQGAP3

The correct interplay between actin and microtubules is one important aspect during initial neuronal growth but also later when neurons grow in response to external and internal signaling cascades. In our mass spectrometry approach we found IQGAP3, a protein, which has been shown to regulate the cross talk between microtubules and actin filaments. IQGAP3 was recently shown to regulate neurite outgrowth in response to Rac1 and CDC42 signaling [Wang et al., 2007] making an interesting potential interaction partner of RIM3γ and RIM4γ. IQGAP3 belongs to the IQGAP (IQ domain-containing GTPase-Activating Protein) family consisting of IQGAP1-3. All IQGAPs posses a calponin homology domain (CHD) responsible for their interaction with actin, several IQ repeats, an IQ motif, which is associated with calcium/calmodulin and a RasGAP related domain (GRD) (Fig 5.16A). The GRD has not been shown to facilitate GTPase activity, it rather interacts directly with and stabilizes Rac1 and CDC42 [Brill et al., 1996]. This is consistent with the finding that IQGAPs function in various cellular processes by remodeling actin filaments and microtubules. Interestingly all IQGAPs have been shown to be involved in aspects of dendritic or axonal growth [Swiech et al., 2011, Wang et al., 2007].

We first tested in mouse neuroblastom cells (NG108 cells) if IQGAP3 localizes to the same cellular compartments as RIM3γ and RIM4γ which would spatially allow their interaction. After overxpression of IQGAP3-GFP in NG108 cells, IQGAP3 revealed a strong localization to the plasma membrane at growing tips of the cell and a diffuse cytosolic distribution. When IQGAP3 was coexpressed with RIM3γ and RIM4γ, all three proteins resided in the cytopplasm of NG108 cells. (Fig 5.15).

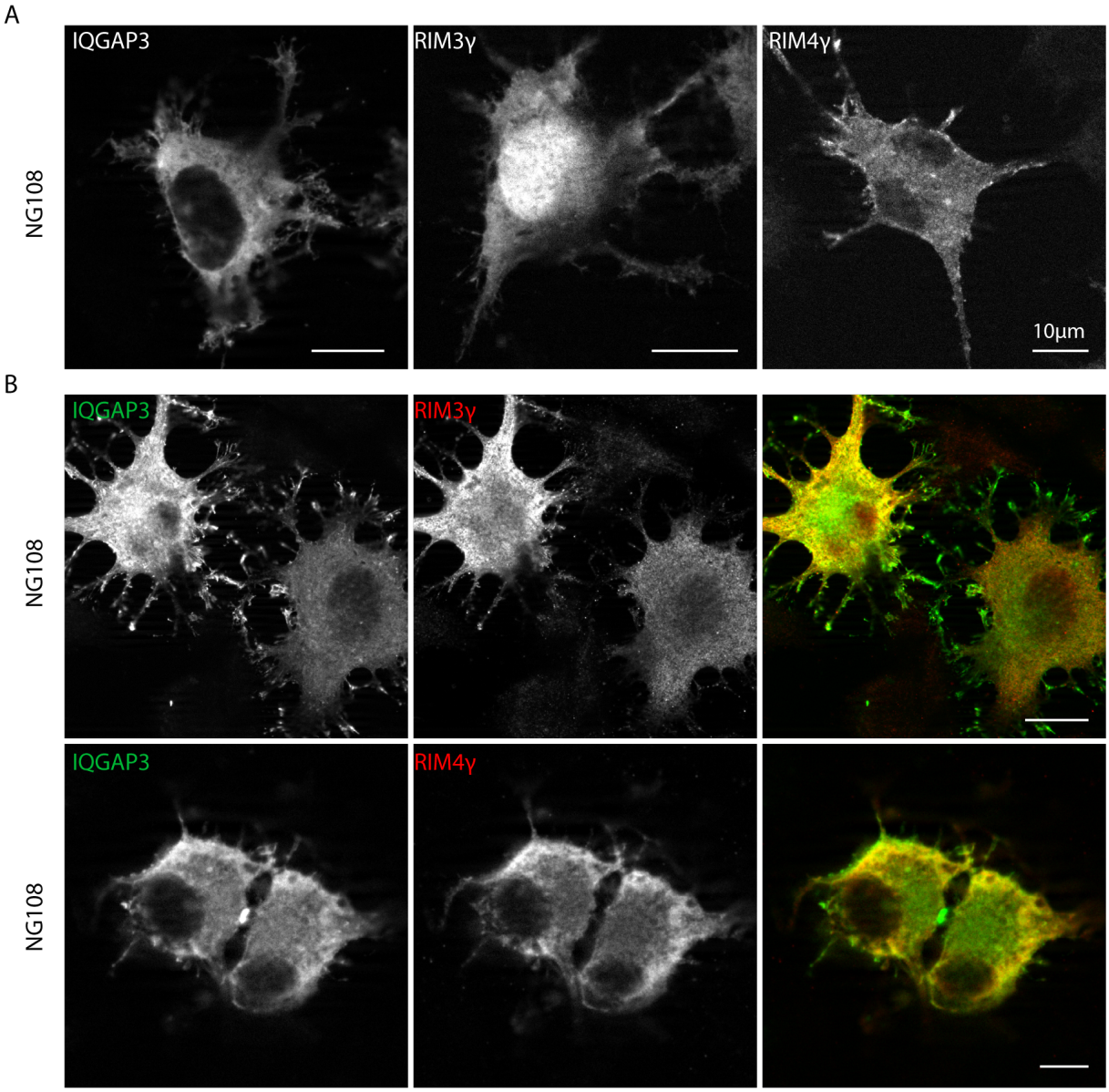

Figure 5.15: **IQGAP3 colocalizes with RIM3γ and RIM4γ in the cytoplasm of NG108 cells. A,** Overexpression of IQGAP3-GFP (left panel) in mouse neuroblastoma cells (NG108 cells) reveals a diffuse cytosolic expression in addition to an enrichment at growing tips of the cell. Middle and right panel show a diffuse distribution of RIM3γ and RIM4γ in cytoplasm after overexpression and antibody labeling. RIM3γ is in addition strongly enriched in the nucleus. **B,** Coexpression of IQGAP3-GFP and RIM3γ and RIM4γ, reveals a colocalization of IQGAP3 and the γ-RIMs in the cytosol of NG108 cells.

In a GST (glutathione-S-transferase)-pulldown assay, GST-RIM3γ and GST-RIM4γ coupled to glutathione agarose were incubated with HEK23T cell lysates expressing IQGAP3-GFP. After purification of the GST-γ-RIMs coupled to agarose beads together with their bound interaction partners, the formed protein complexes were separated by gel electrophoresis and analyzed by western blotting (Fig 5.16B). Due to the high sequence homology in the C_2B domain of all RIM protein family members the binding reaction was also performed with GST-RIM1-C_2B. To control for unspecific interactions the same binding reaction was performed with glutathione-agarose alone and only GST coupled to glutathione-agarose. Immunoblotting against GFP showed a specific binding of IQGAP3-GFP only to GST-RIM3γ, GST-RIM4γ and GST-RIM1-C_2B but not

to the controls (Fig. 5.16C). To further confirm the potential interaction between IQGAP3 and RIM proteins we performed Co-immunoprecipitaions. To this end RIM3γ, RIM4γ and RIM1-C_2A-C_2B-domains fused to an streptavidin-flag (TAP) tag were coexpressed in HEK293Tcells together with IQGAP3-GFP. The *in vivo* formed protein complexes were purified with magnetic beads coupled to antibodies against the flag sequence of the bait proteins affinity tag. After separation by gel electrophoresis and immunoblotting a positive binding was detected with antibody labeling against GFP.

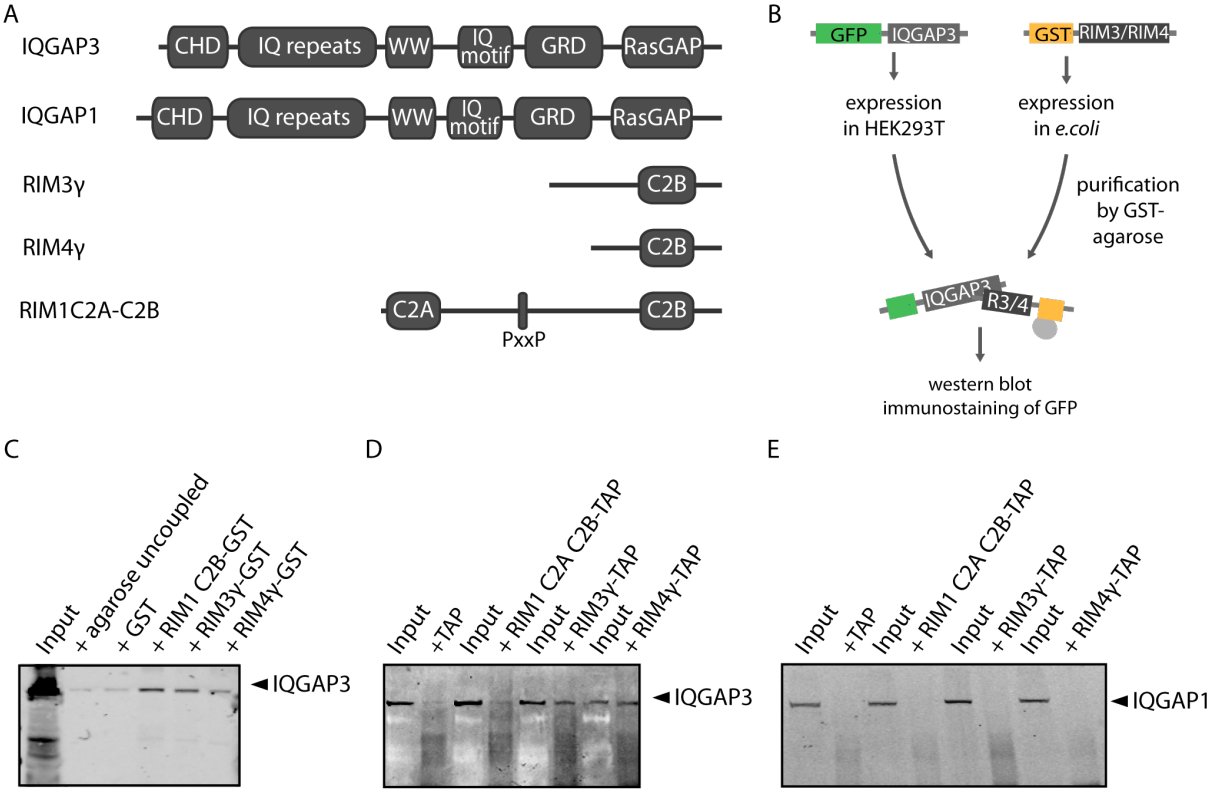

Figure 5.16: **Biochemical analysis of the potential interaction between IQGAP3 and RIM3γ and RIM4γ. A,** Protein domains of IQGAP3, IQGAP1 and the tested interaction partners RIM3γ, RIM4γ and the C2A-C2B domain of RIM1. **B,** Schematic representation of GST-pulldown assays: RIM3γ–GST and RIM4γ–GST were expressed in *e. coli* and purified via coupling to glutathione-agarose. HEK293T cell lysates expressing IQGAP3-GFP were incubated with the purified agarose coupled γ-RIMs. Protein complexes were analyzed by gel electrophoresis and western blot. **C,** GST-pulldown assay with IQGAP3-GFP reveals a binding of IQGAP3 to GST-RIM3γ, GST-RIM4γ and GST-RIM1 C2B-domain whereas the control reactions with uncoupled agarose and GST-agarose do not show a signal. Number of individual experiments n=3. **D,** Co-immunprecipitaion of RIM3γ-streptavidin-flag (TAP), RIM4γ-TAP and RIM1 C2A-C2B-domain-TAP and IQGAP3-GFP with magnetic beads coupled to a flag antibodies further confirm a binding of IQGAP3 to RIM3γ and RIM4γ. Number of individual experiments n=3. **E,** IQGAP1 shows no binding affinity to RIM3γ-TAP, RIM4γ-TAP and RIM1 C2A-C2B-domain-TAP in co-immunoprecipitation assays. Number of individual experiments n=2.

Theses experiments confirmed a binding of IQGAP3 to RIM3γ and RIM4γ and no binding to the TAP tag alone. However the in pulldown assays observed binding of IQGAP3 to RIM1-C_2B-C_2A-domains could not be reproduced in in co-immunoprecipitations (Fig. 5.16,D). Collectively these results suggest an interaction of IQGAP3 with RIM3γ and RIM4γ does take place in living cells. The positive binding to RIM1 in pulldown assays implies, that either IQGAP3 might show in addition a general affinity to C_2B domains or exhibits a rather transient interaction

with RIM1. IQGAP3 shows a high structural homology to IQGAP1 (Fig 5.16A). Therefore we tested in co-immunoprecipitations if also IQGAP1 exhibits an binding affinity towards RIM3γ and RIM4γ. Both γ-RIMs and also the control construct of RIM1 C_2A-C_2B-domains did not show any *in vitro* binding affinity to IQGAP1 (Fig. 5.16E). This further supports the specificity of the interaction between IQGAP3 and RIM3γ and RIM4γ. Taken together IQGAP3 and the γ-RIMs colocalize in the cytosol of neuroblastoma cells. Additionally, biochemical binding assays showed that RIM3γ and RIM4γ interact *in vitro* with IQGAP3. This interaction is specific for IQGAP3 as no interaction with IQGAP1 could be observed supporting a possible role of RIM3γ and RIM4γ in the remodeling of the cytoskeleton during neuronal growth.

5.3.2.3 The presynaptic protein Syd-1

Down regulation of RIM3γ and RIM4γ also affects the correct formation of synaptic structures (chapter 5.2.1), which could be on the one hand caused by the disruption of general growth promoting mechanisms but also on the other hand by a potential synaptic function of RIM3γ and RIM4γ. In the mass spectrometry approach of lysates from whole brain homogenates the synapse-defective-1 protein (Syd-1) was identified as one potential interaction partner of RIM3γ. Genetic approaches identified Syd-1 as one of three core molecules of the presynaptic active zone in flies and worms [Patel et al., 2006]. Presynaptic assembly includes local changes of the actin cytoskeleton followed by the recruitment of the synapse specific protein network. Syd-1 was shown to interact with this actin network at nascent synapses and to be crucial for the concomitant assembly of the presynapse [Chia et al., 2012]. Consistently, the loss of Syd-1 disrupts the localization of multiple presynaptic proteins. In addition Syd-1 coordinates pre- and postsynaptic assembly by interacting with the presynaptic adhesion molecule neurexin, which induces the postsynaptic assembly via its postsynaptic interaction partner neuroligin [Owald et al., 2012]. Because of the reduced synapse number in RIM3γ and RIM4γ knock-down neurons Syd-1 is an interesting potential interaction partner. To gain first insights into the potential interaction between Syd-1 and RIM3γ and RIM4γ we analyzed if the three proteins are colocalized in the same subcellular compartments when overexpressed in HEK293T cells. Overexpressed Syd-1 shows a prominent nuclear localization and a diffuse cytosolic distribution. The same is the case for RIM3γ, when overexpressed in HEK 293T cells. RIM4γ in contrast is absent from the nucleus and diffusely distributed throughout the cytoplasm (Fig. 5.17A). The coexpression of RIM3γ and SYD-1 did not change the localization of both proteins (Fig. 5.17B). However the coepxression of RIM4γ and Syd-1, did lead to the translocation of Syd-1 out of the nucleus indicating a functional interaction (Fig. 5.17B).

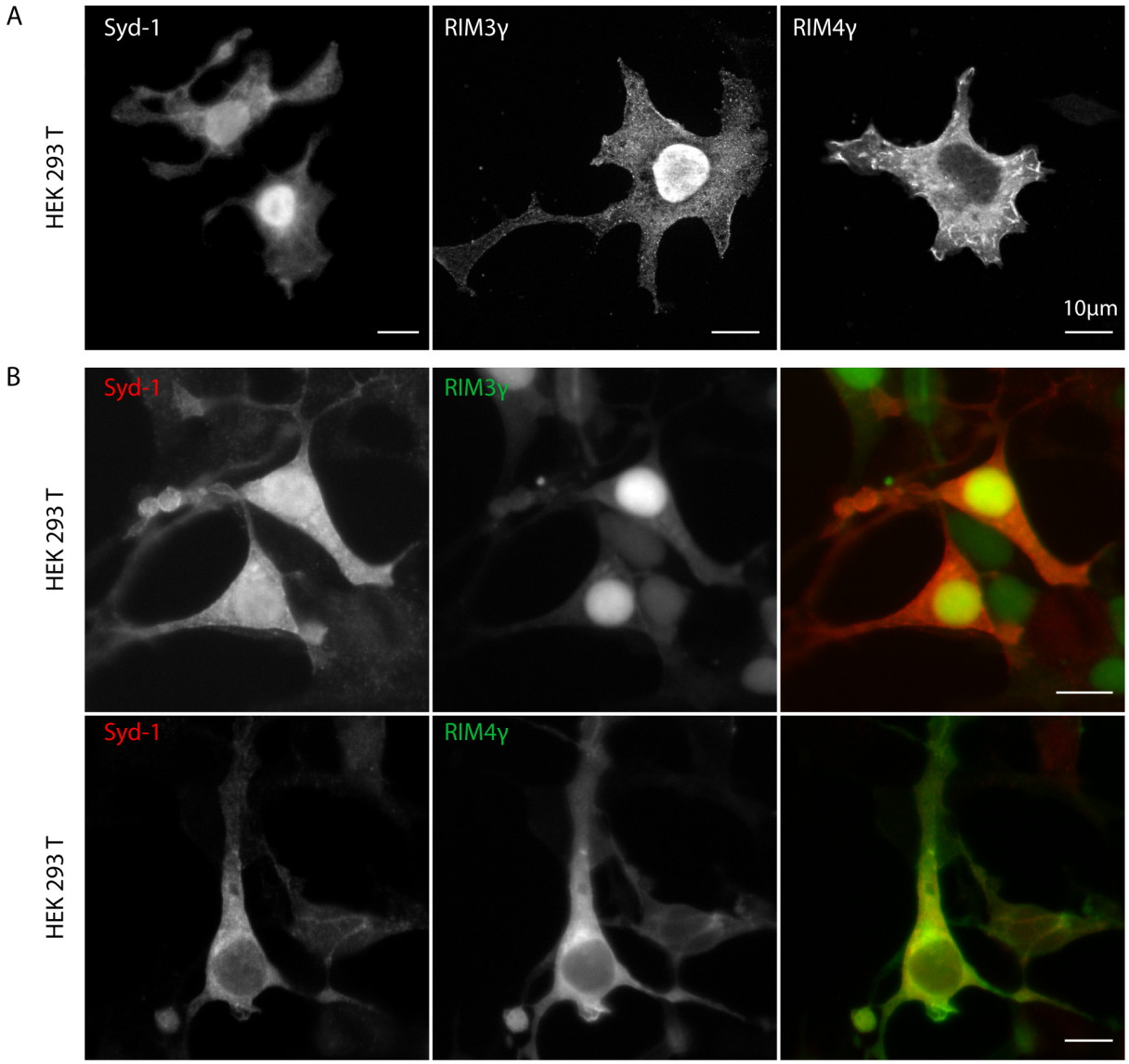

Figure 5.17: **RIM4γ changes the subcellular localization and Syd-1 whereas RIM3γ and SYD-1 reside in nucleus and cytoplasm of HEK293T cells. A,** Overxpression of SYD-1 fused to GFP and RIM3γ and RIM4γ in HEK293T cells. The cells were fixed 48 hours after transfection and immunostained with antibodies against RIM3γ and RIM4γ. **B,** Coexpression of RIM4γ together with SYD-1 leads to a translocation of Syd-1 out of the nucleus, whereas the coexpression of RIM3γ had no effect on the localization of Syd-1.

Next, we investigated the possible interaction between Syd-1 and the γ-RIMs in GST (glutathione-S-transferase)-pulldown assays and immunoprecipitations. Because of the high sequence homology of the C_2B domains of RIM1, RIM3γ and RIM4γ we included the C_2A-C_2B domain of RIM1 in the biochemical interaction studies. In the GST-pulldown assay GST-RIM3γ, GST-RIM4γ, GST-RIM1-C_2B-domain and GST coupled to glutathione agarose were incubated with HEK293T cell lysates expressing Syd-1 fused to a HA (human influenza hemagglutinin) affinity tag. After the incubation step protein complexes were purified, separated by gel electrophoresis and analyzed by western blot. Syd-1 was pulled down from the HEK cell lysates with all three RIM proteins, whereas GST alone was not able to bind Syd-1 (Fig. 5.18A). In a pulldown assay the analyzed interaction takes place in an artificial buffer solution. To test if the interaction between Syd-1 and RIM proteins would also take in place under more physiological conditions

in living cells co-immunoprecitipitations were performed. Syd-1-HA was coexpressed together with RIM3γ, RIM4γ and RIM1-C_2A-C_2B fused to a streptavidin-flag (TAP) affinity tag, after 48 hours the protein complexes were purified with magnetic beads coupled to antibodies against HA. The purified protein complexes were analyzed by gel electrophoresis and western blot. Immunostaining of the western blot with flag antibodies revealed, that syd-1 immunoprecipitated RIM3γ, RIM4 γ and RIM1-C_2A-C_2B (Fig. 5.18B). This further validates the potential interaction between the RIM proteins and Syd-1. Taken together the colocalization studies in HEK293T cells showed, that SYD-1 and γ-RIMs are expressed in the same cellular compartments and might influence the localization of each other. Further we could verify the potential interaction between Syd-1 RIM3γ, RIM4γ and the C_2B domain of RIM1 in biochemical binding studies. However, if this *in vitro* interaction has a functional role in synapse assembly and function needs to be analyzed further.

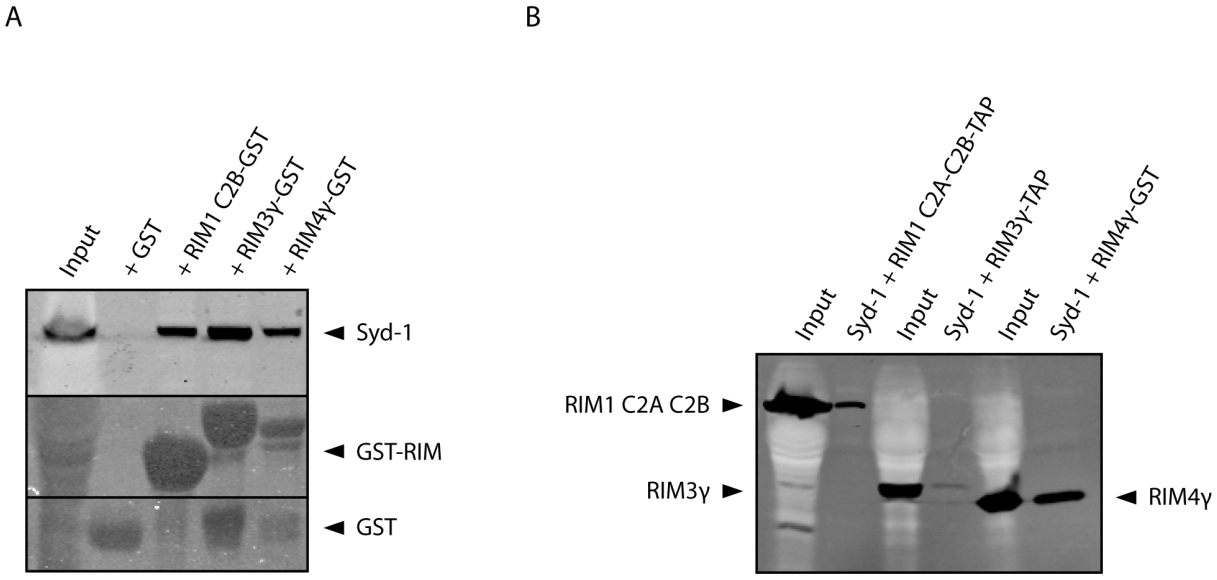

Figure 5.18: **Biochemical analysis of the potential interaction between Syd-1 and RIM3γ and RIM4γ.** **A,** GST pulldown: GST-RIM3γ, GST-RIM4γ and the C2B domain of RIM1 coupled to glutathione-agarose were incubated with HEK cell lysates overexpressing Syd-1-HA. Immunostainigs of the western blot with antibodies against HA reveals a binding of Syd-1 to all three RIM proteins. Number of individual experiments n=3. **B,** Coimmunoprecipitation: RIM3γ-TAP and RIM4γ-TAP and the RIM1 C2A-C2B-domain-TAP were coexpressed with Syd-1-HA in HEK293T cells. Protein complexes were purified with HA antibodies coupled to magnetic beads. The western blot shows a binding of all three RIM proteins to Syd-1. Number of individual experiments n=2

5.4 RIM3γ and RIM4γ knock-out mice

Loss of function studies with shRNA mediated knock-down of a protein of interest are technically restricted to single cells or subsets of cells and specific time points during development. Genetic knock-outs in contrast give the opportunity to study gene and protein function *in vivo* throughout the development and at specific developmental stages. In addition conditional knock-outs allow to study the loss of gene function in specific cell types or brain regions. To get a better understanding of the functional role of RIM3γ and RIM4γ in living animals during different developmental stages and different physiological and pathological conditions we set out to generate conditional and constitutive RIM3γ and RIM4γ knock-out mice.

5.4.1 Generation of RIM3γ and RIM4γ knock-out mice

RIM3γ and RIM4γ knock-out mice were generated with embryonic stem cells produced by the international Knock-out Mouse Project (KOMP) consortium.

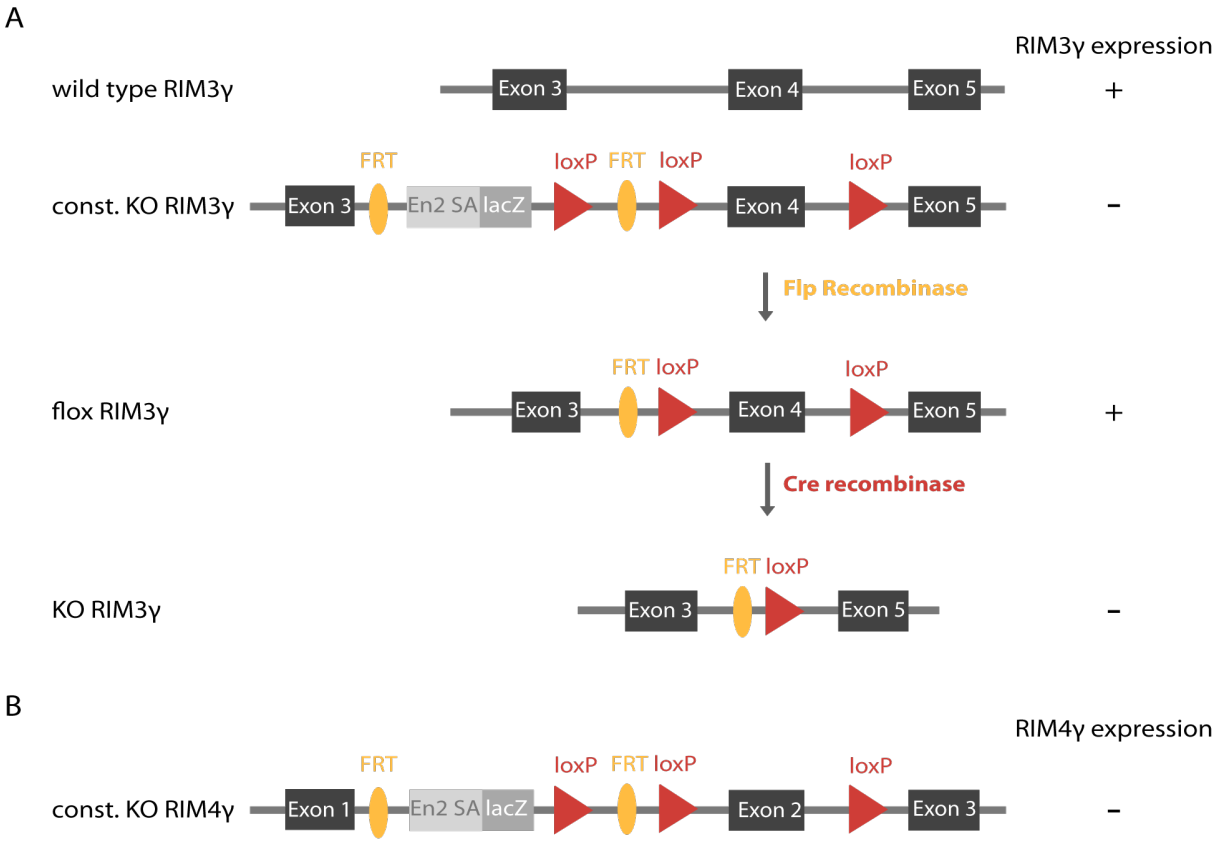

Figure 5.19: **Generation of constitutive and conditional RIM3γ and RIM4γ knock-out mice. A,** Schematic representation of RIM3γ knock-out strategy. RIM3γ wild type alleles lead to normal protein expression of RIM3γ. Introduction of the gene trap cassette in the intro region between exon 3 and 4 leads to splicing of RIM3γ after exon 3 and ablation of protein expression (RIM3**γ**constKO). Recombination by FLP-recombinase leads to excision of the gene trap and a normal expression of the protein (RIM3γflox). Recombination of RIM3γflox by Cre-recombinase to the excision of exon 4 and no protein expression (KO RIM3**γ**). **B,** RIM4γ targeting vector. Introduction of the gene trap cassette in the intro region between exon 1 and 2 leads to splicing of RIM4γ after exon 3 and ablation of protein expression (RIM4γconstKO).

The embryonic stem cells carried the targeting vector against either RIM3γ or RIM4γ, de-

signed to create three different mouse lines (Fig. 5.19). The first line obtained after germ line transmission constitutes a "knock-out first" allele, in which insertion of a splice acceptor-lacZ gene trap cassette disrupts the endogenous RIM3γ and RIM4γ transcripts resulting in a constitutive knock-out (KO) (RIM3γconstKO and RIM4γconstKO). After recombination with a FLP-recombinase expressing mouse line, the FLP-recombinase expression leads to excision of the gene trap cassette and generation of a conditional knock-out (RIM3γflox and RIM4γflox). The conditional knock-out should express wild type levels of RIM3γ or RIM4γ, but can be converted into a null allele by Cre-mediated recombination (RIM3γKO and RIM4γKO) (Fig. 5.19). This system allows to generate a constitutive knock-out, that can be used to study the functional impact on a whole organism caused by the gene ablation from beginning of its development. In addition the conditional knock-out gives the opportunity to ablate the gene of interest at specific time points during development and in the mature organism in specific brain regions or specific neuronal populations

The 'knock-out first' strategy leads in a first step to a conditional knock-out, allowing to analyze the impact of the constitutive genetic ablation of either RIM3γ or RIM4γ on the mouse organism. In the following section results of the characterization of this knock-out-first RIM3γ and RIM4γ mouse lines are shown. In order to verify that insertion of the splice acceptor-casette indeed abolishes RIM3γ and RIM4γ expression we characterized transcript and protein levels in brains of wild type and heterozygous and homozygous RIM3γconstKO (RIM3γ-/-) and RIM4γconstKO (RIM4γ-/-) mice. The level of transcripts was assessed by quantitative real time RT-PCR. RIM3γ transcripts levels were reduced to about 60% in heterozygous and almost abolished in homozygous RIM3γ-/- mice in the hippocampus, cerebellum and cortex. In heterozygous RIM4γ mice transcript levels in hippocampus and cortex showed no significant differences to wild type levels, only in the cerebellum transcript levels were significantly reduced. However homozygous RIM4γ-/- mice exhibited a reduction of RIM4γ transcript to about 30% of wild type levels in all tested brain regions (Fig 5.20 A,B). To analyze if these reduced levels of transcripts also lead to the ablation of the protein quantitative immunoblotting of homogenates from hippocampus, cerebellum and cortex were performed. Staining of the immunoblots with RIM3γ and RIM4γ specific antibodies revealed, that the gene trap had successfully disrupted RIM3γ and RIM4γ protein expression (Fig 5.20 C,D). Protein levels were reduced in both γ-RIM knock-out mouse lines, however the effect was more distinct in RIM3γ knock-out mice especially in the hippocampus (Fig 5.20C-F). Collectively these data show that the gene trap introduced in intron regions of RIM3γ and RIM4γ successfully abolishes the expression of both genes.

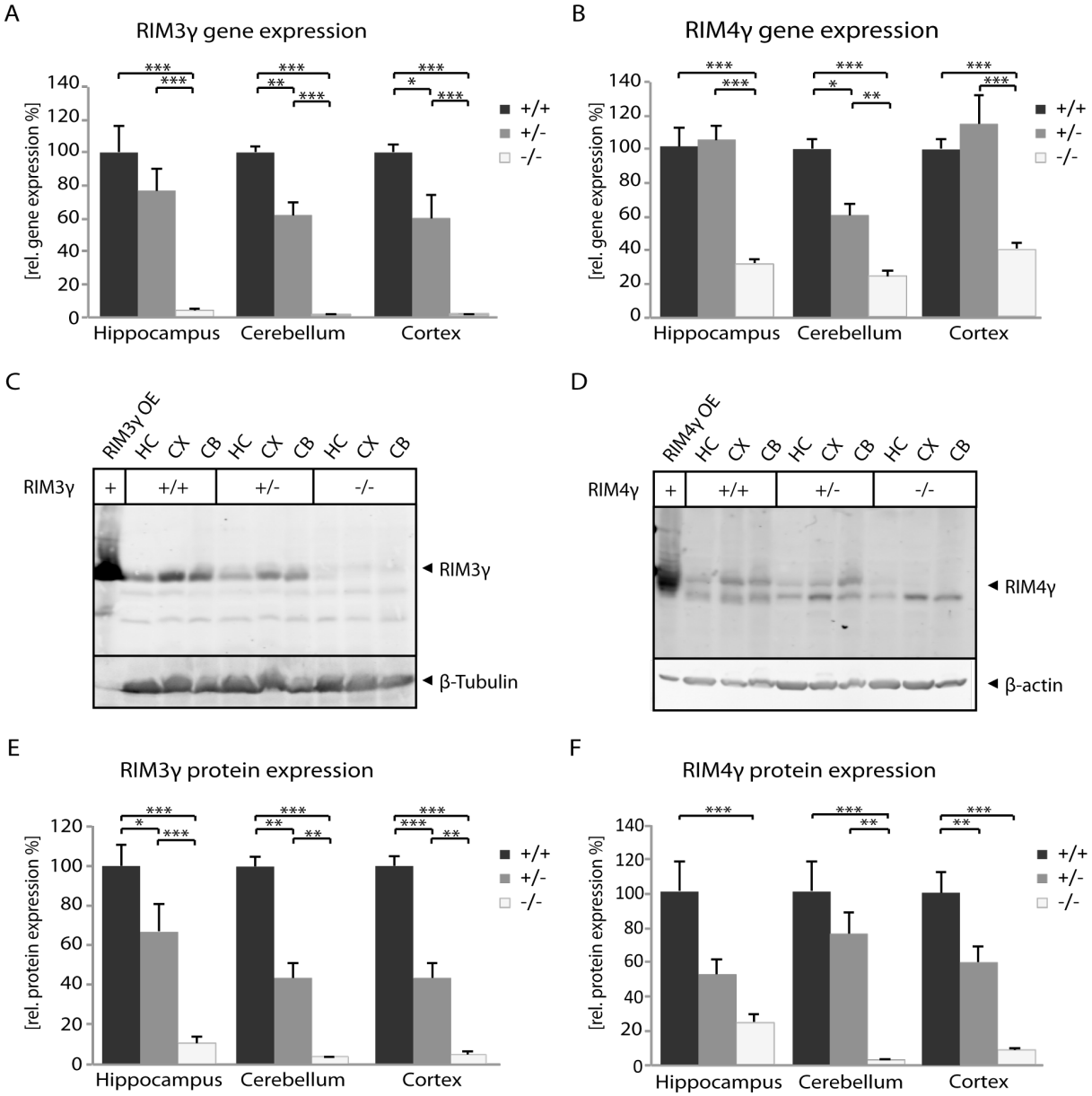

Figure 5.20: **RIM3γ and RIM4γ knock-out abolishes RIM3γ and RIM4γ gene transcription and protein expression. A,B,** Quantitative real time RT-PCR of wild type, heterozygous and homozygous RIM3γconstKO and RIM4γconstKO mice reveals reduced gene transcript levels.(n=10 animals per group) **C,D,** Immunoblots of RIM3γconstKO and RIM4γconstKO mice, show a reduction in protein expression in hippocampus (HC), cerebellum (CB) and cortex. To control for the specificity of the RIM3γ and RIM4γ antibody signal on the immunoblots HEK cell lysates overexpressing the respective γ-RIM were included in the analysis (RIM3γOE, RIM4γOE). **E,F,** Quantification of RIM3γconstKO (n=5 animals per group) and RIM4γconstKO (n=10 animals per group) immunoblots. Significance: two-way ANOVA Bonferoni post Test * = p <0,05 ** <=p 0,01 *** = p<0,001.

5.4.2 RIM3γ and RIM4γ knock-out mice are viable and born at mendelian ratios

Pups of heterozygous RIM3γ and RIM4γ breedings are viable and undistinguishable upon their genotype. Genotypes of heterozygous offspring showed no significant deviation from the expect mendelian distribution in both lines, with about 25% wild type, 50% heterozygous and 25% homozygous knock-out litters (Fig. 5.21A,B).

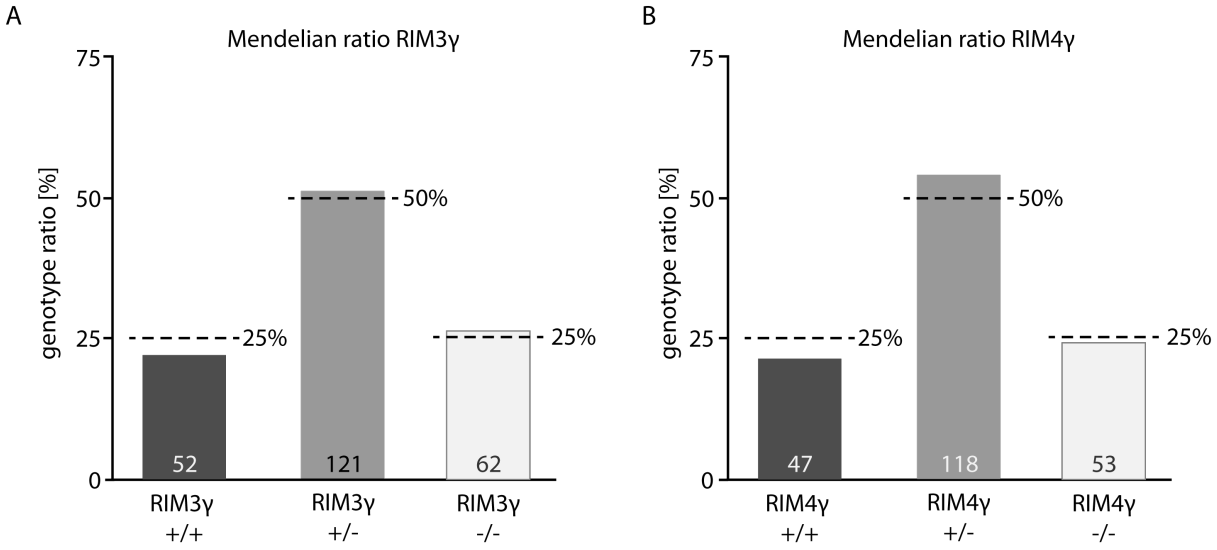

Figure 5.21: **Genotype distribution of pups produced by heterozygous RIM3γ and RIM4γ breeding pairs. A,B)** Genotype frequency of 34 heterozygous RIM3γ mating pairs **(A)** and 38 heterozygous RIM4γ mating pairs **(B)**. Columns represent the percentage of the registered genotype of offspring and dashed lines the expected frequency based on Mendelian inheritance. Numbers in the columns represent numbers of pups for each genotype. Chi-squared statistics reveal no significant deviations from expected Mendelian ratios.

During the first 3 weeks after birth pups deficient for RIM3γ or RIM4γ develop normal and gain weight to the same extend as wild type litter mates. However, around the time of weaning RIM4γ -/- mice suddenly start to loose weight. In order to characterize the onset and extend of the weight loss heterozygous and homozygous RIM4γ -/- and wild type littermates were weighed every five days from postnatal day 5 until an age of 35 days. Around postnatal week 3 RIM4γ -/- mice experience a drastic weight loss up to two grams. Afterwards they gain again in weight but do not reach the wild type level until postnatal day 35 (Fig. 5.22A,B). RIM3γ -/- mice in contrast show no changes in weight compared to wild type and heterozygous litter mates (data not shown).

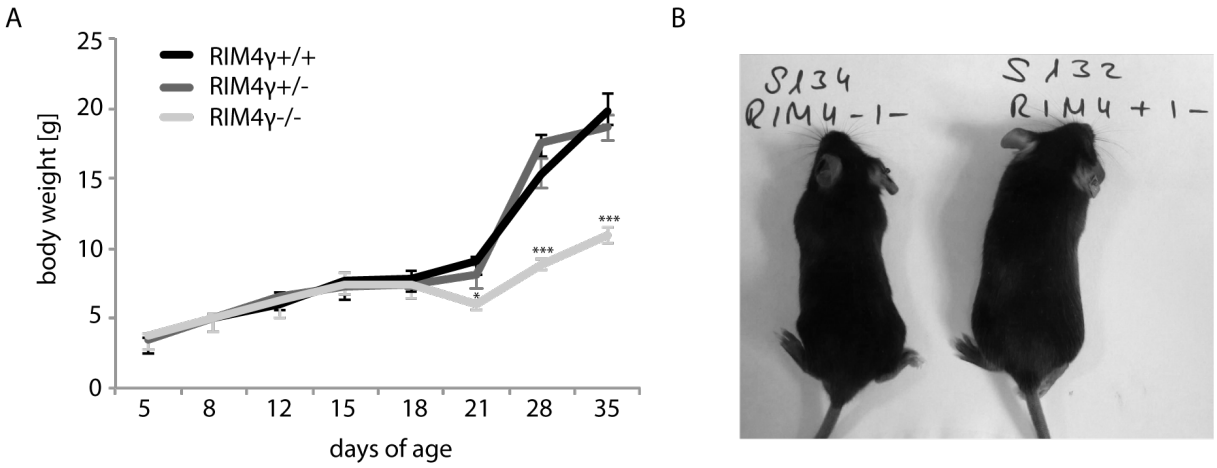

Figure 5.22: **Reduced body weight in RIM4γ -/- mice. A,** Weight reduction in RIM4γ -/- mice becomes evident around postnatal day 21 (significance: two-way ANOVA followed by Bonferoni post test, ***p< 0,001, +/+ n= 5 animals, +/- n= 5 animals, -/- n= 5 animals). **B,** Heterozygous(+/-) and homozygous(-/-) RIM4γ knock-out mice at an age of six weeks. Due to reduced body weight the full knock-out appears smaller than the heterozygous littermate.

5.4.3 RIM4γ knock-out mice show a strong motor phenotype

At the same as the strong weight reduction becomes evident (postnatal week 3) constitutive RIM4γ-/- mice develop episodes of strong hind limb impairments. The duration and frequency of these events was analyzed by video monitoring of two six weeks old RIM4γ -/- mice over five days. During these five days once every 24 hours a 1-4 hours episode of strong movement impairments was observed (Fig 5.23A).

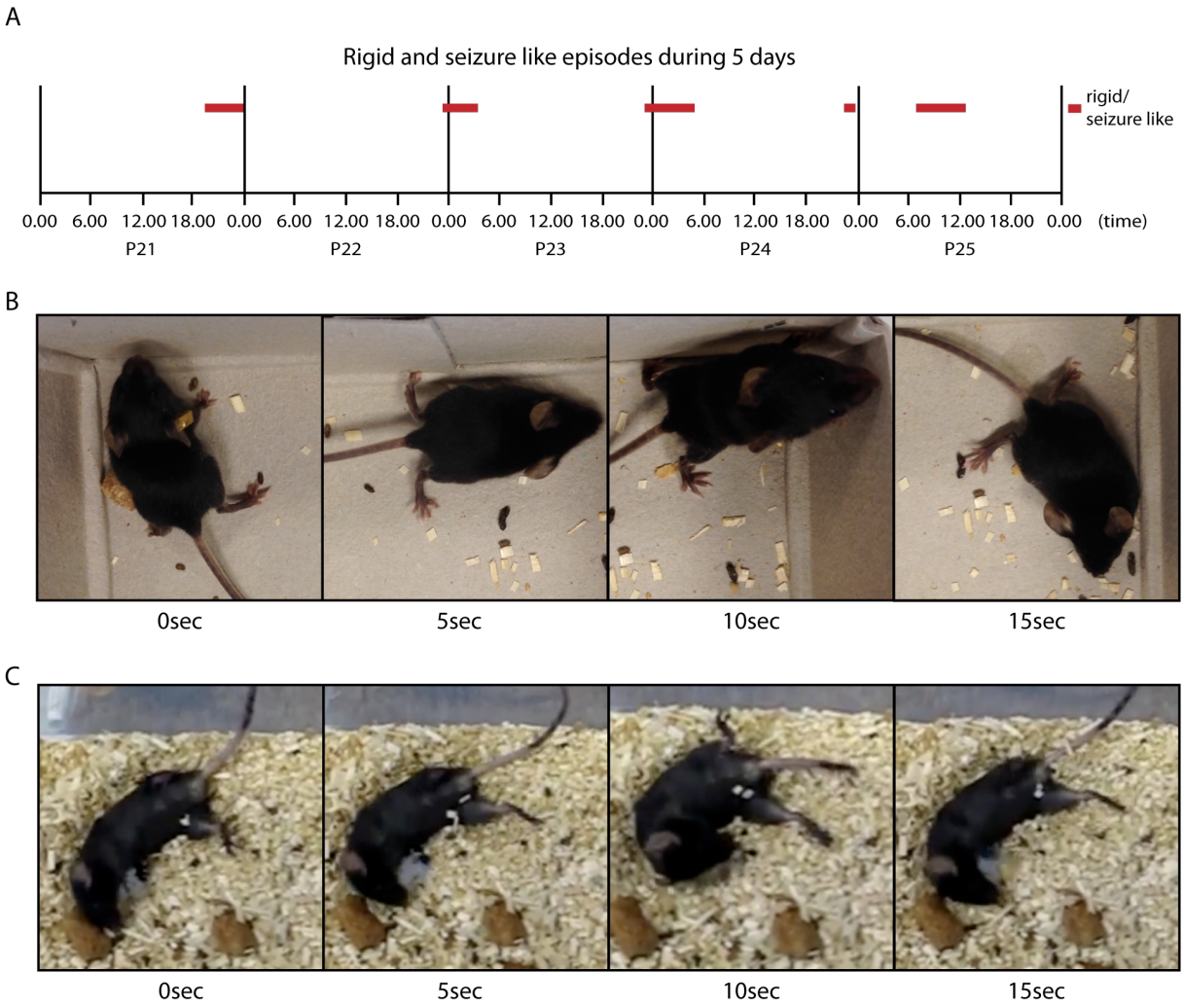

Figure 5.23: **RIM4 knock-out (-/-) mice show episodic motor defecits. A,** Time line of five-day video monitoring of RIM4 γ -/-. Episodes of motor deficits (ataxia and dyskenisia) over 1-4 hours were observed once a day. **B,** Movie of 15 seconds, displayed in images every 5 second of the ataxia /dyskenisia episodes in a five week old RIM4γ -/- mouse. **C,** Images of a 15 second movie showing a RIM4γ -/- mouse (8weeks) experiencing strong epileptic like seizures.

These episodes were composed of rapid uncontrolled movements of the hind limbs and sometimes even front limbs disrupted by phases of immobility, during which the hind limbs appeared stretched out and rigid (Fig 5.23B). Apart from these episodes the animal behaved normally and showed now obvious motor abnormalities. Rarely a phenotype resembling epileptic seizure like behavior was observed in some RIM4γ -/- mice (Fig 5.23C). This strong phenotype was not observed during the 5 day video monitoring. Taken together, RIM4γ -/- mice experience weight

loss at an age of 3 weeks at the same time when they develop a strong motor phenotype.

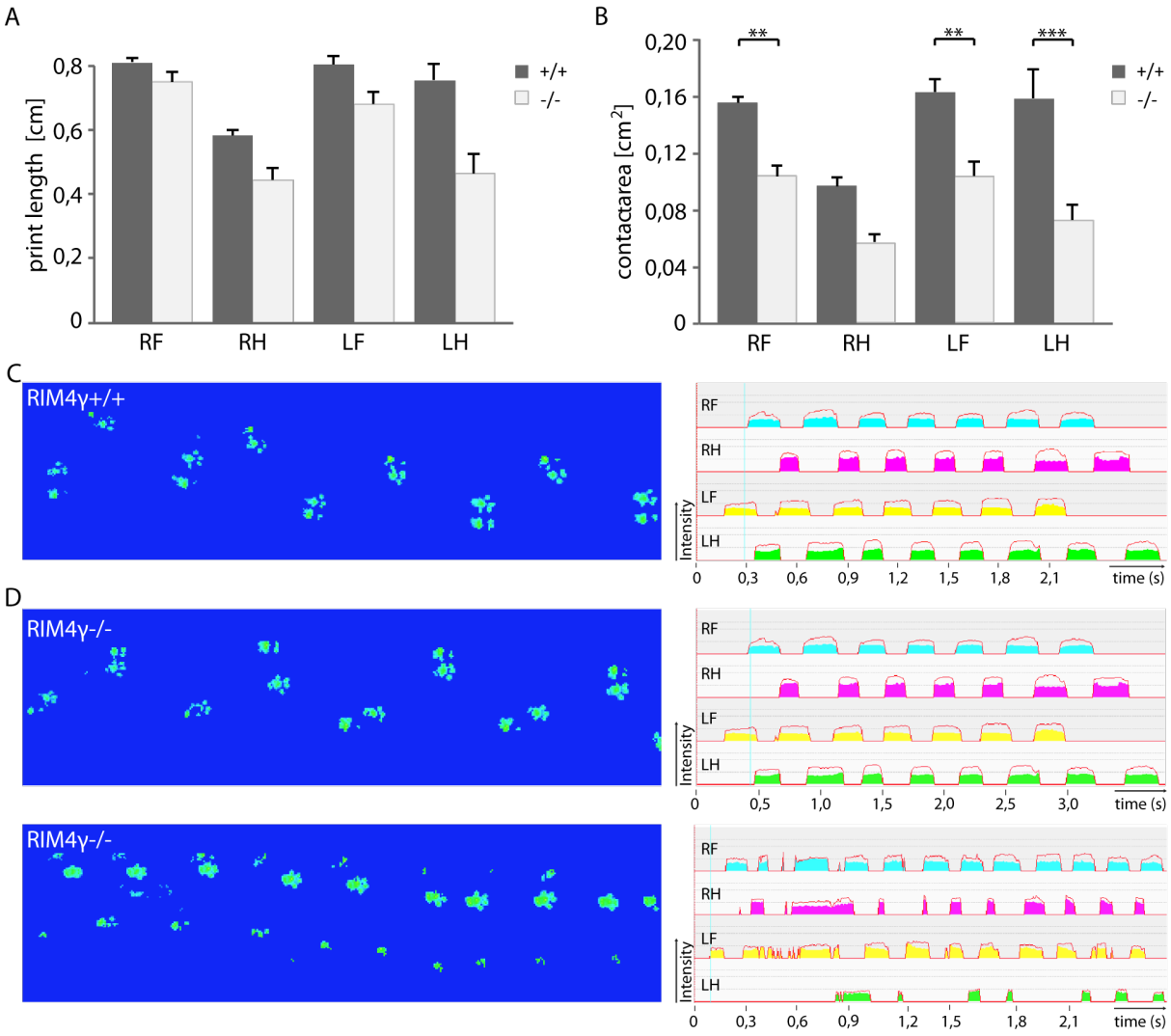

Figure 5.24: **Paw prints of RIM4γ -/- mice. A,B,** Cat walk analysis of 3 RIM4γ -/- mice showing no obvious phenotype and 3 wild type litter mates **A,** Quantification of the paw print length reveals no reduction in the print length of RIM4γ -/- mice. **B,** Quantification of the maximal paw contact area shows a significant reduction in the maximal contact area of the left hind paw in RIM4γ -/- mice during a behavioral inconspicuous phase. **C,** Paw prints and paw print intensities of a 7 weeks old wild type animal. **C,** Paw prints and paw print intensities of a 7 weeks old RIM4γ -/- mouse during a behavioral inconspicuous phase (upper panel) and a episode of strong motoric hind limb impairments (lower panel). Significance: two-way ANOVA **p < 0,01, ***p < 0,001 n= 3 animals per group with 3 trials per mouse.

Gait disorders can be characterized by several motor tests. The CatWalk system is a video based automated gait analysis system developed to evaluate footfall and gait changes in rodents. The CatWalk system consists of an enclosed walkway on a glass plate that is crossed by a mouse from one side of the walkway to the other. Green light enters on the long edge of the glass plate and is completely internally reflected. Only when a mouse's paw makes contact with the glass plate the light is scattered and can escape. The enlightened paw prints are captured by a camera underneath the walkway. RIM4γ -/- mice experience episodes of strong hind limb motor abnormalities, besides theses episodes they appear to walk normally and show no obvious changes in gait. To characterize the motoric hind limb phenotype and identify weaker gait

abnormalities during behavioral inconspicuous phases RIM4γ -/- mice and wild type littermates were analyzed by the CatWalk system. RIM4γ -/- mice experiencing an episode of hind limb impairments were not able to traverse the complete distance of the walk under two minutes, whereas a healthy mouse crosses the walkway in 5-15 seconds. The hind limbs of RIM4γ -/- mice suffering from hind limb impairments barely contacted the glass plate and animals could only push themselves forward by using their front limbs (Fig 5.24D lower panel). For further gait analyzes only RIM4γ -/- mice showing no obvious motor deficits were examined on the Catwalk system (Fig 5.24D upper panel). Quantification of the print length and maximal contact area of all four paws revealed, that RIM4γ -/- mice also suffer from mild gait impairments when they show no obvious motor phenotype. RIM4γ -/- mice showed no significant reduction in print length but in contact area of the left hind paws made with the walk way (Fig. 5.24A,B). This could be either caused by a weakened musculature or by coordination difficulties or both.

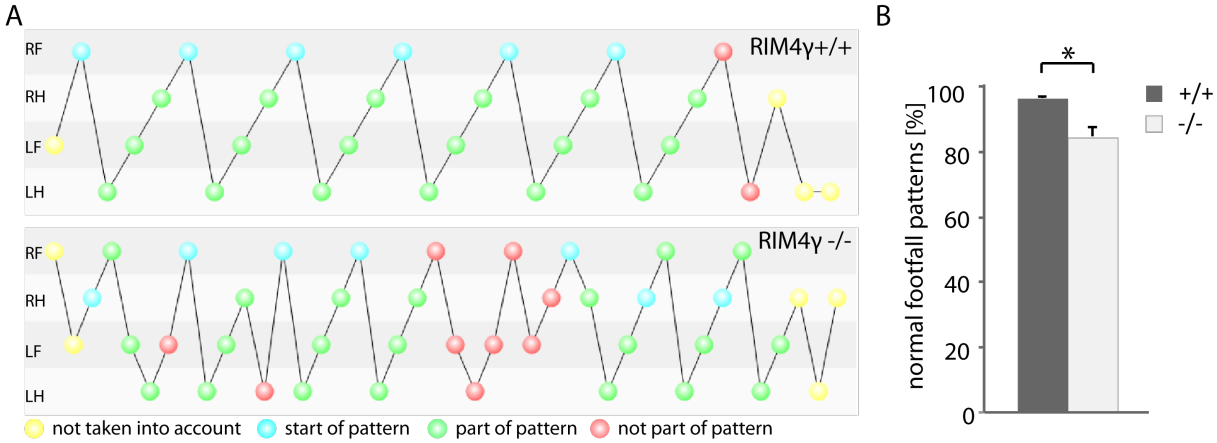

Figure 5.25: **Coordinative disturbances in RIM4γ -/- mice in a behavioral inconspicuous phase. A,** Footfall pattern of a wild type littermate shows a regular step sequence (upper panel), whereas the step sequence of a RIM4γ -/- mouse shows a step sequence disrupted by irregular paw placements (lower panel). **B,** Quantification of the regularity index (number of normal step sequences x 4 / number of paw placements) reveals a higher irregularity of paw placements in RIM4γ -/- mouse. Significance: ttest * p=0,03, n=3 animals per group with 3 trials per mouse.

Mice walking on their four paws use specific step patterns. Deficits in coordination can disrupt these patterns. Therefore coordinative abilities can be characterized by the regularity of step patterns. Common step sequence patterns are defined as cruciate (right front - left front - right - hind - left hind paw or starting with left front) alternate (right front - right hind - left front - left hind or starting with left front) or rotate (left front - right front - right hind - left hind). A measure of interpaw coordination is the regularity index of these footfall patterns, it can be calculated as the number of normal step sequence patterns relative to the paw placements. A healthy fully coordinated animal walking only in the four predefined patterns shows a regularity index of 100% (Fig. 5.25A). Footfall patterns of RIM4γ -/- mice were disrupted by irregular step sequences, which could not be related to the predefined step sequence patterns (Fig 5.25A lower panel, B). Wild type littermates in contrast crossed the walkway in regular step sequences with an average regularity index of 96% (Fig 5.25A upper panel,B).

Another behavioral test for motor coordination and physical endurance of rodents is the rotarod

test. It is composed of a turning cylinder the rotational speed of which can be adjusted from 4 to 40 rotations per minute (rpm). In the test motor skills are assessed by recording the duration and the maximum velocity reached before the mouse falls from the cylinder. The ability of a mouse to stay on the rotating rod during accelerating speed depends on coordination and grip strength of the mouse. We tested the ability of 6 RIM4γ -/- mice and 6 wild type littermates to stay on the rotating rod when the velocity was increased from 4 to 40 rotations per minutes (rpm) during five minutes. The animals were placed on the rotating rod at a speed of 4 rpm, when all animals were walking stablely on the turning cylinder the speed was accelerated. In a first trail the animals were habituated. After habituation mice were tested in 3 subsequent trials with a 15-minute break in between. All animals were tested on 3 different days with one-week recovery time between testing days.

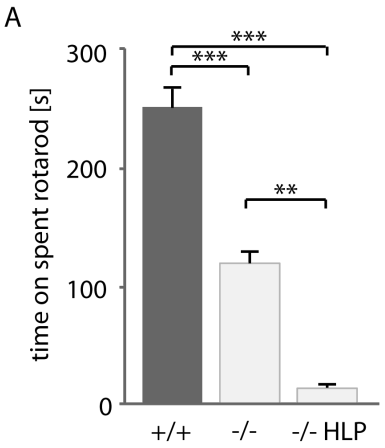

Figure 5.26: **RIM4γ -/- mice exhibit a reduced ability to stay on the rotating rod. A,** 6 RIM4γ -/- mice and 6 wild type littermates were tested on 3 days, 3 times for 5 minutes with an accelerating speed from 4 to 40 rpm. 3 trials of 3 RIM4γ -/- mice experiencing strong hind limb impairments (-/- HLP) were included in the quantification to show the drastic impairments in motor skills. Significance: one-way ANOVA followed by Bonferoni post test, **p<0,01, ***p<0,001

To illustrate the strong differences in motor performance of RIM4γ -/- mice suffering from hind limb impairments and RIM4γ -/- mice showing no obvious motor impairments, 3 trials of RIM4γ -/- animals experiencing an episode of strong hind limb impairments were include in the quantification. Wild type animals mostly stayed on the rod the complete trial and were still walking stabely after 5 minutes at a speed of 40 rpm. RIM4 γ -/- mice were not able to complete the trial and fell of the rotating rod after about 2 minutes at a speed of 20 to 25 rpm. During strong episodes of hind limb impairments RIM4γ -/- mice could not stay on the rotating rod for longer than 15 seconds (Fig 5.26). These results together with the irregular footfall patterns observed in RIM4γ -/- mice suggests that RIM4γ -/- mice suffer from coordinative disturbances also during behavioral inconspicuous phases.

5.4.4 RIM3γ and RIM4γ knock-out mice show no obvious changes in neuronal structures

Knock-down of RIM3γ and RIM4γ at early developmental stages in neuronal cultures and *in vivo* leads to strong reduction in neuronal branching. This implicates that a knock-out of these proteins might lead to the same impairments in neuronal branching or even disturb the correct development of brain structures. In addition the observed phenotype in RIM4γ -/- mice indicates, that RIM4γ -/- mice suffer from neurological deficits accompanied or caused by morphological changes in the brain. Changes in the cerebellar architecture have been associated with mouse models of episodic ataxia and dyskenisia [Mark et al., 2011].

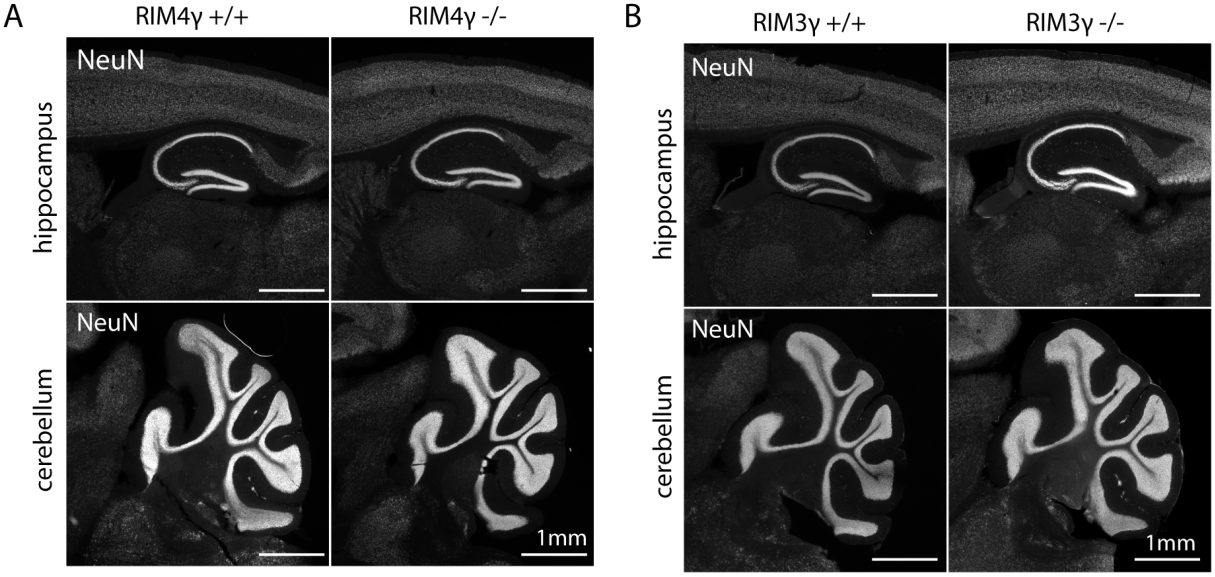

Figure 5.27: **No obvious structural changes in cerebellar and hippocampal architecture in RIM3γ -/- and RIM4γ -/- mice. A,B,** NeuN staining in the cerebellum and hippocampus of RIM4γ -/- and RIM3γ -/- mouse display no obvious differences in comparison to wild type littermates.

Interestingly, levels of RIM4γ protein expression are highest in the cerebellum [Alvaréz-Baron, 2010]. The correct layering and morphology of hippocampus and cerebellum was analyzed in RIM3γ -/- and RIM4γ -/- mice and wild type littermates by staining neuronal cell layers with antibodies against the neuron specific protein NeuN (Fig 5.27). Comparison of the cerebellar and hippocampal morphology after NeuN immunostaining revealed no obvious differences between RIM3γ -/-, RIM4γ -/-mice and wild type littermates. However milder changes in the cellular morphology that do not affect the overall structure of a brain are not detected by this method.

5.4.5 Neuronal activity influences gene expression of RIM3γ and RIM4γ

During increased neuronal activity neurons undergo changes in molecular composition and structure in order to adjust their synaptic strength. This neuronal plasticity has been associated with a variety of physiological processes like learning and memory but also pathological processes like epileptogenesis [Milner et al., 1998, Bausch et al., 2006]. In order to investigate if RIM3γ and RIM4γ gene expression is differentially regulated during neuronal activity we performed quanti-

tative real time RT PCR on mouse hippocampal tissue samples at four different time points after the induction of status epilepticus (SE). SE was induced by the application of pilocarpine, 40 minutes after onset SE was relived by the administration of diazepam. 12, 24, 36 and 72 hours later animals were sacrificed and hippocampal subregions dentate gyrus (DG), cornu amonis 1 (CA1) and cornu amonis 3 (CA3) were microdissected. Quantitative real time RT PCR revealed a significant down regulation of RIM3γ 36 and 72 hours after SE in the DG (Fig. 5.28A). In contrast, RIM4γ was strongly upregulated already 12 hours after SE in all hippocampal subregions. In CA3 this upregulation was most prominent and still detectable 24 hours after SE (Fig. 5.28B). These results suggest that RIM3γ and RIM4γ are involved in the modulation of neuronal transmission or remodeling of neuronal structures after changes in the network activity.

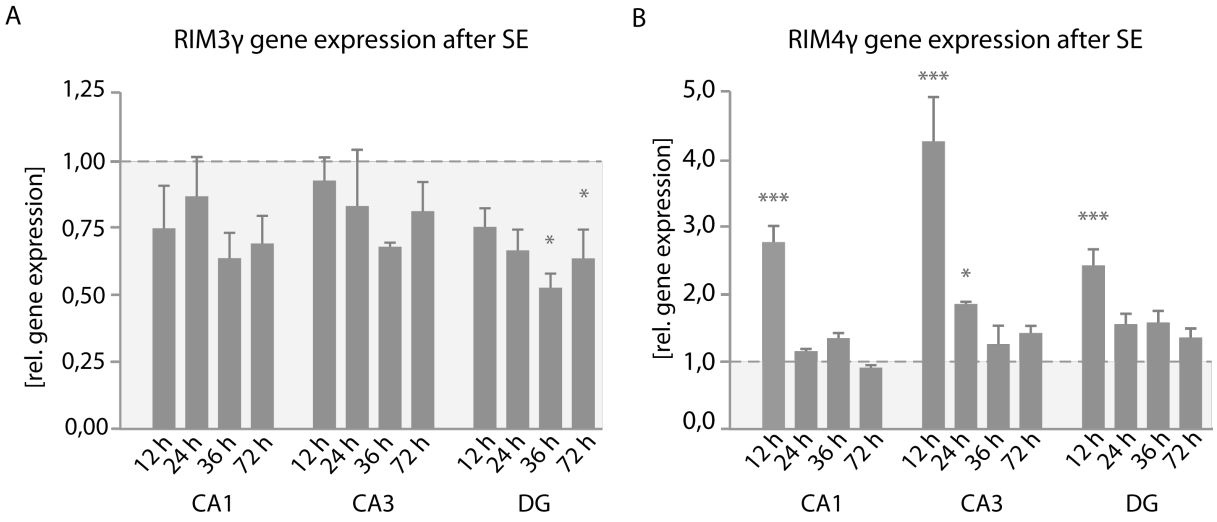

Figure 5.28: **Changes in gene transcription of RIM3γ and RIM4γ after induction of status epilepticus (SE). A,B,** 8 week old wild type mice were subjected to pilocarpine induced SE and hippocampal subregions dentate gyrus (DG) cornu ammonis 1 (CA1) and cornu ammonis 3 (CA3), were microdissected 12, 24, 36 and 72 hours after SE. Gene expression levels are displayed as relative increase in comparison to basal gene expression levels of sham injected animals normalized to 1. **A,** Quantification of real time RT PCR reveals a downregulation of RIM3γ mRNA levels 36 and 72 hours after SE in DG. **B,** Quantification of real time RT PCR reveals an upregulation of RIM4γ in all hippocampal subregions 12 hours after SE and CA3 also 36 hours after SE. Significance: two-way ANOVA followed by Bonferoni post test * = $p < 0{,}05$ *** = $p < 0{,}001$, n=5 for all groups.

6 Discussion

Discussion

At the presynapse the large members of the RIM protein family are centrally involved in the network of active zone proteins [Mittelstaedt et al., 2010]. Through multiple interactions within this network of active zone proteins they participate in several steps of neurotransmitter release and regulate thereby its speed, efficiency and synchrony [Südhof, 2013]. In contrast very little is known about the function of the small γ-RIMs which are composed of only the RIM specific C_2B domain and an isoform specific N-terminus [Wang & Südhof, 2003]. First, shRNA mediated knock-down experiments resulted in a strong growth deficit in primary cultured neurons, suggesting a role of RIM3γ and RIM4γ in neuronal growth and development [Alvarez-Baron et al., 2013]. In this study we set out to analyze the molecular mechanism underlying the role of RIM3γ and RIM4γ during neuronal growth and to identify a possible synaptic function in accordance to the large RIM proteins.

6.1 Subcellular localization of RIM3γ and RIM4γ

Eukaryotic cells are compartmentalized, allowing molecular pathways within the cell to occur more efficiently and in a well orchestrated fashion. During development cellular organelles and functional compartments can change their protein composition to adapt their functionality to changing external conditions. Thus, a distinct subcellular localization pattern of a protein might give first hints on its cellular function.

In accordance to its well-established role at the presynaptic neurotransmitter release site RIM1 shows a specific synaptic localization. RIM3γ and RIM4γ in contrast do not show an exclusive synaptic expression pattern. RIM4γ is present at pre- and postsynaptic compartments but shows no specific localization to these structures and is rather diffusely distributed throughout axons and dendrites. RIM3γ is localized to pre- and postsynaptic compartments and shows in addition a strong enrichment in the nucleus. In this study we identified bioinformatically a nuclear localization signal in the N-terminal sequence of RIM3γ whereas such a signal was not present in the sequence of RIM4γ. By mutating all four amino acids coding for this nuclear localization signal we could prove its functionality and show that this sequence is responsible for the localization of RIM3γ to the nucleus (Fig5.2).

The only protein interaction domain shared between the small γ-RIMs and RIM1α is the C_2B domain. Even though the precise molecular mechanisms determining the presynaptic localization of RIM1 are not fully resolved so far, the C_2B domain of RIM1 was suggested to be involved in targeting RIM1 to the active zone. In *C. elegans* the Liprin-α homolog SYD-2, a binding partner of RIM1's C_2B domain, was shown to be an important regulator in the formation of the

presynaptic active zone [Zhen & Jin, 1999, Schoch et al., 2002]. Accordingly, shRNA mediated knock-down of Liprins-α in primary cultured neurons leads to reduced RIM1 levels at the synapse indicating that the C_2B of RIM1 domain contributes to its localization to the synapse [Spangler et al., 2013]. This suggests, that the C_2B domain of RIM3γ and RIM4γ might be involved in a similar manner in the localization of RIM3γ and RIM4γ, whereas the N-terminal sequences could target the γ-RIMs to non-synaptic localizations. However, the C_2B domain of RIM3γ and RIM4γ was also suggested to be important for the growth promoting effects mediated by RIM3γ and RIM4γ. The strong reduction in neuronal growth after the shRNA mediated knock-down of RIM3γ and RIM4γ can be partially rescued by overexpressing only the C_2B domain of the respective γ-RIM [Alvarez-Baron et al., 2013]. Thus, depending on interactions with other proteins the C_2B domain of RIM3γ and RIM4γ might be on the one hand involved in targeting the γ-RIMs to the synapse and on the other hand in mediating their growth promoting effects.

In our affinity purification - mass spectrometry screen for novel γ-RIM binding proteins several importins were detected as interaction partners of RIM3γ. This and the identification of RIM3γ's nuclear localization signal indicates an active recruitment of RIM3γ into the nucleus. Synapses can adapt their strength in response to increased or reduced network activity, leading to structural changes for exmaple in the protein composition at the active zone [Lazarevic et al., 2013]. An adaptation of synaptic strength can be dependent on changes in gene transcription to meet the changed demand in synapse specific proteins [Cohen & Greenberg, 2008, Ch'ng et al., 2012]. The strong nuclear localization of RIM3γ together with its localization at the synapse suggests a possible function of RIM3γ in synapse to nucleus signaling and in the activity dependent regulation of gene transcription. Signaling form the synapse to the nucleus can occur through a variety of mechanisms including rapid electrochemical, regenerative calcium waves along the endoplasmic reticulum as well as active transport of soluble proteins from the synapse back to the nucleus [Ch'ng & Martin, 2011]. The active transport of proteins from the synapse to the nucleus is mediated by importins. During increased neuronal activity synaptic bound α-importins are released, bind to the nuclear localization signal of potential cargos and initiate their translocation to the nucleus in cooperation with β-importins [Jeffrey et al., 2009]. Once in the nucleus the synaptic cargos can induce alterations in transcriptional programs allowing the cell to answer the changed protein demand at the synapse. An involvement of RIM3γ in the activity dependent signaling from synapse back to the nucleus and the signals that trigger the shuttling of RIM3γ in and out of the nucleus need to be addressed in future studies.

6.2 The growth reduction in RIM3γ and RIM4γ knock-down neurons involves changes in vesicular traffic

The growth of axons and dendrites is regulated by common but also by axon and dendrite specific mechanisms. The shRNA mediated knock-down of RIM3γ and RIM4γ in primary neuronal cultures at DIV 1 resulted in impairments in axonal and dendritic growth. This suggests that RIM3γ and RIM4γ are involved in general growth promoting processes crucial for axon and dendrite development. Neuronal growth and polarization are not only the simple extension of

neuronal branches; these processes involve also the establishment of highly specified neuronal structures, like synapses. Thus, if the maturation of neuronal processes is inhibited one would expect in addition to a reduction of the process length an immaturity of these short preserved branches. This could be verified in the case of RIM3γ and RIM4γ knock-down neurons. The few short branches that were formed in RIM3γ or RIM4γ knock-down neurons had significantly less synapses and dendritic spines. The findings were not observed when a mutated versions of the shRNAs against RIM3γ and RIM4γ with single nucleotide exchanges in the binding site of RIM3γ and RIM4γ were transfected and could be rescued by the coexpression of a shRNA resistant version of the respective γ-RIM confirming the specificity of the knock-down (Fig. 5.4).

Neurite outgrowth can be stimulated by neuronal activity and the concomitant depolarization of neurons. Especially dendritic growth is profoundly regulated by synaptic activity in order to connect the different brain regions correctly [Solem et al., 1995, Wong & Ghosh, 2002]. Taking a possible synaptic role of RIM3γ and RIM4γ in account, impairments in neurotransmitter release due to the loss of RIM3γ and RIM4γ could therefore induce the reduction in neuronal growth. However silencing neuronal activity in primary neuronal cultures had no influence on neurite outgrowth and dendritic complexity (Fig5.5). Thus, possible changes in neurotransmitter release due to the loss of RIM3γ or RIM4γ are most likely not responsible for the growth inhibition of neuronal branches. Additionally, if the growth deficit in RIM3γ and RIM4γ knock-down neurons were caused by a reduced network activity the effect should be abolished, if the cell is surrounded by a network of wild-type neurons. However, the *in vivo* knock-down of RIM3γ and RIM4γ in single neurons surrounded by wild-type neurons in the hippocampus and cortex of rats one day after birth still led to a reduction in neuronal growth (Fig5.6). This reduction in neuronal growth was not observed when the shRNA against RIM3γ was introduced in cortical neurons of 21 days old rats (Fig 5.7). Thus, the growth promoting effect of RIM3γ and RIM4γ seems to be restricted to development of neuronal processes with no influence on the maintenance of the dendritic tree.

One of the most important cellular processes during neuronal growth is the sorting and transport of new proteins and membrane particles to nascent neuronal compartments. New proteins are synthesized in the endoplasmic reticulum and transported to the Golgi apparatus, the main cellular organelle regulating vesicular transport and protein distribution. Consequently, the correct functionality of the Golgi apparatus and the associated protein sorting and distribution is crucial for neuronal growth. Despite a generally high structural stability of the Golgi apparatus various physiological and pathophysiological processes can induce fragmentation of the Golgi structure. For instance it was shown that the accumulation of mutated proteins in the Golgi leads to the disruption of the Golgi structure in several neurodegenerative diseases [Fan et al., 2008]. During neuronal growth the Golgi apparatus undergoes structural remodeling. In early stages of neuronal growth the Golgi is first oriented towards the axons and later when dendritic development starts it reorients itself towards the main dendrite and sends out Golgi outpost into the growing dendrites. Golgi outposts are suggested to be important regulators in local branch induction of dendrites [Horton et al., 2005, Ye et al., 2007, Yadav & Linstedt, 2011]. Interestingly, RIM3γ and RIM4γ knock-down neurons exhibit alterations in the structure of the

Golgi apparatus. Knock-down of RIM3γ leads to a fragmentation and dispersion of the Golgi apparatus throughout the neuron, whereas knock-down of RIM4γ leads to a condensation of the Golgi apparatus in the center of the soma and to a reduction of the total Golgi size (Fig. 5.8). Golgi condensation associated with changes in neuronal morphology was for example observed after the overexpresssion of the microtubule plus end tracking protein CLASP2 [Beffert et al., 2012]. After overexpresion of CLASP2 in neuronal cultures the amount of densely packed, smaller Golgi was increased in comparison to wild type neurons. In contrast to the observed finding in RIM4γ knock-down neurons CLASP2 overexpressing neurons show an increase in axon length and exhibit multiple axons [Beffert et al., 2012]. CLASP2 might lead to an stabilization of the cytoskeleton that promotes neurite outgrowth but impairs the changes in Golgi morphology to induce dendritic branching, whereas in RIM4γ knock-down neurons the functionality of the Golgi apparatus seems to be further impaired leading to the complete inhibition of axonal and dendrite growth.

TTC3, a gene located in the close proximity of the Down critical region on human chromosome 21, was recently shown to inhibit neurite growth through the induction of actin polymerization. Overexpression of TTC3 in primary neuronal cultures impairs neurite extension and leads to a fragmentation of the Golgi apparatus, similar to the observed changes in Golgi morphology after knock-down of RIM3γ [Berto et al., 2014]. Actin remodeling is a key feature of neuronal growth [Neukirchen & Bradke, 2011]. Local actin instability in the growth cone allows for the penetration of microtubules that direct membrane flow from the Golgi into the growing tip leading to the formation of a new neuronal branch. Thus, depolarization of the actin network might lead to a disruption of the Golgi structure in differentiating neurons. The observed fragmentation of the Golgi apparatus and reduction in neuronal growth after overexpression of the actin polymerizing protein TTC3 suggest that the correct balance of actin depolymerizing and polymerizing forces are required to guarantee neuronal growth as well as structural stability and correct membrane flow of the Golgi apparatus. The similar effects on neuronal growth and Golgi morphology of microtubule and actin filament regulating proteins indicate that RIM3γ and RIM4γ's role during neuronal growth involves the correct regulation of cytoskeletal structures. This is further supported by the identification of several cytoskeleton regulating proteins in our affinity-purification mass spectrometry screens for novel γ-RIM binding partners (Fig 5.11, Fig. 5.12).

A further important factor regulating the structure of Golgi morphology is the continuous and correct amount of membrane supply from the endoplasmic reticulum (ER). The incorporation of vesicles arriving from the ER requires the *cis*-Golgi protein GM130. Knock-down of GM130 leads to a disruption of the membrane supply from the ER and breakdown and of the Golgi structure [Marra & Salvatore, 2007]. Thus, an impairment in the incorporation of membrane vesicles send out from the ER could lead to the dispersion of the Golgi apparatus in RIM3γ knock-down neurons and in the case of RIM4γ a reduced membrane input from the ER to the condensation of the Golgi apparatus. Both the condensation and dispersion of the Golgi could additionally disrupt the supply of proteins and membrane at sites of neuronal growth and would explain why axons and dendrites and smaller structures like synapses are affected to the same

degree.

In accordance, changes in vesicular transport of Rab8 and Rab11 marked vesicles were observed in RIM3γ and RIM4γ knock-down neurons while vesicular traffic of Rab6 marked vesicles was unaffected (Fig. 5.9). Here again effects of the two γ-RIMs differed as RIM4γ had overall a stronger effect on vesicular transport than RIM3γ. Rab proteins are thought to act as cellular cargo address labels of the various membrane transports routes within a cell. They are involved in the recruitment of the correct cargos to transport vesicles of specific transport routes and also support the traffic itself by interacting with the cytoskeleton. Furthermore, Rab proteins regulate the corresponding transport routes by controlling vesicle budding at the site of origin and vesicle fusion at the desired destination [Zerial & McBride, 2001]. The three analyzed Rab proteins participate in different aspects of vesicular transport routes and have all been implicated in neuronal growth [Huber et al., 1995, Schlager et al., 2010, Lazo et al., 2013]. Rab8 and Rab6 are both localized to the *trans* Golgi network (TGN) on vesicles leaving the Golgi to travel to the plasma membrane. Rab8 additionally localizes to the recycling endosomes. In a popular model of polarized vesicle traffic, the traffic of rhodopsin in retinal photoreceptors, it was shown that Rab6 and Rab8 seem to interfere with TGN vesicular transport at different stages [Shetty et al., 1998, Deretic et al., 1995]. In this system Rab6 is recruited to vesicles transporting rhodopsin at earlier stages of the transport process than Rab8 and might be a part of the sorting machinery that controls post Golgi vesicle budding [Deretic & Papermaster, 1993]. Rab8 is not needed for budding or the motility of exocytic carriers but required for docking and fusion of vesicles send out from the TGN to the plasma membrane [Grigoriev et al., 2011]. In addition to its role in the transport of TGN vesicles, Rab8 was implicated in neuronal growth through regulating vesicular traffic at the recycling endosomes, a function that is not shared by Rab6 [Hattula et al., 2006]. For instance induced neurite outgrowth in PC12 cells relies on the recruitment of Rab8 to recycling endosomes and in fibroblast the overexpression of Rab8 leads to the formation of neurite like protrusions with the accumulation of actin microfilaments to this protrusion [Kobayashi et al., 2014, Hattula et al., 2006, Peränen et al., 1996]. These functions of Rab8 rely on its recycling activity and not its excocytic role in TGN. Interestingly, Rab8 was also involved in the organization of the Golgi apparatus by recruiting the minus actin motor MyosinIV to the Golgi complex. A disruption of this function leads to a dispersion of the Golgi complex [Sahlender et al., 2005]. The observed changes in the vesicular transport of Rab8 without affecting significantly Rab6 marked transport routes therefore indicate that the knock-down of RIM3γ and RIM4γ preferentially impairs vesicular traffic from the recycling endosome, leading to reduced neuronal growth and disruption of the Golgi structure.

Correspondingly, the loss of RIM3γ and RIM4γ also affected vesicular transport of Rab11, a well-known regulator of the recycling endosome. In non-neuronal cells Rab11 regulates vesicular traffic to the endocytic recycling compartment and from the endocytic recycling compartment to the plasma membrane [Ullrich et al., 1996, Sönnichsen et al., 2000]. The correct trafficking of Rab11 vesicles was shown to be crucial for axonal and dendritic growth and arborization [Takahashi et al., 2012, Takano et al., 2014b, Lazo et al., 2013]. This function of Rab11 seems to be negatively regulated by the lemur kinase 1 (LMTK1). Phosphorylation of LMTK1 by

the Cyclin dependent kinase 5 (CDK5) inhibits Rab11 activity and formation of the endocytic recycling compartment [Takano et al., 2010]. Accordingly, down regulation of LMTK1 leads to an increase in velocity and trafficking length of Rab11 positive vesicles as well as increased neuronal growth. Interestingly, CDK5 was identified as possible interaction partner of RIM3γ and RIM4γ in our screen for novel interaction partners. Thus a hypothetical interference of RIM3γ and RIM4γ with this cascade via CDK5 could explain the observed reduction in the path length and velocity of Rab11vesicular traffic as well as a resulting reduction in axonal and dendritic growth. In addition impaired Rab11 vesicle traffic might change the formation of the recycling endosome and influence other vesicular trafficking routes associated with the recycling endosome like Rab8. This however would not explain the observed differential effects of RIM3γ and RIM4γ on Golgi morphology and vesicular transport routes.

Taken together, the loss of both γ-RIMs leads to a strong reduction in neuronal growth that affects axon and dendrites. The concomitant isoform specific changes in the Golgi morphology and vesicular transport suggest that RIM3γ and RIM4γ contribute to protein and membrane transport during neuronal growth with isoform specific function and are both crucial for neuronal development.

6.3 Affinity-purification mass spectrometry based proteomics reveals cytoskeleton and vesicular trafficking associated proteins as novel γ-RIM binding partners

With two experimental strategies we set out to identify the proteomic interaction partners of RIM3γ and RIM4γ with a focus on novel binding partners that are associated with neuronal growth or the regulation of synaptic transmission. Therefore we used two tissue preparations, whole brain homogenate and the crude synaptosomal fraction and the detergents CL114 and Triton X-100. Analysis of the identified novel γ-RIMs interaction partners revealed that the use of synaptosomal fractions and the detergent Cl114 did successfully increase the amount of synaptic proteins. Cl114 is a detergent of unknown composition, able to solubilize the Triton-X 100 resistant components of the presynaptic active zone. In our last experiment we combined the screens for novel interaction partners in whole brain homogenates solubilized with Triton X-110, crude synaptosomes solubilized with Triton X-100 and crude synaptosomes solubilized with Cl114 in one experiment. In this combinatory approach the use of Cl114 instead of TX-100 had an impact on the amount of identified synaptic proteins rather than the choice of the tissue fraction. However, the levels of synaptic proteins were generally much lower in this combinatory approach when compared to our first independent screen for novel interaction partners in crude synaptosomal fractions. Thus it might be possible that the preparation of the crude synaptosomal fraction in the combinatory experiment was not as pure as in the first experiment. Collectively, by using different tissue fractions and detergents with specific solubilizing characteristics it seems to be possible to resolve the entity of interaction partners of a protein belonging to different cellular compartments as well as differing functional complexes.

Except for the independent screen for novel γ-RIM interaction partners in crude synaptosomal

fractions all experiments revealed a similar distribution of functional categories of novel RIM3γ and RIM4γ interaction partners (Fig 5.11, 5.12). This overlap in novel RIM3γ and RIM4γ can be explained by the high sequence homology of both proteins. In addition the similar effects of RIM3γ and RIM4γ on neuronal growth suggest that both proteins share common interaction partners and participate in the same signaling cascades possibly at different steps. After the affinity purification the RIM3γ and RIM4γ proteome was analyzed by LC-MS/MS (liquid-chromatography-mass spectrometry/mass spectrometry) leading to not only the identification of primary but also secondary and tertiary interactions. Thus if RIM3γ and RIM4γ are involved in the same signal cascades but at different steps this would lead to identification of a similar proteome. The detection of nuclear import receptors as specific interaction partners of only RIM3γ in all approaches however shows that also isoform specific interaction partners could be detected. Furthermore, together with the strong nuclear localization of RIM3γ that is mediated by a nuclear localization signal in its N-terminus the discovery of importins in all experiments shows the potential of affinity-purification mass spectrometry proteomics approaches to identify protein interaction that might be of physiological relevance.

Analysis of the functional categories of detected proteins revealed that cytoskeletal proteins and proteins involved in intracellular traffic of proteins and vesicles constitute large groups of novel interaction partners in all screens. Moreover, most of the proteins that have been identified in multiple experiments could also be associated with these functional groups, suggesting that RIM3γ and RIM4γ are involved in processes of cytoskeleton remodeling and vesicular traffic during neuronal growth. In this context interesting novel γ-RIM interaction partners, that were identified in two of our experiments are three members of the Exocyst complex sec3, sec8 and sec6. The Exocyst complex is an important regulator of site directed exocytosis and was shown to be essential for membrane addition during neurite outgrowth and axon elongation [Vega & Hsu, 2001, Dupraz et al., 2009]. Two of the eight Exocyst subunits, sec3 and Exo70, are associated with the plasma membrane where they act as spatial landmarks and target arriving transport vesicles to the correct fusion site. The other Exocyst subunits (sec5, sec6, sec8, sec15 an Exo84) are directly associated with the transport vesicles. When transport vesicles carrying the six vesicular Exocyst components arrive at the plasma membrane the octameric complex assembles and thereby tethers the vesicles to their fusion site, keeping them in close proximity until the fusion machinery itself arrives [Boyd et al., 2004, Zhang et al., 2005]. Potential interactions of RIM3γ and RIM4γ with the vesicular Exocyst subunit sec8 and the plasma membrane localized subunit sec3 suggest that γ-RIMs are either present on transport vesicles guided by the two exocyst complex components or they influence vesicular traffic through an interaction with the two exocyst components. A key feature of neuronal growth is the site directed fusion of new membrane specifically to sites of outgrowth, this requires a high spatial and temporal control of the fusion event and consequently of the Excocyst complex components [He & Guo, 2009]. Further important regulators of vesicular transport, that were identified in multiple experiments as novel RIM3γ and RIM4γ interaction partners were several members of the Rab protein family. Interestingly, Rab11 vesicles were identified as target vesicles for the Exo70 mediated recruitment to the plasma membrane. Knock-down of Rab11 or Exo70 in cultured HeLa cells inhibits the

fusion of vesicles derived from the recycling endosome and leads to their accumulation at the cell periphery [Takahashi et al., 2012]. The interaction of RIM3γ and RIM4γ with the Exocyst complex and Rab11 could therefore explain the defect in neuronal growth and the disruption of vesicular transport routes leading to an inappropriate supply of membrane to the Golgi and hence a disruption of the Golgi morphology. Two members of the IQGAP family, which are involved in the cross talk of actin and microtubules were identified in two of our experiments. Interestingly, an interaction of IQGAP1, sec3 and sec8 upon CDC42 activation has been reported to play a role in the tumor cell invasion [Sakurai-Yageta et al., 2008]. Thus, IQGAPs could act as a further link between Rho signaling induced local changes in the cytoskeleton and site directed fusion events combining two fundamental processes of neuronal growth. An interaction of RIM3γ and RIM4γ with the Exocyst complex, IQGAPs and Rab proteins might therefore bring these functions together and might explain the observed phenotype after the knock-down of RIM3γ and RIM4γ.

Collectively, the different proteomics approaches led to the successful identification of interesting potential interaction partners in order to elucidate the function of RIM3γ and RIM4γ and a possible role in synaptic transmission. The whole set of proteins was composed of a large amount of cytoskeleton associated proteins and proteins involved in intracellular traffic. The comparison of the data sets of the individual experiments revealed a cluster of proteins that connects signaling pathways involved in cytoskeleton remodeling with site directed vesicular transport and might explain the phenotype observed in RIM3γ and RIM4γ knock-down neurons. Future studies on the interaction γ-RIMs, the Exocyst complex components, IQGAPs, CDC42 effector proteins, Rabs and other proteins identified in multiple screens will help to understand in more detail how the interplay of these protein is involved in signaling cascades and cellular processes to promote axonal and dendritic growth.

6.4 Novel binding partners suggest an involvement of RIM3γ and RIM4γ in several cellular processes explaining their role in neuronal arborization

Interesting candidates identified in the mass spectrometry approaches as potential interaction partner of RIM3γ an RIM4γ are the cell adhesion molecules plakophilin4 and δ-catenin. The interactions of plakophilin4 and RIM3γ an RIM4γ were confirmed *in vitro* (Fig. 5.14). This *in vitro* interactions are not caused by a general affinity of plakophilin4 to C_2 domains, as plakophilin4 did not bind to the C_2A-C_2B-domains of RIM1. Plakophilin4 belongs to a subfamily of armadillo repeat proteins composed of p120catenin, δ-catenin/NPRAP, ARVCF and the more distantly related plakophilins1-3, whereby δ-catenin is most closely related to plakophilin4. δ-catenin is involved in the regulation of dendritic morphology and dendritic spine number by forming a complex with the actin linker protein cortactin as well as RhoGTPases [Kim et al., 2007, Martinez et al., 2003]. RhoGTPases are important regulators of the actin cytoskeleton during various cellular processes including neuronal growth [Bito et al., 2000, Nakayama et al., 2000]. A specific function of plakophilin4 in neuronal growth was not shown yet, however a screen

for interaction partners of plakophilin4 revealed, similar to the identified γ-RIM interaction partners, a high number of cytoskeletal proteins and also a large fraction of proteins involved in vesicular and intercellular traffic [Keil & Hatzfeld, 2013, Keil et al., 2013]. Thus, a potential interaction with plakophilin4 or δ-catenin might link RIM3γ an RIM4γ to signaling cascades involved in the regulation of the cytoskeleton and contribute to their role during neuronal growth.

Another regulator of the cytoskeleton identified as potential interaction partner of RIM3γ and RIM4γ in the mass spectrometry approaches was IQGAP3. This potential interaction between IQGAP3 and the γ-RIMs was verified *in vitro* by GST-pulldown assays and Co-immunoprecipitation (Fig. 5.16). The closely related protein IQGAP1 in contrast showed no binding affinity to RIM proteins (Fig. 5.16). IQGAPs have been suggested as critical regulators of the cross talk between actin an microtubules. Through the direct binding to actin filaments IQGAPs are able to converge Rac1 and CDC42 signals to the actin cytoskeleton and via microtubule associated proteins also to the microtubule network [Mateer et al., 2002, Fukata et al., 2002]. Consistently, IQGAPs are involved in various cellular processes by remodeling actin filaments and microtubules [Brandt & Grosse, 2007, White et al., 2012]. A disruption of the correct interplay of actin and microtubules presumably leads to strong impairments in neuronal growth. shRNA mediated knock-down of IQGAP1 as well as knock-down of its binding partner CLIP170, a microtubule plus end tracking protein, reduces the dendritic complexity in primary cultured neurons. Both knock-down phenotypes can be rescued by addition of the actin polymerizing drug jasplakinolide, suggesting that both proteins are crucially involved in the crosstalk with actin filaments during neuronal growth [Swiech et al., 2011]. Knock-down of the other IQGAP family members, IQGAP2 and IQGAP3 leads to a reduction in NGF (neuronal growth factor) induced neurite outgrowth in PC12 cells and reduced axonal length of primary hippocampal neurons [Wang et al., 2007]. This impairment in neurite outgrowth could not be rescued by the overexpression of CDC42 and Rac1 suggesting that IQGAP2 and IQGAP3 function downstream of Rac1 and CDC42 in the regulation of the cytoskeleton during neuronal growth. An effect on axonal growth was in contrast not observed after the knock-down of IQGAP1. Thus, all members of the IQGAP family seem to be involved conveying growth regulating signals to the cytoskeleton with differential contribution to axonal and dendritic growth. An interaction of RIM3γ and RIM4γ with IQGAP3 is therefore a further link to the modulation of the cytoskeleton during neuronal growth. IQGAP3 and IQGAP2 seem to be important for initial neurite outgrowth and axon elongation whereas IQGAP1 is involved in later stages of neuronal growth during the elaboration of a complex dendritic arbor. The knock-down of RIM3γ and RIM4γ similar to the knock-down of IQGAP3 impaired neurite growth and axonal elongation. This substantiates the possibility that RIM3γ and RIM4γ are involved in neuronal growth by interfering with the transduction of growth regulating signaling on the cytoskeleton via IQGAP3. IQGAP1 showed no binding affinity to RIM proteins further supporting the specificity of the identified interaction in accordance to the differential function of the IQGAPs during neuronal growth. However it remains elusive if the positive binding of the C_2A-C_2B-domains of RIM1 to IQGAP3 in two out of three *in vitro* protein binding assays is due to a general affinity of IQGAP3 to C_2B domains or a specific interaction of IQGAP3 to RIM1. Nevertheless, the reported role

in synaptic plasticity of IQGAP1 as modulator of NMDA receptor traffic and activity [Gao & Frausto, 2011] opens the possibility, that also IQGAP3 might be involved in the organization of the presynapse. This function of IQGAP3 could involve an interaction with RIM1. Interestingly, IQGAP1 was also shown to associate with Golgi membranes together with CDC42 suggesting that IQGAP1 is also involved in the modulation of the Golgi apparatus by local remodeling of the cytoskeleton [McCallum et al., 1998]. Thus, the interaction of RIM3γ and RIM4γ with IQGAP3 could explain the role of both γ-RIMs in neuronal growth and the modulation of the Golgi apparatus assuming a function of IQGAP3 in the modulation of the Golgi apparatus in accordance to IQGAP1.

The high sequence homology between the 7 RIM family members and their shared synaptic localization suggests an involvement in common regulatory mechanisms at the presynapse [Wang et al., 2000, Alvarez-Baron et al., 2013]. In this study the synapse defective protein 1 (Syd-1), a protein involved in the early steps of active zone assembly [Owald et al., 2012] was identified as potential interaction partner of RIM3γ and RIM4γ. This potential interaction with RIM3γ and RIM4γ as well as an interaction with the C_2B domain of RIM1 could be verified in *in vitro* binding assays (Fig 5.18). The initial steps of the presynaptic assembly include local changes of the actin cytoskeleton allowing for the subsequent establishment of the tight protein network of the presynaptic active zone. Syd-1 interacts with this actin network at nascent synapses and is thought to be involved in the recruitment of active zone proteins via its interaction with Liprin-α [Wentzel et al., 2013, Li et al., 2014]. Furthermore, Syd-1 was shown to be involved in coordinating the assembly of pre- and postsynaptic structures in cooperation with the presynaptic adhesion molecule neurexin, which is known to induce assembly of the postsynaptic densities via its postsynaptic partner neuroligin [Owald et al., 2012]. Considering the observed impairments in synapse formation after the knock-down of RIM3γ and RIM4γ as well as their proposed functions in intracellular traffic it can be envisioned that the γ-RIMs are involved in the transport of Syd-1 to the assembling presynapse. Thus, a loss of RIM3γ or RIM4γ would lead to a misslocalization of Syd-1, disrupting the correct assembly of the presynapse and consequently also the coordinative assembly of the postsynapse. However, the strong deficits of neuronal growth suggest that the reduced synapse number observed in RIM3γ and RIM4γ knock-down neurons is rather caused by a disruption of general growth processes. Additionally, the interaction of Syd-1 not only with RIM3γ and RIM4γ but also the C_2B domain of RIM1 suggests, that rather Syd-1 is responsible for the recruitment of RIM proteins to the active zone. The C_2B domain is highly conserved between all RIM family members. Thus if the recruitment of RIM proteins is mediated through a binding of Syd-1 to the C_2B domains, RIM3γ and RIM4γ could act as dominant negative versions and thereby influence the amount of RIM1 at the presynapse. This mechanism would allow RIM3γ and RIM4γ to negatively interfere with the presynaptic release probability and hence synaptic strength. Instead of blocking the binding of RIM to Syd-1, RIM3γ and RIM4γ could also stabilize this interaction by forming a tripartite complex with Syd-1 and RIM1 and promote thereby the assembly of the active zone.

Taken together, the *in vitro* verified interaction of γ-RIMs with IQGAP3 and plakophilin4 propose several mechanisms explaining how RIM3γ and RIM4γ might interfere with the remodeling

of the cytoskeleton as well as intracellular traffic of proteins and membrane during growth and development. However, the questions of how these functions converge and what their individual contributions to the role of RIM3γ and RIM4γ in neuronal arborization are, remain to be answered. The interaction with the presynaptic protein Syd-1 suggests that RIM3γ and RIM4γ exhibit in addition to the growth regulating function a synapse specific role.

6.5 Activity dependent changes in RIM3γ and RIM4γ gene transcription

During increased neuronal activity neurons undergo changes in molecular composition and structure in order to adjust their synaptic strength. This neuronal plasticity has been associated with a variety of physiological processes like learning and memory but also pathological processes like epileptogenesis [Milner et al., 1998, Bausch et al., 2006]. A possible function of RIM3γ and RIM4γ in neuronal plasticity was investigated in a model of episodic brain hyperexcitability, by analyzing the effect of intense neuronal activity on the gene expression of RIM3γ and RIM4γ. In this model a status epilepticus characterized as an episode of intense synchronized neuronal activity is induced by the application of the muscarinic agonist pilocarpine. Mice subjected to pilocarpine induced status epilepticus develop spontaneous seizures after a latency period of two weeks [Pitsch et al., 2007]. 12 hours after status epilepticus the gene exepression of RIM4γ is strongly upregulated in the hippocampus. RIM3γ in contrast shows only a weak down regulation in the dentate gyrus 36 hours after status epilepticus. In accordance RIM4γ was recently shown to be upregulated in the hippocampus after induction of neuronal activity by the application of kainic acid [Hermey et al., 2013]. These results suggest a function in the regulation of synaptic strength for both γ-RIMs with presumably opposing effects of the two isoforms. In the same animal model of epilepsy the gene expression of RIM1 was unchanged in the acute phase after status epilepticus though downregulated 28 days after status epilepticus in the chronic phase when the animals experience spontaneous seizures [Pitsch et al., 2012]. This could be either a compensatory mechanisms of the neuronal network in order reduce synaptic strength and diminish the hyperxcitability of an epileptic brain or the decrease in RIM1 gene expression is part of the pathomechanisms leading to chronic epileptic seizures. In addition RIM1 was shown to be differentially regulated after neuronal silencing [Jiang et al., 2010, Lazarevic et al., 2011]. Both lines of evidence suggest an important role for RIM1 in the adaptation of the synaptic strength during changes in network activity. RIM1 knock-out mice like RIM3γ knock-out mice show no obvious motor phenotype. However, detailed electrophysiological and behavioral experiments revealed that RIM1 knock-out mice do experience impairments in presynaptic release probability resulting in severe learning and memory deficits and schizophrenia related behaviors whereby coordination is unchanged [Powell et al., 2004, Blundell et al., 2010b]. Interestingly, changes in RIM3γ expression levels have been reported in schizophrenia and in lymphoblastoid cells from autism patients. [Weidenhofer et al., 2006, Weidenhofer et al., 2009, Nishimura et al., 2007]. RIM3γ was further identified as a novel candidate gene for autism in a genetic approach [Kumar et al., 2010]. These findings suggest that alterations in the loss of RIM3γ gene expression might

induce the development of neuropsychiatric disorders like schizophrenia and autism in RIM3γ knock-out mice. In the future electrophysiological analysis together with detailed behavioral studies on the phenotypes of RIM3γ and RIM4γ knock-out mice will help to unravel the role of RIM3γ and RIM4γ in synaptic transmission as well as in the development of neurological disorders.

6.6 Strong motor phenotype in RIM4γ knock-out mice

The shRNA mediated knock-down of proteins allows to analyze the function of the protein of interest only in a subset of cells at a specific time point during development. In contrast constitutive knock-out mice allow to study the consequences of the loss of a genes function throughout development on the whole mouse organism. During this study the introduction of a splice acceptor site in an intronic region of the RIM3γ and RIM4γ genes lead to the successful generation of constitutive RIM3γ and RIM4γ knock-out mice. The ablation of the gene of interest was verified on the level of mRNA expression and on the level of protein expression (Fig 5.20). Homozygous RIM3γ knock-out (RIM3γ-/-) mice showed a reduction of 90-99% in mRNA and protein levels depending on the analyzed brain region whereas homozygous RIM4γ knock-out (RIM4γ-/-) mice revealed a only reduced of 70-98%. The constitutive knock-out of RIM4γ was induced by the introduction of a splice acceptor cassette in the intron region between exon one and two. Thus, a successful knock-out should abolish the expression of the full-length protein. It would however still allow the expression of the first exon. The antibodies used to detect RIM4γ on western blots as well as the primers used to detect RIM4γ mRNA, both span boarders of exon one and two. The expression of exon one in the constitutive RIM4γ-/- mice should therefore not be detectable by western blots and quantitative real time RT-PCR with the used antibodies and primers. Endogenous RIM4γ expression in the brain is fairly low, leading to weak signals in western blots and quantitative real time RT-PCR and consequently to small signal to noise ratio. Thus, the detected signals of RIM4γ expression in RIM4γ -/- mice might be or partially caused by a relatively a high background signal. Consistently RIM4γ -/- mice exhibit the highest RIM4γ rest protein expression levels of all tested brain regions in the hippocampus, the region with the lowest endogenous expression levels. Whereas in the cerebellum the region with the highest RIM4γ expression levels in the brain the signal was reduced to 2% of wild type protein expression levels [Alvaréz-Baron, 2010], (Fig 5.20). However, it cannot be excluded that constitutive RIM4γ -/- mice still express low levels of RIM4γ caused by not 100% effective splicing of the introduced gene trap cassette. Analysis of conditional RIM3γ and RIM4γ crossed with a Cre recombinase expressing line leading to the complete excision of the targeted exons will show if the background in western blots and quantitative real time RT-PCR originates from ineffective splicing of the gene trap cassette or by unspecific background signals.

In the first weeks after birth RIM4γ -/- and RIM3γ-/- mice cannot be distinguished from wild type litter mates and show no obvious abnormalities. At three weeks of age, around the time of weaning, RIM4γ -/- mice develop a severe episodic motor phenotype accompanied by a strong reduction in weight whereas RIM3γ-/- mice develop normally (Fig 5.22, 5.23). Gait analysis and

motor tests on a rotating rod revealed that RIM4γ -/- mice also during episodes of no obvious motor impairments experience coordinative disturbances (Fig 5.24, 5.25). These motor deficits might be at least partially contributed to a weakened musculature due to the strong episodes of hind limb impairments and the associated weight loss. The weight reduction in RIM4γ-/- mice starts to develop at the same time as the episodic motor phenotype and might therefore be a secondary effect of the motor phenotype. During episodes of motor impairments RIM4γ-/- mice might be devitalized and less able to reach the food represented in wire-bar cage lids. In addition, the strong motor abnormalities occurring with a frequency of once every 24 hours possibly induce physical stress leading to a higher calorie consumption in RIM4γ -/- mice in comparison to wild type litter mates.

Apart from the frequent episodes of motor disturbances, in rare cases a behavior resembling an event of epileptic seizures was observed in RIM4γ -/- mice. The difference in the frequency of theses two events and also in the difference in the behavioral impact suggest that RIM4γ-/- mice suffer from several neurological impairments leading on the one hand to strong episodic motor deficits affecting mainly the hind limbs and on the other hand in rare cases to epileptic seizure like events.

The growth deficits observed in RIM4γ knock-down neurons suggest that the motor phenotype in RIM4γ-/- mice is caused by impairments in neuronal growth leading to changes in the brain architecture. Histological stainings of neuronal layers revealed no drastic changes in the overall architecture of the hippocampus and the cerebellum of RIM4γ -/- and RIM3γ -/- mice (Fig. 5.27). A functional redundancy of RIM3γ and RIM4γ in neuronal growth is already suggested by the same strong deficits in the neurite growth after the knock-down of either RIM3γ or RIM4γ and further supported by the finding that the growth impairments can be partially rescued by the overexpression of the respective other γ-RIM isoform [Alvarez-Baron et al., 2013]. An upregulation of the respective other γ-RIM isoform in RIM3γ and RIM4γ knock-out mice might therefore help to overcome or milder the deficits in neuronal growth and aborization in RIM3γ -/- and RIM4γ -/- mice. Mildered dendritic growth deficits after the complete knock-out of a protein in comparison to its acute knock-down have been reported for example for δ-cantenin. Both primary cultured neurons transfected with shRNA agains δ-cantenin and cultured neurons from δ-cantenin knock-out mice show are reduction in the total dendritic length and the the number of dendritic endpoints, however this growth impairment was more pronounced in δ-cantenin knock-down neurons [Arikkath et al., 2008]. This suggests that the full knock-out allows the induction of compensatory mechanism in order to weaken the consequences of the protein loss. Interestingly, also the phenotype of reduced glutamatergic synapses after the knock-down of neuroligin-1 could neither be reproduced in neuroligin-1 nor in neuroligin-1, neuroligin-2 and neuroligin-3 triple knock-outs [Varoqueaux et al., 2006, Blundell et al., 2010a]. In-vivo studies on cortical pyramidal neurons in which neuroligin-1 levels had been downregulated from neuronal birth on revealed that the reduction in glutamatergic synapses was not caused by the loss of neuroligin-1 but the differing levels of neuroligin-1 in individual neurons [Kwon et al., 2012]. Thus also the varying levels of RIM3γ or RIM4γ after shRNA mediated knock-down in culture or *in vivo* could lead to a phenotype that would not be observed in the full knock-out.

The observed episodes of rapid uncontrolled movements disrupted by phases of rigid immobility in RIM4γ-/- partially resemble the phenotype of the tottering mouse. Tottering mice carry a mutation in the calcium channel α1a subunit gene (Cacna1a) that encodes for the pore forming protein of P/Q type calcium channels [Fletcher et al., 1996]. Tottering mice experience neurological deficits resulting in ataxia, paroxysomal dyskenisia and behavioral absence seizures resembling petit mal epilepsy. In these mice seizures resembling absence epilepsy have been associated with spike wave discharge whereas episodes of paroxysomal dyskenisia showed no obvious electroencephalographic correlates [Noebels & Sidman, 1979]. The episodes of dyskenisia resemble the observed phenotype in RIM4γ-/- mice. The phenotype observed in tottering mice is accompanied by a local increase in cell death in the cerebellum [Fletcher et al., 1996, Zwingman, 2001]. Studies on the expression pattern of the immediate early gene c-fos after induction of an episode of dyskenisia revealed an increase in neuronal activity in the cerebellum and concomitantly in the cerebal cortex [Campbell & Hess, 1998]. An involvement of the cerebellum in the emergence of the dystonic episodes in tottering mice was further confirmed by the surgical removal of the cerebellum. Cerebellectomy in tottering mice resulted in some cases in a worsening of the baseline ataxia however spontaneous dystonic attacks were abolished [Neychev et al., 2008].

Interestingly, RIM4γ exhibits the highest mRNA expression levels in the cerebellum and was furthermore suggested to be involved in the modulation of the voltage dependent inactivation of P/Q type calcium channels in PC12 cells. In *in-vitro* binding assays RIM4γ was shown to bind to the β4 and β3 subunits of voltage dependent calcium channels (VDCC) and to inhibit the voltage dependent inactivation leading to longer calcium channel opening times [Uriu et al., 2010]. In accordance it was suggested that the phenotype observed in tottering mice might be caused by reduced current density in Purkinje cells and minor effects on P/Q current kinetics including changes in the voltage dependence of inactivation [Wakamori, 1998]. Taken together, the high expression levels of RIM4γ in the cerebellum and the suggested function in the modulation of calcium channel opening times as well as the resembling motor deficits of RIM4γ -/- and tottering mice indicate that the phenotype observed in RIM4γ -/- mice is caused by changes in the electrophysiological properties of the cerebellum. The cerebellum itself does not initiate movements but it contributes to coordination, precision, accuracy and timing. Therefore, the observed coordinative disturbances in the RIM4γ -/- mice during the phenotypic inconspicuous periods further support a dysfunction of the cerebellar circuits in RIM4γ -/- mice. Furthermore, lately RIM1 and RIM2 were associated with the rare dominantly inherited episodic movement disorder paroxysmal dyskinesia (PNKD). PNKD is characterized by childhood onset with involuntary movements in the limbs, trunk, and face manifesting as dystonia, chorea, and athetosis. The causative gene codes for a novel protein PNKD that has been show to localize to the presynapse and shows a binding affinity the C_2B domain of RIM1 and RIM2 [Shen et al., 2015]. With regard to the reported functional redundancy in neuronal growth as well as remodeling of calcium channel opening times of both γ-RIMs it is surprising that RIM3γ -/- mice are behaviorally inconspicuous and do not share the phenotype of RIM4γ -/- mice [Uriu et al., 2010, Alvarez-Baron et al., 2013]. This contradiction suggests that RIM4γ

might rather influence the functionality of the cerebellum through a function that is not shared by RIM3γ. A RIM4γ specific synaptic function is furthermore supported by the strong RIM4γ transcriptional upregulation after the induction of synaptic activity [Hermey et al., 2013]. The loss of RIM4γ could therefore impair synaptic transmission especially in the cerebellum leading to an imbalance and misconnection of neuronal circuits involved in motor coordination.

Taken together, RM4γ -/- mice show a strong episodic motor phenotype and mild coordination disturbances. The high expression levels of RIM4γ in the cerebellum together with the role of the cerebellum in motor coordination suggest that the loss of RIM4γ might impair the correct formation and function of neuronal circuits in the cerebellum leading to the observed phenotype. RIM3γ -/- mice in contrast showed no drastic motor phenotype or changes in overall brain architecture. However, possible deficits in learning and memory and behaviors associated with neuropsychiatric disorders were not investigated in this study and remain to be resolved.

7 Outlook

The findings obtained in this study form the basis for future experiments on the functional role of RIM3γ and RIM4γ.

Our affinity-purification mass spectrometry approaches revealed a substantial number of interesting novel potential γ-RIM interaction partners. Biochemical studies on the interactions with these newly identified binding partners will help to unravel the proteomic connectome of RIM3γ and RIM4γ. In addition, functional assays on the role of these potential interactions in axonal and dendritic growth, Golgi morphology and vesicular traffic will allow, to elucidate the signaling cascades that underlie the role of RIM3γ and RIM4γ in neuronal growth.

In shRNA mediated knock-down experiments we could show that the sudden loss of RIM3γ and RIM4γ leads to strong impairments in neuronal growth *in vivo* and *in vitro*. However, in RIM3γ and RIM4γ knock-out mice the overall brain morphology appears unchanged. Therefore, detailed studies on the morphology of brain structures and of individual neurons of RIM3γ and RIM4γ knock-out mice, including the induction of the gene knock-out at different developmental stages, are required to reveal if possible growth deficits are restricted to specific cell types or compensated during development through the upregulation of other growth promoting proteins.

The characteristics of the strong motor deficits and the coordinative disturbances as well as the high expression levels of RIM4γ in the cerebellum raise the question if an impaired cerebellar function is responsible for the phenotype of RIM4γ knock-out mice. This question can be answered by studying the consequence of a conditional RIM4γ knock-out restricted to the cerebellum or specific neuronal subtypes.

In genexpression assays we could show that RIM3γ and RIM4γ are differentially regulated after pilocarpine induced status epilepticus. This finding together with a possible role of both proteins in synaptic transmission suggest that γ-RIMs might be crucial for the correct function of a healthy brain. Electrophysiological measurements in the hippocampus and cerebellum of RIM3γ and RIM4γ knock-out mice will show if the two γ-RIMs are involved in the establishment of hippocampal and cerebellar circuits and the regulation of synaptic transmission. Furthermore, behavioral tests on RIM3γ and RIM4γ knock-out mice considering changes in learning and memory, schizophrenia related behaviors and the sensitivity to epileptogenic insults will contribute to our knowledge on the role of RIM3γ and RIM4γ in the pathogenesis of neurological disorders as well as in normal brain.

8 Appendix

8.1 Tables of by mass spectrometry identified RIM3γ and RIM4γ binding proteins

8.2 Table 8.1: Proteins identified in the whole mouse brain fraction

gene ID	identified protein	protein score RIM3γ	protein score RIM4γ
intercellular signaling			
1175	Adaptor-related protein complex 2, sigma 1 subunit	210	73
116986	ArfGAP with GTPase domain, ankyrin repeat and PH domain 1		295
9855	FERM, RhoGEF and pleckstrin domain protein 2	235	
9737	G protein-coupled receptor associated sorting protein 2	449	
2778	GNAS complex locus	225	360
84705	GTP binding protein 3 (mitochondrial)	304	112
2770	Guanine nucleotide binding protein (G protein), alpha inhibiting activity polypeptide 1	430	384
2782	Guanine nucleotide binding protein (G protein), beta polypeptide 1	165	213
8471	Insulin receptor substrate 4	1505	1632
5784	protein tyrosine phosphatase, non-receptor type 14	203	123
5905	Ran GTPase activating protein 1		205
79809	Tetratricopeptide repeat domain 21B	215	328
adhesion molecules			
gene ID	identified protein	protein score RIM3γ	protein score RIM4γ
154796	Angiomotin	1547	1610
1495	Catenin (cadherin-associated protein), alpha 1, 102kDa	659	536
1500	Catenin (cadherin-associated protein), delta 1	502	285
57530	Cingulin	611	432
1829	Desmoglein 2	479	
56704	Junctophilin 1	158	257
3987	LIM and senescent cell antigen like domains 1	64	207
5318	Plakophilin2		769

8502	Plakophilin4	129	442
7082	Tight junction protein 1	991	811
intracellular protein and membrane traffic			
gene ID	identified protein	protein score RIM3γ	protein score RIM4γ
8546	Adaptor-related protein complex 3, beta 1 subunit	486	532
8943	Adaptor-related protein complex 3, delta 1 subunit	486	532
1176	Adaptor-related protein complex 3, sigma 1 subunit	221	133
55763	Exocyst complex component 1	491	164
60412	Exocyst complex component 4	404	291
9922	IQ motif and Sec7 domain 1	379	789
9928	Kinesin family member 14	321	404
cytoskeletal proteins and cytoskeleton regulating proteins			
gene ID	identified protein	protein score RIM3γ	protein score RIM4γ
829	Capping protein (actin filament) muscle Z-line, alpha 1	305	215
11135	CDC42 effector protein (RhO GTPase binding) 1		484
1674	Desmin	288	
128239	IQ motif containing GTPase activating protein 3 (IQGAP3)	158	603
55700	MAP7 domain containing 1	139	327
79649	MAP7 domain containing 3		874
253260	RPTOR independent companion of MTOR, complex 2	126	655
89796	Neuron navigator 1	1886	284
6709	Spectrin, alpha, non-erythrocytic 1	3375	2047
6711	Spectrin, beta, non-erythrocytic 1	2333	2143
10381	Tubulin, beta 3		999
synaptic proteins			
gene ID	identified protein	protein score RIM3γ	protein score RIM4γ
8573	Calcium/calmodulin dependent serine protein kinase (MAGUK family)	48	83
5573	Protein kinase, cAMP-dependent, regulatory, type I, alpha	203	123
85360	Synapse defective 1, Rho GTPase, homolog 1 (syd-1)	246	

116841	Synaptosomal-associated protein, 47kDa	313	89
55014	Syntaxin 17	272	
channel proteins			
gene ID	identified protein	protein score RIM3γ	protein score RIM4γ
7417	Voltage dependent anion channel 2	223	89
729317	Voltage dependent anion channel 2 pseudogene	223	89
nuclear proteins			
gene ID	identified protein	protein score RIM3γ	protein score RIM4γ
983	Cyclin dependent kinase 1	385	333
79711	Importin 4	150	
3843	Importin 5	188	
10526	Importin 8	119	
calcium binding proteins			
gene ID	identified protein	protein score RIM3γ	protein score RIM4γ
5954	Reticulocalbin 1, EF-hand calcium binding domain	658	
5955	Reticulocalbin 2, EF-hand calcium binding domain	396	
51150	Stromal cell derived factor 4	453	

8.3 Table 8.2: Proteins identified in crude synaptosomal fractions

gene ID	identified protein	protein score RIM3γ	protein score RIM4γ
synaptic proteins /synaptic vesicle release /synaptogenesis			
12217	Bassoon	35	37
234577	Copine-2	33	
13838	Ephrin type-A receptor 8	39	
20512	Excitatory amino acid transporter 1	69	46
20511	Excitatory amino acid transporter 2	20	
73748	Glutamate decarboxylase-like protein 1		28
17475	Multiple PDZ domain protein	16	
499191	Neugrin		33
235627	Neurobeachin-like protein 2		40
26875	Piccolo	30	
382018	Protein unc-13 homolog A 41		41
116837	Regulating synaptic membrane exocytosis protein 1	68	121
20615	SNARE-associated protein Snapin	30	
27204	Synapsin-3		30
9145	Synaptogyrin-1	60	
20614	Synaptosomal-associated protein 25	51	
27359	Synaptotagmin-like protein 4	37	
20969	Syndecan-1		32
6804	Syntaxin-1A	39	
cytoskeletal components and cytoskeleton regulating proteins			
gene ID	identified protein	protein score RIM3γ	protein score RIM4γ
68743	Actin-binding protein anillin		31
76652	Actin-related protein M1 homolog	35	
70	Actin, alpha cardiac muscle 1	100	
219144	ADP-ribosylation factor-like protein 11	33	
56430	CAP-Gly domain-containing linker protein 1	43	
58804	Cdc42 effector protein 5	30	
208846	Disheveled-associated activator of morphogenesis 1	31	36
17761	Ensconsin (MAP7)		30
56226	Espin	30	
56223	Fascin-3		37
232944	MAP/microtubule affinity-regulating kinase 4	31	

270058	Microtubule-associated protein 1S	30	28
78757	Rapamycin-insensitive companion of mTOR		26
10788	Ras GTPase-activating-like protein IQGAP2		32
22349	Villin-1		31
intracellular protein and membrane traffic			
gene ID	identified protein	protein score RIM3γ	protein score RIM4γ
16476	AP-1 complex subunit beta-1	33	
216963	ARF GTPase-activating protein GIT1	26	
26357	ATP-binding cassette sub-family G member 2	43	
8455	Attractin	36	
13424	Cytoplasmic dynein 1 heavy chain 1	32	
235661	Cytoplasmic dynein 1 light intermediate chain 1	35	
13424	Cytoplasmic dynein 2 heavy chain 1	32	
110084	Dynein heavy chain 8, axonemal	29	
227619	Endoplasmic reticulum mannosyl-oligosaccharide 1,2-alpha-mannosidase		20
211446	Exocyst complex component 3 (Sec 6)	35	
18550	Furin	31	
15194	Huntingtin		33
381290	Plasma membrane calcium-transporting ATPase 4	87	
53421	Protein transport protein Sec61 subunit alpha isoform 1	42	
18844	Plexin-A1	32	
98732	Rab3 GTPase-activating protein non-catalytic subunit	27	38
268451	Rab11 family-interacting protein 4	26	
34110	Rabenosyn-5	29	
19894	Rabphilin-3A	47	
104886	Ras-related protein Rab-15	31	
19338	Ras-related protein Rab-33B	57	
270160	Ras-related protein Rab-39A	19	19
67295	Ras-related protein Rab-3C	57	
19341	Ras-related protein Rab-4A	57	
19346	Ras-related protein Rab-6A	57	

266781	Sorting nexin-17		34
27096	Trafficking protein particle complex subunit 3		32
364137	Transmembrane protein 165		42
adhesion molecules			
gene ID	identified protein	protein score RIM3γ	protein score RIM4γ
75723	Angiomotin-like protein 1		31
70882	Armadillo repeat-containing protein 3		34
102272429	Claudin-7		30
319565	Nesprin-2	36	
17967	Neural cell adhesion molecule 1	44	
18081	Ninjurin-1	29	
23963	Teneurin-1	37	35
channel proteins			
gene ID	identified protein	protein score RIM3γ	protein score RIM4γ
243634	Anoctamin-2		16
228432	Anoctamin-3	30	
102566	Anoctamin-10	27	
1179	Calcium-activated chloride channel regulator 1	26	
12283	Calcium-binding protein 39	36	
53321	Contactin-associated protein 1		29
14609	Gap junction alpha-1 protein	32	
14616	Gap junction alpha-8 protein	31	
16509	Potassium voltage-gated channel subfamily E member	41	
67498	Potassium voltage-gated channel subfamily V member 1	33	31
110876	Sodium channel protein type 2 subunit alpha	35	
22333	Voltage-dependent anion-selective channel protein 1	69	
22335	Voltage-dependent anion-selective channel protein 3	69	
nuclear proteins			
gene ID	identified protein	protein score RIM3γ	protein score RIM4γ
30946	Activator of basal transcription 1	32	
214444	CDK5 regulatory subunit-associated protein 2	30	

69131	Cyclin-dependent kinase 12		29
18555	Cyclin-dependent kinase 16		32
76582	Importin-11	33	
13555	Transcription factor E2F1	37	
15273	Transcription factor HIVEP2	14	
17133	Transcription factor MafF	50	
270627	Transcription initiation factor TFIID subunit 1	30	
22589	Transcriptional regulator ATRX	29	
70207	Translational activator of cytochrome c oxidase 1	33	
calcium binding proteins			
gene ID	identified protein	protein score RIM3γ	protein score RIM4γ
69008	Calcium-binding protein 39-like	36	
26611	Reticulocalbin-2	88	
growth receptors			
gene ID	identified protein	protein score RIM3γ	protein score RIM4γ
18212	BDNF/NT-3 growth factors receptor	31	
50915	Growth factor receptor-bound protein 14		31

8.4 Table 8.3: Proteins identified in the combined mass spectrometry approach

gene ID	identified protein	RIM3γ WB	RIM3γ SS CL114	RIM3γ SS TX100	RIM4γ WB	RIM4γ SS CL114	RIM4γ SS TX100
cytoskeletal proteins and cytoskeleton regulating proteins							
103466	5'-nucleotidase domain-containing protein 3				35,30		
56444	Actin-related protein 10				85,45		
66713	Actin-related protein 2				159,34		
35311	Actin-related protein 2/3 complex subunit 2		136,75		65,67	82,39	
33864	Actin-related protein 2/3 complex subunit 4				102,72		
74117	Actin-related protein 3				164,29		
11518	Alpha-adducin			84,14			
109676	Ankyrin-2				231,91		
11735	Ankyrin-3				90,46		
13821	Band 4.1-like protein 1			212,33			
13822	Band 4.1-like protein 2			91,18			
72832	Cartilage acidic protein 1				215,42		
12631	Cofilin-1	174,89			143,70	388,34	
53321	Contactin-associated protein 1	94,70			319,07		
12721	Coronin-1A				70,29		
76441	Disheveled-associated activator of morphogenesis 2						70,72
13429	Dynamin-1	83,49			410,25		
13726	Emerin	78,24		31,70			
14026	Ena/VASP-like protein				26,47		
53972	Ephexin-1				672,64		
22350	Ezrin					60,71	
14086	Fascin				129,57		
74103	LIM zinc-binding domain-containing Nebulette		115,91			52,08	

50997	MAGUK p55 subfamily member 2	224,46			259,52		
56524	MAGUK p55 subfamily member 6	175,77			141,30		
228355	MAP kinase-activating death domain protein						138,58
208158	MAP6 domain-containing protein 1	78,37			61,41		
17760	Microtubule-associated protein 6	403,93			586,35		
13589	Microtubule-associated protein RP/EB family member 1				74,59		
212307	Microtubule-associated protein RP/EB family member 2	79,96					
100732	Microtubule-associated protein RP/EB family member 3					107,87	
17698	Moesin				37,49		
50884	Nck-associated protein 1				66,19		
18645	Profilin-2				90,65		
52822	Protein RUFY3	179,76			203,13		
110351	Rap1 GTPase-activating protein 1			76,22			
11852	Rho-related GTP-binding protein RhoB					39,38	
18951	Septin-5				47,90		
235072	Septin-7				276,72		
20362	Septin-8					90,12	
53860	Septin-9			38,92			
21894	Talin-1		109,48				
22142	Tubulin alpha-1A chain	15161			13562		
22143	Tubulin alpha-1B chain	15128		11973	13489		8717
22146	Tubulin alpha-1C chain						7437
22151	Tubulin beta-2A chain	33621		30154	28024		19066
73710	Tubulin beta-2B chain			29618			18378
22152	Tubulin beta-3 chain	20802		19992	17990		12160
22153	Tubulin beta-4A chain	25880		23192	20926		13810
22154	Tubulin beta-5 chain	27471		25095	23377		15947

67951	Tubulin beta-6 chain	14700		12592	13068		7600
22388	WD repeat-containing protein 1				113,58		
207615	WD repeat-containing protein 37		40,36				
nuclear proteins / transcription machinery							
gene ID	identified protein	RIM3γ WB	RIM3γ SS CL114	RIM3γ SS TX100	RIM4γ WB	RIM4γ SS CL114	RIM4γ SS TX100
67089	26S protease regulatory subunit 10B		98,77				
19182	26S protease regulatory subunit 6A						76,47
118451	28S ribosomal protein S2, mitochondrial		83,61				
27207	40S ribosomal protein S11					114,90	
20085	40S ribosomal protein S19						47,59
27050	40S ribosomal protein S3		272,73			158,37	
20102	40S ribosomal protein S4, X isoform					36,10	
20115	40S ribosomal protein S7						69,76
19934	60S ribosomal protein L22						108,14
65019	60S ribosomal protein L23						132,55
268449	60S ribosomal protein L23a						99,74
67671	60S ribosomal protein L38	177,56			309,11		
100503670	60S ribosomal protein L5		129,40			94,71	
11737	Acidic leucine-rich nuclear phosphoprotein 32 family member A	88,87					
234734	Alanine-tRNA ligase, cytoplasmic			88,02			
70223	Asparagine–tRNA ligase, cytoplasmic		29,99			44,73	
237397	C2 calcium-dependent domain-containing protein 4C			143,34			

12568	Cyclin-dependent kinase 5		120,31			153,07	159,64
13194	DNA damage-binding protein 1	97,91			260,67		65,21
15502	DnaJ homolog subfamily A member 1	348,60	133,69		932,72	380,59	
56445	DnaJ homolog subfamily A member 2	209,95			235,65		
67838	DnaJ homolog subfamily B member 11				138,78		
23950	DnaJ homolog subfamily B member 6	111,75					94,87
13002	DnaJ homolog subfamily C member 5		45,05			20,61	
56354	DnaJ homolog subfamily C member 7	111,59			139,17		
13628	Elongation factor 1-alpha 2		480,39			713,68	
66656	Elongation factor 1-delta		173,19			107,17	
13631	Elongation factor 2	388,90			139,94		
74195	Elongator complex protein 3					58,15	
13681	Eukaryotic initiation factor 4A-I					116,76	
13682	Eukaryotic initiation factor 4A-II					113,28	
13664	Eukaryotic translation initiation factor 1A	57,46					
13665	Eukaryotic translation initiation factor 2 subunit 2				32,30		
13669	Eukaryotic translation initiation factor 3 subunit A			19,77			
8664	Eukaryotic translation initiation factor 3 subunit D				60,26		
16341	Eukaryotic translation initiation factor 3 subunit I		49,05			39,54	

208643	Eukaryotic translation initiation factor 4 gamma				58,98		
26232	F-box only protein 2				163,24		
23014	F-box only protein 21				284,66		
233038	F-box only protein 50		90,30				
214931	F-box/LRR-repeat protein 16				45,45		
15382	Heterogeneous nuclear ribonucleoprotein A1	115,72			94,32		94,18
56258	Heterogeneous nuclear ribonucleoprotein H2	174,99			403,88		
15387	Heterogeneous nuclear ribonucleoprotein K	804,49			685,93		
76936	Heterogeneous nuclear ribonucleoprotein M	70,03					
15289	High mobility group protein B1					47,30	
16650	Importin subunit alpha-7	151,48	68,06				
70572	Importin-5	80,08					
17975	Nucleolin	68,63					
17955	Nucleosome assembly protein 1-like 1				201,90		
66590	Phenylalanine–tRNA ligase alpha subunit				124,47		
66870	Plasminogen activator inhibitor 1 RNA-binding protein				79,81		
13207	Probable ATP-dependent RNA helicase DDX5				144,47		
110957	Putative ATP-dependent RNA helicase Pl10				163,56		
192196	Putative RNA-binding protein Luc7-like 2	107,91	125,65		122,45		
170791	RNA-binding protein 39						50,18
20382	Serine/arginine-rich splicing factor 2		87,87				
67332	Small nuclear ribonucleoprotein Sm D3	86,06					
71514	Splicing factor, proline- and glutamine-rich	62,64			60,06		

19045	Serine/threonine-protein phosphatase PP1-alpha catalytic subunit					96,3	
229906	Transcription initiation factor IIB	54,69					
66078	tRNA-splicing endonuclease subunit Sen34	226,29					

phosphatase / kinase

gene ID	identified protein	RIM3γ WB	RIM3γ SS CL114	RIM3γ SS TX100	RIM4γ WB	RIM4γ SS CL114	RIM4γ SS TX100
238276	A-kinase anchor protein 5			87,37			
229949	Adenylate kinase isoenzyme 5				290,01		
18573	Calcium/calmodulin-dependent 3',5'-cyclic nucleotide phosphodiesterase 1A				36		
18574	Calcium/calmodulin-dependent 3',5'-cyclic nucleotide phosphodiesterase 1B	123,17			148,68		
18747	Calcium/calmodulin-dependent protein kinase kinase 1				96,79		
12322	Calcium/calmodulin-dependent protein kinase type II subunit alpha	933,49			1487,90		
108058	Calcium/calmodulin-dependent protein kinase type II subunit delta			502,37	762,84		
12301	Calcyclin-binding protein					91,28	
18749	cAMP-dependent protein kinase catalytic subunit beta				99,39		
19084	cAMP-dependent protein kinase type I-alpha regulatory subunit				104,44		

19088	cAMP-dependent protein kinase type II-beta regulatory subunit	91,54			270,09		
12995	Casein kinase II subunit alpha	586,92	91,15	308,31	1081,31	113,12	746,57
13001	Casein kinase II subunit beta				140,63		
13480	Dolichol-phosphate mannosyltransferase						109,84
26398	Dual specificity mitogen-activated protein kinase kinase 4				75,00		
14555	Glycerol-3-phosphate dehydrogenase [NAD(+)], cytoplasmic		130,70			189,23	
333433	Glycerol-3-phosphate dehydrogenase 1-like protein		136,95			205,04	
238024	Ketosamine-3-kinase						59,83
229791	Lipid phosphate phosphatase-related protein type 4		150,27				
228355	MAP kinase-activating death domain protein	283,39			209,66		
26419	Mitogen-activated protein kinase 8				42,74		
117150	Phosphatidylinositol 5-phosphate 4-kinase type-2 gamma			62,64			32,85
18655	Phosphoglycerate kinase 1				455,30		
23969	Protein kinase C and casein kinase substrate in neurons protein 1				153,75	95,32	
18751	Protein kinase C beta type	94,12			634,50		
5582	Protein kinase C gamma type	353,28			660,07		
320472	Protein phosphatase 1E	150,97			428,78		
14208	Protein phosphatase 1G	47,36					

18746	Pyruvate kinase isozymes M1/M2	290,57			1004,45		
19280	Receptor-type tyrosine-protein phosphatase S	95,80					
106504	Serine/threonine-protein kinase 38	987,02			1766,14		
381979	Serine/threonine-protein kinase BRSK1						64,76
13175	Serine/threonine-protein kinase DCLK1				95,51		
70762	Serine/threonine-protein kinase DCLK2						44,45
51792	Serine/threonine-protein phosphatase 2A 65 kDa regulatory subunit A alpha isoform	575,74			924,47		113,82
19053	Serine/threonine-protein phosphatase 2A catalytic subunit beta isoform		153,71		151,00	161,99	
19055	Serine/threonine-protein phosphatase 2B catalytic subunit alpha isoform	379,51	2224,80		659,75	506,30	
72542	Serine/threonine-protein phosphatase PGAM5, mitochondrial		106,34			123,22	
19046	Serine/threonine-protein phosphatase PP1-beta catalytic subunit				121,99		
19047	Serine/threonine-protein phosphatase PP1-gamma catalytic subunit						88,99
14360	Tyrosine-protein kinase Fyn	80,29			140,51		

intracellular protein and membrane traffic

gene ID	identified protein	RIM3γ WB	RIM3γ SS CL114	RIM3γ SS TX100	RIM4γ WB	RIM4γ SS CL114	RIM4γ SS TX100
54401	14-3-3 protein beta/alpha			1071,89			649,95
22627	14-3-3 protein epsilon	2280,82	5240,19	1808,00	1611,89	1313,74	780,57

22629	14-3-3 protein eta	1171,41			669,69		
22628	14-3-3 protein gamma	2960,23		1866,78	1780,81		1145,57
22630	14-3-3 protein theta	1168,40		858,59	687,47		258,63
22631	14-3-3 protein zeta/delta	2285,80		1351,08	1384,78		773,58
15108	3-hydroxyacyl-CoA dehydrogenase type-2				175,68		
11842	ADP-ribosylation factor 3				59,30		
108124	Alpha-soluble NSF attachment protein		263,66		149,06		
11764	AP-1 complex subunit beta-1	278,19					
232910	AP-2 complex subunit sigma			44,42			
64933	AP-3 complex subunit mu-2				360,70		85,32
11777	AP-3 complex subunit sigma-1				96,17		
269774	AP2-associated protein kinase 1					91,64	
216963	ARF GTPase-activating protein GIT1			89,22			
17957	Beta-soluble NSF attachment protein		491,49			153,27	
235604	CaM kinase-like vesicle-associated protein	143,26			360,25		147,37
13016	C-terminal-binding protein 1				88,40		
65945	Calsyntenin-1				69,54		
232370	Calsyntenin-3	80,09					
12757	Clathrin light chain A		49,94				
213827	Coatomer subunit delta	101,22			87,16		
235661	Cytoplasmic dynein 1 light intermediate chain 1				185,14		
234663	Cytoplasmic dynein 1 light intermediate chain 2				75,90		
11258	Dynactin subunit 3				70,42		
108123	Gamma-soluble NSF attachment protein		130,70		90,42	94,91	
23897	HCLS1-associated protein X-1			181,95			215,51

232227	IQ motif and SEC7 domain-containing protein 1						130,49
16560	Kinesin-like protein KIF1A	147,30			196,99		
16564	Kinesin-like protein KIF21A	126,94		155,83	158,97		
18039	Neurofilament light polypeptide				206,39		
234267	Neuronal membrane glycoprotein M6-a				98,22	346,86	
2824	Neuronal membrane glycoprotein M6-b				65,84	209,30	
22343	Protein lin-7 homolog C				154,33	114,80	
69162	Protein transport protein Sec31A				42,49		
14569	Rab GDP dissociation inhibitor beta					248,07	
52055	Rab11 family-interacting protein 5				351,37		
226407	Rab3 GTPase-activating protein catalytic subunit	48,37			90,65		
19894	Rabphilin-3A	107,11			245,26		
19353	Ras-related C3 botulinum toxin substrate 1					146,43	
19325	Ras-related protein Rab-10				153,05		
68365	Ras-related protein Rab-14					110,46	
104886	Ras-related protein Rab-15					49,64	
19339	Ras-related protein Rab-3A				279,63		
67295	Ras-related protein Rab-3C					225,95	
271457	Ras-related protein Rab-5A					60,03	
19346	Ras-related protein Rab-6A				140,95		105,44

19418	Ras-specific guanine nucleotide-releasing factor 2						73,42
19415	RasGAP-activating-like protein 1					51,43	
11852	Rho-related GTP-binding protein RhoB				33,42		
9522	Secretory carrier-associated membrane protein 1		116,51				
73094	SH3-containing GRB2-like protein 3-interacting protein 1	76,74			76,77		
20661	Sortilin						87,03
69150	Sorting nexin-4	114,46			110,43		
27096	Trafficking protein particle complex subunit 3				64,01		
65114	Vacuolar protein sorting-associated protein 35	132,72					
18195	Vesicle-fusing ATPase	2647,27			4638,43		
40919	Vesicular glutamate transporter 2	1203,59			2237,58		

proteasome proteins

gene ID	identified protein	RIM3γ WB	RIM3γ SS CL114	RIM3γ SS TX100	RIM4γ WB	RIM4γ SS CL114	RIM4γ SS TX100
5700	26S protease regulatory subunit 4	77,20			152,17		
23996	26S protease regulatory subunit 6B	188,65			273,25		
19181	26S protease regulatory subunit 7				182,60		
19184	26S protease regulatory subunit 8	156,20			414,02		
69077	26S proteasome non-ATPase regulatory subunit 11	232,54			605,98		

66997	26S proteasome non-ATPase regulatory subunit 12				170,63		
10213	26S proteasome non-ATPase regulatory subunit 14	175,32	87,11		354,03	107,40	
57296	26S proteasome non-ATPase regulatory subunit 8				70,59		
69597	AFG3-like protein 2	66,86					
209318	COP9 signalosome complex subunit 1	141,74			86,01		
26891	COP9 signalosome complex subunit 4				251,40		
59026	E3 ubiquitin-protein ligase HUWE1				112,98		
56736	E3 ubiquitin-protein ligase RNF14				124,41		
20821	E3 ubiquitin-protein ligase TRIM21	34,83			202,33		
69807	E3 ubiquitin-protein ligase TRIM32				124,41		
67059	Obg-like ATPase 1	142,17					
22284	Probable ubiquitin carboxyl-terminal hydrolase FAF-X		66,33	66,33		114,90	114,90
26440	Proteasome subunit alpha type-1		84,39			171,87	
19167	Proteasome subunit alpha type-3	103,49			114,83		
26442	Proteasome subunit alpha type-5				113,55		
26444	Proteasome subunit alpha type-7				75,81		
14467	Protein NipSnap homolog 2			42,30	64,12		
22225	Ubiquitin carboxyl-terminal hydrolase 5			254,19			

22223	Ubiquitin carboxyl-terminal hydrolase isozyme L1					142,26	
107260	Ubiquitin thioesterase OTUB1		100,41		39,39		
217342	Ubiquitin-conjugating enzyme E2 O	135,46	135,46		159,10	159,10	
66589	Ubiquitin-conjugating enzyme E2 variant 1				118,83		
synaptic proteins /synaptic vesicle release /synaptogenesis							
gene ID	identified protein	RIM3γ WB	RIM3γ SS CL114	RIM3γ SS TX100	RIM4γ WB	RIM4γ SS CL114	RIM4γ SS TX100
12331	Adenylyl cyclase-associated protein 1					268,60	
12891	Copine-6				120,54		
13383	Disks large homolog 1				47,76		
20404	Endophilin-A1				160,52		
13838	Ephrin type-A receptor 4			140,80			
26556	Homer protein homolog 1				105,17		
330814	Latrophilin-1				149,34		
116838	Regulating synaptic membrane exocytosis protein 2	3400,23	2726,31				
20965	Synapsin-2	428,38			1070,95		
27204	Synapsin-3			99,89			
26949	Synaptic vesicle membrane protein VAT-1 homolog					84,64	
20972	Synaptogyrin-1			127,31	115,39		
67826	Synaptosomal-associated protein 47				76,83		
20979	Synaptotagmin-1	538,98			1491,77		
20980	Synaptotagmin-2				374,07		
20910	Syntaxin-binding protein 1	531,70			2063,49		

30960	Vesicle-associated membrane protein-associated protein A					37,57	
22318	Vesicle-associated membrane protein 2				349,20		
channel proteins							
gene ID	identified protein	RIM3γ WB	RIM3γ SS CL114	RIM3γ SS TX100	RIM4γ WB	RIM4γ SS CL114	RIM4γ SS TX100
239217	BTB/POZ domain-containing protein KCTD12	33,35			85,06		
14609	Gap junction alpha-1 protein		123,65			104,77	
234267	Neuronal membrane glycoprotein M6-a		312,28			206,72	
12298	Voltage-dependent L-type calcium channel subunit beta-4	145,59			85,91		
adhesion molecules							
gene ID	identified protein	RIM3γ WB	RIM3γ SS CL114	RIM3γ SS TX100	RIM4γ WB	RIM4γ SS CL114	RIM4γ SS TX100
94332	Cell adhesion molecule 3				43,35		
53321	Contactin-associated protein 1					109,36	
13510	Desmoglein-1-alpha		147,97				
109620	Desmoplakin		599,42				
16480	Junction plakoglobin		740,23		117,15		
17967	Neural cell adhesion molecule 1			665,27			173,09
64652	Nischarin					192,51	
18772	Plakophilin-1		634,05				
243743	Plexin-A4					49,28	
70549	Talin-2				258,14		
calcium binding proteins							
gene ID	identified protein	RIM3γ WB	RIM3γ SS CL114	RIM3γ SS TX100	RIM4γ WB	RIM4γ SS CL114	RIM4γ SS TX100

12317	Calreticulin	169,45			1034,43		

8.5 Table 8.4: Proteins identified in all screens

gene ID	identified protein	screen ident. prot X as RIM3γ binding protein	screen ident. prot X as RIM4γ binding protein
phosphatase / kinase			
protein family: Cyclin dependent kinases			
983	Cyclin dependent kinase 1	experiment 1: whole brain	experiment : whole brain
69131	Cyclin-dependent kinase 12		experiment 2: synaptosome CL-114
18555	Cyclin-dependent kinase 16		experiment 2: synaptosome CL-114
214444	CDK5 regulatory subunit-associated protein 2	experiment 2: synaptosome CL-114	
12568	Cyclin-dependent kinase 5	experiment 3: whole brain, synaptosome CL-114	experiment1 : whole brain
protein family: calcium calmodulin dependent kinases			
8573	Calcium/calmodulin dependent serine protein kinase (MAGUK family)	experiment 1: whole brain	experiment1 : whole brain
18747	Calcium/calmodulin-dependent protein kinase kinase 1		experiment 3: whole brain
12322	Calcium/calmodulin-dependent protein kinase type II subunit alpha		experiment 3: whole brain
108058	Calcium/calmodulin-dependent protein kinase type II subunit delta		experiment 3: whole brain, synaptosome TX-100
cytoskeletal proteins/ cytoskeleton associated proteins			
protein family: IQGAP			
gene ID	identified protein	screen ident. prot X as RIM3γ binding protein	screen ident. prot X as RIM4γ binding protein
128239	IQ motif containing GTPase activating protein 3 (IQGAP3)	experiment 1: whole brain	experiment : whole brain
10788	Ras GTPase-activating-like protein IQGAP2		experiment 2: synaptosome CL-114
mTOR complex			
253260	RPTOR independent companion of MTOR, complex 2	experiment 1: whole brain	experiment1 : whole brain
78757	Rapamycin-insensitive companion of mTOR		experiment 2: synaptosome CL-114

CDC42 effector proteins			
11135	CDC42 effector protein (RhO GTPase binding) 1		experiment 1: whole brain
58804	Cdc42 effector protein 5	experiment 2: synaptosome CL-114	
protein family: Fascin			
56223	Fascin-3		experiment 2: synaptosome CL-114
14086	Fascin		experiment 3: whole brain
microtubule associated proteins			
55700	MAP7 domain containing 1	experiment 1: whole brain	experiment1 : whole brain
79649	MAP7 domain containing 3	experiment 1: whole brain	experiment1 : whole brain
17761	Ensconsin (MAP7)		experiment 2: synaptosome CL-114
232944	MAP/microtubule affinity-regulating kinase 4	experiment 2: synaptosome CL-114	
270058	Microtubule-associated protein 1S	experiment 2: synaptosome CL-114	experiment 2: synaptosome CL-114
208158	MAP6 domain-containing protein 1	experiment 3: whole brain	experiment 3: whole brain
17760	Microtubule-associated protein 6	experiment 3: whole brain	experiment 3: whole brain
13589	Microtubule-associated protein RP/EB family member 1		experiment 3: whole brain
212307	Microtubule-associated protein RP/EB family member 2	experiment 3: whole brain	
100732	Microtubule-associated protein RP/EB family member 3		experiment 3: synaptosome CL-114
intracellular protein and vesicle traffic			

Kinesins			
gene ID	identified protein	screen ident. prot X as RIM3γ binding protein	screen ident. prot X as RIM4γ binding protein
9928	Kinesin family member 14	experiment 1: whole brain	experiment1 : whole brain
16560	Kinesin-like protein KIF1A	experiment 3: whole brain	experiment3 : whole brain
16564	Kinesin-like protein KIF21A	experiment 3: whole brain, synaptosome TX-100	experiment3 : whole brain
IQ motif and SEC7 domain-containing protein 1			
232227	IQ motif and SEC7 domain-containing protein 1	experiment 1: whole brain	experiment1 : whole brain experiment 3: synaptosome TX-100

Exocyst complex			
55763	Exocyst complex component 1	experiment 1: whole brain	experiment1 : whole brain
60412	Exocyst complex component 4	experiment 1: whole brain	experiment1 : whole brain
211446	Exocyst complex component 3 (Sec 6)	experiment 2: synaptosome CL-114	
ARF GTPas activating protein GIT1			
216963	ARF GTPase-activating protein GIT1	experiment 2: synaptosome CL-114 experiment 3: synaptosome TX-100	
Rab protein family and Rab related proteins			
98732	Rab3 GTPase-activating protein non-catalytic subunit	experiment 2: synaptosome CL-114	experiment 2: synaptosome CL-114
268451	Rab11 family-interacting protein 4	experiment 2: synaptosome CL-114	
19894	Rabphilin-3A	experiment 2: synaptosome CL-114 experiment 3: whole brain	experiment 3: whole brain
104886	Ras-related protein Rab-15	experiment 2: synaptosome CL-114	experiment 2: synaptosome CL-114 experiment 3: synaptosome CL-114
19338	Ras-related protein Rab-33B	experiment 2: synaptosome CL-114	
270160	Ras-related protein Rab-39A	experiment 2: synaptosome CL-114	experiment 2: synaptosome CL-114
67295	Ras-related protein Rab-3C	experiment 2: synaptosome CL-114	experiment 3: synaptosome CL-114
19341	Ras-related protein Rab-4A	experiment 2: synaptosome CL-114	
19346	Ras-related protein Rab-6A		experiment 3: synaptosome CL-114
14569	Rab GDP dissociation inhibitor beta		experiment 3: synaptosome CL-114
52055	Rab11 family-interacting protein 5		experiment 3: whole brain
226407	Rab3 GTPase-activating protein catalytic subunit	experiment 3: whole brain	experiment 3: whole brain
19325	Ras-related protein Rab-10	experiment 3: synaptosome TX-100	experiment 3: whole brain

68365	Ras-related protein Rab-14		experiment 3: synaptosome CL-114
19339	Ras-related protein Rab-3A	experiment 3: whole brain	experiment 3: whole brain
271457	Ras-related protein Rab-5A		experiment 3: synaptosome CL-114
AP-1 adaptor complex / AP-2 adaptor complex / AP-3 adaptor complex			
11764	AP-1 complex subunit beta-1	experiment 2: synaptosome CL-114 experiment 3: synaptosome TX-100	
232910	AP-2 complex subunit sigma	experiment 3: synaptosome TX-100	
64933	AP-3 complex subunit mu-2		experiment 3: whole brain
11777	AP-3 complex subunit sigma-1	experiment 3: whole brain	
Trafficking particle complex subunit 3			
27096	Trafficking protein particle complex subunit 3		experiment 2: synaptosome CL-114 experiment 3: whole brain
adhesion molecules			

armadillo repeat proteins			
gene ID	identified protein	screen ident. prot X as RIM3γ binding protein	screen ident. prot X as RIM4γ binding protein
1495	Catenin (cadherin-associated protein), alpha 1, 102kDa	experiment 1: whole brain	experiment 1: whole brain
1500	Catenin (cadherin-associated protein), delta 1	experiment 1: whole brain	experiment 1: whole brain
1829	Desmoglein 2	experiment 1: whole brain	
5318	Plakophilin 2		experiment 1: whole brain
8502	Plakophilin 4	experiment 1: whole brain	experiment 1: whole brain
13510	Desmoglein-1-alpha	experiment 3: synaptosome CL-114	
18772	Plakophilin-1	experiment 3: synaptosome CL-114	
neural cell adhesion molecule 1			
17967	Neural cell adhesion molecule 1	experiment 2: synaptosome CL-114	experiment 3: synaptosome TX-100
contactin associated protein 1			

53321	Contactin-associated protein 1	experiment 3: whole brain	experiment 2: synaptosome TX-100 experiment 3: whole brain, synatosome CL-114
synaptic proteins			
synatxins			
gene ID	identified protein	screen ident. prot X as RIM3γ binding protein	screen ident. prot X as RIM4γ binding protein
6804	Syntaxin-1A	experiment 2: synaptosome CL-114	
55014	Syntaxin 17	experiment 1: whole brain	
20910	Syntaxin-binding protein 1	experiment 3: whole brain	experiment 3: whole brain
protein family: RIM			
116837	Regulating synaptic membrane exocytosis protein 1	experiment 2: synaptosome CL-114	experiment 2: synaptosome TX-100
116838	Regulating synaptic membrane exocytosis protein 2	experiment 3: whole brain, synaptosome TX-100	
Copines			
234577	Copine-2	experiment 2: synaptosome CL-114	
12891	Copine-6		experiment 3: whole brain
Ephrin receptors			
13838	Ephrin type-A receptor 8	experiment 2: synaptosome TX-100	
13838	Ephrin type-A receptor 4	experiment 3: synaptosome TX-100	
Synaptosomal associated proteins			
20614	Synaptosomal-associated protein 25	experiment 2: synaptosome CL-114	
116841	Synaptosomal-associated protein, 47kDa		experiment 3: whole brain
Synaptogyrins1			
9145	Synaptogyrin-1	experiment 2: synaptosome CL-114 experiment 3: whole brain	experiment 3: whole brain
Synaptotagmins			
27359	Synaptotagmin-like protein 4	experiment 2: synaptosome CL-114	
20979	Synaptotagmin-1	experiment 3:whole brain	experiment 3:whole brain
Synapsins			

20965	Synapsin-2	experiment 3: whole brain	experiment 3: whole brain
27204	Synapsin-3	experiment 3: synaptosome TX-100	experiment 2: synaptosome CL-114
channel proteins			
voltage dependent anion channels			
gene ID	identified protein	screen ident. prot X as RIM3γ binding protein	screen ident. prot X as RIM4γ binding protein
7417	Voltage dependent anion channel 2	experiment 1: whole brain	experiment 1: whole brain
729317	Voltage dependent anion channel 2 pseudogene	experiment 1: whole brain	experiment 1: whole brain
22333	Voltage-dependent anion-selective channel protein 1	experiment 2: synaptosome CL-114	
22335	Voltage-dependent anion-selective channel protein 3	experiment 2: synaptosome CL-114	
nuclear proteins			
Importins			
gene ID	identified protein	screen ident. prot X as RIM3γ binding protein	screen ident. prot X as RIM4γ binding protein
79711	Importin 4	experiment 1: whole brain	
3843	Importin 5	experiment 1: whole brain experiment 3: whole brain	
10526	Importin 8	experiment 1: whole brain	
76582	Importin-11	experiment 2: synaptosome CL-114	
16650	Importin subunit alpha-7	experiment 3: whole brain, synaptosome CL-114	
Ca^{2+} binding proteins			
Reticulocalbins			
5954	Reticulocalbin 1, EF-hand calcium binding domain	experiment 1: whole brain	
5955	Reticulocalbin 2, EF-hand calcium binding domain	experiment 2: synaptosome CL-114	experiment 1: whole brain

8.6 Supplementary figures

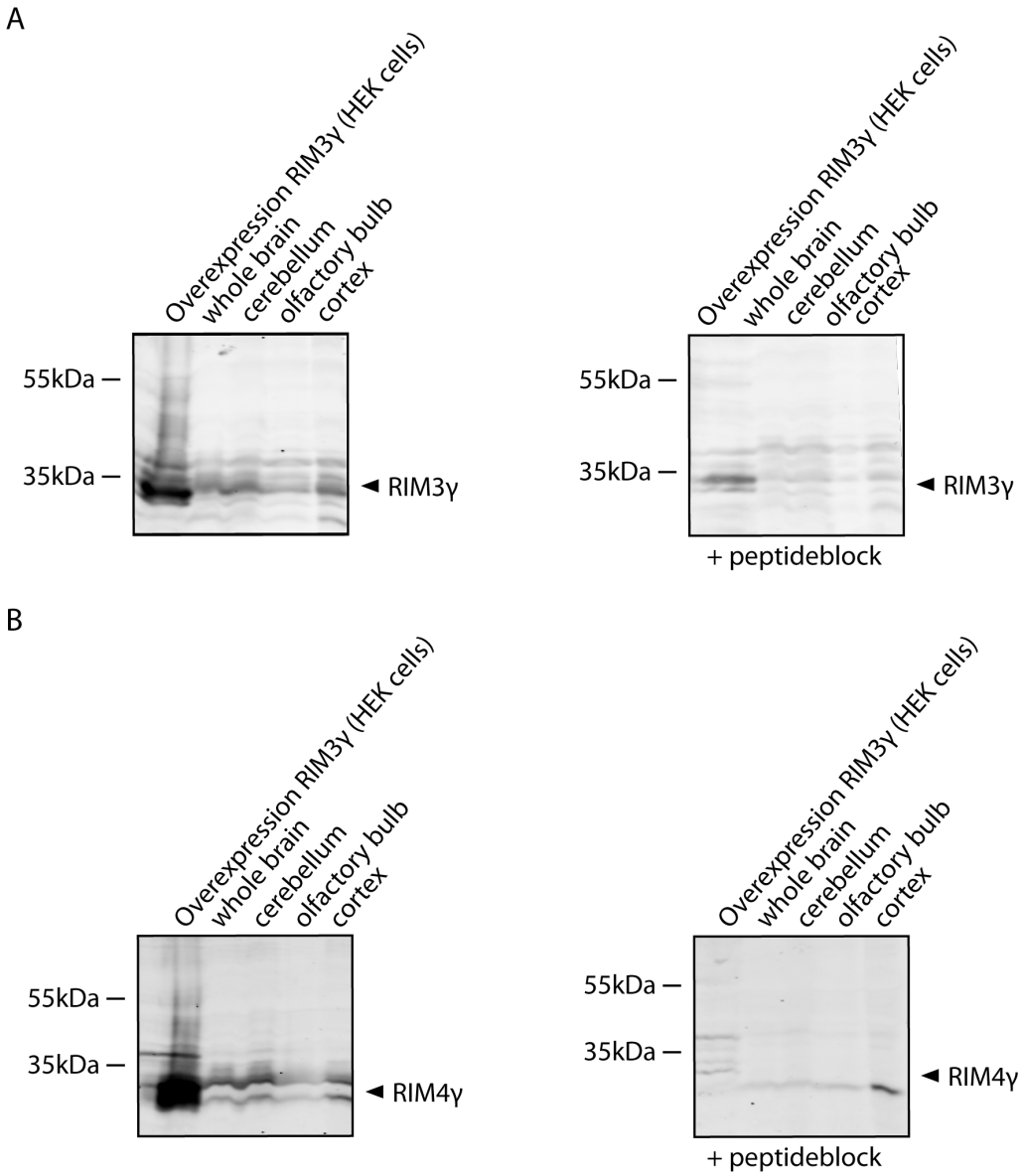

Figure 8.1: **Peptide block reveals specificity of polyclonal RIM3γ and RIM4γ antibodies. A,** Western blots of HEK293T cell lysates overexpressing RIM3γ, whole brain lysates and lysates of only the cerebellum, olfactory bulb and cortex were stained with polyclonal RIM3γ antibodies, revealing a RIM3γ specific band at 35 kDa. When western blots of the same lysates were incubated with polyclonal RIM3γ antibodies that were preincubated with RIM3γ-GST coupled to agarose beads the RIM3γ specific band was strongly reduced. **B,** Western blots of HEK293T cell lysates overexpressing RIM4γ and tissues lysates as described in A, were incubated with polyclonal RIM4γ antibodies revealing a RIM4γ specific band at 30 kDa. However a preincubation of RIM4γ antibodies with RIM4γ-GST coupled to agarose abolished the RIM4γ specific band.

9 Abbreviations

AAV	Adeno-associated virus
AMPA	α-amino-3-hydroxy-5-methyl-4-isoxazolepropionic acid
ANOVA	Analysis of variance
ARVCF	Armadillo repeat gene deleted in Velo-Cardio-Facial syndrome
AZ	Active zone
BICDR	Bicaudal-D related protein
BL6 J mice	Black six J mice
BME	Basal Medium Eagle
bp	Base pair
BSA	Bovine serum albumin
C. elegans	Caenorhabditis elegans
CA	Cornu amonis
Cacna1a	Calcium channel a1a subunit gene
CAMK	Ca^{2+}/calmodulin-dependent protein kinase
CDC42	Cell division control protein 42 homolog
CdH1-APC	Cdh1-anaphase promoting complex
CDK5	Cyclin dependent kinase 5
cDNA	Complementary DNA
CLASP	Cytoplasmic linker associated protein
CLIP	Cytoplasmic linker protein
CMV	Cytomegalie virus
Co-IP	Co-immunoprecipitation
ConstKO	Constitutive knock-out
cortico-LA	Lateral nucleus of the amygdala
CRM1	Chromosome region maintenance 1
ct	Cycle threshold
Cy	Cyanine dye
DEPC	Diethylpyrocarbonate
DG	Dentate Gyrus
DIV	Day in vitro
DMEM	Dulbecco's Modified Eagle's Medium
DNA	Desoxyribonucleic acid
E	Embryonic day
EDTA	Ethylenediaminetetraacetic acid
EphB2 receptor	Ephrin type-B receptor 2

ER	Endoplasmic reticulum
FBS	Fetal bovine serum
FCS	Fetal calf serum
FITC	Fluorescein isothiocyanate
FOX	Forkhead-Box-Proteine
Fw	Forward
GAPs	GTPase activating proteins
GDP	Guanosindiphosphat
GEF	Guanine exchange factors
GFP	Green fluorescent protein
GM130	Golgi matrix protein 130
GRD	Calcium/calmodulin and a Ras-GAP related domain
GRIP	Glutamate receptor-interacting protein
GST	Glutathione-S-transferase
GTP	Guanosintriphosphat
h	Hour
HA	Human influenza hemagglutinin
HAT	Sodium hypoxanthine, aminopterin, thymidine
HBSS	Hank's Buffered Salt Solution
HCL	Hydrochloride
HEK cells	Human embryonic kidney cells
HEPES	4-(2-hydroxyethyl)-1-piperazineethanesulfonic acid
het	Heterozygous
HIV	Human immunodeficiency virus
HLP	Hind limb impairments
ID2	DNA-binding protein inhibitor 2
Ig	Immune globulin
IMDM	Iscove's Modified Dulbecco's Medium
IPTG	Isopropyl b-D-1-thiogalactopyranoside
IQGAP	IQ-motif GTPase-activating protein 1
kb	Kilobase pair
kg	Kilogram
KO	knock-out
KOMP	Knock-out Mouse Project
LAR	Leukocyte commonantigen-related
LAR-RPTPs	LAR-receptor protein tyrosine phosphatases
LB	Luria Broth
LC-MS/MS	Liquid chromatography–mass spectrometry/mass spectrometry
LMTK1	Lemur kinase 1
LTP	Long-term plasticity
M	Molar
MAGUK	Membrane-associated guanylate kinase

MAP	Microtubule associated protein
mDia	Mammalian diaphanous
MEM	Minimum essential medium
mg	Milligramm
min	Minutes
ml	Milliliter
mM	Millimolar
mm	Millimeter
mRNA	Messenger RNA
Munc-13	Mammalian Unc-13 homolog
NA	Numerical aperture
NBQX	2,3-dioxo-6-nitro-1,2,3,4-tetrahydrobenzo-[f]-quinoxalin-7-sulfonamide
NES	Nuclear export signal
NeuroD	Neurogenic differentiation 1
NG108-15	Neuroblastoma glioma cell line 108-15
NLS	Nuclear localization signal
nM	Nanomolar
nm	Nanometer
NPRAP	Neural plakophilin-related armadillo protein
OD	Optical density
OE	Overexpression
P	Postnatal day
PAK	p21-activated kinase
PBS	Phosphate buffered saline
PCR	Polymerase chain reaction
PDZ-domain	Post synaptic density protein-Drosophila disc large tumor suppressor-zonula occludens-1-domain
PEI	Polyethylenimine
pen/strep	Penicillin/streptomycin
PFA	Paraformaldehyde
Pfu	Pyrococcus furiosus
PI	Propidium iodide
PKA	Protein kinase A
PSD	Postsynaptic density
PSM	Peptide spectrum matches
qPCR	Quantitative PCR
Rab	Ras-related in brain
Rac1	Ras-related C3 botulinum toxin substrate 1
Rev	Reverse
RFP	Red fluorescent protein
Rho	Ras homolog
RhoA	Ras homolog gene family, member A

RIMs	Rab3-interacting molecules
RNA	Ribonucleic acid
ROCK	Rho-associated protein kinase
RPM	Rounds per minute
SDS	Sodium dodecyl sulfate
SDS PAGE	SDS polyacryalmid gel electrophoresis
SE	Status epilepticus
sec	Second
SEM	Standard error of mean
SF-TAP	Streptavidin/FLAG-tandem affinity purification
SH3-domain	Src-homology 3-domain
shRNA	Small hairpin RNA
SNAP25	Synaptosomal-associated protein 25
SNARE	Soluble N-ethylmaleimide-sensitive-factor attachment receptor
SYD	Synapse defective
SYN	Synapsin
TAP	Tandem affinity purification
TBS	Tris-buffered saline
TBST	Tris-buffered saline and Tween 20
TEMED	Tetramethylethylenediamine
TGN	Trans-Golgi-network
TIPs	Microtubule plus end tracking proteins
TX-100	Triton X-100
VSV-G	Vesicular stomatitis virus
WAVE	Wiskott–Aldrich syndrome protein
WB	Western blot
µl	Microliter
µm	Micrometer

10 Bibliography

Bibliography

[Aleman & Kahn, 2005] Aleman, A. & Kahn, R. S. (2005). Strange feelings: do amygdala abnormalities dysregulate the emotional brain in schizophrenia? *Progress in neurobiology*, 77(5), 283–98.

[Alvaréz-Baron, 2010] Alvaréz-Baron, E. (2010). *Localization and functional role of RIM3γ and RIM4γ , the small members of the RIM protein family.* PhD thesis, University Bonn.

[Alvarez-Baron et al., 2013] Alvarez-Baron, E., Michel, K., Mittelstaedt, T., Opitz, T., Schmitz, F., Beck, H., Dietrich, D., Becker, A. J., & Schoch, S. (2013). RIM3γ and RIM4γ are key regulators of neuronal arborization. *The Journal of neuroscience : the official journal of the Society for Neuroscience*, 33(2), 824–39.

[Amano et al., 1996] Amano, M., Ito, M., Kimura, K., Fukata, Y., Chihara, K., Nakano, T., Matsuura, Y., & Kaibuchi, K. (1996). Phosphorylation and Activation of Myosin by Rho-associated Kinase (Rho-kinase). *Journal of Biological Chemistry*, 271(34), 20246–20249.

[Arakawa et al., 2003] Arakawa, Y., Bito, H., Furuyashiki, T., Tsuji, T., Takemoto-Kimura, S., Kimura, K., Nozaki, K., Hashimoto, N., & Narumiya, S. (2003). Control of axon elongation via an SDF-1alpha/Rho/mDia pathway in cultured cerebellar granule neurons. *The Journal of cell biology*, 161(2), 381–91.

[Arber et al., 1998] Arber, S., Barbayannis, F. a., Hanser, H., Schneider, C., Stanyon, C. a., Bernard, O., & Caroni, P. (1998). Regulation of actin dynamics through phosphorylation of cofilin by LIM-kinase. *Nature*, 393(6687), 805–9.

[Arikkath et al., 2008] Arikkath, J., Israely, I., Tao, Y., Mei, L., Liu, X., & Reichardt, L. F. (2008). Erbin controls dendritic morphogenesis by regulating localization of delta-catenin. *The Journal of neuroscience : the official journal of the Society for Neuroscience*, 28(28), 7047–56.

[Arlotta et al., 2005] Arlotta, P., Molyneaux, B. J., Chen, J., Inoue, J., Kominami, R., & Macklis, J. D. (2005). Neuronal subtype-specific genes that control corticospinal motor neuron development in vivo. *Neuron*, 45(2), 207–21.

[Bard & Malhotra, 2006] Bard, F. & Malhotra, V. (2006). The formation of TGN-to-plasma-membrane transport carriers. *Annual review of cell and developmental biology*, 22, 439–55.

[Barr & Lambright, 2010] Barr, F. & Lambright, D. G. (2010). Rab GEFs and GAPs. *Current opinion in cell biology*, 22(4), 461–70.

[Bausch et al., 2006] Bausch, S. B., He, S., Petrova, Y., Wang, X.-M., & McNamara, J. O. (2006). Plasticity of both excitatory and inhibitory synapses is associated with seizures in-

duced by removal of chronic blockade of activity in cultured hippocampus. *Journal of neurophysiology*, 96(4), 2151–67.

[Beffert et al., 2012] Beffert, U., Dillon, G. M., Sullivan, J. M., Stuart, C. E., Gilbert, J. P., Kambouris, J. a., & Ho, A. (2012). Microtubule Plus-End Tracking Protein CLASP2 Regulates Neuronal Polarity and Synaptic Function. *The Journal of neuroscience : the official journal of the Society for Neuroscience*, 32(40), 13906–16.

[Berto et al., 2014] Berto, G. E., Iobbi, C., Camera, P., Scarpa, E., Iampietro, C., Bianchi, F., Gai, M., Sgrò, F., Cristofani, F., Gärtner, A., Dotti, C. G., & Di Cunto, F. (2014). The DCR protein TTC3 affects differentiation and Golgi compactness in neurons through specific actin-regulating pathways. *PloS one*, 9(4), e93721.

[Betz & Bewick, 1992] Betz, W. J. & Bewick, G. S. (1992). Optical analysis of synaptic vesicle recycling at the frog neuromuscular junction. *Science (New York, N.Y.)*, 255(5041), 200–3.

[Bito et al., 2000] Bito, H., Furuyashiki, T., Ishihara, H., Shibasaki, Y., Ohashi, K., Mizuno, K., Maekawa, M., Ishizaki, T., & Narumiya, S. (2000). A critical role for a Rho-associated kinase, p160ROCK, in determining axon outgrowth in mammalian CNS neurons. *Neuron*, 26(2), 431–41.

[Blundell et al., 2010a] Blundell, J., Blaiss, C. a., Etherton, M. R., Espinosa, F., Tabuchi, K., Walz, C., Bolliger, M. F., Südhof, T. C., & Powell, C. M. (2010a). Neuroligin-1 deletion results in impaired spatial memory and increased repetitive behavior. *The Journal of neuroscience : the official journal of the Society for Neuroscience*, 30(6), 2115–29.

[Blundell et al., 2010b] Blundell, J., Kaeser, P. S., Südhof, T. C., & Powell, C. M. (2010b). RIM1alpha and interacting proteins involved in presynaptic plasticity mediate prepulse inhibition and additional behaviors linked to schizophrenia. *The Journal of neuroscience : the official journal of the Society for Neuroscience*, 30(15), 5326–33.

[Boyd et al., 2004] Boyd, C., Hughes, T., Pypaert, M., & Novick, P. (2004). Vesicles carry most exocyst subunits to exocytic sites marked by the remaining two subunits, Sec3p and Exo70p. *The Journal of cell biology*, 167(5), 889–901.

[Brandt & Grosse, 2007] Brandt, D. T. & Grosse, R. (2007). Get to grips: steering local actin dynamics with IQGAPs. *EMBO reports*, 8(11), 1019–23.

[Brill et al., 1996] Brill, S., Li, S., & Lyman, C. (1996). The Ras GTPase-activating-protein-related human protein IQGAP2 harbors a potential actin binding domain and interacts with calmodulin and Rho family GTPases. *Molecular and cellular biology and cellular biology.*

[Brown et al., 2007] Brown, T. C., Correia, S. S., Petrok, C. N., & Esteban, J. a. (2007). Functional compartmentalization of endosomal trafficking for the synaptic delivery of AMPA receptors during long-term potentiation. *The Journal of neuroscience : the official journal of the Society for Neuroscience*, 27(48), 13311–5.

[Burbank & Mitchison, 2006] Burbank, K. & Mitchison, T. (2006). Microtubule dynamic instability. *Current Biology*, 16(14), 516–517.

[Burridge & Wennerberg, 2004] Burridge, K. & Wennerberg, K. (2004). Rho and Rac Take Center Stage. *Cell*, 116, 167–179.

[Caceres et al., 1992] Caceres, a., Mautino, J., & Kosik, K. S. (1992). Suppression of MAP2 in cultured cerebellar macroneurons inhibits minor neurite formation. *Neuron*, 9(4), 607–18.

[Campbell & Hess, 1998] Campbell, D. & Hess, E. (1998). Cerebellar circuitry is activated during convulsive episodes in the tottering (tg/tg) mutant mouse. *Neuroscience*, 85(3), 773–783.

[Castillo et al., 1994] Castillo, P., Weisskopf, M., & Nicoll, R. (1994). The Role of Ca 2+ Channels in Hippocampal Mossy Fiber Synaptic Transmission and Long-Term Potentiation. *Neuron*, 12, 261–269.

[Castillo et al., 2002] Castillo, P. E., Schoch, S., Schmitz, F., & Su, T. C. (2002). RIM1a is required for presynaptic long-term potentiation. *Nature*, (pp. 327–330).

[Chandrasekaran & Bonchev, 2013] Chandrasekaran, S. & Bonchev, D. (2013). A Network View on Parkinsons Disease. *Computational and structural ...*, (April).

[Chia et al., 2012] Chia, P. H., Patel, M. R., & Shen, K. (2012). NAB-1 instructs synapse assembly by linking adhesion molecules and F-actin to active zone proteins. *Nature neuroscience*, 15(2), 234–42.

[Ch'ng & Martin, 2011] Ch'ng, T. H. & Martin, K. C. (2011). Synapse-to-nucleus signaling. *Current opinion in neurobiology*, 21(2), 345–52.

[Ch'ng et al., 2012] Ch'ng, T. H., Uzgil, B., Lin, P., Avliyakulov, N. K., O'Dell, T. J., & Martin, K. C. (2012). Activity-dependent transport of the transcriptional coactivator CRTC1 from synapse to nucleus. *Cell*, 150(1), 207–21.

[Cohen & Greenberg, 2008] Cohen, S. & Greenberg, M. (2008). Communication Between the Synapse and the Nucleus in Neuronal Development, Plasticity, and Disease. *Annual review of cell and ...*, (pp. 183–209).

[Daniels, 1973] Daniels, M. (1973). Fine structural changes in neurons and nerve fibers associated with colchicine inhibition of nerve fiber formation in vitro. *The Journal of cell biology*, 58, 463–470.

[Dawson et al., 2001] Dawson, H. N., Ferreira, a., Eyster, M. V., Ghoshal, N., Binder, L. I., & Vitek, M. P. (2001). Inhibition of neuronal maturation in primary hippocampal neurons from tau deficient mice. *Journal of cell science*, 114(Pt 6), 1179–87.

[de Forges et al., 2012] de Forges, H., Bouissou, A., & Perez, F. (2012). Interplay between microtubule dynamics and intracellular organization. *The international journal of biochemistry & cell biology*, 44(2), 266–74.

[de la Torre-Ubieta & Bonni, 2011] de la Torre-Ubieta, L. & Bonni, A. (2011). Transcriptional regulation of neuronal polarity and morphogenesis in the mammalian brain. *Neuron*, 72(1), 22–40.

[de la Torre-Ubieta et al., 2010] de la Torre-Ubieta, L., Gaudillière, B., Yang, Y., Ikeuchi, Y., Yamada, T., DiBacco, S., Stegmüller, J., Schüller, U., Salih, D. a., Rowitch, D., Brunet, A., & Bonni, A. (2010). A FOXO-Pak1 transcriptional pathway controls neuronal polarity. *Genes & development*, 24(8), 799–813.

[De Matteis & Luini, 2008] De Matteis, M. A. & Luini, A. (2008). Exiting the Golgi complex. *Nature reviews. Molecular cell biology*, 9(4), 273–84.

[Deng et al., 2011] Deng, L., Kaeser, P. S., Xu, W., & Südhof, T. C. (2011). RIM proteins activate vesicle priming by reversing autoinhibitory homodimerization of Munc13. *Neuron*, 69(2), 317–31.

[Deretic et al., 1995] Deretic, D., Huber, L., & Ransom, N. (1995). rab8 in retinal photoreceptors may participate in rhodopsin transport and in rod outer segment disk morphogenesis. *Journal of cell ...*, 224, 215–224.

[Deretic & Papermaster, 1993] Deretic, D. & Papermaster, D. (1993). Rab6 is associated with a compartment that transports rhodopsin from the trans-Golgi to the site of rod outer segment disk formation in frog retinal photoreceptors. *Journal of cell science*, 813, 803–813.

[DiTella et al., 1996] DiTella, M., Feiguin, F., & Carri, N. (1996). MAP-1B/TAU functional redundancy during laminin-enhanced axonal growth. *Journal of cell ...*, 477, 467–477.

[Dunah et al., 2005] Dunah, A. W., Hueske, E., Wyszynski, M., Hoogenraad, C. C., Jaworski, J., Pak, D. T., Simonetta, A., Liu, G., & Sheng, M. (2005). LAR receptor protein tyrosine phosphatases in the development and maintenance of excitatory synapses. *Nature neuroscience*, 8(4), 458–67.

[Dupraz et al., 2009] Dupraz, S., Grassi, D., Bernis, M. E., Sosa, L., Bisbal, M., Gastaldi, L., Jausoro, I., Cáceres, A., Pfenninger, K. H., & Quiroga, S. (2009). The TC10-Exo70 complex is essential for membrane expansion and axonal specification in developing neurons. *The Journal of neuroscience : the official journal of the Society for Neuroscience*, 29(42), 13292–301.

[Edwards et al., 1999] Edwards, D. C., Sanders, L. C., Bokoch, G. M., & Gill, G. N. (1999). Activation of LIM-kinase by Pak1 couples Rac/Cdc42 GTPase signalling to actin cytoskeletal dynamics. *Nature cell biology*, 1(5), 253–9.

[Edwards et al., 2014] Edwards, M., Zwolak, A., Schafer, D. a., Sept, D., Dominguez, R., & Cooper, J. a. (2014). Capping protein regulators fine-tune actin assembly dynamics. *Nature reviews. Molecular cell biology*, (September).

[Elia et al., 2006] Elia, L. P., Yamamoto, M., Zang, K., & Reichardt, L. F. (2006). p120 catenin regulates dendritic spine and synapse development through Rho-family GTPases and cadherins. *Neuron*, 51(1), 43–56.

[Fan et al., 2008] Fan, J., Hu, Z., Zeng, L., Lu, W., Tang, X., Zhang, J., & Li, T. (2008). Golgi apparatus and neurodegenerative diseases. *International journal of developmental neuroscience : the official journal of the International Society for Developmental Neuroscience*, 26(6), 523–34.

[Farah et al., 2005] Farah, C. A., Liazoghli, D., Perreault, S., Desjardins, M., Guimont, A., Anton, A., Lauzon, M., Kreibich, G., Paiement, J., & Leclerc, N. (2005). Interaction of microtubule-associated protein-2 and p63: a new link between microtubules and rough endoplasmic reticulum membranes in neurons. *The Journal of biological chemistry*, 280(10), 9439–49.

[Ferreira et al., 1989] Ferreira, a., Busciglio, J., & Cáceres, a. (1989). Microtubule formation

and neurite growth in cerebellar macroneurons which develop in vitro: evidence for the involvement of the microtubule-associated proteins, MAP-1a, HMW-MAP2 and Tau. *Brain research. Developmental brain research*, 49(2), 215–28.

[Flavell & Greenberg, 2008] Flavell, S. W. & Greenberg, M. E. (2008). Signaling mechanisms linking neuronal activity to gene expression and plasticity of the nervous system. *Annual review of neuroscience*, 31, 563–90.

[Fletcher et al., 1996] Fletcher, C. F., Lutz, C. M., O'Sullivan, T. N., Shaughnessy, J. D., Hawkes, R., Frankel, W. N., Copeland, N. G., & Jenkins, N. a. (1996). Absence epilepsy in tottering mutant mice is associated with calcium channel defects. *Cell*, 87(4), 607–17.

[Fornerod et al., 1997] Fornerod, M., Ohno, M., Yoshida, M., & Mattaj, I. (1997). CRM1 Is an Export Receptor for Leucine-Rich Nuclear Export Signals. *Cell*, 90, 1051–1060.

[Fourcaudot & Gambino, 2008] Fourcaudot, E. & Gambino, F. (2008). cAMP/PKA signaling and RIM1 mediate presynaptic LTP in the lateral amygdala. *Proceedings of the ...*, 105(39).

[Fujita et al., 2013] Fujita, A., Koinuma, S., Yasuda, S., Nagai, H., Kamiguchi, H., Wada, N., & Nakamura, T. (2013). GTP hydrolysis of TC10 promotes neurite outgrowth through exocytic fusion of Rab11- and L1-containing vesicles by releasing exocyst component Exo70. *PloS one*, 8(11), e79689.

[Fukata et al., 2002] Fukata, M., Watanabe, T., Noritake, J., Nakagawa, M., Yamaga, M., Kuroda, S., Matsuura, Y., Iwamatsu, A., Perez, F., & Kaibuchi, K. (2002). Rac1 and Cdc42 capture microtubules through IQGAP1 and CLIP-170. *Cell*, 109(7), 873–85.

[Gao & Frausto, 2011] Gao, C. & Frausto, S. (2011). IQGAP1 regulates NR2A signaling, spine density, and cognitive processes. *The Journal of ...*, 31(23), 8533–8542.

[Gardner et al., 2013] Gardner, M. K., Zanic, M., & Howard, J. (2013). Microtubule catastrophe and rescue. *Current opinion in cell biology*, 25(1), 14–22.

[Garvalov et al., 2007] Garvalov, B. K., Flynn, K. C., Neukirchen, D., Meyn, L., Teusch, N., Wu, X., Brakebusch, C., Bamburg, J. R., & Bradke, F. (2007). Cdc42 regulates cofilin during the establishment of neuronal polarity. *The Journal of neuroscience : the official journal of the Society for Neuroscience*, 27(48), 13117–29.

[Gaudilliere et al., 2004] Gaudilliere, B., Konishi, Y., De la Iglesia, N., Yao, G.-I., & Bonni, A. (2004). A CaMKII-NeuroD Signaling Pathway Specifies Dendritic Morphogenesis. *Neuron*, 41, 229–241.

[Gerber et al., 2008] Gerber, S. H., Rah, J.-C., Min, S.-W., Liu, X., de Wit, H., Dulubova, I., Meyer, A. C., Rizo, J., Arancillo, M., Hammer, R. E., Verhage, M., Rosenmund, C., & Südhof, T. C. (2008). Conformational switch of syntaxin-1 controls synaptic vesicle fusion. *Science (New York, N.Y.)*, 321(5895), 1507–10.

[Goelet et al., 1986] Goelet, P., Castellucci, V., Schacher, S., & Kandel, E. (1986). The long term and the short of long-term memory- a molecular framework. *Nature*.

[Govek et al., 2005] Govek, E.-E., Newey, S. E., & Van Aelst, L. (2005). The role of the Rho GTPases in neuronal development. *Genes & development*, 19(1), 1–49.

[Gracheva et al., 2008] Gracheva, E. O., Hadwiger, G., Nonet, M. L., & Richmond, J. E. (2008). Direct interactions between C. elegans RAB-3 and Rim provide a mechanism to target vesicles to the presynaptic density. *Neuroscience letters*, 444(2), 137–42.

[Graf et al., 2006] Graf, E. R., Kang, Y., Hauner, A. M., & Craig, A. M. (2006). Structure function and splice site analysis of the synaptogenic activity of the neurexin-1 beta LNS domain. *The Journal of neuroscience : the official journal of the Society for Neuroscience*, 26(16), 4256–65.

[Grigoriev et al., 2007] Grigoriev, I., Splinter, D., Keijzer, N., Wulf, P. S., Demmers, J., Ohtsuka, T., Modesti, M., Maly, I. V., Grosveld, F., Hoogenraad, C. C., & Akhmanova, A. (2007). Rab6 regulates transport and targeting of exocytotic carriers. *Developmental cell*, 13(2), 305–14.

[Grigoriev et al., 2011] Grigoriev, I., Yu, K. L., Martinez-Sanchez, E., Serra-Marques, A., Smal, I., Meijering, E., Demmers, J., Peränen, J., Pasterkamp, R. J., van der Sluijs, P., Hoogenraad, C. C., & Akhmanova, A. (2011). Rab6, Rab8, and MICAL3 cooperate in controlling docking and fusion of exocytotic carriers. *Current biology : CB*, 21(11), 967–74.

[Grosshans et al., 2006] Grosshans, B. L., Ortiz, D., & Novick, P. (2006). Rabs and their effectors: achieving specificity in membrane traffic. *Proceedings of the National Academy of Sciences of the United States of America*, 103(32), 11821–7.

[Gu et al., 2006] Gu, C., Zhou, W., Puthenveedu, M. a., Xu, M., Jan, Y. N., & Jan, L. Y. (2006). The microtubule plus-end tracking protein EB1 is required for Kv1 voltage-gated K+ channel axonal targeting. *Neuron*, 52(5), 803–16.

[Hakak et al., 2001] Hakak, Y., Walker, J. R., Li, C., Wong, W. H., Davis, K. L., Buxbaum, J. D., Haroutunian, V., & Fienberg, a. a. (2001). Genome-wide expression analysis reveals dysregulation of myelination-related genes in chronic schizophrenia. *Proceedings of the National Academy of Sciences of the United States of America*, 98(8), 4746–51.

[Han et al., 2011] Han, Y., Kaeser, P. S., Südhof, T. C., & Schneggenburger, R. (2011). RIM determines Ca2+ channel density and vesicle docking at the presynaptic active zone. *Neuron*, 69(2), 304–16.

[Hattula et al., 2006] Hattula, K., Furuhjelm, J., Tikkanen, J., Tanhuanpää, K., Laakkonen, P., & Peränen, J. (2006). Characterization of the Rab8-specific membrane traffic route linked to protrusion formation. *Journal of cell science*, 119(Pt 23), 4866–77.

[Hazuka et al., 1999] Hazuka, C. D., Foletti, D. L., Hsu, S. C., Kee, Y., Hopf, F. W., & Scheller, R. H. (1999). The sec6/8 complex is located at neurite outgrowth and axonal synapse-assembly domains. *The Journal of neuroscience : the official journal of the Society for Neuroscience*, 19(4), 1324–34.

[He & Guo, 2009] He, B. & Guo, W. (2009). The exocyst complex in polarized exocytosis. *Current opinion in cell biology*, 21(4), 537–42.

[Hemby et al., 2002] Hemby, S. E., Ginsberg, S. D., Brunk, B., & Arnold, S. E. (2002). Gene Expression Profile for Schizophrenia. *Arch. Gen. Psychiatry*, 59(July).

[Hermey et al., 2013] Hermey, G., Mahlke, C., Gutzmann, J. J., Schreiber, J., Blüthgen, N., &

Kuhl, D. (2013). Genome-wide profiling of the activity-dependent hippocampal transcriptome. *PloS one*, 8(10), e76903.

[Higashida et al., 2004] Higashida, C., Miyoshi, T., Fujita, A., Oceguera-Yanez, F., Monypenny, J., Andou, Y., Narumiya, S., & Watanabe, N. (2004). Actin polymerization-driven molecular movement of mDia1 in living cells. *Science (New York, N.Y.)*, 303(5666), 2007–10.

[Hoogenraad et al., 2007] Hoogenraad, C. C., Feliu-Mojer, M. I., Spangler, S. a., Milstein, A. D., Dunah, A. W., Hung, A. Y., & Sheng, M. (2007). Liprinalpha1 degradation by calcium/calmodulin-dependent protein kinase II regulates LAR receptor tyrosine phosphatase distribution and dendrite development. *Developmental cell*, 12(4), 587–602.

[Hoogenraad et al., 2005] Hoogenraad, C. C., Milstein, A. D., Ethell, I. M., Henkemeyer, M., & Sheng, M. (2005). GRIP1 controls dendrite morphogenesis by regulating EphB receptor trafficking. *Nature neuroscience*, 8(7), 906–15.

[Horton & Ehlers, 2003] Horton, A. C. & Ehlers, M. D. (2003). Dual modes of endoplasmic reticulum-to-Golgi transport in dendrites revealed by live-cell imaging. *The Journal of neuroscience : the official journal of the Society for Neuroscience*, 23(15), 6188–99.

[Horton et al., 2003] Horton, A. C., Ehlers, M. D., & Carolina, N. (2003). Neuronal Polarity and Trafficking Review. 40, 277–295.

[Horton et al., 2005] Horton, A. C., Rácz, B., Monson, E. E., Lin, A. L., Weinberg, R. J., & Ehlers, M. D. (2005). Polarized secretory trafficking directs cargo for asymmetric dendrite growth and morphogenesis. *Neuron*, 48(5), 757–71.

[Hsu et al., 1999] Hsu, S. C., Hazuka, C. D., Foletti, D. L., & Scheller, R. H. (1999). Targeting vesicles to specific sites on the plasma membrane: the role of the sec6/8 complex. *Trends in cell biology*, 9(4), 150–3.

[Hsu et al., 1996] Hsu, S. C., Ting, a. E., Hazuka, C. D., Davanger, S., Kenny, J. W., Kee, Y., & Scheller, R. H. (1996). The mammalian brain rsec6/8 complex. *Neuron*, 17(6), 1209–19.

[Huang & Zakharenko, 2005] Huang, Y. & Zakharenko, S. (2005). Genetic evidence for a protein-kinase-A-mediated presynaptic component in NMDA-receptor-dependent forms of long-term synaptic potentiation. *Proceedings of the ...*, 102(26), 9365–9370.

[Huber et al., 1995] Huber, L. a., Dupree, P., & Dotti, C. G. (1995). A deficiency of the small GTPase rab8 inhibits membrane traffic in developing neurons. *Molecular and cellular biology*, 15(2), 918–24.

[Ikeuchi et al., 2009] Ikeuchi, Y., Stegmüller, J., Netherton, S., Huynh, M. A., Masu, M., Frank, D., Bonni, S., & Bonni, A. (2009). A SnoN-Ccd1 pathway promotes axonal morphogenesis in the mammalian brain. *The Journal of neuroscience : the official journal of the Society for Neuroscience*, 29(13), 4312–21.

[Jaworski et al., 2008] Jaworski, J., Hoogenraad, C. C., & Akhmanova, A. (2008). Microtubule plus-end tracking proteins in differentiated mammalian cells. *The international journal of biochemistry & cell biology*, 40(4), 619–37.

[Jeffrey et al., 2009] Jeffrey, R. a., Ch'ng, T. H., O'Dell, T. J., & Martin, K. C. (2009). Activity-dependent anchoring of importin alpha at the synapse involves regulated binding to the cy-

toplasmic tail of the NR1-1a subunit of the NMDA receptor. *The Journal of neuroscience : the official journal of the Society for Neuroscience*, 29(50), 15613–20.

[Jiang et al., 2010] Jiang, X., Litkowski, P. E., Taylor, A. a., Lin, Y., Snider, B. J., & Moulder, K. L. (2010). A role for the ubiquitin-proteasome system in activity-dependent presynaptic silencing. *The Journal of neuroscience : the official journal of the Society for Neuroscience*, 30(5), 1798–809.

[Jordens et al., 2005] Jordens, I., Marsman, M., Kuijl, C., & Neefjes, J. (2005). Rab proteins, connecting transport and vesicle fusion. *Traffic (Copenhagen, Denmark)*, 6(12), 1070–7.

[Kaeser, 2011] Kaeser, P. S. (2011). Pushing synaptic vesicles over the RIM. *Cellular logistics*, 1(3), 106–110.

[Kaeser et al., 2012] Kaeser, P. S., Deng, L., Fan, M., & Südhof, T. C. (2012). RIM genes differentially contribute to organizing presynaptic release sites. *Proceedings of the National Academy of Sciences of the United States of America*, 109(29), 11830–5.

[Kaeser et al., 2011] Kaeser, P. S., Deng, L., Wang, Y., Dulubova, I., Liu, X., Rizo, J., & Südhof, T. C. (2011). RIM proteins tether Ca2+ channels to presynaptic active zones via a direct PDZ-domain interaction. *Cell*, 144(2), 282–95.

[Kaeser et al., 2008] Kaeser, P. S., Kwon, H.-B., Chiu, C. Q., Deng, L., Castillo, P. E., & Südhof, T. C. (2008). RIM1alpha and RIM1beta are synthesized from distinct promoters of the RIM1 gene to mediate differential but overlapping synaptic functions. *The Journal of neuroscience : the official journal of the Society for Neuroscience*, 28(50), 13435–47.

[Kawauchi et al., 2010] Kawauchi, T., Sekine, K., Shikanai, M., Chihama, K., Tomita, K., Kubo, K.-i., Nakajima, K., Nabeshima, Y.-I., & Hoshino, M. (2010). Rab GTPases-dependent endocytic pathways regulate neuronal migration and maturation through N-cadherin trafficking. *Neuron*, 67(4), 588–602.

[Keil & Hatzfeld, 2013] Keil, R. & Hatzfeld, M. (2013). The armadillo protein p0071 is involved in Rab11-dependent recycling. *Journal of cell science*, (October).

[Keil et al., 2013] Keil, R., Schulz, J., & Hatzfeld, M. (2013). p0071/PKP4, a multifunctional protein coordinating cell adhesion with cytoskeletal organization. *Biological chemistry*, 394(8), 1005–17.

[Kim et al., 2007] Kim, H., Han, J., Park, J., Oh, M., James, S., Chang, S., Lu, Q., Lee, K., Ki, H., Song, W., & Kim, K. (2007). -Catenin-induced Dendritic Morphogenesis: AN ESSENTIAL ROLE OF p190RhoGEF INTERACTION THROUGH AKT1-MEDIATED PHOSPHORYLATION. *Journal of Biological Chemistry*, 283(2), 977–987.

[Kirschner & Mitchison, 1986] Kirschner, M. & Mitchison, T. (1986). Beyond self-assembly: from microtubules to morphogenesis. *Cell*, 45(3), 329–42.

[Kiyonaka et al., 2007] Kiyonaka, S., Wakamori, M., Miki, T., Uriu, Y., Nonaka, M., Bito, H., Beedle, A. M., Mori, E., Hara, Y., De Waard, M., Kanagawa, M., Itakura, M., Takahashi, M., Campbell, K. P., & Mori, Y. (2007). RIM1 confers sustained activity and neurotransmitter vesicle anchoring to presynaptic Ca2+ channels. *Nature neuroscience*, 10(6), 691–701.

[Klöpper et al., 2012] Klöpper, T. H., Kienle, N., Fasshauer, D., & Munro, S. (2012). Untangling the evolution of Rab G proteins: implications of a comprehensive genomic analysis. *BMC biology*, 10(1), 71.

[Kobayashi et al., 2014] Kobayashi, H., Etoh, K., Ohbayashi, N., & Fukuda, M. (2014). Rab35 promotes the recruitment of Rab8, Rab13 and Rab36 to recycling endosomes through MICAL-L1 during neurite outgrowth. *Biology open*, 3(9), 803–14.

[Köhrmann et al., 1999] Köhrmann, M., Haubensak, W., Hemraj, I., Kaether, C., Leß mann, V. J., & Kiebler, M. A. (1999). Fast , Convenient , and Effective Method to Transiently Transfect Primary Hippocampal Neurons. *Journal of neuroscience research*, 835(August), 831–835.

[Kumar et al., 2010] Kumar, R. a., Sudi, J., Babatz, T. D., Brune, C. W., Oswald, D., Yen, M., Nowak, N. J., Cook, E. H., Christian, S. L., & Dobyns, W. B. (2010). A de novo 1p34.2 microdeletion identifies the synaptic vesicle gene RIMS3 as a novel candidate for autism. *Journal of medical genetics*, 47(2), 81–90.

[Kwon et al., 2012] Kwon, H.-B., Kozorovitskiy, Y., Oh, W.-J., Peixoto, R. T., Akhtar, N., Saulnier, J. L., Gu, C., & Sabatini, B. L. (2012). Neuroligin-1-dependent competition regulates cortical synaptogenesis and synapse number. *Nature neuroscience*, 15(12), 1667–74.

[Lasorella et al., 2006] Lasorella, A., Stegmüller, J., Guardavaccaro, D., Liu, G., Carro, M. S., Rothschild, G., de la Torre-Ubieta, L., Pagano, M., Bonni, A., & Iavarone, A. (2006). Degradation of Id2 by the anaphase-promoting complex couples cell cycle exit and axonal growth. *Nature*, 442(7101), 471–4.

[Lazarevic et al., 2013] Lazarevic, V., Pothula, S., Andres-Alonso, M., & Fejtova, A. (2013). Molecular mechanisms driving homeostatic plasticity of neurotransmitter release. *Frontiers in cellular neuroscience*, 7(December), 244.

[Lazarevic et al., 2011] Lazarevic, V., Schöne, C., Heine, M., Gundelfinger, E. D., & Fejtova, A. (2011). Extensive remodeling of the presynaptic cytomatrix upon homeostatic adaptation to network activity silencing. *The Journal of neuroscience : the official journal of the Society for Neuroscience*, 31(28), 10189–200.

[Lazo et al., 2013] Lazo, O. M., Gonzalez, A., Ascaño, M., Kuruvilla, R., Couve, A., & Bronfman, F. C. (2013). BDNF regulates Rab11-mediated recycling endosome dynamics to induce dendritic branching. *The Journal of neuroscience : the official journal of the Society for Neuroscience*, 33(14), 6112–22.

[LeClerc et al., 1993] LeClerc, N., Kosik, K. S., Cowan, N., Pienkowski, T. P., & Baas, P. W. (1993). Process formation in Sf9 cells induced by the expression of a microtubule-associated protein 2C-like construct. *Proceedings of the National Academy of Sciences of the United States of America*, 90(13), 6223–7.

[Leung et al., 1996] Leung, T., Chen, X. Q., Manser, E., & Lim, L. (1996). The p160 RhoA-binding kinase ROK alpha is a member of a kinase family and is involved in the reorganization of the cytoskeleton. *Molecular and cellular biology*, 16(10), 5313–27.

[Li & Higgs, 2003] Li, F. & Higgs, H. (2003). The mouse Formin mDia1 is a potent actin nucleation factor regulated by autoinhibition. *Current biology*, 13, 1335–1340.

[Li et al., 2014] Li, L., Tian, X., Zhu, M., Bulgari, D., Böhme, M. a., Goettfert, F., Wichmann, C., Sigrist, S. J., Levitan, E. S., & Wu, C. (2014). Drosophila Syd-1, liprin-α, and protein phosphatase 2A B' subunit Wrd function in a linear pathway to prevent ectopic accumulation of synaptic materials in distal axons. *The Journal of neuroscience : the official journal of the Society for Neuroscience*, 34(25), 8474–87.

[Lipska & Weinberger, 2000] Lipska, B. K. & Weinberger, D. R. (2000). To model a psychiatric disorder in animals: schizophrenia as a reality test. *Neuropsychopharmacology : official publication of the American College of Neuropsychopharmacology*, 23(3), 223–39.

[Llinás et al., 1992] Llinás, R., Sugimori, M., & Silver, R. B. (1992). Microdomains of high calcium concentration in a presynaptic terminal. *Science (New York, N.Y.)*, 256(5057), 677–9.

[Lonart et al., 2003] Lonart, G., Schoch, S., Kaeser, P., & Larkin, C. (2003). Phosphorylation of RIM1α by PKA Triggers Presynaptic Long-Term Potentiation at Cerebellar Parallel Fiber Synapses. *Cell*, 115, 49–60.

[Luo, 2000] Luo, L. (2000). Rho GTPases in neuronal morphogenesis. *Nature reviews. Neuroscience*, 1(3), 173–80.

[Ma et al., 2011] Ma, C., Li, W., Xu, Y., & Rizo, J. (2011). Munc13 mediates the transition from the closed syntaxin-Munc18 complex to the SNARE complex. *Nature structural & molecular biology*, 18(5), 542–9.

[Maclean & Bowie, 2011] Maclean, D. M. & Bowie, D. (2011). Transmembrane AMPA receptor regulatory protein regulation of competitive antagonism: a problem of interpretation. *The Journal of physiology*, 589(Pt 22), 5383–90.

[Mark et al., 2011] Mark, M. D., Maejima, T., Kuckelsberg, D., Yoo, J. W., Robert, A., Shah, V., Gutierrez, D., Moreno, R. L., Kruse, W., Jeffrey, L., & Herlitze, S. (2011). Delayed postnatal loss of P/Q type calcium channels recapitulates the absence epilepsy, dyskinesia, and ataxia phenotypes of genomic Cacna1A mutations. *Journal of Neuroscience*, 31(11), 4311–4326.

[Marra & Salvatore, 2007] Marra, P. & Salvatore, L. (2007). The Biogenesis of the Golgi Ribbon: The Roles of Membrane Input from the ER and of GM130. *Molecular biology of . . .*, 18(May), 1595–1608.

[Martinez et al., 2003] Martinez, M. C., Ochiishi, T., Majewski, M., & Kosik, K. S. (2003). Dual regulation of neuronal morphogenesis by a delta-catenin-cortactin complex and Rho. *The Journal of cell biology*, 162(1), 99–111.

[Martinez et al., 1994] Martinez, O., Schmidt, a., Salaméro, J., Hoflack, B., Roa, M., & Goud, B. (1994). The small GTP-binding protein rab6 functions in intra-Golgi transport. *The Journal of cell biology*, 127(6 Pt 1), 1575–88.

[Mateer et al., 2002] Mateer, S. C., McDaniel, A. E., Nicolas, V., Habermacher, G. M., Lin, M.-J. S., Cromer, D. a., King, M. E., & Bloom, G. S. (2002). The mechanism for regulation

of the F-actin binding activity of IQGAP1 by calcium/calmodulin. *The Journal of biological chemistry*, 277(14), 12324–33.

[Maxfield & McGraw, 2004] Maxfield, F. R. & McGraw, T. E. (2004). Endocytic recycling. *Nature reviews. Molecular cell biology*, 5(2), 121–32.

[McCallum et al., 1998] McCallum, S. J., Erickson, J. W., & Cerione, R. a. (1998). Characterization of the Association of the Actin-binding Protein , IQGAP , and Activated Cdc42 with Golgi Membranes. *Journal of Biological Chemistry*, 273(35), 22537–22544.

[Meberg & Bamburg, 2000] Meberg, P. J. & Bamburg, J. R. (2000). Increase in neurite outgrowth mediated by overexpression of actin depolymerizing factor. *The Journal of neuroscience : the official journal of the Society for Neuroscience*, 20(7), 2459–69.

[Meinrenken et al., 2002] Meinrenken, C. J., Borst, J. G. G., & Sakmann, B. (2002). Calcium secretion coupling at calyx of held governed by nonuniform channel-vesicle topography. *The Journal of neuroscience : the official journal of the Society for Neuroscience*, 22(5), 1648–67.

[Michaelides et al., 2005] Michaelides, M., Holder, G. E., Hunt, D. M., Fitzke, F. W., Bird, a. C., & Moore, a. T. (2005). A detailed study of the phenotype of an autosomal dominant cone-rod dystrophy (CORD7) associated with mutation in the gene for RIM1. *The British journal of ophthalmology*, 89(2), 198–206.

[Miki et al., 1998] Miki, H., Suetsugu, S., & Takenawa, T. (1998). WAVE, a novel WASP-family protein involved in actin reorganization induced by Rac. *The EMBO journal*, 17(23), 6932–41.

[Miki et al., 2007] Miki, T., Kiyonaka, S., & Uriu, Y. (2007). Mutation Associated with an Autosomal Dominant Cone-Rod Dystrophy CORD7 Modifies RIM1-Mediated Modulation of Voltage-Dependent Ca2+ Channels. *Channels*, 1(3), 144–147.

[Milner et al., 1998] Milner, B., Squire, L., & Kandel, E. (1998). Cognitive Neuroscience and the Study of Memory. *Neuron*, 20, 445–468.

[Mittelstaedt et al., 2010] Mittelstaedt, T., Alvaréz-Baron, E., & Schoch, S. (2010). RIM proteins and their role in synapse function. *Biological chemistry*, 391(6), 599–606.

[Miyata et al., 1999] Miyata, T., Maeda, T., & Lee, J. (1999). NeuroD is required for differentiation of the granule cells in the cerebellum and hippocampus. *Genes & development*, (pp. 1647–1652).

[Molyneaux et al., 2007] Molyneaux, B. J., Arlotta, P., Menezes, J. R. L., & Macklis, J. D. (2007). Neuronal subtype specification in the cerebral cortex. *Nature reviews. Neuroscience*, 8(6), 427–37.

[Mori et al., 2013] Mori, Y., Matsui, T., & Fukuda, M. (2013). Rabex-5 protein regulates dendritic localization of small GTPase Rab17 and neurite morphogenesis in hippocampal neurons. *The Journal of biological chemistry*, 288(14), 9835–47.

[Murthy et al., 2003] Murthy, M., Garza, D., Scheller, R. H., & Schwarz, T. L. (2003). Mutations in the exocyst component Sec5 disrupt neuronal membrane traffic, but neurotransmitter release persists. *Neuron*, 37(3), 433–47.

[Nakayama et al., 2000] Nakayama, a. Y., Harms, M. B., & Luo, L. (2000). Small GTPases Rac and Rho in the maintenance of dendritic spines and branches in hippocampal pyramidal

neurons. *The Journal of neuroscience : the official journal of the Society for Neuroscience*, 20(14), 5329–38.

[Neukirchen & Bradke, 2011] Neukirchen, D. & Bradke, F. (2011). Neuronal polarization and the cytoskeleton. *Seminars in cell & developmental biology*, 22(8), 825–33.

[Neychev et al., 2008] Neychev, V. K., Fan, X., Mitev, V. I., Hess, E. J., & Jinnah, H. a. (2008). The basal ganglia and cerebellum interact in the expression of dystonic movement. *Brain : a journal of neurology*, 131(Pt 9), 2499–509.

[Nishimura et al., 2007] Nishimura, Y., Martin, C. L., Vazquez-Lopez, A., Spence, S. J., Alvarez-Retuerto, A. I., Sigman, M., Steindler, C., Pellegrini, S., Schanen, N. C., Warren, S. T., & Geschwind, D. H. (2007). Genome-wide expression profiling of lymphoblastoid cell lines distinguishes different forms of autism and reveals shared pathways. *Human molecular genetics*, 16(14), 1682–98.

[Noebels & Sidman, 1979] Noebels, J. & Sidman, R. (1979). Inherited Epilepsy : Spike-Wave and Focal Motor Seizures in the mutant mouse tottering. *Science*, 204(June).

[Owald et al., 2012] Owald, D., Khorramshahi, O., Gupta, V. K., Banovic, D., Depner, H., Fouquet, W., Wichmann, C., Mertel, S., Eimer, S., Reynolds, E., Holt, M., Aberle, H., & Sigrist, S. J. (2012). Cooperation of Syd-1 with Neurexin synchronizes pre- with postsynaptic assembly. *Nature neuroscience*, 15(9), 1219–26.

[Pardo & Eberhart, 2007] Pardo, C. a. & Eberhart, C. G. (2007). The neurobiology of autism. *Brain pathology (Zurich, Switzerland)*, 17(4), 434–47.

[Park et al., 2004] Park, M., Penick, E. C., Edwards, J. G., Kauer, J. a., & Ehlers, M. D. (2004). Recycling endosomes supply AMPA receptors for LTP. *Science (New York, N.Y.)*, 305(5692), 1972–5.

[Patel et al., 2006] Patel, M. R., Lehrman, E. K., Poon, V. Y., Crump, J. G., Zhen, M., Bargmann, C. I., & Shen, K. (2006). Hierarchical assembly of presynaptic components in defined C. elegans synapses. *Nature neuroscience*, 9(12), 1488–98.

[Peifer & McCrea, 1992] Peifer, M. & McCrea, P. (1992). The vertebrate adhesive junction proteins beta-catenin and plakoglobin and the Drosophila segment polarity gene armadillo form a multigene family with similar properties. *The Journal of cell . . .*, 118(3), 681–691.

[Peränen et al., 1996] Peränen, J., Auvinen, P., Virta, H., Wepf, R., & Simons, K. (1996). Rab8 promotes polarized membrane transport through reorganization of actin and microtubules in fibroblasts. *The Journal of cell biology*, 135(1), 153–67.

[Pfenninger, 2009] Pfenninger, K. H. (2009). Plasma membrane expansion: a neuron's Herculean task. *Nature reviews. Neuroscience*, 10(4), 251–61.

[Pitsch et al., 2012] Pitsch, J., Opitz, T., Borm, V., Woitecki, A., Staniek, M., Beck, H., Becker, A. J., & Schoch, S. (2012). The presynaptic active zone protein RIM1α controls epileptogenesis following status epilepticus. *The Journal of neuroscience : the official journal of the Society for Neuroscience*, 32(36), 12384–95.

[Pitsch et al., 2007] Pitsch, J., Schoch, S., Gueler, N., Flor, P. J., van der Putten, H., & Becker,

a. J. (2007). Functional role of mGluR1 and mGluR4 in pilocarpine-induced temporal lobe epilepsy. *Neurobiology of disease*, 26(3), 623–33.

[Platta & Stenmark, 2011] Platta, H. W. & Stenmark, H. (2011). Endocytosis and signaling. *Current opinion in cell biology*, 23(4), 393–403.

[Pollard & Cooper, 2009] Pollard, T. & Cooper, J. (2009). Actin, a Central Player in Cell Shape and Movement. *Science*, 326(5957), 1208–1212.

[Polleux et al., 2007] Polleux, F., Ince-Dunn, G., & Ghosh, A. (2007). Transcriptional regulation of vertebrate axon guidance and synapse formation. *Nature reviews. Neuroscience*, 8(5), 331–40.

[Pommereit & Wouters, 2007] Pommereit, D. & Wouters, F. S. (2007). An NGF-induced Exo70-TC10 complex locally antagonises Cdc42-mediated activation of N-WASP to modulate neurite outgrowth. *Journal of cell science*, 120(Pt 15), 2694–705.

[Powell et al., 2004] Powell, C. M., Schoch, S., Monteggia, L., Barrot, M., Matos, M. F., Feldmann, N., Südhof, T. C., & Nestler, E. J. (2004). The presynaptic active zone protein RIM1alpha is critical for normal learning and memory. *Neuron*, 42(1), 143–53.

[Qian & Noebels, 2001] Qian, J. & Noebels, J. L. (2001). Presynaptic Ca2+ channels and neurotransmitter release at the terminal of a mouse cortical neuron. *The Journal of neuroscience : the official journal of the Society for Neuroscience*, 21(11), 3721–8.

[Regehr & Mintz, 1994] Regehr, W. & Mintz, I. (1994). Participation of Multiple Calcium Channel Types in Transmission at Single Climbing Fiber to Purkinje Cell Synapses. *Neuron*, 12, 605–613.

[Richmond et al., 2001] Richmond, J. E., Weimer, R. M., & Jorgensen, E. M. (2001). An open form of syntaxin bypasses the requirement for UNC-13 in vesicle priming. *Nature*, 412(6844), 338–41.

[Rohatgi et al., 2000] Rohatgi, R., Ho, H. Y., & Kirschner, M. W. (2000). Mechanism of N-WASP activation by CDC42 and phosphatidylinositol 4, 5-bisphosphate. *The Journal of cell biology*, 150(6), 1299–310.

[Rohatgi et al., 1999] Rohatgi, R., Ma, L., Miki, H., Lopez, M., Kirchhausen, T., Takenawa, T., & Kirschner, M. W. (1999). The interaction between N-WASP and the Arp2/3 complex links Cdc42-dependent signals to actin assembly. *Cell*, 97(2), 221–31.

[Sabatini & Regehr, 1999] Sabatini, B. & Regehr, W. (1999). TIMING OF SYNAPTIC TRANSMISSION. *Annual Review of Physiology*, (1).

[Sahlender et al., 2005] Sahlender, D. a., Roberts, R. C., Arden, S. D., Spudich, G., Taylor, M. J., Luzio, J. P., Kendrick-Jones, J., & Buss, F. (2005). Optineurin links myosin VI to the Golgi complex and is involved in Golgi organization and exocytosis. *The Journal of cell biology*, 169(2), 285–95.

[Sakurai-Yageta et al., 2008] Sakurai-Yageta, M., Recchi, C., Le Dez, G., Sibarita, J. B., Daviet, L., Camonis, J., D'Souza-Schorey, C., & Chavrier, P. (2008). The interaction of IQGAP1 with the exocyst complex is required for tumor cell invasion downstream of Cdc42 and RhoA. *The Journal of cell biology*, 181(6), 985–998.

[Satoh et al., 2008] Satoh, D., Sato, D., Tsuyama, T., Saito, M., Ohkura, H., Rolls, M. M., Ishikawa, F., & Uemura, T. (2008). Spatial control of branching within dendritic arbors by dynein-dependent transport of Rab5-endosomes. *Nature cell biology*, 10(10), 1164–71.

[Scharfman, 2008] Scharfman, H. E. (2008). Epilepsy as an Example of Neural Plasticity. *Neuroscientist*, 8(2), 154–173.

[Scheiffele et al., 2000] Scheiffele, P., Fan, J., Choih, J., Fetter, R., & Serafini, T. (2000). Neuroligin expressed in nonneuronal cells triggers presynaptic development in contacting axons. *Cell*, 101(6), 657–69.

[Schlager et al., 2010] Schlager, M. a., Kapitein, L. C., Grigoriev, I., Burzynski, G. M., Wulf, P. S., Keijzer, N., de Graaff, E., Fukuda, M., Shepherd, I. T., Akhmanova, A., & Hoogenraad, C. C. (2010). Pericentrosomal targeting of Rab6 secretory vesicles by Bicaudal-D-related protein 1 (BICDR-1) regulates neuritogenesis. *The EMBO journal*, 29(10), 1637–51.

[Schliwa, 2006] Schliwa, M. (2006). *Molecular motors*, volume 422.

[Schoch et al., 2002] Schoch, S., Castillo, P. E., Jo, T., Mukherjee, K., Geppert, M., Wang, Y., Schmitz, F., Malenka, R. C., & Südhof, T. C. (2002). RIM1alpha forms a protein scaffold for regulating neurotransmitter release at the active zone. *Nature*, 415(6869), 321–6.

[Sharma et al., 2007] Sharma, V. M., Litersky, J. M., Bhaskar, K., & Lee, G. (2007). Tau impacts on growth-factor-stimulated actin remodeling. *Journal of cell science*, 120(Pt 5), 748–57.

[Shen et al., 2015] Shen, Y., Ge, W.-P., Li, Y., Hirano, A., Lee, H.-Y., Rohlmann, A., Missler, M., Tsien, R. W., Jan, L. Y., Fu, Y.-H., & Ptáček, L. J. (2015). Protein mutated in paroxysmal dyskinesia interacts with the active zone protein RIM and suppresses synaptic vesicle exocytosis. *Proceedings of the National Academy of Sciences of the United States of America*, (pp. 1–7).

[Shetty et al., 1998] Shetty, K. M., Kurada, P., & O'Tousa, J. E. (1998). Rab6 Regulation of Rhodopsin Transport inDrosophila. *Journal of Biological Chemistry*, 273(32), 20425–20430.

[Sisodiya et al., 2007] Sisodiya, S. M., Thompson, P. J., Need, A., Harris, S. E., Weale, M. E., Wilkie, S. E., Michaelides, M., Free, S. L., Walley, N., Gumbs, C., Gerrelli, D., Ruddle, P., Whalley, L. J., Starr, J. M., Hunt, D. M., Goldstein, D. B., Deary, I. J., & Moore, A. T. (2007). Genetic enhancement of cognition in a kindred with cone-rod dystrophy due to RIMS1 mutation. *Journal of medical genetics*, 44(6), 373–80.

[Solem et al., 1995] Solem, M., McMahon, T., & Messing, R. (1995). Depolarization-Induced Neurite Outgrowth in PC12 Cells Requires Permissive , Low Level NGF Receptor Stimulation and Activation of Calcium / Calmodulin-Dependent Protein Kinase. *The Journal of neuroscience*, 75(September), 5966–5975.

[Sönnichsen et al., 2000] Sönnichsen, B., De Renzis, S., Nielsen, E., Rietdorf, J., & Zerial, M. (2000). Distinct membrane domains on endosomes in the recycling pathway visualized by multicolor imaging of Rab4, Rab5, and Rab11. *The Journal of cell biology*, 149(4), 901–14.

[Spangler et al., 2013] Spangler, S. a., Schmitz, S. K., Kevenaar, J. T., de Graaff, E., de Wit, H., Demmers, J., Toonen, R. F., & Hoogenraad, C. C. (2013). Liprin-α2 promotes the presynaptic

recruitment and turnover of RIM1/CASK to facilitate synaptic transmission. *The Journal of cell biology*, 201(6), 915–28.

[Stegmüller et al., 2006] Stegmüller, J., Konishi, Y., Huynh, M. A., Yuan, Z., Dibacco, S., & Bonni, A. (2006). Cell-intrinsic regulation of axonal morphogenesis by the Cdh1-APC target SnoN. *Neuron*, 50(3), 389–400.

[Stephan et al., 2009] Stephan, K. E., Friston, K. J., & Frith, C. D. (2009). Dysconnection in schizophrenia: from abnormal synaptic plasticity to failures of self-monitoring. *Schizophrenia bulletin*, 35(3), 509–27.

[Sudhof, 2004] Sudhof, T. C. (2004). The synaptic vesicle cycle. *Annual review of neuroscience*, 27, 509–47.

[Südhof, 2012] Südhof, T. C. (2012). The presynaptic active zone. *Neuron*, 75(1), 11–25.

[Südhof, 2013] Südhof, T. C. (2013). Neurotransmitter release: the last millisecond in the life of a synaptic vesicle. *Neuron*, 80(3), 675–90.

[Swiech et al., 2011] Swiech, L., Blazejczyk, M., Urbanska, M., Pietruszka, P., Dortland, B. R., Malik, A. R., Wulf, P. S., Hoogenraad, C. C., & Jaworski, J. (2011). CLIP-170 and IQGAP1 cooperatively regulate dendrite morphology. *The Journal of neuroscience : the official journal of the Society for Neuroscience*, 31(12), 4555–68.

[Takahashi et al., 2012] Takahashi, S., Kubo, K., Waguri, S., Yabashi, A., Shin, H.-W., Katoh, Y., & Nakayama, K. (2012). Rab11 regulates exocytosis of recycling vesicles at the plasma membrane. *Journal of cell science*, 125(Pt 17), 4049–57.

[Takahashi & Momiyama, 1993] Takahashi, T. & Momiyama, A. (1993). Different types of calcium channels mediate central synaptic transmission. *Nature*.

[Takano et al., 2012] Takano, T., Tomomura, M., Yoshioka, N., Tsutsumi, K., Terasawa, Y., Saito, T., Kawano, H., Kamiguchi, H., Fukuda, M., & Hisanaga, S.-i. (2012). LMTK1/AATYK1 is a novel regulator of axonal outgrowth that acts via Rab11 in a Cdk5-dependent manner. *The Journal of neuroscience : the official journal of the Society for Neuroscience*, 32(19), 6587–99.

[Takano et al., 2010] Takano, T., Tsutsumi, K., Saito, T., Asada, A., Tomomura, M., Fukuda, M., & Hisanaga, S.-i. (2010). AATYK1A phosphorylation by Cdk5 regulates the recycling endosome pathway. *Genes to cells : devoted to molecular & cellular mechanisms*, 15(7), 783–97.

[Takano et al., 2014a] Takano, T., Urushibara, T., Yoshioka, N., Saito, T., Fukuda, M., Tomomura, M., & Hisanaga, S.-I. (2014a). LMTK1 regulates dendritic formation by regulating movement of Rab11A-positive endosomes. *Molecular biology of the cell*, 25(11), 1755–68.

[Takano et al., 2014b] Takano, T., Urushibara, T., Yoshioka, N., Saito, T., Fukuda, M., Tomomura, M., & Hisanaga, S.-I. (2014b). LMTK1 regulates dendritic formation by regulating movement of Rab11A-positive endosomes. *Molecular biology of the cell*.

[Takei et al., 2000] Takei, Y., Teng, J., Harada, a., & Hirokawa, N. (2000). Defects in axonal elongation and neuronal migration in mice with disrupted tau and map1b genes. *The Journal of cell biology*, 150(5), 989–1000.

[Temburni et al., 2004] Temburni, M. K., Rosenberg, M. M., Pathak, N., McConnell, R., & Jacob, M. H. (2004). Neuronal nicotinic synapse assembly requires the adenomatous polyposis coli tumor suppressor protein. *The Journal of neuroscience : the official journal of the Society for Neuroscience*, 24(30), 6776–84.

[TerBush et al., 1996] TerBush, D. R., Maurice, T., Roth, D., & Novick, P. (1996). The Exocyst is a multiprotein complex required for exocytosis in Saccharomyces cerevisiae. *The EMBO journal*, 15(23), 6483–94.

[Ullrich et al., 1996] Ullrich, O., Reinsch, S., & Urbé, S. (1996). Rab11 regulates recycling through the pericentriolar recycling endosome. *The Journal of cell biology*, 135(4), 913–924.

[Uriu et al., 2010] Uriu, Y., Kiyonaka, S., Miki, T., Yagi, M., Akiyama, S., Mori, E., Nakao, A., Beedle, A. M., Campbell, K. P., Wakamori, M., & Mori, Y. (2010). Rab3-interacting molecule gamma isoforms lacking the Rab3-binding domain induce long lasting currents but block neurotransmitter vesicle anchoring in voltage-dependent P/Q-type Ca2+ channels. *The Journal of biological chemistry*, 285(28), 21750–21767.

[Varoqueaux et al., 2006] Varoqueaux, F., Aramuni, G., Rawson, R. L., Mohrmann, R., Missler, M., Gottmann, K., Zhang, W., Südhof, T. C., & Brose, N. (2006). Neuroligins determine synapse maturation and function. *Neuron*, 51(6), 741–54.

[Vega & Hsu, 2001] Vega, I. E. & Hsu, S. C. (2001). The exocyst complex associates with microtubules to mediate vesicle targeting and neurite outgrowth. *Journal of Neuroscience*, 21(11), 3839–3848.

[Villarroel-Campos et al., 2014] Villarroel-Campos, D., Gastaldi, L., Conde, C., Caceres, A., & Gonzalez-Billault, C. (2014). Rab-mediated trafficking role in neurite formation. *Journal of neurochemistry*.

[Wakamori, 1998] Wakamori, M. (1998). Single Tottering Mutations Responsible for the Neuropathic Phenotype of the P-type Calcium Channel. *Journal of Biological Chemistry*, 273(52), 34857–34867.

[Wang et al., 2007] Wang, S., Watanabe, T., Noritake, J., Fukata, M., Yoshimura, T., Itoh, N., Harada, T., Nakagawa, M., Matsuura, Y., Arimura, N., & Kaibuchi, K. (2007). IQGAP3, a novel effector of Rac1 and Cdc42, regulates neurite outgrowth. *Journal of cell science*, 120(Pt 4), 567–577.

[Wang et al., 1997] Wang, Y., Okamoto, M., Schmitz, F., Hofmann, K., & Südhof, T. C. (1997). Rim is a putative Rab3 effector in regulating synaptic-vesicle fusion. *Nature*, 388(6642), 593–8.

[Wang & Südhof, 2003] Wang, Y. & Südhof, T. C. (2003). Genomic definition of RIM proteins: evolutionary amplification of a family of synaptic regulatory proteins. *Genomics*, 81(2), 126–137.

[Wang et al., 2000] Wang, Y., Sugita, S., & Sudhof, T. C. (2000). The RIM/NIM family of neuronal C2 domain proteins. Interactions with Rab3 and a new class of Src homology 3 domain proteins. *The Journal of biological chemistry*, 275(26), 20033–44.

[Watanabe et al., 1997] Watanabe, N., Madaule, P., Reid, T., Ishizaki, T., Watanabe, G., Kakizuka, a., Saito, Y., Nakao, K., Jockusch, B. M., & Narumiya, S. (1997). p140mDia, a

mammalian homolog of Drosophila diaphanous, is a target protein for Rho small GTPase and is a ligand for profilin. *The EMBO journal*, 16(11), 3044–56.

[Watanabe et al., 2009] Watanabe, T., Noritake, J., Kakeno, M., Matsui, T., Harada, T., Wang, S., Itoh, N., Sato, K., Matsuzawa, K., Iwamatsu, A., Galjart, N., & Kaibuchi, K. (2009). Phosphorylation of CLASP2 by GSK-3beta regulates its interaction with IQGAP1, EB1 and microtubules. *Journal of cell science*, 122(Pt 16), 2969–79.

[Watanabe et al., 2004] Watanabe, T., Wang, S., Noritake, J., Sato, K., Fukata, M., Takefuji, M., Nakagawa, M., Izumi, N., Akiyama, T., & Kaibuchi, K. (2004). Interaction with IQGAP1 links APC to Rac1, Cdc42, and actin filaments during cell polarization and migration. *Developmental cell*, 7(6), 871–83.

[Weidenhofer et al., 2006] Weidenhofer, J., Bowden, N. a., Scott, R. J., & Tooney, P. a. (2006). Altered gene expression in the amygdala in schizophrenia: up-regulation of genes located in the cytomatrix active zone. *Molecular and cellular neurosciences*, 31(2), 243–50.

[Weidenhofer et al., 2009] Weidenhofer, J., Scott, R. J., & Tooney, P. a. (2009). Investigation of the expression of genes affecting cytomatrix active zone function in the amygdala in schizophrenia: effects of antipsychotic drugs. *Journal of psychiatric research*, 43(3), 282–90.

[Wentzel et al., 2013] Wentzel, C., Sommer, J., Nair, R., Stiefvater, A., Sibarita, J.-B., & Scheiffele, P. (2013). mSYD1A, a Mammalian Synapse-Defective-1 Protein, Regulates Synaptogenic Signaling and Vesicle Docking. *Neuron*, 78(6), 1012–1023.

[White et al., 2012] White, C. D., Erdemir, H. H., & Sacks, D. B. (2012). IQGAP1 and its binding proteins control diverse biological functions. *Cellular signalling*, 24(4), 826–34.

[Wickstead & Gull, 2011] Wickstead, B. & Gull, K. (2011). The evolution of the cytoskeleton. *The Journal of cell biology*, 194(4), 513–25.

[Williams et al., 2004] Williams, S. N., Locke, C. J., Braden, A. L., Caldwell, K. a., & Caldwell, G. a. (2004). Epileptic-like convulsions associated with LIS-1 in the cytoskeletal control of neurotransmitter signaling in Caenorhabditis elegans. *Human molecular genetics*, 13(18), 2043–59.

[Witte & Bradke, 2008] Witte, H. & Bradke, F. (2008). The role of the cytoskeleton during neuronal polarization. *Current opinion in neurobiology*, 18(5), 479–487.

[Wong & Ghosh, 2002] Wong, R. O. L. & Ghosh, A. (2002). Activity-dependent regulation of dendritic growth and patterning. *Nature reviews. Neuroscience*, 3(10), 803–12.

[Wyszynski et al., 2002] Wyszynski, M., Kim, E., & Dunah, A. (2002). Interaction between GRIP and liprin-α/SYD2 is required for AMPA receptor targeting. *Neuron*, 34, 39–52.

[Yadav & Linstedt, 2011] Yadav, S. & Linstedt, A. D. (2011). Golgi positioning. *Cold Spring Harbor perspectives in biology*, 3(5).

[Yamada et al., 1971] Yamada, K. M., Spooner, B. S., & Wessells, N. K. (1971). Ultrastructure and function of growth cones and axons of cultured nerve cells. *The Journal of cell biology*, 49(3), 614–35.

[Yap & Winckler, 2012] Yap, C. C. & Winckler, B. (2012). Harnessing the power of the endosome to regulate neural development. *Neuron*, 74(3), 440–51.

[Ye et al., 2007] Ye, B., Zhang, Y., Song, W., Younger, S. H., Jan, L. Y., & Jan, Y. N. (2007). Growing dendrites and axons differ in their reliance on the secretory pathway. 130(4), 717–729.

[Yu & Rasenick, 2006] Yu, J.-Z. & Rasenick, M. M. (2006). Tau associates with actin in differentiating PC12 cells. *FASEB journal : official publication of the Federation of American Societies for Experimental Biology*, 20(9), 1452–61.

[Zerial & McBride, 2001] Zerial, M. & McBride, H. (2001). Rab proteins as membrane organizers. *Nature reviews. Molecular cell biology*, 2(2), 107–17.

[Zhang et al., 2005] Zhang, X., Zajac, A., Zhang, J., Wang, P., Li, M., Murray, J., TerBush, D., & Guo, W. (2005). The critical role of Exo84p in the organization and polarized localization of the exocyst complex. *The Journal of biological chemistry*, 280(21), 20356–64.

[Zhen & Jin, 1999] Zhen, M. & Jin, Y. (1999). The liprin protein SYD-2 regulates the differentiation of presynaptic termini in C. elegans. *Nature*, 401(6751), 371–5.

[Zwingman, 2001] Zwingman, T. (2001). Rocker is a new variant of the voltage-dependent calcium channel gene Cacna1a. *The Journal of ...*, 21(4), 1169–1178.

11 Acknowledgements

The realization of my PhD would not have possible with the help and the support of others therefore I would like to express my gratitude to all the people who contributed to this work and accompanied me on my journey to this thesis.

I would like to thank Prof. Dr. Susanne Schoch for believing in pharmacists and giving me the opportunity to do my thesis work in her lab and discover my passion for science. Her enthusiasm and never ending curiosity about scientific questions was always a great source of motivation and kept me going also through the frustrating times.

I cordially thank Prof. Dr. Albert Haas for being the co-advisor of my Ph.D. thesis and Prof. Dr. Walter Witke and Prof. Dr. Alf Lamprecht for their time as part of my thesis committee.

I would like to thank Prof. Dr. Heinz Beck and Prof. Dr. Dirk Dietrich for their helpful questions, critics, suggestions and comments.

I would like to thank the whole Schoch Becker lab with all its present and past members who have been here during the last five years for the help support understanding and friendship.

Elena, ich danke dir für dein Vertrauen in mich dir eine würdige Nachfolgerin zu sein und deine Hilfe bei meinen ersten Schritten im Labor.

Tobi ohne Dich wäre diese Arbeit schon an den kleinsten Dingen gescheitert. Ich danke dir für eine wunderbare Freundschaft unendlich viel Geduld und deine Liebe zum Detail.

Verena, ich danke dir für all die glücklichen und auch die traurigen Momente die ich mit dir erleben durfte. In unseren Herzen wirst du immer bei uns sein.

Barbara, du warst eine großartige Büromitbewohnerin die mich mit viel Geduld und Keksen durch die Höhen und Tiefen der letzten Jahre begleitet hat. Ich danke dir für deine Freundschaft, Unterstützung und deine immer fortwährende wissenschaftliche und auch unwissenschaftliche Neugierde und Begeisterung.

Alex auch dir danke ich genauso wie Tobi im Besonderen für deine Unterstützung in technischen Fragen. Ohne dich wäre die gesamte AG Schoch Becker verloren und die gedruckte Form dieser

Arbeit nicht mal halb so schön geworden.

Eva, Katharina und Anne euch danke ich für eure fortwährende Unterstützung und Hilfsbereitschaft. Ihr wart immer ein Lichtblick am Schoch-Becker Himmel und habt es geschafft habt das sogar ich als Schwabe Weiberfastnacht vermissen werde.

Sabine, dir danke ich für die wunderschönsten Neurone und deine aufopferungsvolle Hilfe bei allen größeren und kleineren Nöten des Laboralltags.

Lioba, dir möchte ich für deine Hilfe im RIM3/4 Genotypisierungsmarathon danken ohne dich würde ich noch immer pipettieren.

I would like to thank all members of the AG Beck and AG Dietrich lab for lively discussions at seminars and their always friendly and helpful cooperation.

Leonie, dir danke ich von ganzem Herzen für deine für mich immer offenen Ohren, all die langen Nächte, vielen Kletterabende, sonnigen Nachmittage auf Ollis Balkon, Konzerte, Ballettbesuche und so vieles mehr. Letztendlich für eine wunderbare Freundschaft die den Venusberg hoffentlich lange überdauern wird.

Holger und Olli auch euch möchte ich für eure Freundschaft und Unterstützung in den letzten Jahren Danken und all die schönen Stunden außerhalb des Labors.

Ein großer Dank geht an meine Familie, ihr habt die Grundsteine dieser Arbeit gelegt und wart in allen Lebenslagen eine großartige Unterstützung. Im Besonderen möchte ich meinen Eltern dafür danken dass sie mir die Augen für die Fragen und Wunder unserer Welt geöffnet haben und stets unbeirrbar an mich geglaubt haben. Holger auch dir gilt ein ganz besonderer Dank dafür, dass du der gutherzigste und geduldigste Bruder bist, den man sich nur wünschen kann.

Tony I am very thankful and happy that this thesis brought us together. I would like to thank you for being extraordinary supportive and patient during the last years of my PhD. All the sunny Dutch days and the great Zeeuwse mosselen gave me the strength to bring this thesis journey to an end.